JSCSEN 76(2)155–315(2011)

International Year of CHEMISTRY 2011

Journal of the Serbian Chemical Society

Electronic Version

VOLUME 76

No 2

BELGRADE 2011

Available on line at

www.shd.org.rs/JSCS/

The full search of JSCS is available through

DOAJ DIRECTORY OF OPEN ACCESS JOURNALS

www.doaj.org

Journal of the Serbian Chemical Society
JSCS-info@shd.org.rs • www.shd.org.rs/JSCS

J. Serb. Chem. Soc. Vol. 76, No. 2 (2011)

CONTENTS

Published by the Serbian Chemical Society
Karnegijeva 4/III, 11000 Belgrade, Serbia
Printed by the Faculty of Technology and Metallurgy
Karnegijeva 4, P.O. Box 35-03, 11120 Belgrade, Serbia

Journal of the Serbian Chemical Society
JSCS-info@shd.org.rs • www.shd.org.rs/JSCS
J. Serb. Chem. Soc. *76* (2) 155–163 (2011)
JSCS–4108
UDC 66.095.11+547.857.8:678.746:547–316
Original scientific paper

Friedel–Crafts acylation of arenes with carboxylic acids using polystyrene-supported aluminum triflate

KAVEH PARVANAK BOROUJENI[1]* and KAMRAN PARVANAK[2]

[1]*Department of Chemistry, Shahrekord University, Shahrekord 115 and* [2]*Islamic Azad University, Shahr-e-Rey Branch, Iran*

(Received 15 February, revised 1 September 2010)

Abstract: Cross-linked polystyrene-supported aluminum triflate (Ps–Al(OTf)$_3$) has been shown to be a mild, efficient, and chemoselective heterogeneous Lewis acid catalyst for the acylation of aromatic compounds. The catalyst can be easily prepared from cheap starting materials, is stable (as a bench top catalyst) and is reusable.

Keywords: acylation; ketones; aluminum triflate; polystyrene.

INTRODUCTION

Friedel–Crafts acylation of arenes is of great importance in both laboratory work and industry processes to synthesize aromatic ketones.[1,2] Usually, this reaction is performed using acid chlorides or anhydrides[3–12] or carboxylic acids[13–25] as acylating agents in the presence of protic acids or Lewis acids. Acylation of arenes using carboxylic acids is preferable to the acylation *via* acid chlorides or anhydrides because the former reaction produces only water as a by-product, which meets recent requirements for environmentally benign chemical processes. Furthermore, carboxylic acids are stable and more available compounds and their handling is much easier than that of the corresponding acid chlorides or anhydrides. However, only a few studies on the use of carboxylic acids as acylating agents have been reported and many of these procedures have serious drawbacks, such as a need for the use of stoichiometric or excess amounts of catalyst in the reactions, tedious work-up, environmental pollution, long reaction times, high reaction temperatures, highly corrosive conditions, the formation of various by-products and the use of moisture-sensitive, non-recyclable or difficult to handle catalysts. In view of this, a reliable method for this useful reaction involving heterogeneous catalysts is demanded.

* Corresponding author. E-mail: parvanak-ka@sci.sku.ac.ir
doi: 10.2298/JSC100215010P

Triflic acid (trifluoromethanesulfonic acid), known to be a strong acid, is suitable for use as a catalyst for synthetic applications.[26–28] However, the recovery of the triflic acid from the reaction mixture results in the formation of large amounts of waste, which is environmentally unacceptable. In continuation of our ongoing program to develop environmentally benign methods using heterogeneous Lewis acid catalysts, it was found that Ps–Al(OTf)$_3$ is a good solid catalyst for highly chemoselective dithioacetalization of carbonyl compounds.[29] Along this line, it is herein reported that Ps–Al(OTf)$_3$ is also an effective and highly chemoselective catalyst for the acylation of aromatic compounds with carboxylic acids under mild reaction conditions (Scheme 1).

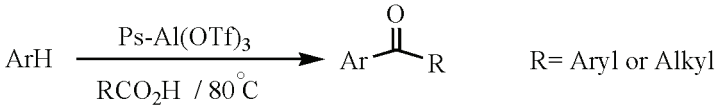

Scheme 1. Acylation of arenes with carboxylic acids using Ps–Al(OTf)$_3$.

EXPERIMENTAL

The employed chemicals were either self-prepared or were purchased from Merck and Fluka. Polystyrene (8 % divinylbenzene, prepared *via* suspension polymerization, using poly(vinylpyrrolidone) 90 K as the suspension agent, grain size range: 0.25–0.6 mm) was obtained from the Iran Polymer and Petrochemical Institute. Capacity of the catalyst was determined by gravimetric method and atomic absorption technique using a Philips PU9400X atomic absorption spectrophotometer. Reaction monitoring and purity determination of the products were accomplished by GLC or TLC on silica-gel polygram SILG/UV254 plates. Gas chromatography was performed on a Shimadzu GC 14-A. The IR spectra were recorded on a Shimadzu model 8300 FT-IR spectrophotometer. The NMR spectra were recorded on a Bruker Advance DPX-300 spectrometer.

Preparation of Ps–Al(OTf)$_3$

This catalyst was prepared as reported in the literature.[29] The determined loading of Al(OTf)$_3$ was 0.41 mmol g^{-1}.

Typical experimental procedure

To a solution of arene (5 mmol) and carboxylic acid (3.5 mmol) was added 0.35 mmol of Ps–Al(OTf)$_3$ and the reaction mixture was stirred at 80 °C. After completion of the reaction (monitored by TLC and GC), the catalyst was filtered off and washed with CH_2Cl_2. The filtrate was washed with 10 % $NaHCO_3$ solution (2×10 mL) and water (2×10 mL) and the organic layer was dried over anhydrous Na_2SO_4. The unreacted anisole was removed by vacuum distillation and the aryl ketone product was isolated in high purity in yields from 87 to 97 %. Whenever required, the products were purified by column chromatography (silica gel) using petroleum ether–ethyl acetate as the eluent, whereby pure ketone was obtained.

RESULTS AND DISCUSSION

Ps–Al(OTf)$_3$ was prepared by the exchange reaction between cross-linked polystyrene supported $AlCl_3$ (Ps–$AlCl_3$) and triflic acid in Freon-113 under reflux conditions. Using catalytic amounts of this catalyst in the Friedel–Crafts

acylation of arenes with carboxylic acids as acylating agents under solvent-free conditions, high to excellent yields of product were obtained (Table I). The optimum molar ratio of Ps–Al(OTf)$_3$ to carboxylic acid was 0.1:1. From the results, it is clear that Ps–Al(OTf)$_3$ is capable of catalyzing not only the acylation of activated arenes, but also of deactivated arenes (Table I, entries 1–23). The methodology showed the excellent positional selectivity as the *para* substituted product was formed almost exclusively. Naphthalene, 2-methoxynaphthalene and anthracene underwent acylation with high regioselectivity in 87–93 % yields (Table I, entries 24–30). It was satisfying to observe that even heterocyclic compounds, such as furan, thiophene and pyrrole, were smoothly converted into the corresponding ketones, a conversion which is otherwise problematic in the presence of strong acid catalysts (Table I, entries 31–36). These reactions were regioselective, affording only the 2-acyl product in high to excellent yields. The acylation of indole with benzoic acid in the presence of Ps–Al(OTf)$_3$ was also studied and the corresponding indolyl aryl ketone was obtained with high regioselectivity in 90 % yield (Table I, entry 37). No *N*-substituted products were observed under these reaction conditions. Acylation of highly deactivated arenes, such as nitrobenzene and 1,2-dichlorobenzene failed.

TABLE I. Acylation of arenes with carboxylic acids catalyzed by Ps–Al(OTf)$_3$ (all reactions performed at 80 °C in the absence of solvent, unless otherwise indicated. The molar ratio of Ps–Al(OTf)$_3$:carboxylic acid is 0.1:1)

Entry	Arene	Carboxylic acid	Product	Time h	Yield, % (*o*:*m*:*p*)[a]	Ref.
1		$PhCO_2H$	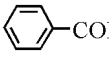	3.3	90 –	20,30
2	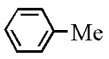	$PhCO_2H$	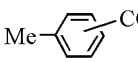	3	92 (6:3:91)	25
3		*p*-$NO_2C_6H_4CO_2H$	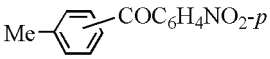	3.1	90 (3:0:97)	25
4		$CH_3(CH_2)_2CO_2H$	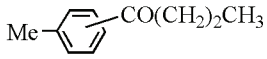	2.9	95 (4:3:93)	13
5		$CH_3(CH_2)_5CO_2H$	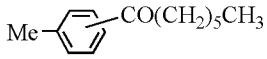	2.9	94 (5:3:92)	13
6		$CH_3(CH_2)_6CO_2H$	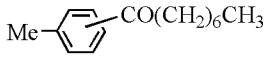	3	88 (4:0:96)	13
7		$CH_3(CH_2)_{10}CO_2H$	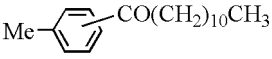	3.1	85 (4:0:96)	13
8	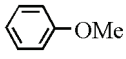	$PhCO_2H$	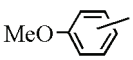	3	94 (4:0:96)	25
9		*p*-$MeOC_6H_4CO_2H$	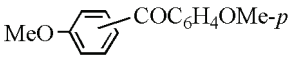	2.9	95 (5:3:92)	15,25
10		$MeCO_2H$	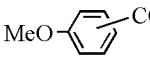	2.9	94 (6:4:90)	31–33

TABLE I. Continued

Entry	Arene	Carboxylic acid	Product	Time h	Yield, % (*o*:*m*:*p*)[a]	Ref.
11	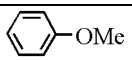	$PhCH_2CO_2H$	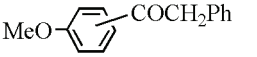	2.8	94 (6:4:90)	34
12		$PhCH{=}CHCO_2H$	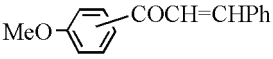	3.1	90 (3:0:97)	25,35
13		$CH_3(CH_2)_2CO_2H$	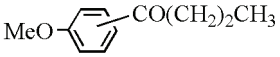	2.7	97 (5:4:91)	16,18
14		$CH_3(CH_2)_5CO_2H$	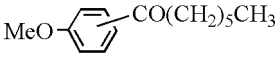	2.8	95 (5:3:92)	16,18
15		$CH_3(CH_2)_6CO_2H$	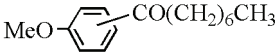	3	93 (3:0:97)	16,18
16		$CH_3(CH_2)_{10}CO_2H$	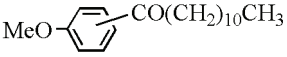	3	92 (3:0:97)	16,18
17	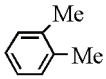	$CH_3(CH_2)_5CO_2H$	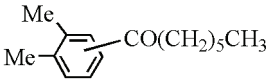	3	90 (95:5)[b]	21
18	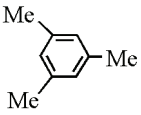	$PhCO_2H$	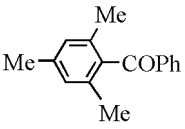	2.9	93 –	25
19		$MeCO_2H$	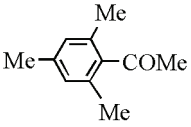	2.8	94 –	18,36
20	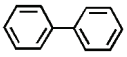	$PhCO_2H$	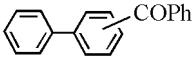	3.1	88 (3:4:97)[c]	30
21	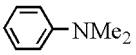	$PhCO_2H$	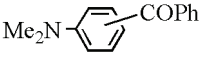	3	91 (7:3:90)	7,30
22		$PhCO_2H$	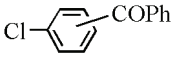	3.5	87 (4:3:93)	30
23		$MeCO_2H$	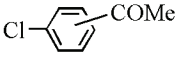	3.3	89 (5:3:92)	30
24		$MeCO_2H$	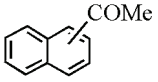	3.3	88 (3:97)[c,d]	18
25	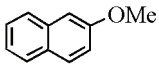	$PhCO_2H$	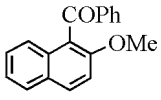	3.1	93[c] –	25
26		$p\text{-}NO_2C_6H_4CO_2H$	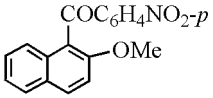	3	90[c] –	25
27		$MeCO_2H$	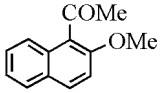	3.1	90[c] –	18,37

TABLE I. Continued

Entry	Arene	Carboxylic acid	Product	Time h	Yield, % (*o*:*m*:*p*)[a]	Ref.
28	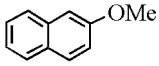	$PhCH_2CO_2H$	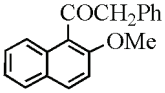	3	90[c] –	18,38
29	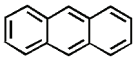	$PhCO_2H$	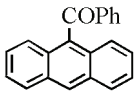	3.4	87[c] –	25
30		$MeCO_2H$	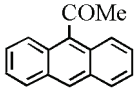	3.3	89[c] –	18,37
31		$PhCO_2H$	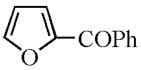	3.5	89[e] –	20,39
32		$MeCO_2H$	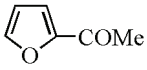	3.3	90[e]	5,40
33		*p*-$NO_2C_6H_4CO_2H$		3.6	89[e] –	5
34		$MeCO_2H$	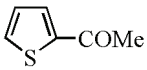	3.6	92[e]	5,41
35	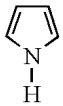	$PhCO_2H$	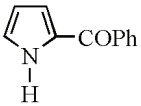	3.4	87[e] –	5,42
36		$MeCO_2H$	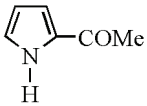	3.3	89[e] –	18,42
37	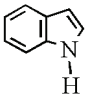	$PhCO_2H$	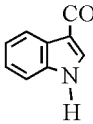	4	90[c] –	43–45

[a]Isolated yields. Isomer distribution based on ^{1}H-NMR spectroscopy and GC. All products are known compounds and were identified by comparison of their physical and spectral data with those of authentic samples; [b]isomer distribution of the 3,4-dimethylphenyl isomer to the 2,3-dimethylphenyl isomer; [c]the reaction was performed in 1,2-dichloroethane; [d]α:β ratio; [e]the reaction was performed at 60 °C.

When Ps–$Al(OTf)_3$ was used as the catalyst in the acylation reactions, no band corresponding to –CO stretching in the IR spectrum of Ps–$Al(OTf)_3$ was observed after the reactions in either the presence or absence of substrate, indicating that polystyrene itself did not undergo acylation under the employed experimental conditions. Probably acylation reactions are not favored with Ps–$Al(OTf)_3$ as a π complex is formed between the polystyrene and $Al(OTf)_3$.[29,46] By-product formation was not observed in the studied reactions. Steric crowding

of the supported catalyst influences the positional selectivity (isomer distribution) observed in the acylation of aromatic compounds.

To determine whether the reaction occurs in the solid matrix of Ps–Al(OTf)$_3$ or whether Al(OTf)$_3$ simply released into the reaction medium is responsible for the acylation reaction, Ps–Al(OTf)$_3$ was added to toluene and the mixture was stirred at 80 °C for 2 h. Then, the catalyst was filtered off and the filtrate was analyzed for its aluminum content, which showed a negligible release of Al(OTf)$_3$. The filtrate was found to be inactive for acylation reaction. These observations indicate that Ps–Al(OTf)$_3$ is stable under the employed reaction conditions and there was no leaching of acid moieties during the studied reactions.

One notable achievement of this solid acid catalyst was intramolecular Friedel–Crafts acylation. For example, 4-phenylbutanoic acid cyclized in nitrobenzene at 80 °C in the presence of Ps–Al(OTf)$_3$ to afford the desired 1-tetralone in 94 % yield (Scheme 2).

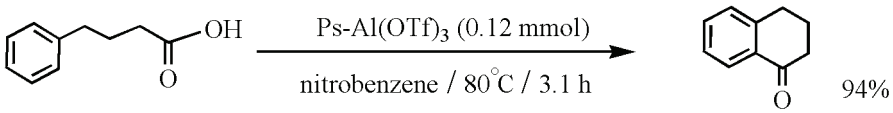

Scheme 2. Intramolecular Friedel–Crafts acylation using Ps–Al(OTf)$_3$.

Ps–Al(OTf)$_3$ recovered after a reaction can be washed with dichloromethane and used again at least five times without any noticeable loss of catalytic activity (Scheme 3). The capacity of the catalyst after five uses was 0.40 mmol Al(OTf)$_3$ per gram of polymeric catalyst.

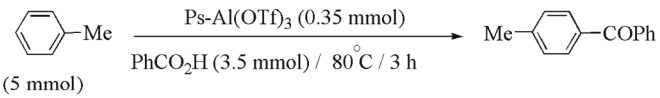

Use	1	2	3	4	5
Yield, %	92	92	90	90	89

Scheme 3. Acylation of toluene using recovered Ps–Al(OTf)$_3$ (recovered catalyst was successfully reused).

A comparison of the efficiency of Ps–Al(OTf)$_3$ catalyst with some of those reported in the literature is given in Table II. As can be seen, in addition to having the general advantages attributed to solid supported catalysts, Ps–Al(OTf)$_3$ also has good efficiency compared to other recently reported catalysts.

Representative spectral data of some of the obtained compounds are given below.

TABLE II. Comparison of the catalytic activity of Ps–Al(OTf)$_3$ against other reported catalysts for the acylation of anisole and toluene with carboxylic acids

Arene	Carboxylic acid	Catalyst	Temperature, °C	Time, h	Yield, % (*o*:*p*)
Anisole	Benzoic acid	Ps–Al(OTf)$_3$	80	3	94(4:96)
		$AlPW_{12}O_{40}$	120	10	92[18]
		$AlPW_{12}O_{40}$/TFAA[a]	25	2.5	96[18]
		P_2O_5/Al_2O_3	85	5	65[25]
Anisole	Heptanoic acid	Ps–Al(OTf)$_3$	80	2.8	95(5:92)
		HZSM-5 zeolite	150	48	5[14]
		Eu(NTf$_2$)$_3$	250	6	87(3:97)[21]
Anisole	Octanoic acid	Ps–Al(OTf)$_3$	80	3	93(3:97)
		$Cs_{2.5}H_{0.5}PW_{12}O_{40}$	110	5	45(1:73)[16]
		Beta zeolite	155	6	42.6(1:38)[22]
Anisole	Dodecanoic acid	Ps–Al(OTf)$_3$	80	3	92(3:97)
		$FePW_{12}O_{40}$	160	1	97(2:98)[24]
Toluene	Octanoic acid	Ps–Al(OTf)$_3$	80	3	88(4:96)
		CeNaY zeolite	150	48	75(3:94)[13]

[a]Trifluoroacetic anhydride

4-Methylbenzophenone. IR (KBr, cm^{-1}): 1660 (C=O). ^{1}H-NMR (300 MHz, $CDCl_3$, δ / ppm): 2.51 (3H, *s*), 7.51 (2H, *d*, *J* = 8.31 Hz), 7.87–8.15 (7H, *m*).

1-(4-Methoxyphenyl)-3-phenyl-2-propen-1-one. IR (KBr, cm^{-1}): 1650 (C=O). ^{1}H-NMR (300 MHz, $CDCl_3$, δ / ppm): 3.91 (3H, *s*), 6.99 (2H, *d*, *J* = 8.71 Hz), 7.47 (3H, *m*), 7.59 (1H, *d*, *J* = 15.15 Hz), 7.69 (2H, *m*), 7.86 (1H, *d*, *J* = 15.15 Hz), 8.11 (2H, *d*, *J* = 8.71 Hz).

1-(3,4-Dimethylphenyl)-1-heptanone. IR (KBr, cm^{-1}): 1685 (C=O). ^{1}H-NMR (300 MHz, $CDCl_3$, δ / ppm): 0.82–0.91 (3H, *m*), 1.23–1.41 (6H, *m*), 1.63–1.74 (2H, *m*), 2.26–2.33 (6H, *m*), 2.80 (0.1H, *t*, *J* = 7.2Hz, 2,3-dimethyl isomer), 2.90 (1.9H, *t*, *J* = 7.2 Hz, 3,4-dimethyl isomer), 7.11 (0.05H, *t*, *J* = 7.2 Hz, 2,3-dimethyl isomer), 7.13–7.20 (1H, *m*), 7.25 (0.05H, *d*, *J* = 7.2 Hz, 2,3-dimethyl isomer), 7.65 (0.95H, *d*, *J* = 7.2 Hz, 3,4-dimethyl isomer), 7.70 (0.95H, *d*, *J* = 7.2 Hz, 3,4-dimethyl isomer).

2,4,6-Trimethylbenzophenone. IR (KBr, cm^{-1}): 1669 (C=O). ^{1}H-NMR (300 MHz, $CDCl_3$, δ / ppm): 2.2 (6H, *s*, 2- and 6-Me), 2.4 (3H, *s*, 4-Me), 6.91 (2H, *s*, aromatic protons of mesityl group), 7.45 (2H, *m*), 7.55 (1H, *m*), 7.81 (2H, *m*).

1-Benzoyl-2-methoxynaphthalene. IR (KBr, cm^{-1}): 1665 (C=O). ^{1}H-NMR (300 MHz, $CDCl_3$, δ / ppm): 3.88 (3H, *s*), 7.31–7.52 (7H, *m*), 7.55–8.12 (4H, *m*).

CONCLUSIONS

In conclusion, a convenient and chemoselective method of the acylation of aromatic compounds has been devised. The significant advantages of this methodology are mild reaction conditions, high to excellent yields, solvent-free conditions and easy preparation and handling of the catalyst. In addition, the use

of Ps–Al(OTf)$_3$ resulted in a reduction in the unwanted and hazardous waste that is produced during conventional homogeneous processes.

Acknowledgements. We gratefully acknowledge the partial support of this study by the Shahrekord University and the Islamic Azad University, Shahr-e-Ray branch Research Council, Iran.

ИЗВОД

ФРИДЕЛ–КРАФТСОВО АЦИЛОВАЊЕ АРЕНА КАРБОКСИЛНИМ КИСЕЛИНАМА ПОМОЋУ АЛУМИНИЈУМ-ТРИФЛАТА НА ПОЛИСТИРЕНУ

KAVEH PARVANAK BOROUJENI[1] и KAMRAN PARVANAK[2]

[1]*Department of Chemistry, Shahrekord University, Shahrekord 115 и* [2]*Islamic Azad University, Shahr-e-Rey Branch, Iran*

Показано је да је Луисова киселина алуминијум-трифлат на унакрсно повезаном полистирену благ, ефикасан и хемоселективан катализатор за ациловање ароматичних једињења. Катализатор се лако припрема из јефтиних полазних једињења, стабилан је и може се више пута користити.

(Примљено 15. фебруара, ревидирано 1. септембра 2010)

REFERENCES

1. R. Jensen, G. Goldman, in *Friedel-Crafts and Related Reactions*, Vol. III, G. Olah, Ed., Wiley Interscience, New York, 1964, p. 1319
2. G. Franck, J. W. Stadelhofer, *Industrial Aromatic Chemistry*, Springer-Verlag, Berlin, 1988
3. S. Paul, P. Nanda, R. Gupta, A. Loupy, *Synthesis* (2003) 2877
4. M. Hosseini Sarvari, S. Sharghi, *J. Org. Chem.* **69** (2004) 6953
5. M. L. Kantam, K. V. S. Ranganath, M. Sateesh, K. B. S. Kumar, B. M. Choudary, *J. Mol. Catal. A* **225** (2005) 15
6. M. J. Earle, U. Hakala, C. Hardacre, J. Karkkainen, B. J. McAuley, D. W. Rooney, K. R. Seddon, J. M. Thompson, K. Wahala, *Chem. Commun.* (2005) 903
7. M. Gopalakrishnan, P. Sureshkumar, V. Kanagarajan, J. Thanusu, *Catal. Commun.* **6** (2005) 753
8. D. O. Jang, K. S. Moon, D. H. Cho, J. G. Kim, *Tetrahedron Lett.* **47** (2006) 6063
9. G. Sartori, R. Maggi, *Chem. Rev.* **106** (2006) 1077
10. C. Li, W. Liu, Z. Zhao, *Catal. Commun.* **8** (2007) 1834
11. F. Zayed, L. Greiner, P. S. Schulz, A. Lapkin, W. Leitner, *Chem. Commun.* (2008) 79
12. R. G. D. Noronha, A. C. Fernandes, C. C. Romao, *Tetrahedron Lett.* **50** (2009) 1407
13. B. Chiche, A. Finiels, C. Gauthier, P. Geneste, *J. Org. Chem.* **51** (1986) 2128
14. Q. L. Wang, Y. Ma, X. Ji, H. Yan, Q. Qiu, *J. Chem. Soc., Chem. Commun.* (1995) 2307
15. Y. Ma, Q. L. Wang, W. Jiang, B. Zuo, *Appl. Catal. A* **165** (1997) 199
16. J. Kaur, I. V. Kozhevnikov, *Chem. Commun.* (2002) 2508
17. D. M. Cui, M. Kawamura, S. Shimada, T. Hayashi, M. Tanaka, *Tetrahedron Lett.* **44** (2003) 4007
18. H. Firouzabadi, N. Iranpoor, F. Nowrouzi, *Tetrahedron* **60** (2004) 10843
19. D. M. Cui, C. Zhang, M. Kawamura, S. Shmada, *Tetrahedron Lett.* **45** (2004) 1741
20. M. Hosseini Sarvari, H. Sharghi, *Synthesis* (2004) 2165

21. M. Kawamura, D. M. Cui, S. Shimada, *Tetrahedron* **62** (2006) 9201
22. S. G. Wagholikar, P. S. Niphadkar, S. Mayadevi, S. Sivasanker, *Appl. Catal. A* **317** (2007) 250
23. M. M. Khodaei, A. Alizadeh, E. Nazari, *Tetrahedron Lett.* **48** (2007) 4199
24. K. I. Shimizu, K. Nimini, A. Satsuma, *Catal. Commun.* **9** (2008) 980
25. A. R. Hajipour, A. Zarei, L. Khazdooz, A. E. Ruoho, *Synth. Commun.* **39** (2009) 2702
26. G. A. Olah, O. Farooq, S. M. F. Farnia, J. A. Olah, *J. Am. Chem. Soc.* **110** (1988) 2560
27. D. B. G. Williams, M. C. Lawton, *Green Chem.* **10** (2008) 914
28. D. B. G. Williams, M. L. Shaw, M. J. Green, C. W. Holzapfel, *Angew. Chem. Int. Ed.* **47** (2008) 560
29. K. Parvanak Boroujeni, A. R. Massah, *React. Funct. Polym.* **66** (2006) 1126
30. S. Paul, P. Nanda, R. Gupta, A. Loupy, *Synthesis* (2003) 2877
31. J. R. Desmurs, M. Labrouillere, C. L. Roux, H. Gaspard, A. Laporterie, J. Dubac, *Tetrahedron Lett.* **38** (1997) 8871
32. S. Kobayashi, S. Iwamoto, *Tetrahedron Lett.* **39** (1998) 4697
33. X. Chen, M. Yu, M. Wang, *J. Chem. Res.* (2005) 80
34. C. J. Chapman, C. G. Frost, J. P. Hartley, A. J. Whittle, *Tetrahedron Lett.* **42** (2001) 773
35. A. Sasse**,** X. Ligneau, B. Sadek, S. Elz, H. H. Pertz, C. R. Ganellin, J. M. Arrang, J. C. Schwartz, W. Schunack, H. Stark, *Arch. Pharm. (Weinheim Ger.)* **334** (2001) 45
36. A. Kawada, S. Mitamura, S. Kobayashi, *Synlett* (1994) 545
37. N. Gatti, *Tetrahedron Lett.* **31** (1990) 3933
38. S. Pivsa-Art, K. Okura, M. Miura, S. Murata, M. Nomura, *J. Chem. Soc., Perkin Trans. 1* (1994) 1703
39. L. Strekowski, R. L. Wydra, M. T. Cegla, A. Czarny, S. Patterson, *J. Org. Chem.* **54** (1989) 6120
40. A. Kawada, S. Mitamura, S. Kobayashi, *J. Chem. Soc., Chem. Commun.* (1996) 183
41. K. Nomiya, Y. Sugaya, S. Sasa, M. Miwa, *Bull. Chem. Soc. Jpn.* **53** (1980) 2089
42. S. Cadamuro, I. Degani, S. Dughera, R. Fochi, A. Gatti, C. Prandi, *Gazz. Chim. Ital.* **120** (1990) 619
43. E. Akgün, U. Pindur, J. Müller, *J. Heterocycl. Chem.* **20** (1983) 1303
44. *Dictionary of Organic Compounds*; 6th ed., Vol. 9, Chapman and Hall, London, 1996, p. 566
45. Y. Miki, Y. Tsuzaki, C. Kai, H. Hachiken, *Heterocycles* **57** (2002) 1635
46. D. C. Neckers, *J. Macromol. Soc. Chem.* **24** (1987) 431.

Journal of the Serbian Chemical Society
JSCS-info@shd.org.rs • www.shd.org.rs/JSCS
J. Serb. Chem. Soc. *76* (2) 165–175 (2011)
JSCS–4109
UDC 542.913+547.367+547.79:615.281/.282
Original scientific paper

Synthesis of selected 5-thio-substituted tetrazole derivatives and evaluation of their antibacterial and antifungal activities

VARADARAJI DHAYANITHI[1], SUBAN SHAFI SYED[1], KUBARAN KUMARAN[1], KASI REGURAMAN JAI SANKAR[1], RAMASWAMY VENKAT RAGAVAN[2], PALUSA SANATH KUMAR GOUD[3], NALILU SUCHETHA KUMARI[4] and HARI NARAYAN PATI[5]*

[1]*P.G. and Research Department of Chemistry, Islamiah College, Vaniyambadi 632 752,* [2]*Chemistry Division, School of Science and Humanities, VIT University, Vellore 632 014* [3]*N. E. T. College of Pharmacy, Raichur 584 102,* [4]*Department of Biochemistry, K. S. Hegde Medical Academy, Mangalore 574 162 and* [5]*Department of Chemistry, Sambalpur University, Jyoti Vihar 768 019, India*

(Received 21 April 2009, revised 13 September 2010)

Abstract: Several 5-thio-substituted tetrazole derivatives were efficiently synthesized by a three-step process. The substituted tetrazol-5-thiol, namely, 1-benzyl-1*H*-tetrazole-5-thiol (**2**) was prepared by refluxing commercially available benzyl isothiocyanate (**1**) with sodium azide in water. The second step was the synthesis of 1-benzyl-5-[(3-bromopropyl)thio]-1*H*-tetrazole (**3**) by thioalkylation of tetrazole-5-thiol **2** with 1,3-dibromopropane in tetrahydrofuran. Finally, the 5-thio-substituted tetrazole derivatives **4a**–**i** were prepared by condensation of **3** with the corresponding amine or thiol. The structures of the newly synthesized compounds were characterized by NMR, LC/MS/MS, IR spectral data and elemental analysis. All the synthesized compounds were screened for their antibacterial and antifungal activities.

Keywords: substituted thiol; tetrazole; 1,3-dibromopropane; antibacterial; antifungal.

INTRODUCTION

Tetrazole and its derivatives have attracted interest because of their unique structure and their applications as antihypertensive, anti-allergic, antibiotic and anticonvulsant agents.[1–5] Number of publications and patents on the preparation, properties and applications of tetrazole derivatives is increasing every year with respect to other heterocyclic systems. Development of the tetrazole chemistry has been largely associated with the wide-scale application of these compounds in medicine, biochemistry, agriculture, *etc*.[1–9] The tetrazole functionality plays an

* Corresponding author. E-mail: hnpati@gmail.com
doi: 10.2298/JSC090421001D

important role in medicinal chemistry, primarily due to its ability to serve as the bioequivalent (bioisostere) of the carboxylic acid group,[10] and also the class of tetrazole compounds has been used both as anticancer and antimicrobial agents.[1–5] In particular, 1-substituted tetrazole and 5-thio-substituted tetrazoles have been used in the synthesis of pharmacologically active drugs.[11–19]

Tetrazoles are quite suitable ligands and can serve as replacement for carboxylic acids not only in medicinal chemistry, but also in supramolecular chemistry. Most importantly, tetrazoles are highly flexible ligands and can adapt easily to different binding modes.[20–23] As there is also a need for new and effective broad-spectrum antifungal and antibacterial agents, it was decided to exploit this interest by ascertaining the molecular features essential for activity and utilizing them to develop a new class of drugs. Prompted by the various biological activities of tetrazole and its 5-thio substituted derivatives, the synthesis of a novel series of 5-thio substituted tetrazole derivatives and a study of their biological activities was envisioned. Thus, the synthesis of the new 5-thio substituted tetrazole derivatives **3** and **4a**–**i** (Scheme 1 and Table I) and an evaluation of their antibacterial and antifungal properties were the objectives of this study.

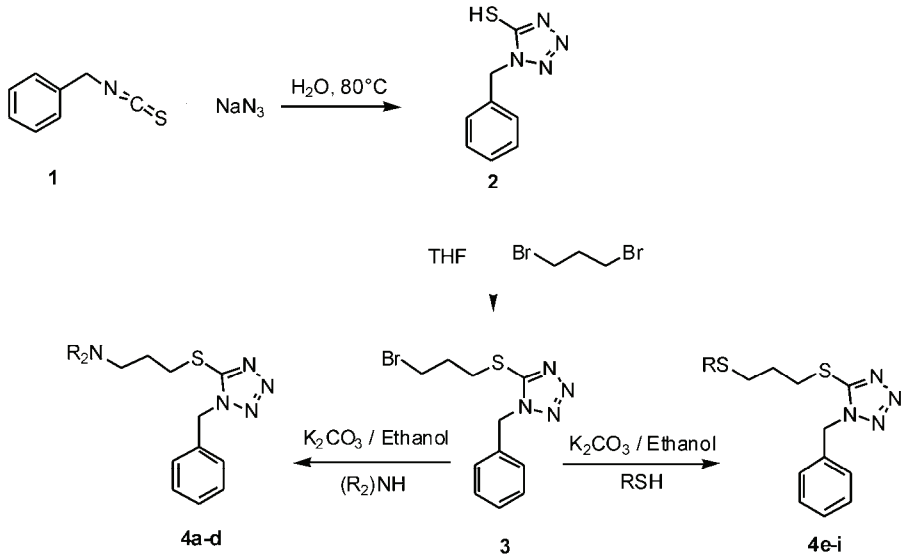

Scheme 1. Synthesis scheme for the compounds.

RESULTS AND DISCUSSION

Synthesis

In order to prepare a variety of derivatives of 1-benzyl-5-(propylthio)-1*H*--tetrazole, 1-benzyl-5-[(3-bromopropyl)thio]tetrazole (**3**) was prepared as a precursor. Preparation of 1-benzyl-5-[(3-bromopropyl)thio]tetrazole was accom-

plished as given in Scheme 1. As depicted in Scheme 1, reaction between commercially available benzyl isothiocyanate (**1**) and sodium azide in water provided 1-benzyl-1*H*-tetrazole-5-thiol[24] (**2**) in good yield. The isolated compound **2** was treated with 1,3-dibromopropane in tetrahydrofuran to give an intermediate, 1-benzyl-5-[(3-bromopropyl)thio]-1*H*-tetrazole (**3**). The synthon **3** is a new compound and reported here for the first time. Compound **3** was treated with corresponding amines or thiols to afford the 5-thio-substituted tetrazole derivatives **4a**–**i**.

TABLE I. Structure of the substituent (R) in the compounds **4a**–**i**

Compound	$(R_2)N$	Compound	R
3	Br	**4e**	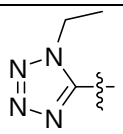
4a	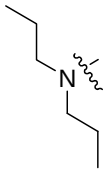	**4f**	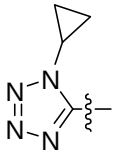
4b	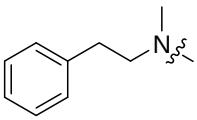	**4g**	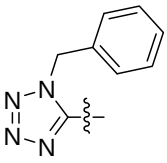
4c	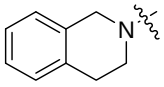	**4h**	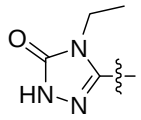
4d	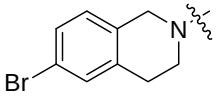	**4i**	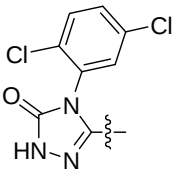

Characterization

The structures of the synthesized compounds were elucidated by ^{1}H-NMR, ^{13}C-NMR, LC–MS and IR spectroscopy, and elemental analysis, the results of which are given below.

*1-Benzyl-5-[(3-bromopropyl)thio]-1*H*-tetrazole (**3**).* Anal. Calcd. for $C_{11}H_{14}BrN_4S$: C, 42.14; H, 4.47; N, 17.88 %. Found: C, 42.08; H, 4.46; N,

17.85 %. IR (KBr, cm^{-1}): 2964 (C–H), 1496 (N=N), 1453 (C=C), 1389 (C=N). ^{1}H-NMR (400 MHz, $CDCl_3$, δ / ppm): 2.29–2.36 (2H, *qn*), 3.42–3.49 (4H, *m*), 5.42 (2H, *s*), 7.27–7.44 (5H, *m*). ^{13}C-NMR (100 MHz, $CDCl_3$, δ / ppm): 31.2, 31.5, 153.4, 51.0, 128.1, 129.0, 129.1, 132.7. MS Calcd. for $C_{11}H_{14}BrN_4S$: 313.22; Found: M^++1, 312.9, 314. 9. MS/MS (*m*/*z*): 262.2, 233.6, 178.2, 102.0, 90.7.

*3-(1-Benzyl-1*H*-tetrazol-5-ylthio)*-N,N-*dipropylpropan-1-amine* ***(4a)***. Yield: 62 %; Anal. Calcd. for $C_{17}H_{27}N_5S$: C, 61.17; H, 8.10; N, 20.99 %. Found: C, 61.08; H, 8.08; N, 21.03 %. IR (KBr, cm^{-1}): 2957 (C–H), 1497 (N=N), 1455 (C=C), 1388 (C=N). ^{1}H-NMR (400 MHz, $CDCl_3$, δ / ppm): 0.84–0.88 (6H, *t*), 1.36–1.46 (4H, *m*), 1.85–1.91 (2H, *qn*), 2.30–2.34 (4H, *t*), 2.46–2.50 (2H, *t*), 3.33––3.37 (2H, *t*), 5.41 (2H, *s*), 7.27–7.39 (5H, *m*). ^{13}C-NMR (100 MHz, $CDCl_3$, δ / / ppm): 11.9, 20.2, 26.9, 31.5, 56.0, 52.3, 128.0, 128.8, 129.0, 133.0, 154.3. MS calculated for $C_{17}H_{27}N_5S$: 333.49; Found: M^++1, 334.0. MS/MS (*m*/*z*): 233.4, 174.2, 132.3, 104.2, 90.1.

*3-(1-Benzyl-1*H*-tetrazol-5-ylthio)*-N-*methyl*-N-*phenethylpropan-1-amine* ***(4b)***. Yield: 78 %. Anal. Calcd. for $C_{20}H_{25}N_5S$: C, 65.30; H, 6.80; N, 19.05 %. Found: C, 65.37; H, 6.79; N, 19.09 %. IR (KBr, cm^{-1}): 2947 (C–H), 1496 (N=N), 1453 (C=C), 1389 (C=N). ^{1}H-NMR (400 MHz, $CDCl_3$, δ / ppm): 1.89––1.94 (2H, *qn*), 2.26 (3H, *s*), 2.45–2.49 (2H, *t*), 2.56–2.60 (2H, *t*), 2.71–2.76 (2H, *t*), 3.26–3.30 (2H, *t*), 5.39 (2H, *s*), 7.17–7.36 (10H, *m*). ^{13}C-NMR (100 MHz, $CDCl_3$, δ / ppm): 26.8, 31.2, 33.7, 41.9, 50.8, 55.5, 59.4, 125.9, 128.1, 128.3, 128.7, 128.9, 129.0, 132.9, 140.4, 154.2. MS calculated for $C_{20}H_{25}N_5S$: 367.51; Found: M^++1, 368.1. MS/MS (*m*/*z*): 368.1, 339.8, 233.2, 208.0, 176.1, 105.2, 90.9.

*2-[3-(1-Benzyl-1*H*-tetrazol-5-ylthio)propyl]-1,2,3,4-tetrahydroisoquinoline* ***(4c)***. Yield: 78 %; Anal. Calcd. for $C_{20}H_{23}N_5S$: C, 65.66; H, 6.29; N, 19.15 %. Found: C, 65.60; H, 6.30; N, 19.16 %. IR (KBr, cm^{-1}): 2922 (C–H), 1497 (N=N), 1453 (C=C), 1388 (C=N). ^{1}H-NMR (400 MHz, $CDCl_3$, δ / ppm): 2.0––2.08 (2H, *qn*), 2.57–2.60 (2H, *t*), 2.67–2.70 (2H, *t*), 2.86–2.88 (2H, *t*), 3.36–3.39 (2H, *t*), 3.59 (2H, *s*), 5.37 (2H, *s*), 6.99–7.33 (9H, m). ^{13}C-NMR (100 MHz, $CDCl_3$, δ / ppm): 26.7, 50.9, 31.5, 29.1, 50.8, 56.0, 56.3, 128.1, 129.0, 125.6, 126.1, 126.5, 128.6, 128.8, 133.0, 134.2, 134.6, 154.2. MS calculated for $C_{20}H_{23}N_5S$: 365.50; Found: M^++1, 366.1; M^++K adduct: 404.2. MS/MS (*m*/*z*): 338.0, 233.1, 206.1, 101.9, 91.0.

*2-[3-(1-Benzyl-1*H*-tetrazol-5-ylthio)propyl]-6-bromo-1,2,3,4-tetrahydroiso-quinoline* ***(4d)***. Yield: 72 %; Anal. Calcd. for $C_{20}H_{22}BrN_5S$: C, 54.01; H, 4.95; N, 15.75 %. Found: C, 54.10; H, 4.95; N, 15.72 %. IR (KBr, cm^{-1}) 2924 (C–H), 1482 (N=N), 1453 (C=C), 1388 (C=N). ^{1}H-NMR (400 MHz, $CDCl_3$, δ / ppm): 2.00–2.06 (2H, *qn*), 2.55–2.58 (2H, *t*), 2.65–2.68 (2H, *t*), 2.77–2.80 (2H, *t*), 3.35––3.38 (2H, *t*), 3.53 (2H, *s*), 5.37 (2H, *s*), 6.93–7.33 (8H, *m*). ^{13}C-NMR (100

MHz, $CDCl_3$, δ / ppm): 26.6, 50.1, 28.5, 45.9, 31.4, 55.4, 56.0, 119.0, 128.1, 129.0, 128.8, 129.1, 129.3, 132.9, 133.3, 136.9, 154.2. MS calculated for $C_{20}H_{22}BrN_5S$: 444.39; Found: M^++1, 444.1. MS/MS (*m*/*z*): 415.9, 284.0, 102.2, 91.0.

*1-Benzyl-5-[3-(1-ethyl-1*H*-tetrazol-5-ylthio)propylthio]-1*H*-tetrazole* (***4e***). Yield: 68 %; Anal. Calcd. for $C_{14}H_{18}N_8S_2$: C, 46.35; H, 4.97; N, 30.90 %. Found: C, 46.26; H, 4.96; N, 30.82 %. IR (KBr, cm^{-1}): 2983 (C–H), 1496 (N=N), 1433 (C=C), 1390 (C=N). ^{1}H-NMR (400 MHz, $CDCl_3$, δ / ppm): 1.48––1.52 (3H, *t*), 2.27–2.34 (2H, *qn*), 3.40–3.44 (4H, *q*), 4.24–4.29 (2H, *q*), 5.44 (2H, *s*), 7.26–7.38 (5H, *m*). ^{13}C-NMR (100 MHz, $CDCl_3$, δ / ppm): 14.2, 28.8, 31.3, 31.6, 42.6, 51.0, 128.0, 128.9, 129.0, 132.8, 152.8, 153.5. MS calculated for $C_{14}H_{18}N_8S_2$: 362.48; Found: M^++1, 363.1; M^++Na adduct: 385.2; M^++K adduct: 401.0. MS/MS (*m*/*z*): 335.0, 306.2, 265.0, 233.0, 105.9, 91.0.

*1-Benzyl-5-[3-(1-cyclopropyl-1*H*-tetrazol-5-ylthio)propylthio]-1*H*-tetrazole* (***4f***). Yield: 70 %; Anal. Calcd. for $C_{15}H_{18}N_8S_2$: C, 48.07; H, 4.81; N, 29.91 %. Found: C, 48.13; H, 4.80; N, 29.89 %. IR (KBr, cm^{-1}): 2938 (C–H), 1496 (N=N), 1454 (C=C), 1392 (C=N). ^{1}H-NMR (400 MHz, $CDCl_3$, δ / ppm): 1.22––1.29 (4H, *m*), 2.29–2.36 (2H, *qn*), 3.35–3.37 (1H, *m*), 3.41–3.45 (4H, *q*), 5.44 (2H, *s*), 7.26–7.39 (5H, *m*). ^{13}C-NMR (100 MHz, $CDCl_3$, δ / ppm): 6.8, 28.8, 27.8, 30.8, 31.7, 51.0, 128.1, 128.9, 129.0, 132.8, 153.5, 155.5. MS calculated for $C_{15}H_{18}N_8S_2$: 374.49; Found: M^++1, 375.3; M^++Na adduct: 397.0; M^++K adduct: 413.1. MS/MS (*m*/*z*): 265.4, 233.4, 183.3, 102.0, 91.2.

*5,5'-[1,3-Propanediylbis(thio)]bis(1-benzyl-1*H*-tetrazole)* (***4g***). Yield: 41 %; Anal. Calcd. for $C_{19}H_{20}N_8S_2$: C, 53.70; H, 4.71; N, 26.38 %. Found: C, 53.78; H, 4.72; N, 26.43 %. IR (KBr, cm^{-1}): 2942 (C–H), 1496 (N=N), 1453 (C=C), 1389 (C=N). ^{1}H-NMR (400 MHz, $CDCl_3$, δ / ppm): 2.21–2.28 (2H, *qn*), 3.33––3.37 (4H, *t*), 5.41 (4H, *s*), 7.25–7.37 (10H, *m*). ^{13}C-NMR (100 MHz, $CDCl_3$, δ / ppm): 28.7, 31.5, 50.8, 128.0, 128.8, 128.9, 133.0, 153.5. MS calculated for $C_{19}H_{20}N_8S_2$: 424.55; Found: M^++1, 425.4; M^++Na adduct: 447.1. MS/MS (*m*/*z*): 282.9, 265.2, 233.0, 130.9, 102.0, 90.9.

*5-[3-(1-Benzyl-1*H*-tetrazol-5-ylthio)propylthio]-4-ethyl-2,4-dihydro-3*H*-1,2,4-triazol-3-one* (***4h***). Yield: 48 %; Anal. Calcd. for $C_{15}H_{19}N_7OS_2$: C, 47.68; H, 5.03; N, 25.96 %. Found: C, 47.78; H, 5.02; N, 25.99 %. IR (KBr, cm^{-1}): 1751 (C=O), 2936 (C–H), 3100 (N–H), 1523 (N=N), 1451 (C=C), 1389 (C=N). ^{1}H-NMR (400 MHz, $CDCl_3$, δ / ppm): 1.27–1.30 (3H, *t*), 2.21–2.28 (2H, *qn*), 3.15–3.19 (2H, *t*), 3.42–3.45 (2H, *t*), 3.66–3.72 (2H, *q*), 5.45 (2H, *s*), 7.29–7.37 (5H, *m*), 11.34 (1H, *bs*). ^{13}C-NMR (100 MHz, $CDCl_3$, δ / ppm): 14.2, 28.7, 29.8, 31.7, 36.6, 51.0, 128.0, 128.9, 129.0, 132.8, 143.4, 153.5, 155.9. MS calculated for $C_{15}H_{19}N_7OS_2$: 377.49; Found: M^++1, 378.4. MS/MS (*m*/*z*): 308.0, 233.3, 218.1, 186.0, 101.9, 91.0.

*5-[3-(1-Benzyl-1*H*-tetrazol-5-ylthio)propylthio]-4-(2,5-dichlorophenyl)-2,4--dihydro-3*H*-1,2,4-triazol-3-one (**4i**)*. Yield: 39 %. Anal. Calcd. for $C_{19}H_{17}Cl_2N_7OS_2$: C, 46.11; H, 3.44; N, 19.82 %. Found: C, 46.16; H, 3.43; N, 19.76 %. IR (KBr, cm^{-1}): 1718 (C=O), 2900 (C–H), 1519 (N=N), 1478 (C=C), 1425 (C=N). ^{1}H-NMR (400 MHz, $CDCl_3$, δ / ppm): 2.15–2.20 (2H, *qn*), 3.05–3.08 (2H, *t*), 3.33––3.38 (2H, *t*), 5.40 (2H, *s*), 7.24–7.51 (7H, *m*), 10.94 (1H, *s*). ^{13}C-NMR (100 MHz, $CDCl_3$, δ / ppm): 28.5, 29.8, 31.6, 51.0, 128.1, 128.9, 129.0, 130.4, 130.7, 131.5, 131.6, 131.8, 132.8, 133.5, 143.7, 153.5, 154.6. MS calculated for $C_{19}H_{17}Cl_2N_7OS_2$: 494.42; Found: M^++1, 493.8. MS/MS (*m*/*z*): 334.1, 309.1, 302.0, 288.0, 265.6, 233.4, 165.3, 102.2, 91.2.

In the IR spectra, the bands due to –N=N– and C=N group, present in all compounds, were observed at about 1500 and 1388 cm^{-1}, respectively. The bands at about 1244 and 985 cm^{-1} are characteristic for the tetrazole ring system.[25] In the ^{1}H-NMR spectra, the 1-substituted benzylic protons appeared as singlet at about δ 5.4 ppm in all the derivatives. The other methylene protons appeared as quintets and triplets at about δ 2.2 to 2.3 ppm and 3.3 to 3.5 ppm, respectively. The aromatic protons were observed at about δ 6.9 to 7.4 ppm. In the ^{13}C-NMR spectra of all the synthesized compounds, tetrazole carbon and aromatic carbon peaks were observed at δ 153.5 and 128.0 to 129.5 ppm, respectively. In the mass spectra, an appropriate molecular ion peak (M^++1) was obtained for all the derivatives from ESI–MS.

Antibacterial activity

The results of the antibacterial studies against *Staphylococcus aureus*, *Escherichia coli*, *Pseudomonas aeruginosa* and *Klebsiella pneumoniae* bacterial strains are given in Table II and compared with the standard ampicillin drug. Interestingly, out of eleven compounds, nine compounds were found to have

TABLE II. Antibacterial activities of the compounds **2**, **3** and **4a–i** (zone of inhibition in mm; minimum inhibitory concentration (*MIC*), in mg mL^{-1}, is given in parenthesis)

Compound	*S. aureus*	*E. coli*	*P. aeruginosa*	*K. pneumoniae*
2	15 (6.25)	<10 (50)	<10 (50)	<10 (50)
3	20 (6.25)	18 (6.25)	19 (6.25)	19 (6.25)
4a	17 (6.25)	18 (6.25)	<10 (50)	<10 (50)
4b	18 (6.25)	17 (6.25)	<10 (50)	<10 (50)
4c	17 (6.25)	18 (6.25)	<10 (50)	<10 (50)
4d	19 (6.25)	19 (6.25)	<10 (50)	<10 (50)
4e	20 (6.25)	19 (6.25)	<10 (50)	<10 (50)
4f	17 (6.25)	17 (6.25)	<10 (50)	<10 (50)
4g	20 (6.25)	19 (6.25)	19 (6.25)	20 (6.25)
4h	<10 (50)	<10 (50)	<10 (50)	<10 (50)
4i	19 (6.25)	17 (6.25)	<10 (50)	<10 (50)
Ampicillin	22 (6.25)	23 (6.25)	20 (6.25)	22 (6.25)

good antibacterial activity. Among these compounds **3** and **4g** were most active against the four bacterial organisms. Compounds **4a**–**f** and **4i** showed good growth inhibition towards *S. aureus* and *E. coli*, and pronounced growth inhibition for *P. aeruginosa* and *K. pneumoniae*. The remaining compounds, **2** and **4h**, were found to be less active against the four bacterial organisms.

Antifungal activity

The results of the antifungal studies against *Aspergillus flavus*, *Aspergillus fumigatus*, *Penicillium marneffei* and *Trichophyton mentagrophytes* are given in Table III and compared with the standard itraconazole drug. It was observed that most of the compounds exhibited good antifungal activity. Compounds **2** and **4h** were less active against all the tested organisms. Compounds **4a**–**f** and **4i** showed good antifungal activity against *P. marneffei* and *T. mentagrophytes*, and pronounced antifungal activity towards the other two fungal organisms. On the other hand, compounds **3** and **4g** showed the highest antifungal activity against all four fungal strains, namely *A. flavus*, *A. fumigatus*, *P. marneffei* and *T. menta-grophytes*.

TABLE III. Antifungal activities of the compounds **2**, **3** and **4a–i** (zone of inhibition in mm, *MIC*, in mg mL^{-1}, is given in parenthesis)

Compound	*T. mentagrophytes*	*P. marneffei*	*A. flavus*	*A. fumigatus*
2	13 (6.25)	<10 (50)	<10 (50)	<10 (50)
3	19 (6.25)	17 (6.25)	20 (6.25)	19 (6.25)
4a	19 (6.25)	18 (6.25)	<10 (50)	<10 (50)
4b	18 (6.25)	19 (6.25)	<10 (50)	<10 (50)
4c	18 (6.25)	17 (6.25)	<10 (50)	<10 (50)
4d	19 (6.25)	18 (6.25)	<10 (50)	<10 (50)
4e	19(6.25)	18 (6.25)	<10 (50)	<10 (50)
4f	18 (6.25)	19 (6.25)	<10 (50)	<10 (50)
4g	20 (6.25)	18 (6.25)	19 (6.25)	20 (6.25)
4h	<10 (50)	<10 (50)	<10 (50)	<10 (50)
4i	19 (6.25)	17 (6.25)	<10 (50)	<10 (50)
Itraconazole	21(6.25)	20 (6.25)	21 (6.25)	19 (6.25)

EXPERIMENTAL

The ^{1}H-NMR, ^{13}C-NMR and DEPT experiments were performed on an Oxford AS 400 NMR instrument (Varian, City, USA) with a dual broad band. The ^{1}H-NMR chemical shift values are reported on the δ scale in ppm relative to TMS (δ = 0 ppm) and the ^{13}C-NMR chemical shifts values are reported relative to $CDCl_3$ (δ = 72.5 ppm). The IR spectra were recorded on a Perkin Elmer spectrum 100 FT-IR model. Column chromatography was performed with silica gel 60–120 mesh (Merck, Mumbai, India.). All the compounds were routinely checked for completion of the reaction on silica gel 60 F254 TLC plates and their spots were visualized by exposure to a UV lamp, iodine vapor or $KMnO_4$ reagents. The liquid chromatography part of the LC–MS system consisted of an Agilent-1100 series quaternary gradient pump with a degasser, an auto sampler and a column oven. The MS/MS part of the sys-

tem contained an API-2000 system (Sciex, Applied Bio-Systems, Canada). The yields are reported as isolated yield after purification of the compounds.

*Procedure for the preparation of 1-benzyl-5-[(3-bromopropyl)thio]-1*H*-tetrazole (**3**)*

To a solution of 1,3-dibromopropane (10 g, 50 mmol) in tetrahydrofuran (200 mL), 1--benzyl-1*H*-tetrazole-5-thiol (**2**) (1.92 g, 10 mM) was added portionwise at 25–30 °C and then stirred for 3 h at the same temperature. The reaction was monitored by TLC. After completion of reaction, the reaction mixture was concentrated to dryness and the crude product was purified by column chromatography (eluent 35 % ethyl acetate–hexane). Product **3** was obtained as light brown colored gummy mass (52 % yield).

*General procedure for the preparation of derivatives **4a–i***

To a mixture of 1-benzyl-5-[(3-bromopropyl)thio]-1*H*-tetrazole (**3**) (10 mmol) and anhydrous powdered K_2CO_3 (20 mmol) in ethanol (10 mL), the corresponding amine or thiol (1.2 equivalent) was added at 25 °C and stirred at this temperature for 2–3 h. The reaction was monitored by TLC. After completion of the reaction; the reaction mixture was concentrated to dryness. The residue was dissolved in dichloromethane (20 mL) and washed with water. The organic layer was concentrated under reduced pressure to give the crude product. The final product was isolated by column purification. The column was started at 10 % ethyl acetate with petroleum ether and slowly increased to 60 % ethyl acetate. Finally, the compound was isolated at 25 to 30 % ethyl acetate in petroleum ether.

Antibacterial activity

The tetrazole derivatives (**2**, **3** and **4a–i**) were investigated for their inhibition of growth against *Staphylococcus aureus* (ATCC-25923), *Escherichia coli* (ATCC-25922), *Pseudomonas aeruginosa* (ATCC-27853) and *Klebsiella pneumoniae* (recultured) bacterial strains by the disc diffusion method.[26-31] Batches of 100 discs (Whatman filter paper No. 1, 6 mm diameter) were each dispensed to a screw capped bottle and sterilized by dry heat at 140 °C for 1 h. Solutions of the test compounds were prepared at different concentrations in dimethylformamide (DMF). 1mL containing 100 times the amount of prepared solution in each disc was added to each bottle, which contained 100 discs. The disc of each concentration was placed in triplicate in a nutrient agar medium separately seeded with fresh bacteria. The incubation was realized at 37 °C for 24 h. Solvent and growth controls were kept separate; the zones of inhibition and minimum inhibitory concentration (*MIC*) were measured.

Antifungal activity

The newly synthesized compounds were also investigated for their antifungal activity against four fungal strains, namely, *Aspergillus flavus* (NCIM No.524), *Aspergillus fumigatus* (NCIM No.902), *Penicillium marneffei* (recultured) and *Trichophyton mentagrophytes* (recultured). Sabouraud agar media was prepared by dissolving peptone (1 g), D-glucose (4 g) and agar (2 g) in sterile water (100 mL) and the pH was adjusted to 5.7. Normal saline was used to make a suspension of the spores of the fungal strain for seeding. A loopful of particular fungal strain was transferred to 3 mL of saline to obtain a suspension of the corresponding species. Agar media (20 mL) was poured into each petri dish. Excess of the suspension was decanted and the plates were dried by placing them in an incubator at 37 °C for 1 h. Using an agar punch, wells (8 mm diameter) were made on these seeded agar plates and from 6.25 to 50 μg mL^{-1} of the test compounds in DMSO was added into each well labeled disc. Controls were run using DMSO at the same concentration as used with the test compounds. The petri dishes were pre-

pared in triplicate and maintained at 37 °C for 3 to 4 days. The antifungal activity was determined by measuring the diameter of the inhibition zone.[32,33]

CONCLUSIONS

In conclusion, a series of new 5-thio-substituted tetrazole derivatives were successfully synthesized. The antimicrobial screening suggests that all the synthesized compounds showed moderate to good activity against the tested organisms. Among the newly synthesized compounds, **4g** and **3** showed the most promising antibacterial and antifungal activities. Hence, the fact that the compounds prepared in this study are chemically unrelated to the current medication, suggests that further work with similar types of analogues is clearly warranted.

Acknowledgements. The authors thank the Department of Chemistry, Islamiah College and Sambalpur University for support of their research.

ИЗВОД

СИНТЕЗА ОДАБРАНИХ 5-ТИО СУПСТИТУИСАНИХ ДЕРИВАТА ТЕТРАЗОЛА И ОДРЕЂИВАЊЕ ЊИХОВЕ АНТИБАКТЕРИЈСКЕ И АНТИФУНГАЛНЕ АКТИВНОСТИ

VARADARAJI DHAYANITHI[1], SUBAN SHAFI SYED[1], KUBARAN KUMARAN[1], KASI REGURAMAN JAI SANKAR[1], RAMASWAMY VENKAT RAGAVAN[2], PALUSA SANATH KUMAR GOUD[3], NALILU SUCHETHA KUMARI[4] и HARI NARAYAN PATI[5]

[1]P.G. and Research Department of Chemistry, Islamiah College, Vaniyambadi 632 752, India, [2]Chemistry Division, School of Science and Humanities, VIT University, Vellore 632 014, [3]N. E. T. College of Pharmacy, Raichur 584 102, [4]Department of Biochemistry, K. S. Hegde Medical Academy, Mangalore 574 162 и [5]Department of Chemistry, Sambalpur University, Jyoti Vihar 768 019, India

Извршена је синтеза нових деривата 5-тио-тетразола. Супституисани тетразол-5-тиол, 1-бензил-1*H*-тетразол-5-тиол (**2**) добијен је загревањем на температури кључања комерцијално доступног бензил-изотиоцијаната (**1**) са натријум-азидом у води. У другом реакционом кораку добијен је 1-бензил-5-[(3-бромпропил)тио]-1*H*-тетразол (**3**) тиоалкиловањем тетразол-5-тиола (**2**) са 1,3-дибромпропаном у тетрахидрофурану. Коначно, деривати 5-тио-тетразола **4a**–**i** добијени су кондензациојом (**3**) са одговарајућим аминима или тиолима. Структуре добијених једињења одређене су NMR, LC/MS/MS и IC спектроскопијом и микроанализом. Свим синтетисаним једињењима испитана је антибактеријска и антифунгална активност.

(Примљено 21. априла 2009, ревидирано 13. септембра 2010)

REFERENCES

1. S. Bergmans, J. Hunt, A. Roach, P. Goldsmith, *Epilepsy Res*. **75** (2007) 18
2. L. V. Myznikov, A. Hrabalek, G. I. Koldobskii, *Chem. Heterocycl. Compd.* **43** (2007) 1
3. H. D. Klaubert, J. H. Sellstedt, C. J. Guinosso, S. C. Bell, R.J. Capetola, *J. Med. Chem*. **24** (1981) 748
4. J. H. Toney, P. M. D. Fitzgerald, N. Grover Sharma, S. H. Olson, W. J. May, J. G. Sundelof, D. E. Venderwall, K. A. Cleary, S. K. Grant, J. K. Wu, J. W. Kozarich, D. L. Pompliano, G. G. Hammond, *Chem. Biol*. **5** (1998) 185
5. R. N. Butter, in *Comprehensive Heterocyclic Chemistry*, A. R. Katritzky, C. W. Rees, Eds., Vol. **5**, Part 4A, Pergamon Press, New York, 1984, p. 791

6. M. J. Schocken, R. W. Creekmore, G. Theodoridis, G. J. Nystrom, R. A. Robinson, *Appl. Environ. Micobiol*. **55** (1989) 1220
7. S. J. Lim, Y. Sunohara, H. Matsumoto, *J. Pestic. Sci*. **32** (2007) 249
8. Y. Tamura, F. Watanabe, T. Nakatani, K. Yasui, M. Fuji, T. Komurasaki, H. Tsuzuki, R. Maekawa, T. Yoshioka, K. Kawada, K. Sugita, M. Ohtani, *J. Med. Chem.* **41** (1998) 640
9. C. Kikuchi, H. Nagaso, T. Hiranuma, M. Koyama, *J. Med. Chem*. **42** (1999) 533
10. A. Burger, *Prog. Drug Res*. **37** (1991) 287
11. J. Buynak, V. Doppalapudi, A. S. Rao, D. N. Srishkumar, G. Adam, *Bioorg. Med. Chem. Lett.* **10** (2000) 847
12. L. D. George, J. R. E. Hoover, United States patent, 3867380 (1975)
13. L. D George, J. R. E. Hoover, United States patent, 3968226 (1976)
14. D. Walker, H. H. Silvestri, D.A. Johnson, United States patent, 4223135 (1980)
15. M. J. Genin, D. A. Allwine, D. J. Anderson, M. R. Barbachyn, D. E. Emmert, S. Garmon, D. R. Graber, K. C. Grega, J. S. Hester, D. K. Hutchinson., J. Morris, R. J. Reischer, C. W. Ford, G. E. Zurenko, C. J. Hamel, R. D. Schaadt, D. Stapert, H. Yagi, *J. Med. Chem*. **43** (2000) 953
16. E. Muraglia, O. D. Kinzel, R. Laufer, M. D. Miller, G. Moyer, V. Munshi, F. Orvieto, M. C. Palumbi, G. Pescatore, M. Rowley, P. D. Williams, V. Summa, *Bioorg. Med. Chem. Lett*. **16** (2006) 2748
17. J. A. O'Meara, A. Jakalian, S. La Plante, P. R. Bonneau, R. Coulombe, A. M. Faucher, I. Guse, S. Landry, J. Racine, B. Simoneau, B. Thavonrkham, C. Yoakim, *Bioorg. Med. Chem. Lett*. **17** (2007) 3362
18. T. L. Shih, M. R. Candelore, M. A. Cascieri, S. H. L. Chiu, L. F. Colwell Jr., L. Deng, W. P. Feeney, M. J. Forrest, G. J. Hom, D. E. Macintyre, R. R. Miller, R. A. Stearns, C. D. Strader, L. Tota, M. J. Wyvratt, M. H. Fisher, A. E. Weber, *Bioorg. Med. Chem. Lett*. **9** (1999) 1251
19. K. J. Shin, K. D. Koo, K. H. Yoo, D. C. Kim, D. J. Kim, S. W. Park, *Bioorg. Med. Chem. Lett*. **10** (2000) 1421
20. R. R. Wexler, W. J. Greenlee, J. D. Irvin, M. R. Goldberg, K. Prendergast, R. D. Smith, P. B. W. M. J. Timmermans, *J. Med. Chem.* **39** (1996) 625
21. K. Noda, Y. Saad, A. Kinoshita, T. P. Boyle, R. M. Graham, A. Husain, S. S. Karnik**,** *J. Biol. Chem*. **270** (1995) 2284
22. Y. Goldgur, R. Craigie, G. H. Cohen, T. Fujiwara, T. Yoshinaga, T. Fujishita, H. Sugimoto, T. Endo, H. Murai, D. R. Davies, *Proc. Nat. Acad. Sci.* **96** (1999) 13040
23. A. Kraft, F. Osterod, R. Frohlich, *J. Org. Chem.* **64** (1999) 6425
24. H. W. Altland, *J. Org. Chem*. **21** (1976) 3395
25. R. M. Silverstein, G. C. Bassler, T. C. Morrill, *Spectrometric Identification of Organic Compounds*, Wiley, New York, 1981, p. 95
26. R. Cruickshank, J. P. Duguid, B. P. Marmion, R. H. A. Swain, *Medicinal Microbiology* 12th ed., Vol. 2, Churchill Livingstone, London, 1975, p. 196
27. R. Skov, R. Smyth, A. R. Larsen, N. M. Frimodt, G. Kahlmeter, *J. Antimicrob. Chemother*. **55** (2005) 157
28. B. A. Arthington, M. Motley, D. W. Warnock, C. J. Morrison, *J. Clin. Microbiol.* **38** (2000) 2254
29. R. Villanueva, G. Bou, *J. Antimicrob. Chemother*. **55** (2005) 379
30. D. F. J. Brown, D. I. Edwards, P. M. Hawkey, D. Morrison, G. L. Ridgway, K. J. Towner, W. D. Wren, *J. Antimicrob. Chemother.* **56** (2005) 1000

31. N. M. Broekema, T. T. Van, T. A. Monson, S. A. Marshall, D. M. Warshauer, *J. Clin. Microbiol*. **47** (2009) 217
32. M. Ashok, B. S. Holla, N. Suchetha, *Eur. J. Med. Chem*. **42** (2007) 380
33. B. S. Holla, M. Mahalinga, M. S. Karthikeyan, P. M. Akberali, N. Suchetha, *Bioorg. Med. Chem.* **14** (2006) 2040.

Journal of the Serbian Chemical Society
JSCS-info@shd.org.rs • www.shd.org.rs/JSCS
J. Serb. Chem. Soc. *76* (2) 177–188 (2011)
JSCS–4110
UDC 547.856+542.913:667.281.1
Original scientific paper

Novel 2-phenyl-3-{4'-[*N*-(4"-aminophenyl)carbamoyl]-phenyl}--quinazoline-4(3*H*)one-6-sulphonic acid based mono azo reactive dyes

DIVYESH R. PATEL and KESHAV C. PATEL*

Department of Chemistry, Veer Narmad South Gujarat University, Surat 395 007, Gujarat, India

(Received 25 February 2009, revised 23 September 2010)

Abstract: A series of new heterocyclic mono azo reactive dyes **7a**–**m** were prepared by diazotization of 2-phenyl-3-{4'-[*N*-(4"-aminophenyl)carbamoyl]-phenyl}-quinazoline-4(3*H*)-one-6-sulphonic acid (**3**) and coupling with various cyanurated coupling components **6a**–**m** and their dyeing performance on silk, wool and cotton fibres was assessed. These dyes were found to give a variety of colour shades with very good depth and levelness on the fibres. All the compounds were identified by conventional method (IR and ^{1}H-NMR) and elemental analyses. The percentage dye bath exhaustion on different fibres was reasonably good and acceptable. The dyed fibre showed moderate to very good fastness to light, washing and rubbing.

Keyword: quinazoline-4(3*H*)-one; mono azo reactive dyes; dyeing; fastness properties.

INTRODUCTION

In recent years, the development of new structures of reactive dyes has been a subject of interest and many novel structures useful in commercial application to silk, wool and cotton, as well as their blends with other fibres, have been discovered. The utility of quinazoline derivatives for the production of some commercial dyes and pigment, both for natural and man-made fibre, is known.[1,2] Intensive efforts have been made in the investigation of mono azo dyes containing a heterocyclic moiety, such as amino quinazoline,[3] as the diazo component owing to the marked bathochromic effect of such groups compared to the corresponding benzoid compound.[4]

In view of encouraging reports about the technical applications of the dyes based on the 4-oxoquinazoline system,[5,6] it was considered of interest to under-

* Corresponding author. E-mail: divyeshpatel_905@yahoo.com
doi: 10.2298/JSC090225021P

take the synthesis and study of the dyeing properties of azo dyes based on 2-styryl-3-(2'-chlorophenyl)-6-amino-4-oxoquinazoline.

In the present investigation, the synthetic pathway to 2-phenyl-3-{4'-[*N*-(4"--aminophenyl)carbamoyl]-phenyl}-quinazoline-4(3*H*)-one-6-sulphonic acid (**3**) from a readily available starting material, *i.e.*, 5-sulpho anthranilic acid, was examined. The effect of the presence of the $–SO_3Na$ and –CONH–groups in the quinazoline-based structure of the reactive dyes was studied in relation to the colour and dyeing properties of the heterocyclic reactive dyes **7a**–**m**.

The general structure of the reactive dyes **7a**–**m** is:

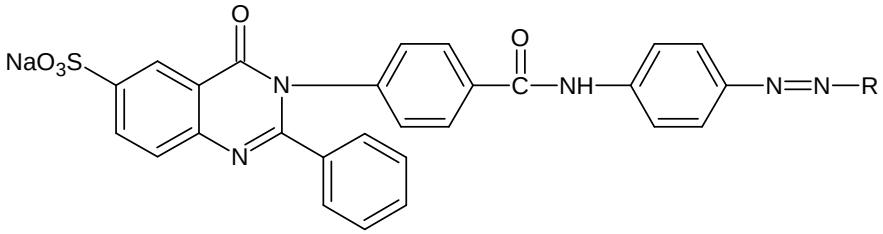

where R = various 4-nitroanilino cyanurated coupling components (**6a**–**m**).

RESULTS AND DISCUSSION

Chemistry

The new series of reactive dyes **7a**–**m** containing the quinazolinone and benzanilide moieties were synthesized by condensation of benzoxazine derivative **1** and the diaminobenzanilide moiety **3**. This condensed product on diazotization and coupling with various 4-nitroanililno cyanurated coupling components **6a**–**m** produced a novel series of heterocyclic reactive dyes. These series of dyes have found wide application in the dyeing of wool, silk and cotton fibres. The presence of quinazolinone structure in the dye molecule results in excellent dyeing properties, including low sublimation and high thermal stability.

Characterization of the isolated intermediates and dyes

*2-Phenyl-4-oxo-3,1-benzoxazine-6-suphonic acid (**1**)*. Yield 85 %; m.p. 107 °C; Anal. Calcd. for $C_{14}H_9O_5NS$: C, 55.44; H, 2.99; N, 4.62 %. Found: C, 55.40; H, 2.95; N, 4.60 %. IR (KBr, cm^{-1}) 1750 (C=O stretching of benzoxazine), 1380 (C–N stretching of benzoxazine), 1042 (S=O stretching of sulphonic acid group). ^{1}H NMR (300 MHz, DMSO-d_6, δ / ppm): 11.2 (1H, *s*, SO_3H), 6.72–8.05 (8H, *m*, Ar–H).

*4,4'-Diaminobenzanilide (**2**)*. Yield 75 %; m.p. 205 °C; Anal. Calcd. for $C_{13}H_{13}ON_3$: C, 68.70; H, 5.77; N, 18.49 %. Found: C, 68.65; H, 5.72; N, 18.44 %. IR (KBr, cm^{-1}) 1695 (C=O stretching of amide group), 3325, 2985 (N–H stretching (asym. and sym.) of amide group). ^{1}H-NMR (300 MHz, DMSO-d_6, δ / ppm): 8.62 (1H, *s*, –CONH), 5.74 (4H, *s*, 2 $–NH_2$), 6.72–8.25 (8H, *m*, Ar–H).

*2-Phenyl-3{4'-[N-(4"-aminophenyl)carbamoyl]-phenyl}-quinazoline-4-(3*H*)--one-6-sulphonic acid (**3**)*. Yield 75 %, m. p. 193 °C. Anal. Calcd. for $C_{27}H_{20}O_5N_4S_1$: C, 63.27; H, 3.93; N, 10.93 %. Found: C, 63.92; H, 3.88; N, 10.90 %. IR (KBr, cm^{-1}): 3515 (N–H stretching of primary $–NH_2$ group), 1675 (C=O stretching of quinazolinone), 1395 (C–N stretching of quinazoline structure), 1040 (S=O stretching of $–SO_3H$ group), 3415, 2995 (asym. and sym. N–H stretching of amide). ^{1}H-NMR (300 MHz, DMSO-d_6, δ / ppm) 5.78 (2H, *s*, $–NH_2$), 8.64 (1H, *s*, –CONH), 11.6 (1H, *s*, $–SO_3H$), 6.78–8.15 (16H, *m*, Ar–H).

*Sodium 5-(4-chloro-6-(4-nitrophenylamino)-1,3,5-triazin-2-ylamino)-4-hydroxy-3-((4-(imino(4-(4-oxo-2-phenyl-6-sulfonatoquinazolin-3(4*H*)-yl)phenyl)methoxy)phenyl)diazenyl)naphthalene-2,7-disulfonate (**7a**)*. Yield: 85 %; Anal. Calcd. for $C_{46}H_{27}O_{14}N_{11}ClS_3Na_3$: C, 47.69; H, 2.35; N, 13.30. Found: C, 47.63; H, 2.31; N, 13.28 %. IR (KBr, cm^{-1}): 3360–3680 (O–H and N–H stretching of –OH and $–NH_2$ groups), 1660 (C=O stretching of quinazoline ring), 1430 (N=N stretching of azo group), 1382 (C–N), 1360, 1112, 1049 (S=O stretching of sulphonates), 1501, 1308 (N=O asym. and sym. stretching of nitro group), 762 (C–Cl stretching of chloro group). ^{1}H-NMR (300 MHz, DMSO-d_6, δ / ppm): 4.32 (1H, *s*, –OH), 4.16 (2H, *s*, 2 –NH), 8.65 (1H, *s*, –CONH), 6.82–7.95 (23H, *m*, Ar–H).

*Sodium 3-(4-((4-((7-(4-chloro-6-(4-nitrophenylamino)-1,3,5-triazin-2-ylamino)-1-hydroxy-3-sulfonatonaphthalen-2-yl)diazenyl)phenoxy)(imino)methyl)phenyl)-4-oxo-2-phenyl-3,4-dihydroquinazoline-6-sulfonate (**7b**)*. Yield: 83 %; Anal. Calcd. for $C_{46}H_{28}O_{11}N_{11}ClS_2Na_2$: C, 52.30; H, 2.67; N, 14.58 %. Found: C, 52.26; H, 2.63; N, 14.55 %, IR (KBr, cm^{-1}): 3360–3680 (O–H and N–H stretching of –OH and $–NH_2$ groups), 1662 (C=O stretching of quinazoline ring), 1425 (N=N stretching of azo group), 1380 (C–N), 1360, 1115, 1055 (S=O stretching of sulphonates), 1510, 1310 (N=O asym. and sym. stretching of nitro group), 765 (C–Cl stretching of chloro group). ^{1}H-NMR (300 MHz, DMSO-d_6, δ / ppm): 4.35 (1H, *s*, –OH), 4.12 (2H, *s*, 2 –NH), 8.62 (1H, *s*, –CONH), 6.81–7.90 (24H, *m*, Ar–H).

*Sodium 3-(4-((4-((6-(4-chloro-6-(4-nitrophenylamino)-1,3,5-triazin-2-ylamino)-1-hydroxy-3-sulfonatonaphthalen-2-yl)diazenyl)phenoxy)(imino)methyl)phenyl)-4-oxo-2-phenyl-3,4-dihydroquinazoline-6-sulfonate (**7c**)*. Yield: 78 %; Anal. Calcd. For $C_{46}H_{28}O_{11}N_{11}ClS_2Na_2$: C, 52.30; H, 2.67; N, 14.58 %. Found: C, 52.25; H, 2.62; N, 14.56 5. IR (KBr, cm^{-1}): 3350–3700 (O–H and N–H stretching of –OH and $–NH_2$ groups), 1656 (C=O stretching of quinazoline ring), 1420 (N=N stretching of azo group), 1385 (C–N), 1340, 1110, 1045 (S=O stretching of sulphonates), 1505, 1315 (N=O asym. and sym. stretching of nitro group), 760 (C–Cl stretching of chloro group). ^{1}H-NMR (300 MHz, DMSO-d_6, δ / ppm): 4.38 (1H, *s*, –OH), 4.18 (2H, *s*, 2 –NH), 8.66 (1H, *s*, –CONH), 6.85–7.92 (24H, *m*, Ar–H).

Sodium 3-(4-((4-((6-((4-chloro-6-(4-nitrophenylamino)-1,3,5-triazin-2-yl)-(methyl)amino)-1-hydroxy-3-sulfonatonaphthalen-2-yl)diazenyl)phenoxy)(imi-

*no)methyl)phenyl)-4-oxo-2-phenyl-3,4-dihydroquinazoline-6-sulfonate (**7d**)*. Yield: 82 %; Anal. Calcd. for $C_{47}H_{30}O_{11}N_{11}ClS_2Na_2$: C, 52.74; H, 2.83; N, 14.39 %. Found: C, 52.70; H, 2.80; N, 14.36 %. IR (KBr, cm^{-1}): 3355–3690 (O–H and N–H stretching of –OH and $–NH_2$ groups), 1670 (C=O stretching of quinazoline ring), 1435 (N=N stretching of azo group), 1380 (C–N), 1365, 1115, 1045 (S=O stretching of sulphonates), 1510, 1310 (N=O asym. and sym. stretching of nitro group), 766 (C–Cl stretching of chloro group). ^{1}H-NMR (300 MHz, DMSO-d_6, δ / ppm): 4.31 (1H, *s*, –OH), 4.20 (1H, *s*, –NH), 8.57 (1H, *s*, –CONH), 8.62 (1H, *s*, –CONH), 6.86–7.92 (24H, *m*, Ar–H).

*Sodium 3-(4-((4-((6-((4-chloro-6-(4-nitrophenylamino)-1,3,5-triazin-2-yl)-(phenyl)amino)-1-hydroxy-3-sulfonatonaphthalen-2-yl)diazenyl)phenoxy)(imino)methyl)phenyl)-4-oxo-2-phenyl-3,4-dihydroquinazoline-6-sulfonate (**7e**)*. Yield: 84 %; Anal. Calcd. for $C_{52}H_{32}O_{11}N_{11}ClS_2Na_2$: C, 55.15; H, 2.85; N, 13.60 %. Found: C, 55.10; H, 2.81; N, 13.57 %. IR (KBr, cm^{-1}): 3360–3700 (O–H and N–H stretching of –OH and $–NH_2$ groups), 1665 (C=O stretching of quinazoline ring), 1430 (N=N stretching of azo group), 1385 (C–N), 1370, 1110, 1040 (S=O stretching of sulphonates), 1505, 1310 (N=O asym. and sym. stretching of nitro group), 765 (C–Cl stretching of chloro group). ^{1}H-NMR (300 MHz, DMSO-d_6, δ / ppm): 4.32 (1H, *s*, –OH), 4.15 (H, *s*, –NH), 8.68 (1H, *s*, –CONH), 6.78–8.05 (29H, *m*, Ar–H).

*Sodium 4-(4-chloro-6-(4-nitrophenylamino)-1,3,5-triazin-2-ylamino)-5-hydroxy-6-((4-(imino(4-(4-oxo-2-phenyl-6-sulfonatoquinazolin-3(4*H*)-yl)phenyl)methoxy)phenyl)diazenyl)naphthalene-1,3-disulfonate (**7f**)*. Yield: 77 %; Anal. Calcd. for $C_{46}H_{27}O_{14}N_{11}ClS_3Na_3$: C, 47.69; H, 2.37; N, 13.30 %. Found: C, 47.63; H, 2.33; N, 13.28 %. IR (KBr, cm^{-1}): 3345–3690 (O–H and N–H stretching of –OH and $–NH_2$ groups), 1670 (C=O stretching of quinazoline ring), 1425 (N=N stretching of azo group), 1365 (C–N), 1375, 1105, 1042 (S=O stretching of sulphonates), 1510, 1315 (N=O asym. and sym. stretching of nitro group), 765 (C–Cl stretching of chloro group). ^{1}H-NMR (300 MHz, DMSO-d_6, δ / ppm): 4.30 (1H, *s*, –OH), 4.12 (2H, *s*, 2 –NH), 8.65 (1H, *s*, –CONH), 6.83–7.98 (23H, *m*, Ar–H).

*Sodium 3-(4-((4-((1-(4-chloro-6-(4-nitrophenylamino)-1,3,5-triazin-2-ylamino)-5-sulfonatonaphthalen-2-yl)diazenyl)phenoxy(imino)methyl)phenyl)-4-oxo-2--phenyl-3,4-dihydroquinazoline-6-sulfonate (**7g**)*. Yield: 76 %; Anal. Calcd. for $C_{46}H_{28}O_{10}N_{11}ClS_2Na_2$: C, 53.11; H, 2.71; N, 14.81 %. Found: C, 53.09; H, 2.68; N, 14.78 %. IR (KBr, cm^{-1}): 3355–3705 (O–H and N–H stretching of –OH and $–NH_2$ groups), 1662 (C=O stretching of quinazoline ring), 1430 (N=N stretching of azo group), 1372 (C–N), 1372, 1115, 1052 (S=O stretching of sulphonates), 1505, 1315 (N=O asym. and sym. stretching of nitro group), 766 (C–Cl stretching of chloro group). ^{1}H-NMR (300 MHz, DMSO-d_6, δ / ppm): 4.18 (2H, *s*, 2 –NH), 8.70 (1H, *s*, –CONH), 6.75–7.93 (25H, *m*, Ar–H).

Sodium 3-(4-((4-((2-(4-chloro-6-(4-nitrophenylamino)-1,3,5-triazin-2-ylamino)-6-sulfonatonaphthalen-1-yl)diazenyl)phenoxy)(imino)methyl)phenyl)-4-oxo-

*2-phenyl-3,4-dihydroquinazoline-6-sulfonate (**7h**)*. Yield: 80 %; Anal. Calcd. for $C_{46}H_{28}O_{10}N_{11}ClS_2Na_2$: C, 53.11; H, 2.71; N, 14.81 %. Found: C, 53.08; H, 2.67; N, 14.77 %. IR (KBr, cm^{-1}): 3350–3715 (O–H and N–H stretching of –OH and $–NH_2$ groups), 1665 (C=O stretching of quinazoline ring), 1435 (N=N stretching of azo group), 1380 (C–N), 1360, 1118, 1050 (S=O stretching of sulphonates), 1505, 1310 (N=O asym. and sym. stretching of nitro group), 762 (C–Cl stretching of chloro group). ^{1}H-NMR (300 MHz, DMSO-d_6, δ / ppm): 4.17 (2H, *s*, 2 –NH), 8.68 (1H, *s*, –CONH), 6.82–7.98 (25H, *m*, Ar–H).

*Sodium 3-(4-((4-((2-(4-chloro-6-(4-nitrophenylamino)-1,3,5-triazin-2-ylamino)naphthalene-1-yl)diazenyl)phenoxy)(imino)methyl)phenyl)-4-oxo-2-phenyl-3,4-dihydroquinazoline-6-sulfonate (**7i**)*. Yield: 82 %; Anal. Calcd. for $C_{46}H_{28}O_7N_{11}ClSNa_2$: C, 58.88; H, 3.12; N, 16.04 %. Found: C, 58.84; H, 3.09; N, 16.01 %. IR (KBr, cm^{-1}): 3350–3700 (O–H and N–H stretching of –OH and $–NH_2$ groups), 1670 (C=O stretching of quinazoline ring), 1422 (N=N stretching of azo group), 1388 (C–N), 1365, 1120, 1060 (S=O stretching of sulphonates), 1510, 1315 (N=O asym. and sym. stretching of nitro group), 760 (C–Cl stretching of chloro group). ^{1}H-NMR (300 MHz, DMSO-d_6 / δ, ppm): 4.15 (2H, *s*, 2 –NH), 8.65 (1H, *s*, –CONH), 6.86–7.95 (26H, *m*, Ar–H).

*Sodium 3-(4-((4-((2-(4-chloro-6-(4-nitrophenylamino)-1,3,5-triazin-2-ylamino)-5-sulfonatonaphthalen-1-yl)diazenyl)phenoxy)(imino)methyl)phenyl)-4-oxo--2-phenyl-3,4-dihydroquinazoline-6-sulfonate (**7j**)*. Yield: 85 %; Anal. Calcd. for $C_{46}H_{27}O_{13}N_{11}ClS_3Na_3$: C, 48.36; H, 2.38; N, 13.49 %. Found: C, 48.32; H, 2.34; N, 13.46 %. IR (KBr, cm^{-1}): 3360–3700 (O–H and N–H stretching of –OH and $–NH_2$ groups), 1660 (C=O stretching of quinazoline ring), 1445 (N=N stretching of azo group), 1380 (C–N), 1360, 1113, 1047 (S=O stretching of sulphonates), 1505, 1308 (N=O asym. and sym. stretching of nitro group), 765 (C–Cl stretching of chloro group). ^{1}H-NMR (300 MHz, DMSO-d_6, δ / ppm): 4.14 (2H, *s*, 2 –NH), 8.61 (1H, *s*, –CONH), 6.85–7.93 (25H, *m*, Ar–H).

*Sodium 3-(4-((4-((1-(4-chloro-6-(4-nitrophenylamino)-1,3,5-triazin-2-ylamino)-8-sulfonatonaphthalen-2-yl)diazenyl)phenoxy)(imino)methyl)phenyl)-4-oxo--2-phenyl-3,4-dihydroquinazoline-6-sulfonate (**7k**)*. Yield: 80 %; Anal. Calcd. For $C_{46}H_{28}O_{10}N_{11}ClS_2Na_2$: C, 53.11; H, 2.71; N, 14.81 %. Found: C, 53.06; H, 2.68; N, 14.76 %. IR (KBr, cm^{-1}): 3355–3700 (O–H and N–H stretching of –OH and $–NH_2$ groups), 1675 (C=O stretching of quinazoline ring), 1440 (N=N stretching of azo group), 1385 (C–N), 1360, 1112, 1055 (S=O stretching of sulphonates), 1511, 1307 (N=O asym. and sym. stretching of nitro group), 763 (C–Cl stretching of chloro group). ^{1}H-NMR (300 MHz, DMSO-d_6, δ / ppm): 4.16 (2H, *s*, 2 –NH), 8.66 (1H, *s*, –CONH), 6.78–7.96 (25H, *m*, Ar–H).

*Sodium 8-(4-chloro-6-(4-nitrophenylamino)-1,3,5-triazin-2-ylamino)-7-((4--(imino(4-(4-oxo-2-phenyl-6-sulfonatoquinazolin-3(4*H*)-yl)phenyl)methoxy)phenyl)diazenyl)naphthalene-1,3,6-trisulfonate (**7l**)*. Yield: 85 %; Anal. Calcd. for

$C_{46}H_{26}O_{16}N_{11}ClS_4Na_4$: C, 44.40; H, 2.11; N, 12.38 %. Found: C, 44.36; H, 2.08; N, 12.34 %. IR (KBr, cm^{-1}): 3360–3705 (O–H and N–H stretching of –OH and $–NH_2$ groups), 1662 (C=O stretching of quinazoline ring), 1445 (N=N stretching of azo group), 1382 (C–N), 1365, 1120, 1048 (S=O stretching of sulphonates), 1510, 1315 (N=O asym. and sym. stretching of nitro group), 766 (C–Cl stretching of chloro group). ^{1}H-NMR (300 MHz, DMSO-d_6, δ / ppm): 4.18 (2H, *s*, 2 –NH), 8.62 (1H, *s*, –CONH), 6.76–7.96 (23H, *m*, Ar–H).

*Sodium 4-(4-chloro-6-(4-nitrophenylamino)-1,3,5-triazin-2-ylamino)-5-hydroxy-6-((4-(imino(4-(4-oxo-2-phenyl-6-sulfonatoquinazolin-3(4*H*)-yl)phenyl)methoxy)phenyl)diazenyl)naphthalene-1,7-disulfonate (**7m**)*. Yield: 78 %; Anal. Calcd. for $C_{46}H_{27}O_{14}N_{11}ClS_3Na_3$: C, 47.69; H, 2.35; N, 13.30 %. Found: C, 47.64; H, 2.31; N, 13.26 %. IR (KBr, cm^{-1}): 3370–3705 (O–H and N–H stretching of –OH and $–NH_2$ groups), 1665 (C=O stretching of quinazoline ring), 1445 (N=N stretching of azo group), 1380 (C–N), 1355, 1120, 1045 (S=O stretching of sulphonates), 1505, 1310 (N=O asym. and sym. stretching of nitro group), 760 (C–Cl stretching of chloro group). ^{1}H-NMR (300 MHz, DMSO-d_6, δ / ppm): 4.35 (1H, *s*, –OH), 4.15 (2H, *s*, 2 –NH), 8.62 (1H, *s*, –CONH), 6.75–7.98 (23H, *m*, Ar–H).

Spectral properties

The absorption maxima (λ_{max}) and logarithm of the molar extinction coefficient (log ε) of all the prepared dyes **7a**–**m** are given in Table I. The absorption maxima of **7a**–**m** were recorded in DMF solution. The absorption maxima were in the range of 475–543 nm. The value of logarithm of molar extinction co-efficient (log ε) of the dyes **7a**–**m** were in the range 4.15–4.42, indicating their good absorption intensity.

TABLE I. Exhaustion and fixation data of the synthesised dyes **7a**–**m** (S – silk, W – wool, C – cotton)

Dye	Colour	λ_{max} / nm	log ε	Exhaustion, %			Fixation, %		
				S	W	C	S	W	C
7a	Pink	543	4.42	75.50	70.80	70.55	91.53	91.08	91.44
7b	Reddish brown	503	4.30	73.30	66.82	67.66	88.78	89.25	84.85
7c	Brown	495	4.22	70.80	70.47	69.72	85.54	92.42	85.57
7d	Orange	485	4.15	69.55	65.55	73.78	89.14	87.81	88.89
7e	Reddish brown	475	4.27	67.87	66.18	69.45	91.84	85.54	87.55
7f	Light brown	520	4.32	72.60	71.15	69.57	84.02	88.75	86.87
7g	Light orange	485	4.30	70.35	68.80	71.88	85.70	84.65	91.49
7h	Orange	480	4.15	75.45	66.27	71.52	90.12	91.81	88.78
7i	Orange	475	4.40	68.80	68.40	65.17	86.73	86.84	84.38
7j	Light yellow	490	4.25	71.23	67.23	72.60	90.45	87.45	87.58
7k	Brown	485	4.27	75.95	65.17	68.28	91.82	84.47	85.88
7l	Orange	475	4.30	69.95	69.96	70.70	90.16	89.29	86.57
7m	Greenish yellow	525	4.23	72.55	68.82	68.04	91.52	88.91	88.92

Dyeing of fibres

All the dyes (**7a**–**m**) were applied on silk, wool and cotton fabrics in 2 % shade according to the usual procedure.[7] The variation in the hues of the dyed fabric result from both the nature and position of the substituent present on the naphthalene ring. The remarkable degree of levelness after washing indicates good penetration and affinity of these dyes for the fabric.

Exhaustion and fixation study

Dye uptake by the fibre was measured by sampling the dye bath before and dyeing. The absorbance of diluted dye solution was measured at the λ_{max} of the dye. Percentage dye bath exhaustion was calculated using following relationship:

$$\text{Exhaustion (\%)} = 100\frac{\text{Initial O.D.} - \text{Final O.D.}}{\text{Initial O.D.}}$$

The percentage exhaustion[8] of 2 % dyeing on cotton ranged from 65 to 74 %, for silk fabric from 67 to 75 % and wool from 65 to 71 %. The percentage fixation[9] of 2 % dyeing on cotton fabric ranged from 84 to 91 %, for silk from 84 to 92% and for wool from 84 to 90 % (the obtained results are summarized in Table I).

Fastness properties

The light fastness of all the reactive dyes (**7a**–**m**) on silk, wool and cotton fibres is moderate to very good. The obtained result of washing fastness of the dyes for silk, wool and cotton fibres showed they are good to excellent. Fastness to rubbing (dry and wet) of the dyed pattern was moderate to very good for silk, wool and cotton fibres (Table II). These are attributed to the good penetration and affinity of the dyes for the fibres.

TABLE II. Fastness properties of the synthesised dyes **7a**–**m** (S – silk, W – wool, C – cotton; light fastness: 1 – poor, 2 – slight, 3 – moderate, 4 – fair, 5 – good, 6 – very good; wash and rubbing fastness: 1 – poor, 2 – fair, 3 – good, 4 – very good, 5 – excellent)

Dye	Light fastness			Wash fastness			Rubbing fastness					
							Dry			Wet		
	S	W	C	S	W	C	S	W	C	S	W	C
7a	5	6	4	5	4–5	4	4–5	3–4	3	3–4	4	5
7b	4	4–5	4–5	4	4	3–4	3–4	3	4	4	4	3
7c	5	5	3	5	3–4	3	4	4–5	5	3–4	6	4
7d	3	4	5	4	4	4	3–4	3	4	4	4–5	3–4
7e	4	3–4	3	3–4	3–4	5	3	5	3	3	4–5	4
7f	4–5	4	4	4–5	4	4–5	4–5	3–4	3–4	3–4	4	3–4
7g	6	4	3	3	4	3–4	4–5	4	4	3	4	4
7h	4	5	4–5	4	5	4	4	3–4	3	4	4–5	5
7i	4	5	4–5	4	4	3–4	3	3	3–4	5	3	5
7j	3–4	5	3	3–4	3	4–5	5	4	3	3	4	3
7k	4	4–5	4	5	4–5	3–4	4	4	3–4	5	4–5	4

TABLE II. Continued

Dye	Light fastness			Wash fastness			Rubbing fastness					
							Dry			Wet		
	S	W	C	S	W	C	S	W	C	S	W	C
7l	4	5	3–4	3–4	4	5	4	4–5	3	4–5	3	3–4
7m	5–6	4	5	4–5	3–4	4–5	3–4	4	3–4	4	3	4–5

EXPERIMENTAL

General

All the melting points (m.p.) were determined in open capillaries and are uncorrected. Elemental analysis for carbon, hydrogen and nitrogen were realised on a Carlo Erba 1108 elemental analyzer. The purity of all the dyes has been checked by TLC[10] using aluminium plates coated with silica gel 60 F254 (Merck), eluent *iso*-butanol:*n*-propanol:ethyl acetate:water (2:4:1:3). The IR spectra were recorded in KBr on a Perkin-Elmer model-881 spectrophotometer and the ^{1}H-NMR spectra on a Brucker DRX-300 (300 MHz FT-NMR) instrument using TMS as the internal standard and DMSO-*d*6 as the solvent. Chemical shifts are given in δ (ppm). Absorption spectra were recorded on a Beckman DB-GT Grating spectrophotometer. The light fastness was assessed in accordance with BS: 1006-1978.[11] The rubbing fastness test was performed with a Crockmeter (Atlas) in accordance with AATCC-1961[12] and the wash fastness test in accordance with IS: 765-1979.[13]

*Preparation of 2-phenyl-4-oxo-3,1-benzoxazine-6-suphonic acid (**1**)[14]*

Benzoyl chloride (140.5 g, 1.0 mol) was added dropwise over the period of 1 h to 5-sulpho anthranilic acid (217 g, 1.0 mol) dissolved in pyridine (60 ml), under constant stirring at 8 °C. After the completion of the addition, the reaction mixture was stirred for 30 min at room temperature. At the end of the reaction, a solid mass was obtained, which was filtered, washed successively with sodium bicarbonate solution (to remove unreacted acid) and then with water, dried and recrystallized from rectified spirit. (The general route for the preparation of 2-phenyl-4-oxo-3,1-benzoxazine-6-suphonic acid (**1**) is outlined in Scheme 1).

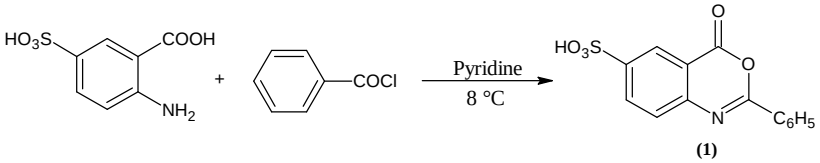

(1)

Scheme 1. Synthetic route to 2-phenyl-4-oxo-3,1-benzoxazine-6-sulphonic acid (**1**).

*Preparation of 4,4'-diaminobenzanilide (**2**)*

The title compound was prepared by the process described in the literature.[15] (The general route for the preparation of 4,4'-diaminobenzanilide (**2**) is outlined in Scheme 2).

*Preparation of 2-phenyl-3{4'-[*N*-(4"-aminophenyl)carbamoyl]-phenyl}-quinazoline-4-(3*H*)--one-6-sulphonic acid (**3**)[16]*

A mixture of compound **1** (0.05 mol) and **2** (0.05 mol) in dry pyridine (50 ml) was heated under reflux for 6 h under anhydrous reaction conditions and then allowed to cool to room temperature. The reaction mixture was treated with dilute HCl and stirred. A solid separate out which was filtered off and washed with water to remove any adhered pyridine. The

thus obtained crude quinazoline was dried under vacuum and recrystallized from 50 vol.% ethanol in water). (The general route for the preparation of compound **3** is outlined in Scheme 3).

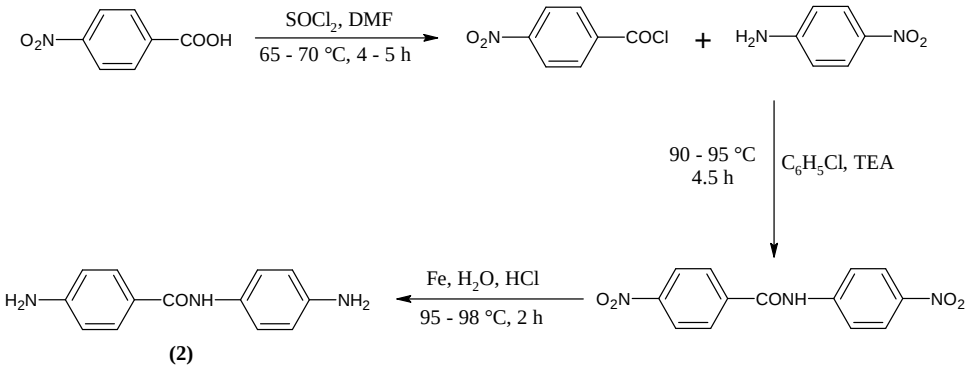

Scheme 2. Synthetic route to the diaminobenzanilide (**2**).

*Diazotation of 2-phenyl-3{4'-[*N*-(4"-aminophenyl)carbamoyl]-phenyl}-quinazoline-4-(3*H*)--one-6-sulphonic acid (**4**)*

Compound **3** (2.56 g, 0.005 mol) was suspended in water (60 ml). Hydrochloric acid (0.36 g) was added dropwise to this well-stirred suspension. The mixture was gradually heated up to 70 °C until a clear solution was obtained. The solution was cooled to 0–5 °C in an ice bath. A solution of $NaNO_2$ (0.6 g) in water (4 ml) previously cooled to 0 °C was then added over a period of five minutes with stirring. The stirring was continued for 1 h, maintaining the same temperature. The excess of nitrous acid (gave a positive test on starch-iodide paper) was decomposed with the required amount of sulphamic acid. The thus obtained clear diazo solution **4** at 0–5 °C was used for the subsequent coupling reaction. (The general route for the preparation of compound **4** is outlined in Scheme 3).

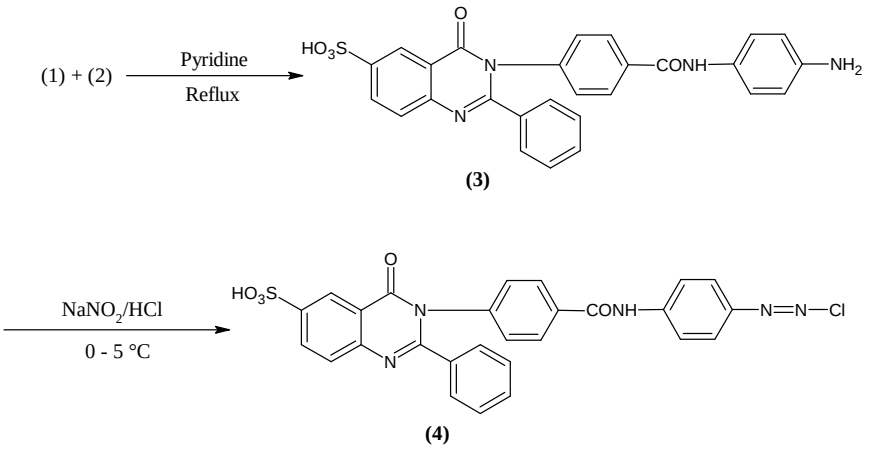

Scheme 3. Synthetic route to 2-phenyl-3-{4'-[*N*-(4"-aminophenyl)carbamoyl]-phenyl}-quinazoline-4-(3*H*)-one-6-sulphonic acid (**3**) and its diazonium salt **4**.

Preparation of 4-nitro anilino cyanurated H-acid

*Cyanuration of H-acid (**5a**)*. Cyanuric chloride (1.85 g, 0.01 mol) was stirred in acetone (25 ml) at a temperature below 5 °C for a period of an hour. A neutral solution of H acid (3.19 g, 0.01mol) in aqueous sodium carbonate solution (10 % w/v) was then added in small amounts over about an hour. The pH was maintained neutral by the simultaneous addition of sodium carbonate solution (1 % w/v). The reaction mixture was stirred at 0–5 °C for further 4 h when a clear solution was obtained. (The general route for the preparation of compound **5a** is outlined in Scheme 4). The resultant solution was used for the condensation reaction with 4-nitro aniline.

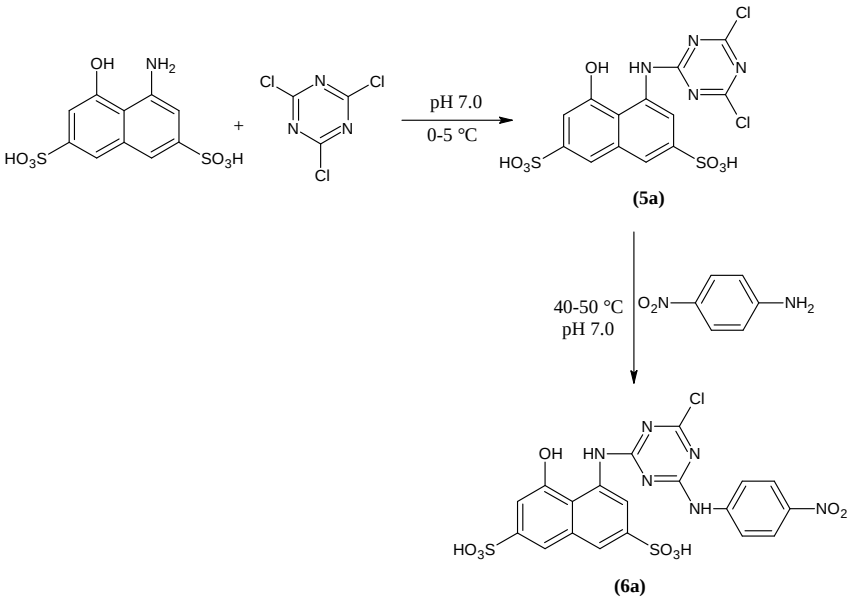

Scheme 4. Synthetic route to the cyanurated H-acid **5** and 4-nitro anilinocyanurated H-acid **6a**.

*Condensation with 4-nitro aniline (preparation of 4-nitro anilino cyanurated H-acid **6a**)*

The temperature of the ice-cooled well-stirred solution of cyanurated H-acid **5** (4.67 g, 0.01 mol) was gradually raised to 45 °C in about 30 min. To this cyanurated H-acid, 4-nitro aniline (1.38 g, 0.01 mol) was added dropwise at the same temperature, during a period of 30 min, maintaining the pH neutral by the simultaneous addition of sodium bicarbonate (1 % w/v). After completion of the addition, stirring was continued for a further 3 h. The thus obtained 4-nitro anilino cyanurated H-acid solution was subsequently used for the further coupling reaction. (The general route for the preparation of compound **6a** is outlined in Scheme 4).

*Formation of the dye **7a***

To an ice cold and stirred solution of 4-nitro anilino cyanurated H-acid **6a** (5.68 g, 0.01 mol), a freshly prepared diazo solution **4** (2.8 g, 0.005 mol) was added dropwise over a period of 10–15 min. The pH was maintained at 7.5 to 8.5 by the simultaneous addition of sodium carbonate solution (10 % w/v). During the coupling, a purple solution was formed. The stirring was continued for 3–4 h, maintaining the temperature below 5 °C. The reaction mixture was heated to 60 ºC and sodium chloride was added until a coloured material precipitated.

The mixture was stirred for 1 h, filtered and washed with a small amount of sodium chloride solution (5 % w/v). The solid was dried at 80–90 °C and extracted with DMF. The dye was precipitated by diluting the DMF-extract with excess chloroform. The violet dye was then filtered, washed with chloroform and dried at 60 °C. Yield: 85 %. (The general route for the preparation of compound (**7a**) is outlined in Scheme 5).

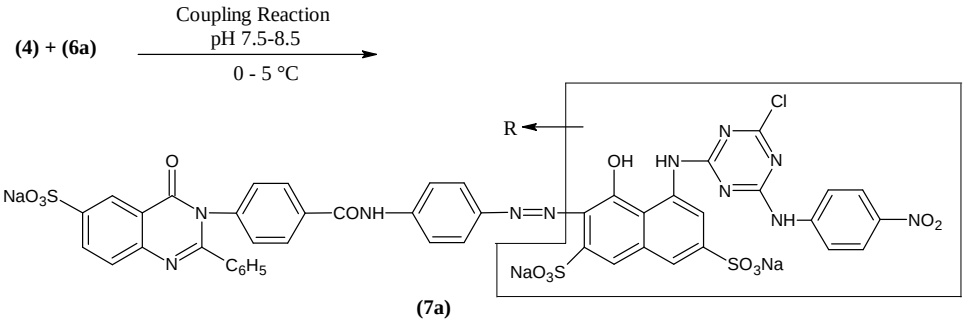

(7a)

Scheme 5. Synthetic route to dye **7a** (R: different 4-nitro aniline cyanurated coupling components (**6a**–**m**)).

Following the above-described procedure, other reactive dyes **7b**–**m** were synthesized using the required 4-nitro anilino cyanurated coupling components, *i.e.*, Gamma acid (**6b**), J-acid (**6c**), *N*-methyl-J-acid (**6d**), *N*-phenyl-J-acid (**6e**), Chicago acid (**6f**), Laurant acid (**6g**), Bronner acid (**6h**), Tobias acid (**6i**), sulpho Tobias acid (**6j**), Peri acid (**6k**), Koch acid (**6l**) and K-acid (**6m**).

CONCLUSIONS

Reactive dyes based on 2-phenyl- 3-{4'-[*N*-(4"-aminophenyl)carbamoyl]--phenyl}-quinazoline-4-(3*H*)-one-6-sulphonic acid were synthesized. These dyes give mostly pink, yellow and brown shades on silk, wool and cotton fabric having good to excellent washing fastness properties. The remarkable degree of levelness after washing indicates good penetration and affinity of these dyes for the fabrics. Exhaustion and fixation of these dyes are very good, which indicates that the dyes have good affinity and solubility with the fabrics. The presence of the quinazolinone structure in the dye molecules results in low sublimation and high thermal stability.

Acknowledgements. The authors express their gratitude to the Head, Department of Chemistry, V. N. S. G. University, Surat, India, for providing the necessary research facility. In addition, thanks go to SAIF, Chandigarh for the spectral data and Atul Ltd., Atul for providing the dyeing and analytical facilities.

И З В О Д

НОВЕ АЗО БОЈЕ ДОБИЈЕНЕ ИЗ 2-ФЕНИЛ-3-{4'-[*N*-(4"-АМИНОФЕНИЛ)КАРБАМОИЛ]--ФЕНИЛ}-КИНАЗОЛИН-4-(3*H*)-ОН-6-СУЛФОНСКЕ КИСЕЛИНЕ

DIVYESH R. PATEL и KESHAV C. PATEL

Department of Chemistry, Veer Narmad South Gujarat University, Surat 395 007, Gujarat, India

Серија нових хетероцикличних моно азо реактивних боја **7a–m** добијена је куповањем производа диазотовања 2-фенил-3-{4'-[*N*-(4"-аминофенил)карбамоил]-фенил}-киназолин-4--(3*H*)-он-6-сулфонске киселине (**3**) са различитим цијануринским компонентама за куповање (**6a**–**m**) и испитиване су њихове способности бојења свиле, вуне и памука. Утврђено је да ове боје дају различиту покривеност са добром дубином и нијансом бојења влакана. Сва једињења окарактерисана су уобичајеним спектроскопским методама (IC и NMR) и елементалном анализом. Обојена влакна имају добру постојаност према светлу, прању и трљању.

(Примљено 25. фебруара 2009, ревидирано 23. септембра 2010)

REFERENCES

1. E. N. Abrahart, *Dyes and their Intermediate*, Edward Arnold Publisher, London, 1976, p. 170
2. A. Arcoria, S. Fisichella, G. Scarlata, *Ann. Chim. (Rome)* **61** (1971) 846
3. D. N. Naik, K. R. Desai, *Dyes Pigments* **14** (1990) 1
4. M. A. Weaver, L. Shuttle Worth, *Dyes Pigments* **3** (1982) 81
5. A. Arcoria, S. Fisichella, G. Scarlata, *Boll. Sci. Fac. Chim. Ind. Bolongo* **27** (1969) 57 [C. A. 71/1969 103150]
6. B. R. Modi, N. R. Desai, B. D. Mistry, K. R. Desai, *Proc. Nat. Acad. Sci. A* **65** (1995) 17
7. V. A. Shenai, *Chemistry of Dyes and Principles of Dyeing*, Sevak Publication, Bombay, 1973
8. V. Iyer, A. M. Gurjar, K. S. Bhyrappa, *Indian J. Fiber Text. Res.* **18** (1993) 120
9. *The Analytical Chemistry of Synthetic Dyes*, K. Venkatraman, Ed., Wiley, New York, 1977, p. 524
10. B. Fried J. Sherma, *Thin Layer Chromatography: Technique and Application*, Marcel Dekker, New York, 1982
11. *BS 1006: Standard Test Method* (1978) (UK), ISO 105 (1994) (India)
12. *AATCC Test Method* (1961) p-8
13. *ISO 765: Indian Standard* (1979)
14. V. P. Trivedi, N. K. Undavia, P. B. Trivedi, *J. Indian Chem. Soc.* **81** (2004) 506
15. G. M. Simu, S. A. Chicu, N. Morin, W. Schmidt, E. Sisu, *Turk. J. Chem.* **28** (2004) 579
16. V. K. Pandey, S. K. Saxena, M. N. Joshi, *J. Indian Chem. Soc.* **84** (2007) 593.

Journal of the Serbian Chemical Society
JSCS-info@shd.org.rs • www.shd.org.rs/JSCS
J. Serb. Chem. Soc. *76* (2) 189–199 (2011)
JSCS–4111
UDC 547.93+547.47+546.33–38:*verapamil
Original scientific paper

Effect of sodium salts of 3*α*,12*α*-dihydroxy-7-oxo-5*β*-cholanoic and 3,7,12-trioxo-5*β*-cholanoic acids on verapamil hydrochloride in biophysical–chemical model experiments

MIHALJ M. POŠA[1*#], VALÉRIA J. GUZSVÁNY[2#], MOMIR M. MIKOV[1] and JANOŠ J. ČANADI[2#]

[1]*Department of Pharmacy, Faculty of Medicine, Hajduk Veljkova 3, University of Novi Sad, 21000 Novi Sad and* [2]*Department of Chemistry, Faculty of Sciences, University of Novi Sad, Trg Dositeja Obradovića 3, 21000 Novi Sad, Serbia*

(Received 19 June, revised 13 September 2010)

Abstract: It is known that certain bile acids have a promotive effect on the action of some drugs. Special attention is paid to bile acids having oxo groups instead of OH groups in the steroid skeleton of their molecule, since these derivatives have a lower hemolytic potential (membrane toxicity). This study examined the effects of sodium salts of 3*α*,12*α*-dihydroxy-7-oxo-5*β*-cholanoic acid (7-oC) and 3,7,12-trioxo-5*β*-cholanoic acid (3,7,12-toC) on the adsorption of verapamil hydrochloride on activated carbon (model of the cell membrane). The interaction was followed by measuring the effect of verapamil on the functional dependence between the spin-lattice relaxation time T_1 (protons of the C18 angular group of the bile acid molecule) and the bile acid concentration in deuterated chloroform (model of the cell membrane lipid phase). Whether a depot effect of verapamil exists when 7-oC and 3,7,12-toC (in the form of methyl esters) are present in chloroform was also investigated. It was found that 7-oC exhibited a significant effect in the experiments with verapamil, whereas 3,7,12-toC showed no difference of the measured parameters with respect to the control. This indicates that bile acid molecules should have OH groups bound to the steroid nucleus, in order to exhibit an effect on the monitored physico–chemical parameters of verapamil.

Key words: Bile acid oxo derivatives; verapamil; spin-lattice relaxation time.

INTRODUCTION

Bile acids are amphiphilic molecules[1,2] which, apart from their well-known physiological roles, such as micellar solubilization of lipids during digestion and regulation of biosynthesis and cholesterol homeostasis,[3] also participate in a

* Corresponding author. E-mail: mihaljp@uns.ac.rs
# Serbian Chemical Society member.
doi: 10.2298/JSC090619023P

number of metabolic pathways as regulators, *i.e.*, modulators of nuclear receptors (farnesoid X (FXR)) of enzymes, ionic channels (large conductance Ca^{2+}-activated K^+ channel (BK_{Ca})), *etc*.[4,5] More recently, bile acid analogues have been increasingly used to treat metabolic disturbances (obesity, hypertriglyceridemia, type 2 diabetes, atherosclerosis and hypertension). Pharmacological applications of certain bile acids are based on their ability to increase drug transport through the cell membrane or through the complex blood-brain barrier. In these interactions, the mechanism of bile acid action is observed as a change of the integrity of the membranes of complex biological structures (epithelial, buccal, dermal, *etc*.) by weakening or breaking *tight junctions* between cells, thus enhancing paracellular transport. In addition, when bile acids are present at levels close to their critical micellar concentrations (*CMC*) or exceeding them, they modify the structure of the cell membrane by withdrawing phospholipids and forming mixed micelles, which results in increased disorder, *i.e.*, increased probability of the formation of water pool in the cell membrane.[4] Besides, on the membrane surface or in its interior, bile acids may form complexes with some drugs which mediate the rate of drug passage through the cell membrane.[3,6–9]

Oxo derivatives of bile acids are suitable for pharmacological investigations in view of the high values of their *CMC*s, which diminish their membrane toxicity, *i.e.*, hemolytic potential.[10]

The aim of this study was to use a biophysical-chemical model to examine experimentally the interaction of 3*α*,12*α*-dihydroxy-7-oxo-5*β*-cholanoic acid (7-oC) and 3,7,12-trioxo-5*β*-cholanoic acid (3,7,12-toC) with verapamil hydrochloride (Fig. 1). Namely, it is known that in *in vitro* experiments certain bile acid salts increase the adsorption of verapamil hydrochloride in the intestinal epithelium in rats, which assumes the formation of a complex between the drug (non-ionized form) and bile acid molecules (non-ionized form) in the lipophilic membrane phase[9]. The study was also concerned with the influence of Na salts of 7-oC and 3,7,12-toC on the adsorption of verapamil hydrochloride on activated carbon (model of the cell membrane surface and small intestine surface). Finally, the study dealt with the interaction between these bile acids (non-ionized form) and verapamil (molecular form, *i.e.*, base) in $CDCl_3$ (hydrophobic interior of the cell membrane), studied by the ^{1}H-NMR relaxation method. When experiment was concerned with the modeling of the processes in the small intestine or in the intercellular space, the bile acid was assumed to be in the form of its sodium salt and verapamil in the form of hydrochloride (adsorption on activated carbon), whereas when the experiment was concerned with modeling in the membrane lipid phase (NMR relaxation experiment), the bile acid and verapamil were assumed to be in their non-ionized forms.

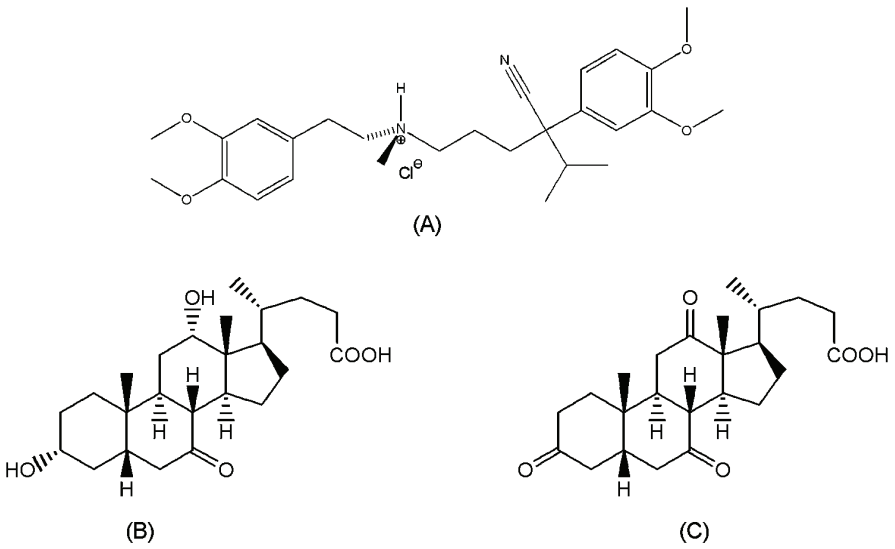

Fig. 1. A) Verapamil hydrochloride (5-[(3,4-dimethoxyphenyl)methylamino]-2-(3,4-dimethoxyphenyl)-2-isopropylvaleronitrile, hydrochloride), B) 3*α*,12*α*-dihydroxy-7-oxo-5*β*-cholanoic acid (7-oxodeoxycholic acid, 7-oC) and C) 3,7,12-trioxo-5*β*-cholanoic acid (3,7,12-trioxocholanoic acid; 3,7,12-toC).

EXPERIMENTAL

Materials

Cholic acid (Sigma, New Zealand, 98 %) was used for the synthesis of 7-oC according to the procedure by Tullar,[11] whereas 3,7,12-toC was prepared by the procedure of Fieser and Rajagoplan.[12] The other employed chemicals were obtained commercially, *i.e.*, Verapamil hydrochloride, verapamil (Sigma, New Zealand, 99.9 %), $CDCl_3$ (Aldrich, 99.99 %), $CHCl_3$ (Sigma, HPLC grade), KH_2PO_4 (Lachner, analytical reagent grade), Na_3PO_4 (Lachner, analytical reagent grade), $FeCl_3$ (Lachner, 98 %), $CrCl_3$ (Lachner, 98 %) and activated carbon (Darco G-60 powder). Double distilled water was used throughout.

Adsorption on activated carbon

For this purpose, a series of solutions of verapamil hydrochloride of the concentration of 0.125, 0.25, 0.5, 0.75, 1.00, 1.25, and 1.50 mg ml^{-1}, pH 7.4, were made to contain also sodium salts of 7-oC or 3,7,12-toC at concentrations of 0.5 *CMC* and *CMC*. The control was the solution of the drug without a bile acid. To each solution, including the control, 20 mg of activated carbon was added and the suspension was stirred for 30 min. After centrifugation (3000 rpm, 10 min), the verapamil hydrochloride concentration was measured in the supernatant by spectrophotometry (Agilent 8453) at 280 nm. The results are presented as the equilibrium amount of the adsorbed drug per unit mass of the adsorbent as a function of drug concentration in the supernatant.

Adsorption of verapamil hydrochloride was also measured in the presence of 10 mM solution of iron(III) chloride and chromium(III) chloride at 0.5 *CMC* of the sodium salt of 7-oC at pH 7.4. In doing this, the adsorbent was separated and the tested drug was extracted with chloroform (2×5 ml) from the supernatant pH 3.5, then the extract was passed through a solid-

-phase extraction column (Oesis), to bind the metal ions potentially present in the chloroform. The concentration of verapamil (molecular, *i.e.*, basic, form) in the chloroform solution was determined spectrophotometrically (285 nm).

^{1}H-NMR relaxation experiment

The starting solutions of 7-oC and 3,7,12-toC acids (non-ionized form, 60 mM in $CDCl_3$) were diluted with deuterated chloroform to obtain solutions of the concentrations ranging from 2 to 60 mM, each solution being also 4 mM in verapamil (molecular, *i.e.*, basic form). Control measurements were performed in pure $CDCl_3$. The experiments were performed at 23 °C on a Bruker AC-250 instrument. The ^{1}H-NMR spectra were recorded in a spectral window of 3200 Hz. The spin-lattice relaxation time was determined by fast inversion–recovery experiments (180°-τ-90°-AQC).[13-15] The area of the bile acid signal was measured at nine different times τ.

Depot experiment

The experiment was performed on an apparatus specially made for this purpose.[8] It consisted of two vertical glass tubes **A** and **B** mounted on a glass cylinder **C** (Fig. 2). Tube **A** contains an aqueous solution of verapamil hydrochloride (5 ml, 30 mM, pH 7.4) and it represents the verapamil hydrochloride solution in contact with the intestine epithelium. In the control experiment, the horizontal cylinder **C** contained chloroform, whereas in the experiments involving bile acids it contained solutions of the bile acid methyl ester in chloroform, 18 mM in one and 36 mM in the other experiment. The horizontal cylinder **C** corresponds to a complex membrane structure in the biological system (*e.g.*, the intestine epithelium membrane), whereas tube **B** contains buffer (5 ml, pH 7.4). The head of one peristaltic pump supplying fresh buffer pH 7.4 and to the head of a second peristaltic pump conducting the buffer from the tube **B**. As the pumping flow rate of both pumps was 2 ml min^{-1}, there was no change in the solution volume in tube **B** (Master flex 7523-60, pump head: L/S-Easy-Load II 77200-60, L/S-Tubing 13). The pumping flow rate is 2 ml min^{-1}; hence there is no change in the solution volume in tube **B**. In this way, the blood flow in a capillary around a tissue was modeled. In the horizontal cylinder **C**, three magnets are placed in the middle and two at the sites of its connection to the vertical tubes (300 rpm). After 3 h, the chloroform solution from the horizontal tube **C** was withdrawn (through tube **A**) and the verapamil concentration determined by spectrophotometry (Agilent 8453).

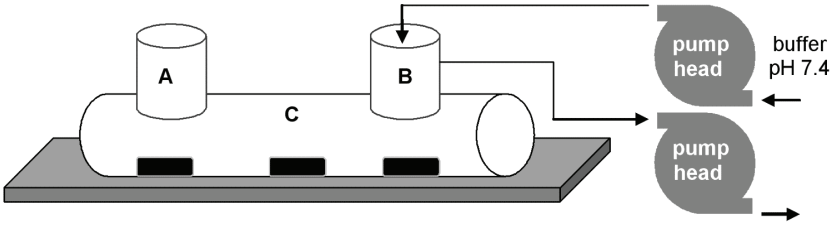

Fig. 2. Sketch of the setup for testing the depot effect.

RESULTS AND DISCUSSION

Adsorption on activated carbon

This part of the investigation represents the model of the surface action of bile acid salts at the water–cell membrane interface, where the bile acid salts are

adsorbed, modifying thus the boundary surface of the cell membrane.[7] Hjelm *et al*.[16] and Nicol *et al*.[17] in their studies of mixed micelles between lecithin (phospholipid) and bile acid salts proposed the model of caped-rod micelle in which the lecithin molecules are arranged radially, with the polar groups oriented towards the surface and separated by bile acid molecules, whereby the β-side of the steroid skeleton is oriented towards the hydrocarbon residues of the fatty acids from the lecithin molecules. This model for the orientation of bile acid molecules can also be acceptable for the case of their incorporation in the phospholipid cell membrane, where the hydrophilic α-side of the bile acid molecules is oriented towards the extracellular space. A similar situation arises also in the adsorption of bile acid salts on activated carbon, where the α-side of the steroid skeleton is directed to the interior of the solution.

The adsorption isotherms of verapamil hydrochloride in the presence and absence of Na-7-oC in the aqueous medium at the concentration of 0.5 *CMC* are shown in Fig. 3. The curve of verapamil hydrochloride adsorption shows an abrupt rise with increasing equilibrium concentration of the drug, and saturation is attained already at a relatively low concentration. The effect of Na-7-oC on verapamil hydrochloride was evidenced by a change of its saturation mass per unit mass of adsorbent. Namely, the Na-7-oC steroid skeleton has two proton donor--acceptor OH groups that form hydrogen bonds with the methoxy groups and nitrile group of verapamil hydrochloride, and the formation of this complex increased the amount of verapamil hydrochloride adsorbed. In the presence of Na--3,7,12-toC (0.5 *CMC*), however, the saturation mass of verapamil hydrochloride decreased abruptly (0.075±0.012) compared to the control value (0.138±0.006), which is probably the result of the formation of the complex with verapamil hyd-

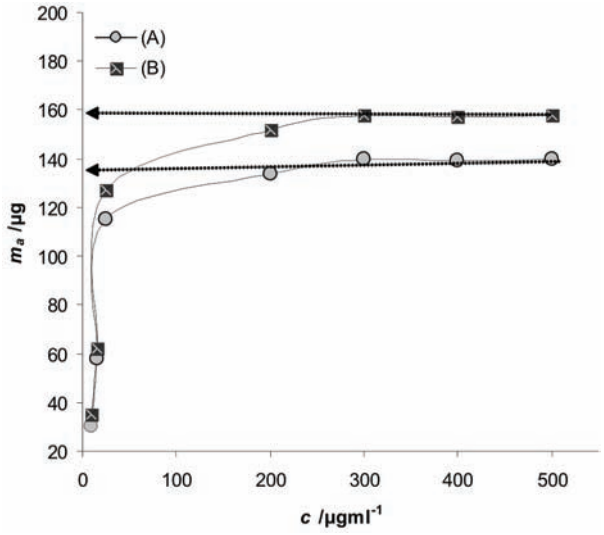

Fig. 3. Adsorption isotherms (adsorbed mass of verapamil hydrochloride per unit mass of activated carbon m_a) as a function of the equilibrium concentration of verapamil hydrochloride c: A) without bile acid salts – control, and B) with Na-7-oC, pH 7.4.

rochloride (Table I). Namely, Na-3,7,12-toC competes in the process of verapamil hydrochloride adsorption, occupying part of the activated carbon surface, increasing thus the coverage of the adsorbent, which lowers the adsorption of the drug. In fact, in the process of adsorption on activated carbon, each of the investigated bile acid salts acts as a competitor to verapamil. However, the adsorbed Na-7-oC forms a hydrogen-bonded complex with verapamil hydrochloride, which then shifts the equilibrium towards its adsorption.

TABLE I. Saturation masses of verapamil hydrochloride, pH 7.4

Na salt of bile acid	Concentration of Na salts of bile acids	Saturation mass of verapamil hydrochloride, mg g^{-1}		
		Buffered solution	Buffered solution + Fe(III)	Buffered solution + Cr(III)
Control	–	0.138±0.006	0.130±0.008	0.135±0.007
7-oC	0.5 *CMC*	0.156±0.004	0.072±0.010	0.071±0.010
	CMC	0.105±0.006	0.069 ±0.008	0.058 ±0.04
3,7,12-toC	0.5 *CMC*	0.078±0.010	0.084±0.007	0.080±0.010
	CMC	0.073±0.012	0.075±0.008	0.070±0.005

If the sodium salts of the tested bile acids were present at levels exceeding their CMC values, then the saturation mass of verapamil hydrochloride decreased compared to the control value (Table I). In the presence of Na-7-oC (0.105± ±0.006), the decrease of the verapamil hydrochloride saturation mass was significantly larger than in the presence of Na-3,7,12-toC (0.073±0.012). Namely, the Na-7-oC has a larger hydrophobic area[18] and hence is more efficient in forming mixed micelles with verapamil hydrochloride in solution, which results in a shift of the equilibrium towards desorption. In the presence of Na-3,7,12-toC, the verapamil hydrochloride saturation mass is not statistically different from that observed at 0.5 *CMC*. Since the three oxo groups in the Na-3,7,12-toC were shifted to the *β*-side of the steroid skeleton, which caused a decrease in its hydrophobic area, this bile acid salt has a lower tendency to form mixed micelles with verapamil hydrochloride.

Ions of chromium(III) and iron(III) hindered the formation of the hydrogen--bonded complex between verapamil hydrochloride and Na-7-oC. Namely, the presence of these ions at the 0.5 *CMC* of Na-7-oC caused no increase in the saturation mass of verapamil hydrochloride, but its decrease was observed compared to the control value (Table I). This is probably a consequence of the formation of complexes between Na-7-oC and the metal ions, which hinders the formation of hydrogen bonds with verapamil hydrochloride.

^{1}H-NMR relaxation experiment

Formation of the aggregates between 7-oC (non-ionized form) and verapamil (molecular form, 4 mM, to avoid self-association) in deuterated chloroform was

investigated by the ^{1}H-NMR relaxation technique. Fig. 4A shows the ^{1}H-NMR spectra of a mixture of 7-oC (60 mM) and verapamil (4 mM) recorded by the 180°-τ-90°-AQC method are shown in Fig. 4A. On the other hand, Fig. 4B presents the time τ dependence of the area of the signal I of the angular C18 methyl group of 7-oC after inversion by 180° (which are the corresponding spectra from Fig. 4A). The parameter of this functional dependence is the spin-lattice relaxation time T_1, which was also determined for the other investigated concentrations c_{BA}, both for 7-oC itself and for the mixture 7-oC + verapamil (4 mM). The functional dependence between the concentration c_{BA} and the spin-lattice relaxation time T_1 is shown in Fig. 4C, from which it can be seen that at the bile acid concentration exceeding 8 mM (curve I: 7-oC in $CDCl_3$, without verapamil) an abrupt jump appears, which indicates a change in the size (mass) of the molecule under observation, *i.e.*, the formation of aggregates. Namely, the observed increase in the mass of the particles retards their thermal motion, which also re-

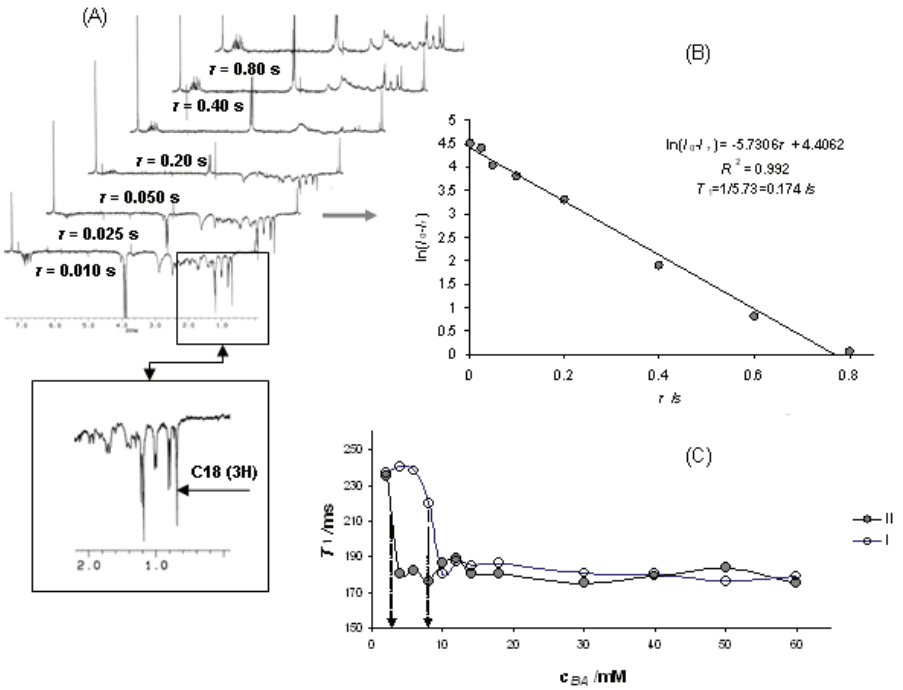

Fig. 4. A) ^{1}H-NMR spectra of a mixture of 7-oC (60 mM in $CDCl_3$) and verapamil (4 mM) obtained by the 180°-τ-90°-AQC method. Each spectrum was recorded at different times τ after the inversion (180°); B) change of the area of the signal of the C18 group of 7-oD as a function of the time after the inversion; C) relaxation time T_1 for the protons of the C18 methyl group of 7-oD as a function of the concentration c_{BA} (I in the absence and II in the presence of verapamil).

sults in a decrease of the relaxation rate (decay of the T_1 value), *i.e.*, there is a slower return of the spin system to the Bolcman equilibrium state. For solutions in deuterated chloroform, this can be explained by the Oakenfull Model[19] of bile acid aggregates, according to which the bile acid monomers are connected by hydrogen bonds *via* the α-sides of the steroid ring system, forming reverse micelles in chloroform (Fig. 5A). By simulating the molecular dynamics, Partay *et al.*[20] confirmed the possibility of the existence of the Oakenfull model for cholic and deoxycholic acids. If verapamil (4 mM) was also present in the deuterated chlo-

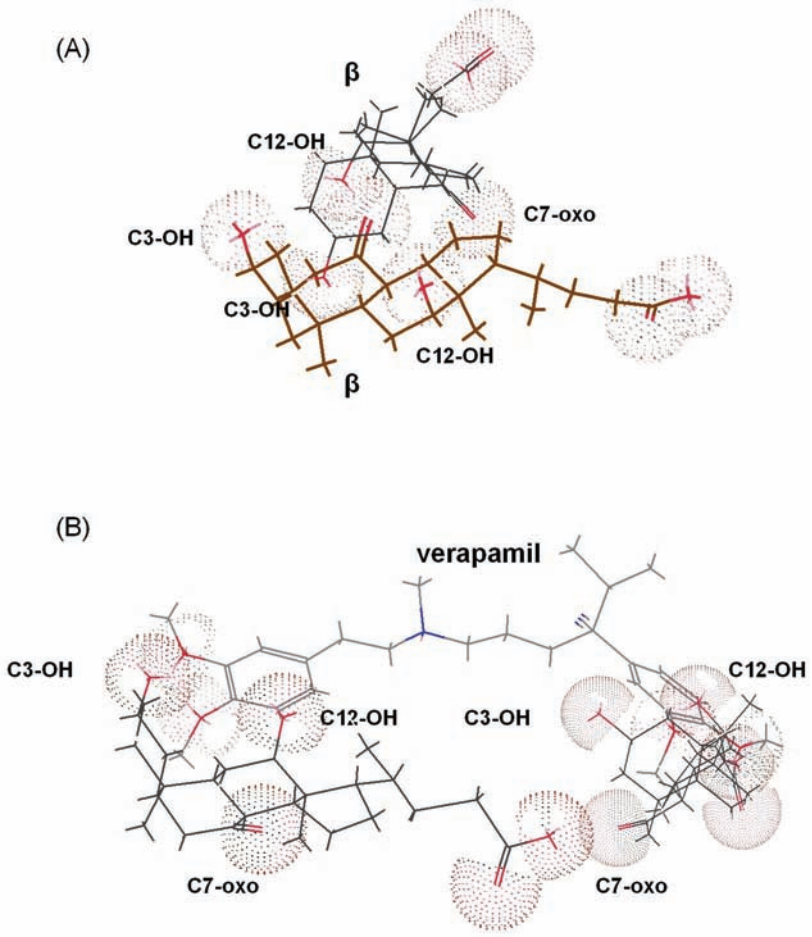

Fig. 5. A) The Oakenfull model of the aggregate (reverse micelle) of the 7-oC dimer (7-oC molecules are mutually bonded by the hydrogen bonds between the C12–OH group of the one and C7–oxo group of the other molecule); B) aggregate between the verapamil molecule and 7-oC (hydrogen bonds are formed between the verapamil methoxy group and the C3– and C12–OH groups of 7-oC, as well as between the C7–oxo group of the one and carboxylic function of the other molecule of the bile acid).

roform, then the function $T_1 = f(c_{BA})$ has an abrupt jump after the 2 mM concentration of 7-oC (Fig. 4C, curve II), which suggests that interaction between the bile acid molecule and the drug occurred. A study of the molecular models indicates that the formation of hydrogen bonds between the verapamil methoxy groups and the C3 (*i.e.*, C12) OH group of the bile acid in the aggregate of verapamil and 7-oC are sterically possible. For such an aggregate, the energy optimization shows that the distance between the carboxylic group of one and the C7 oxo group of the other bile acid molecule may also allow the formation of hydrogen bonds (Fig. 5B). The fact that curve II, even at higher 7-oC concentrations, did not return to its initial value (237 ms) although the $CDCl_3$ contained only 4 mM verapamil, may mean that verapamil has a catalytic role in the formation of the Oakenfull aggregates at higher bile acid concentrations. Namely, in the verapamil–bile acid aggregate, due to the mutual orientation and proximity (entropy effect), the 7-oC molecules may form hydrogen bonds between themselves, thus releasing verapamil molecules.

Verapamil had no influence on the course of the function $T_1 = f(c_{BA})$ when 3,7,12-toC was the tested bile acid.

Depot experiment

The verapamil concentration in chloroform was significantly higher (*t*-test, $p < 0.05$) compared to the control value when the chloroform contained the methyl ester of 7-oC (methyl esters of bile acids are used to prevent the passage of bile acids to an aqueous solution). On the other hand, the verapamil concentration did not differ from the control value when the chloroform contained the methyl ester of 3,7,12-toC (Table II). Therefore, the presence of methyl ester of 7-oC decreased the rate of verapamil transfer from chloroform (model of the membrane, *i.e.* of the epithelial cell) to the flowing buffer pH 7.4 (model of the capillary); thus, the existence of the depot effect was confirmed.

TABLE II. Verapamil concentration (mM) after 3 h of transport from the aqueous medium to chloroform; concentrations of bile acid methyl esters in chloroform: 18 (c_1) and 36 mM (c_2)

Bile acid	c_1	c_2
Control	2.02±0.16	
7-oC	5.41±0.43	7.85±0.39
3,7,12-toC	2.09±0.05	2.12±0.07

CONCLUSIONS

If the concentration of Na-7-oC is below its *CMC* value, the adsorption of verapamil hydrochloride is enhanced compared to the control. In deuterated chloroform, an abrupt change on the curve $T_1 = f(c_{BA})$ in the presence of verapamil appears at a 7-oC concentration of 2 mM (in the absence of verapamil it appears after 8 mM), which indicates the existence of interaction between 7-oC

and the investigated drug. In the depot experiment, the presence of the methyl ester of 7-oC prevents the transition of verapamil from chloroform to the aqueous buffer solution. Therefore, in the considered physico-chemical model systems, of the two tested bile acids only 7-oC showed a significant effect on verapamil, which indicates that a bile acid molecule has to contain OH groups in its steroid skeleton for interaction with verapamil. Namely, a prerequisite for the formation of hydrogen bonds with the proton-accepting methoxy groups of verapamil is that the bile acid molecule must have proton donors. In addition, the absence of an effect of 3,7,12-toC on verapamil confirms in an indirect way the importance of the hydrogen bonds that are formed between the tested drug and 7-oC molecules.

Acknowledgment. This work was supported by the Ministry of Science and Technological Development of the Republic of Serbia (Project No. 23006).

И З В О Д

УТИЦАЈ НАТРИЈУМОВИХ СОЛИ 3α,12α-ДИХИДРОКСИ-7-ОКСО-5β-ХОЛАНСКЕ И 3,7,12-ТРИОКСО-5β-ХОЛАНСКЕ КИСЕЛИНЕ НА ВЕРАПАМИЛ-ХИДРОХЛОРИД У БИОФИЗИЧКО–ХЕМИЈСКИМ МОДЕЛ ЕКСПЕРИМЕНТИМА

МИХАЉ М. ПОША[1], ВАЛЕРИА Ј. ГУЖВАЊ[2], МОМИР М. МИКОВ[1] и ЈАНОШ Ј. ЧАНАДИ[2]

[1]Катедра за фармацију, Медицински факултет, Универзитет у Новом Саду, Хајдук-Вељкова 3, 21000 Нови Сад и [2]Департман за хемију, ПМФ, Универзитет у Новом Саду, Трг Д. Обрадовића 3, 21000 Нови Сад

Познато је да одређене жучне киселине испољавају промоторно деловање на неке лекове. Нарочита пажња се посвећује жучним киселинама код којих су OH групе у стероидном скелету супституисане оксо групама, пошто се код ових деривата смањује хемолтички потенцијал (мембранотоксичност). У раду је испитиван утицај Na-соли 3α,12α-дихидрокси-7--оксо-5β-холанске киселине (7-oC) и 3,7,12-триоксо-5β-холанске киселине (3,7,12-toC) на адсорпцију верапамил-хидрохлорида на активном угљу (модел ћелијске мембране). Праћен је ефекат верапамила на функцију зависности спин-решетка релаксационог времена T_1 (протон C18 ангуларне групе молекула жучне киселине) од концентрације жучне киселине у деутерисаном хлороформу (модел липидне фазе ћелијске мембране). Такође је испитивана могућност појаве депо ефекта верапамила уколико су жучне киселине 7-oC и 3,7,12-toC (у облику метил естра) присутне у хлороформу. Нађено је да значајан ефекат у овим експериментима има само 7-oC, док 3,7,12-toC не показује деловање у односу на контролне вредности испитиваних параметара. Ово указује на то да жучна киселина мора имати OH групе везане за стероидно језгро да би могла испољавати ефекат на физичко-хемијске параметре верапамила.

(Примљено 19. јуна, ревидирано 13. септембра 2010)

REFERENCES

1. M. Calabresi, P. Andreozzi, C. La Mesa, *Molecules* **12** (2007) 1731
2. A. Roda, A. F. Hofmann, K. J. Mysels, *J. Biol. Chem.* **258** (1983) 6362
3. M. Mikov, J. P. Fawcett, *Bile Acids*, Mediset Publisher, Geneva, Switzerland, 2007, p. 178
4. C. Thomas, R. Pellicciari, M. Pruzanski, J. Auwerx, K. Schoonjans, *Nature Rev. Drug Discov.* **7** (2008) 676

5. M. A. Dopico, V. J. Walsh, J. Singer, *J. Gen. Physiol.* **119** (2002) 251
6. C. Bowe, L. Mokhtarzadeh, P. Venkatesen, S. Babu, H. Axelrod, M. J. Sofia, R. Kakarla, T. Y. Chan, J. S. Kim, H. J. Lee, G. L. Amidon, S. Y. Choe, S. Walker, D. Kahne, *Proc. Natl. Acad. Sci. USA* **94** (1997) 12218
7. G. S. Gordon, A. C. Moses, R. D. Silver, J. R. Flier, M. C. Carey, *Proc. Natl. Acad. Sci. USA* **82** (1985) 7419
8. M. Poša, V. Guzsvány, J. Csanádi, S. Kevrešan, K. Kuhajda, *Eur. J. Pharm. Sci.* **34** (2008) 281
9. M. Poša, K. Kuhajda, *J. Serb. Chem. Soc.* **75** (2010) 433
10. M. Poša, K. Kuhajda, *Steroids* **75** (2010) 424
11. B. F. Tullar, US Patent 2 549 947 (1951)
12. L. F. Fieser, S. Rajagopalan, *J. Am. Chem. Soc.* **72** (1950) 5530
13. M. Poša, V. Guzsvány, J. Csanádi, *Colloid Surf. B* **74** (2009) 84
14. M. Poša, V. Guzsvány, J. Csanádi, J. Borbás, F. Gaál, *Acta Chim. Slov.* **56** (2009) 807
15. S. Gouin, X. X. Zhu, *Langmuir* **14** (1998) 4025
16. R. P. Hjelm, P. Thiyagaragan, D. S. Sivia, P. Lindner, H. Alkan, D. Schwahn, *Prog. Colloid Polym. Sci.* **81** (1990) 225
17. J. Wylie-Nichols, J. Ozarowski, *Biochemistry* **29** (1990) 4600
18. M. Poša, S. Kevrešan, M. Mikov, V. Ćirin-Novta, K. Kuhajda, *Colloids Surf. B* **64** (2008) 151
19. D. G. Oakenfull, L. R. Fisher, *J. Phys. Chem.* **81** (1977) 1838
20. D. G. Oakenfull, L. R. Fisher, *J. Phys. Chem.* **82** (1978) 2443
21. B. L. Partay, P. Jedlovszky, M. Sega, *J. Phys. Chem. B.* **111** (2007) 9886.

Journal of the Serbian Chemical Society
JSCS-info@shd.org.rs • www.shd.org.rs/JSCS
J. Serb. Chem. Soc. *76* (2) 201–210 (2011)
JSCS–4112
UDC 547.722+546.17:542.913+547.78+547.861.3:579.8
Original scientific paper

Synthesis and biological activity of 5-nitrofuran-containing (1,3,4-thiadiazol-2-yl)piperazine moieties as a new type of anti-*Helicobacter pylori* heterocycles

MOHAMMAD HASSAN MOSHAFI[1], AZADEH YAHYA-MEYMANDI[2], SEYED ESMAEIL SADAT-EBRAHIMI[2], SAEED EMAMI[3], MARYAM NAKHJIRI[2], FARIDEH SIAVOSHI[4], MARYAM OMRANI[4], MOHSEN VOSOOGHI[2], ESKANDAR ALIPOUR[5], ABBAS SHAFIEE[2] and ALIREZA FOROUMADI[2]*

[1]Department of Pharmaceutical Microbiology, Faculty of Pharmacy, Kerman University of Medical Sciences, Kerman, [2]Department of Medicinal Chemistry, Faculty of Pharmacy and Pharmaceutical Sciences Research Center, Tehran University of Medical Sciences, Tehran, [3]Department of Medicinal Chemistry and Pharmaceutical Sciences Research Center, Faculty of Pharmacy, Mazandaran University of Medical Sciences, Sari, [4]Microbiology Department, Faculty of Sciences, University of Tehran, Tehran and [5]Department of Chemistry, Islamic Azad University, Tehran-North Branch, Zafar St., Tehran, Iran

(Received 24 March, revised 18 October 2010)

Abstract: In order to find new and potent drug candidates for the treatment of *Helicobacter pylori* infections, in this study attention was focused on the synthesis and anti-*H. pylori* activity of a series of 5-(5-nitrofuran-2-yl)-1,3,4-thiadiazoles containing piperazinyl functionality at the C-2 position of the 1,3,4--thiadiazole ring. The synthesis of 1-[5-(5-nitrofuran-2-yl)-1,3,4-thiadiazol-2--yl]piperazine derivatives **3a**–**h** and pyrrolidine derivative **3i** was achieved with a versatile and efficient synthetic route *via* 2-chloro-5-(5-nitrofuran-2-yl)-1,3,4--thiadiazole. The inhibitory activity of the new derivatives **3a**–**i** against twenty clinical *H. pylori* strains was evaluated by the disc diffusion method and compared with the commercially available standard drug metronidazole. Resulting biological data indicated that most compounds exhibited strong inhibitory activity even at doses lower than 2 μg/disc (average zone of inhibition >20 mm) while metronidazole had little or no growth inhibition at this dose. Compound **3c** containing the *N*-benzoylpiperazin-1-yl moiety showed the most potent inhibitory activity.

Keywords: synthesis; 1,3,4-thiadiazole; 5-nitrofuran; antibacterial activity; *Helicobacter pylori*.

* Corresponding author. E-mail: aforoumadi@yahoo.com
doi: 10.2298/JSC100324013M

INTRODUCTION

Helicobacter pylori is considered the major causative bacterium responsible in gastric ulcer, and other gastro-duodenal inflammatory symptoms and complications.[1] Eradication of these pathogens leads to a significant reduction of gastric ulcers, which may also lead to the prevention of mucosa associated lymphoid tissue (MALT) malignancies.[2] Several regimens are arranged under dual, triple and quadruple therapy aiming at higher treatment and eradication rates. The most effective treatment regimens include a combination of antibiotics (beta--lactams, macrolides and quinolones), bactericidal agents (bismuth salts) and antiprotozoal agents (metronidazole).[3,4] The most significant risk factor in the treatment protocols are the emergence of resistant strains.[5] The pattern of local prevalence of antimicrobial resistant strains varies in different regions of the world. There are reports on the activity of furazolidone (a nitrofuran analog) on *H. pylori* strains resistant to metronidazole (a nitroimidazole analog) in Iran and neighboring countries.[6] Thus, the search for new types of nitroheterocyclic compounds, including nitrofurans, is an attractive therapeutic target to find new and potent drug candidates for the treatment of *H. pylori* infections.

Recently, as part of an ongoing research program to find new and potent drug candidates for the treatment of *H. pylori* infection, attention was focused on the synthesis and anti-*H. pylori* activity of a series of 5-(nitroaryl)-1,3,4-thiadiazoles.[7–11] With this point of view and the potent biological activity of 2-(5--nitrofuran-2-yl)-1,3,4-thiadiazoles, the synthetic strategy is now focused on the introduction of a cyclic amine functionality at the C-2 position of the 1,3,4-thiadiazole ring. Accordingly, it was decided to synthesize and evaluate a series of 1-[5-(5-nitrofuran-2-yl)-1,3,4-thiadiazol-2-yl]piperazine derivatives.

RESULTS AND DISCUSSION

Chemistry

The synthesis of 1-[5-(5-nitrofuran-2-yl)-1,3,4-thiadiazol-2-yl]piperazine derivatives **3a**–**h** and the pyrrolidine derivative **3i** was achieved employing a versatile and efficient synthetic route *via* 2-chloro-5-(5-nitrofuran-2-yl)-1,3,4--thiadiazole (**2**) (Scheme 1). The intermediate **2** was prepared from commercially available 5-nitrofurfurylidene diacetate (**1**) according to previously described methods.[12,13] Nucleophilic substitution of the chloro- compound **2** with (un)substituted piperazines in refluxing ethanol afforded compounds **3a** and **3d**–**h** in good yields. Similarly, the reaction of compound **2** with pyrrolidine in refluxing ethanol yielded compound **3i**. *N*-Acetylation of the unsubstituted piperazine derivative **3a** with acetic anhydride produced compounds **3b**. Reaction of piperazine derivative **3a** with benzoyl chloride in benzene/pyridine afforded the *N*-benzoyl piperazine derivative **3c**.

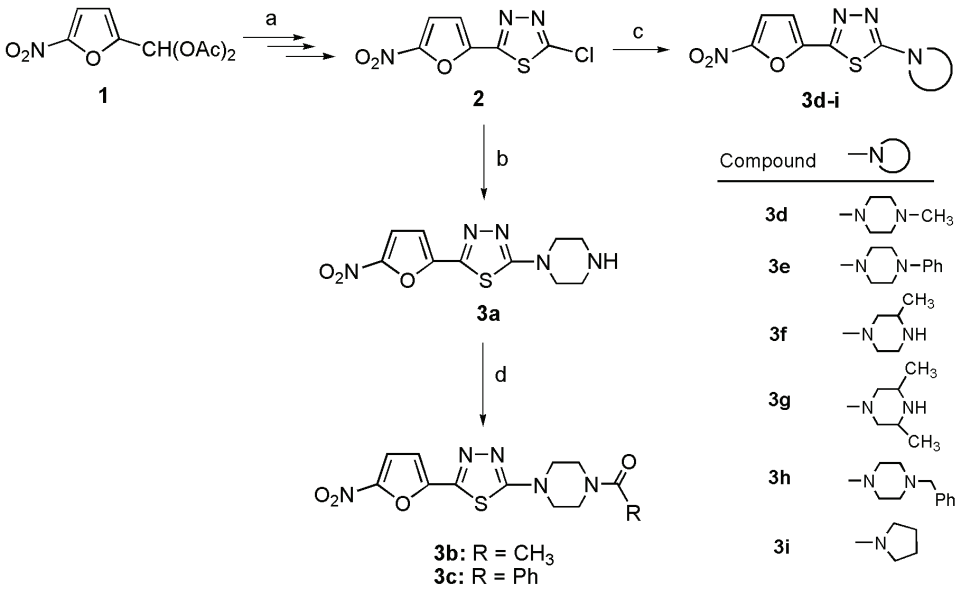

Scheme 1. Synthesis of compounds **3a**–**i**. a) Ref. 11: *i*) thiosemicarbazide, EtOH, reflux, 1h; *ii*) $NH_4Fe(SO_4)_2 \cdot 12H_2O$, H_2O, reflux, 16 h; *iii*) $NaNO_2$, HCl, Cu, 0 °C→r.t, 3 h; b) piperazine, EtOH, reflux, 3h; c) substituted piperazine or pyrrolidine, EtOH, reflux, 2–3 h; d) acetic anhydride, acetic acid, reflux, 20 min, r.t, 12 h; or benzoyl chloride, benzene, pyridine, 24 h.

Analytic and spectral characterization

The structures of compounds **3a**–**i** were confirmed using IR, ^{1}H-NMR and mass spectrometry.

*1-[5-(5-Nitrofuran-2-yl)-1,3,4-thiadiazol-2-yl]piperazine (**3a**)*. Yield: 73 %; m.p.: 214–216 °C; Anal. Calcd. for $C_{10}H_{11}N_5O_3S$: C, 42.70; H, 3.94; N, 24.90 %. Found: C, 42.77; H, 3.80; N, 25.06 %. IR (KBr, cm^{-1}): 3431 (N–H), 1551 and 1347 (NO_2). ^{1}H-NMR (80 MHz. $CDCl_3$, δ / ppm): 7.85 (1H, *d*, 4-H furan, J = = 4.0 Hz), 7.42 (1H, *d*, 3-H furan, J = 4.0 Hz), 3.82–3.30 (5H, *m*, $2CH_2$ and NH piperazine), 3.19–2.99 (4H, *m*, piperazine). MS (*m*/z, %): 281 (M^+, 10), 225 (10), 82 (18), 69 (71), 67 (100).

*1-Acetyl-4-[5-(5-nitrofuran-2-yl)-1,3,4-thiadiazol-2-yl]piperazine (**3b**)*. Yield: 66 %; m.p.: 221–223 °C; Anal. Calcd. for $C_{12}H_{13}N_5O_4S$: C, 44.58; H, 4.05; N, 21.66 %. Found: C, 44.55; H, 3.88; N, 21.53 %. IR (KBr, cm^{-1}): 1664 (C=O), 1556 and 1352 (NO_2). ^{1}H-NMR (80 MHz, $CDCl_3$, δ / ppm): 7.41 (1H, *d*, 4-H furan, J = 4.0 Hz), 7.2 (1H, *d*, 3-H furan, J = 4.0 Hz), 3.95–3.45 (8H, *m*, piperazine), 2.17 (3H, *s*, CH_3). MS (*m*/*z*, %): 323 (M^+, 10), 165 (12), 239 (12), 110 (19), 100 (23), 237 (25), 224 (35), 53 (100).

*1-Benzoyl-4-[5-(5-nitrofuran-2-yl)-1,3,4-thiadiazol-2-yl]piperazine (**3c**)*. Yield: 63 %, m.p.: 225–227 °C; Anal. Calcd. for $C_{17}H_{15}N_5O_4S$: C, 52.98; H, 3.92; N,

18.17 %. Found: C, 53.08; H, 3.90; N, 18.11 %. IR (KBr, cm^{-1}): 1639 (C=O), 1555 and 1362 (NO_2). ^{1}H-NMR (80 MHz, $CDCl_3$, δ / ppm): 7.42 (1H, *d*, 4-H furan, *J* = 4.0 Hz), 7.24 (1H, *d*, 3-H furan, *J* = 4.0 Hz), 7.30–7.10 (5H, *m*, phenyl), 3.95–3.65 (8H, *m*, piperazine). MS (*m*/*z*, %): 385 (M^+, 5), 236 (10), 148 (10), 166 (20), 77 (63), 105 (100).

*1-Methyl-4-[5-(5-nitrofuran-2-yl)-1,3,4-thiadiazol-2-yl]piperazine (**3d**)*. Yield: 46 %; m.p.: 199–202 °C; Anal. Calcd. for $C_{11}H_{13}N_5O_3S$: C, 44.74; H, 4.44; N, 23.71 %. Found: C, 44.80; H, 4.27; N, 23.70 %. IR (KBr, cm^{-1}): 1551 and 1352 (NO_2). ^{1}H-NMR (80 MHz, $CDCl_3$,) *δ* / ppm): 7.45 (1H, *d*, 4-H furan, *J* = 4.0 Hz), 7.15 (1H, *d*, 3-H furan, *J* = 4.0 Hz), 3.80–3.55 (4H, *m*, piperazine), 2.65–2.48 (4H, *m*, piperazine), 2.35 (3H, *s*, N–Me piperazine). MS (*m*/*z*, %): 295 (M^+, 10), 83 (42), 68 (100).

*1-[5-(5-Nitrofuran-2-yl)-1,3,4-thiadiazol-2-yl]-4-phenylpiperazine (**3e**)*. Yield: 42 %; m.p.: 202–205 °C (dec); Anal. Calcd. for $C_{16}H_{15}N_5O_3S$: C, 53.77; H, 4.23; N, 19.60 %. Found: C, 53.94; H, 4.26; N, 19.44 %. IR (KBr, cm^{-1}): 1555 and 1357 (NO_2). ^{1}H-NMR (80 MHz, $CDCl_3$, *δ* / ppm): 7.45 (1H, *d*, 4-H furan, *J* = 4.0 Hz), 7.4–7.2 (5H, *m*, phenyl), 6.98 (1H, *d*, 3-H furan, *J* = 4.0 Hz), 3.94––3.73 (4H, *m*, piperazine), 3.45–3.29 (4H, *m*, piperazine). MS (*m*/*z*, %): 357 (M^+, 8), 77 (6), 161 (9), 143 (22), 102 (60), 132 (100).

*3-Methyl-1-[5-(5-nitrofuran-2-yl)-1,3,4-thiadiazol-2-yl]piperazine (**3f**)*. Yield: 52 %; m.p.: 124–125 °C; Anal. Calcd. for $C_{11}H_{13}N_5O_3S$: C, 44.74; H, 4.44; N, 23.71 %. Found: C, 44.67; H, 4.30; N, 23.64 %. IR (KBr, cm^{-1}): 3421 (N–H), 1556 and 1349 (NO_2). ^{1}H-NMR (80 MHz, $CDCl_3$, *δ* / ppm): 7.42 (1H, *d*, 4-H furan, *J* = 4.0 Hz), 7.15 (1H, *d*, 3-H furan, *J* = 4.0 Hz), 4.05–3.75 (5H, *m*, $2CH_2$ and NH piperazine), 3.28–2.85 (3H, *m*, CH_2 and CH piperazine), 1.16 (3H, *d*, CH_3, *J* = 5.8 Hz). ^{13}C-NMR (125 MHz, $CDCl_3$, *δ* / ppm): 19.3, 45.1, 50.1, 50.5, 57.2, 124.7, 128.8, 140.5, 149.5, 151.6, 172.6. MS (*m*/*z*, %): 295 (M^+, 8), 83 (22), 70 (100).

*3,5-Dimethyl-1-[5-(5-nitrofuran-2-yl)-1,3,4-thiadiazol-2-yl]piperazine (**3g**)*. Yield: 30 %; m.p.: 126–129 °C; Anal. Calcd. for $C_{12}H_{15}N_5O_3S$: C, 46.59; H, 4.89; N, 22.64 %. Found: C, 46.60; H, 5.03; N, 22.71 %. IR (KBr, cm^{-1}): 3431 (N–H), 1549 and 1347 (NO_2). ^{1}H-NMR (80 MHz, $CDCl_3$, *δ* / ppm): 7.40 (1H, *d*, 4-H furan, *J* = 4.0 Hz), 7.47 (1H, *d*, 3-H furan, *J* = 4.0 Hz), 4.05–3.75 (2H, *m*, 2CH piperazine), 3.15–2.75 (5H, *m*, $2CH_2$ and NH piperazine), 1.16 (6H, *d*, $2CH_3$, *J* = 5.8 Hz,). ^{13}C-NMR (125 MHz, $CDCl_3$, *δ* / ppm): 19.2, 50.2, 56.6, 102.3, 113.8, 145.5, 148.5, 153.1, 172.8. MS (*m*/*z*, %): 309 (M^+, 7), 252 (7), 223 (7), 130 (8), 95 (15), 84 (42), 81 (90) ,70 (100).

*1-Benzyl-4-[5-(5-nitrofuran-2-yl)-1,3,4-thiadiazol-2-yl]piperazine (**3h**)*. Yield: 50 %; m.p.: 151–154 °C (dec); Anal. Calcd. for $C_{17}H_{17}N_5O_3S$: C, 54.97; H, 4.61; N, 18.86 %. Found: C, 55.04; H, 4.69; N, 18.72 %. IR (KBr, cm^{-1}): 1547 and 1352 (NO_2). ^{1}H-NMR (80 MHz, $CDCl_3$, *δ* / ppm): 7.44 (1H, *d*, 4-H furan,

J = 4.0 Hz), 7.40–7.20 (5H, *m*, phenyl), 7.14 (1H, *d*, 3-H furan, *J* = 4.0 Hz), 3.80–3.49 (6H, *m*, piperazine and CH_2–Ph), 2.75–2.40 (4H, *m*, piperazine). ^{13}C--NMR (125 MHz, $CDCl_3$, δ / ppm): 50.1, 51.9, 62.8, 124.8, 127.4, 128.4, 128.7, 129.1, 137.3, 140.4, 149.7, 151.6, 172.4. MS (*m*/*z*, %): 371 (M^+, 8), 166 (8), 159 (20), 132 (20), 55 (24), 146 (70), 89 (80), 91 (100).

*2-(5-Nitrofuran-2-yl)-5-pyrrolidin-1-yl-1,3,4-thiadiazole (**3i**)*. Yield: 58 %; m.p.: 247–249 °C; Anal. Calcd. for $C_{10}H_{10}N_4O_3S$: C, 45.11; H, 3.79; N, 21.04 %. Found: C, 45.50; H, 3.61; N, 21.00 %. IR (KBr, cm^{-1}): 1541 and 1349 (NO_2); ^{1}H-NMR (80 MHz, , δ / ppm): 7.40 (1H, *d*, 4-H furan, *J* = 4.0 Hz), 7.15 (1H, *d*, 3-H furan, *J* = 4.0 Hz), 3.88–3.38 (4H, *m*, pyrrolidine), 2.35–1.93 (4H, *m*, pyrrolidine). ^{13}C-NMR (125 MHz, $CDCl_3$, δ / ppm): 25.7, 51.1, 109.9, 113.9, 144.5, 148.9, 153.1, 169.1. MS (*m*/*z*, %): 266 (M^+, 50), 147 (6), 132 (15), 237 (15), 114 (30), 192 (39), 100 (39), 70 (100).

Anti-Helicobacter pylori *activity*

The growth inhibitory activity of the nitrofuran derivatives **3a**–**i** against *H. pylori* was evaluated using the paper disc diffusion method.[14,15] The diameters of the inhibition zone of title compounds were compared with the commercially available antibacterial metronidazole. Different doses of the compounds were loaded on standard discs (6 mm diameter), which were then placed on a Muller––Hinton agar plate, previously inoculated with bacterial suspension. After incubation for 3–5 days at 37 °C, the inhibition zone around each disc was recorded. All tests were performed in triplicate and the antibacterial activity is given as the mean of inhibition diameters (mm) produced by the title compounds. The compounds **3a**–**i** were initially evaluated against three *H. pylori* strains at a high dose of 32 μg/disc and the results are summarized in Table I. Generally, the antibacterial activity of compounds can be classified as follows: strong response, zone diameter >20 mm; moderate response, zone diameter 16–20 mm; weak response, zone diameter 11–15 mm; and little or no response, zone diameter <10 mm. The results given in Table I revealed that all the synthesized nitrofuran analogs **3a**–**i**, exhibited strong antimicrobial activity against *H. pylori* strains at a dose of 32 μg/disc (inhibition zone diameter >20 mm).

Due to the strong inhibitory activity of compounds **3a**–**i** at 32 μg/disc, all compounds were further tested at the doses lower than 32 μg/disc against a broader panel of *H. pylori* strains (twenty clinical isolates). The antibacterial activities of the target compounds at doses of 16, 8, 4, 2, 1, 0.5 and 0.25 μg/disc against 20 clinical isolates of *H. pylori* are given in Table II as the average diameters of the inhibition zones.

The inhibition zone diameters of compounds at different doses indicate that all compounds exhibit higher inhibitory activity against the clinical isolates of *H. pylori* compared to the standard drug, metronidazole. The inhibition zone dia-

meters of all compounds were on average more than 20 mm at 8 μg/disc, which is greater than that of metronidazole. Compounds **3a**–**d** showed strong growth inhibitory activity at doses of 4 and 2 μg/disc, while metronidazole had very weak activity at these doses. The *N*-benzoylpiperazine derivative **3c** had strong activity even at 0.5 μg/disc (inhibition zone = 20 mm). The inhibition zone diameters at the lowest dose (0.25 μg/disc), indicated that the *N*-acetyl and *N*-benzoyl compounds (**3b** and **3c**, respectively) still had a weak growth inhibition while the remaining compounds showed little or no activity at this dose.

TABLE I. *In vitro* antibacterial activity of compounds **3a**–**i** at 32 μg/disc against *H. pylori* using the disc diffusion method

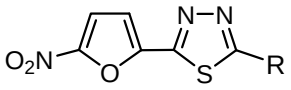

Compound	R	Inhibition zone diameter[a], mm (range)
3a	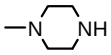	50 (44–60)
3b	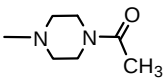	45.3 (45–48)
3c	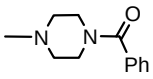	42.6 (44–47)
3d	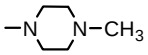	48.6 (47–51)
3e	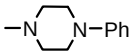	23 (19–33)
3f	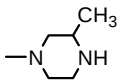	42 (42–44)
3g	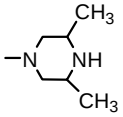	41 (40–46)
3h	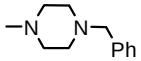	28 (25–31)
3i		46 (46–48)

[a]The anti-*Helicobacter pylori* activity was determined by the paper disc diffusion bioassay. All tests were performed in triplicate and the antibacterial activity is expressed as the mean of the inhibition diameters produced by the title compounds

The comparison of inhibition zone diameters produced by title compounds revealed that substitution of piperazine moiety by *N*-phenyl, *N*-benzyl, 3-methyl and 3,5-dimethyl diminished the inhibitory activity against clinical isolates of *H. pylori*. In contrast, *N*-benzoylation of the piperazine ring increased the anti-*H.*

pylori activity. In addition, the introduction of *N*-methyl or *N*-acetyl groups on the piperazine ring did not improve the antibacterial activity against *H. pylori*.

TABLE II. Inhibition zone diameters of compounds **3a–i** at different doses against 20 clinical *H. pylori* isolates. Antibacterial activities are expressed as the mean of inhibition zone diameters (mm). Range of inhibition zone diameters against 20 clinical *H. pylori* isolates are given in parenthesis

Compound	Concentration, μg/disc						
	0.25	0.5	1	2	4	8	16
3a	7.9 (6–10)	12.6 (6–15)	17.9 (11–30)	23.8 (14–40)	29. 6 (17–50)	33. 6 (21–57)	43.5 (28-60)
3b	11.8 (6–19)	16.7 (6–22)	19.7 (14–30)	23.1 (15–50)	29.7 (15–60)	34.8 (20–60)	40.4 (24–60)
3c	15.1 (6–20)	20.1 (11–30)	24.1 (14–30)	28.8 (11–43)	35.2 (18–49)	41.2 (20–55)	49.1 (34–60)
3d	8.2 (6–11)	14.8 (6–20)	18.1 (10–28)	22.9 (14–38)	28.2 (15–60)	34.1 (21–60)	40.6 (30–60)
3e	6.5 (6–9)	7.6 (6–10)	12.3 (6–16)	17.3 (10–30)	18.4 (11–40)	21.4 (12–40)	23.9 (15–41)
3f	6 (6)	7.1 (6–10)	8.5 (6–10)	13.0 (6–20)	19.3 (8–30)	23.1 (12–37)	30.8 (18–50)
3g	6 (6)	8.4 (6–15)	12.7 (6–16)	17.8 (15–22)	20.7 (15–25)	20.5 (15–25)	21.5 (18–25)
3h	7.7 (6–9)	11.1 (6–17)	15.2 (8–20)	19.8 (6–28)	22.6 (10–26)	23.5 (15–30)	24.8 (18–30)
3i	6.7 (6–9)	8.5 (6–12)	13.2 (6–17)	19.9 (12–26)	25.3 (18–33)	33.3 (24–39)	38.1 (26–49)
Metronidazole	6	6	9.2 (4–21)	13.1 (6–19)	16.0 (8–26)	19.8 (11–27)	24.1 (17–32)

EXPERIMENTAL

The purity of the synthesized compounds was confirmed by thin layer chromatography (TLC) using various solvents of different polarities. Merck silica gel 60 F254 plates were applied for the analytical TLC. Melting points were measured using a Kofler hot-stage apparatus and are uncorrected. The IR spectra were obtained on a Shimadzu 470 (Shimadzu, Tokyo, Japan) spectrophotometer (potassium bromide disks). Nuclear magnetic resonance spectra were determined in $CDCl_3$ containing TMS as an internal standard using Bruker 80 or 500 spectrometers. The mass spectra were recorded on a Finnigan MAT TSQ-70 spectrometer at 70 eV. Elemental analyses were realized on a CHN-O-rapid elemental analyzer (Heraeus GmbH, Hanau, Germany) for C, H and N, and the results were within ±0.4 % of the theoretical values. All reagents were purchased from Merck and Aldrich and used as such without purification. The solvents employed in the reactions were previously distilled.

General procedure for the synthesis of 1-[5-(5-nitrofuran-2-yl)-1,3,4 thiadiazol-2-yl]piperazine derivatives

To a mixture of 2-chloro-5-(5-nitrofuran-2-yl)-1,3,4-thiadiazole (**2,** 231 mg, 1.0 mmol) in ethanol (15 ml), appropriate substituted piperazine (1.0 mmol) was added and refluxed for 3 h.

The completion of reaction was monitored by TLC. After cooling, the separated solid was filtered off and re-crystallized from ethanol.

*Synthesis of 1-acetyl-4-[5-(5-nitrofuran-2-yl)-1,3,4-thiadiazol-2-yl]piperazine (**3b**)*

Acetic anhydride (3 ml) was added to a mixture of 1-[5-(5-nitrofuran-2-yl)-1,3,4-thiadiazol-2-yl]piperazine (**3a**, 280 mg, 1.0 mmol) in acetic acid (12.5 ml) and refluxed for 20 min. The mixture was stirred at room temperature overnight and then poured in to ice-water. The yellow precipitate was separated and washed with water and crystallized from ethanol to give pure compound **3b**.

*Synthesis of 1-benzoyl-4-[5-(5-nitrofuran-2-yl)-1,3,4-thiadiazol-2-yl]piperazine (**3c**)*

Benzoyl chloride (70.5 mg, 0.5 mmol) was added under stirring to a suspension of 1-[5--(5-nitrofuran-2-yl)-1,3,4-thiadiazol-2-yl] piperazine (**3a**, 140 mg, 0.5 mmol) in benzene (1 ml) and pyridine (0.5 ml) at 0–5 °C and then, the reaction mixture was stirred at room temperature for 24 h. After evaporation of solvents under reduced pressure, the residue was washed with water and crystallized from ethanol to give compound **3c**.

*Synthesis of 2-(5-nitrofuran-2-yl)-5-pyrrolidin-1-yl-1,3,4-thiadiazole (**3i**)*

A mixture of 2-chloro-5-(5-nitrofuran-2-yl)-1,3,4-thiadiazole (**2**, 231 mg, 1.0 mmol) and pyrrolidine (70 mg, 1.0 mmol) in ethanol (10 ml) was refluxed for 1 h. After completion of the reaction, the orange precipitate was filtered and crystallized from ethanol.

CONCLUSIONS

In this study, attention was focused on the synthesis and anti-*Helicobacter pylori* activity of a series of 5-(5-nitrofuran-2-yl)-1,3,4-thiadiazoles containing a piperazinyl functionality at the C-2 position of the 1,3,4-thiadiazole ring. The synthesis of the 1-[5-(5-nitrofuran-2-yl)-1,3,4-thiadiazol-2-yl]piperazine derivatives **3a**–**h** and the pyrrolidine derivative **3i** was achieved using a versatile and efficient synthetic route *via* 2-chloro-5-(5-nitrofuran-2-yl)-1,3,4-thiadiazole. Based on the resulting biological data, compound **3c** containing the *N*-benzoyl-piperazin-1-yl moiety showed the most potent inhibitory activity against *H. pylori* strains. The potent activity and straightforward synthesis of these nitrofurans suggest that they are potential candidates for the development of new anti-*H. pylori* agents.

Acknowledgments. This work was supported by grants from the Research Council of Tehran University of Medical Sciences and the Iran National Science Foundation (INSF).

ИЗВОД

СИНТЕЗА И БИОЛОШКА АКТИВНОСТ 5-НИТРОФУРАНА, КОЈИ САДРЖЕ (1,3,4-ТИАДИАЗОЛ-2-ИЛ)ПИПЕРАЗИНСКУ СТРУКТУРУ, КАО НОВИ ТИП АНТИ-*Helicobacter pylori* ХЕТЕРОЦИКЛА

MOHAMMAD HASSAN MOSHAFI[1], AZADEH YAHYA-MEYMANDI[2], SEYED ESMAEIL SADAT-EBRAHIMI[2], SAEED EMAMI[3], MARYAM NAKHJIRI[2], FARIDEH SIAVOSHI[4], MARYAM OMRANI[4], MOHSEN VOSOOGHI[2], ESKANDAR ALIPOUR[5], ABBAS SHAFIEE[2] и ALIREZA FOROUMADI[2]

[1]Department of Pharmaceutical Microbiology, Faculty of Pharmacy, Kerman University of Medical Sciences, Kerman, [2]Department of Medicinal Chemistry, Faculty of Pharmacy and Pharmaceutical Sciences Research Center, Tehran University of Medical Sciences, Tehran, [3]Department of Medicinal Chemistry and Pharmaceutical Sciences Research Center, Faculty of Pharmacy, Mazandaran University of Medical Sciences, Sari, [4]Microbiology Department, Faculty of Sciences, University of Tehran, Tehran u [5]Department of Chemistry, Islamic Azad University, Tehran-North Branch, Zafar St., Tehran, Iran

У циљу проналажења новог ефикасног лека за лечење од инфекција изазваних *Helicobacter pylori* нашу пажњу усмерили смо према синтези и испитивању анти-*H. pylori* активности серије 5-(5-нитрофуран-2-ил)-1,3,4-тиадиазола који садрже пиперазинилни структурни фрагмент у положају C-2 1,3,4-тијадиазолског прстена. Синтеза деривата 1-[5-(5-нитрофуран-2-ил)-1,3,4-тиадиазол-2-ил]пиперазина **3a**–**h** и пиролидинског деривата **3i** постигнута је преко интермедијера 2-хлор-5-(5-нитрофуран-2-ил)-1,3,4-тиадиазола. Користећи диск-дифузиону методу испитана је инхибиторна активност нових деривата **3a**–**i** према двадесет клиничких сојева *H. pylori* и извршено је поређење добијених резултата са резултатима активности метронидазола, комерцијалног стандарда. Добијени резултати показују да већина једињења показује јаку инхибиторну активност чак и при дозама мањим од 2 μg/диск (просечна зона инхибиције је >20 mm), док метронидазол показује малу инхибицију или потпуно одсуство инхибиције при истим дозама. Највећу инхибицију показује једињење **3c** које садржи *N*-бензоилпиперазин-1-ил фрагмент.

(Примљено 24. марта, ревидирано 18. октобра 2010)

REFERENCES

1. A. L. Blum, *Scand. J. Gastroenterol.* **31** (1996) 24
2. F. Chimenti, B. Bizzarri, A. Bolasco, D. Secci, P. Chimenti, S. Carradori, A. Granese, D. Rivanera, D. Lilli, A. Zicari, M. M. Scaltrito, F. Sisto, *Bioorg. Med. Chem. Lett.* **17** (2007) 3065
3. P. Malfertheiner, F. Megraud, C. O'Morain, F. Bazzoli, E. El Omar, D. Graham, R. Hunt, T. Rokkas, N. Vakil, E. J. Kuipers, *Gut* **56** (2007) 772
4. C. W. Howden, R. H. Hunt, *Am. J. Gastroenterol.* **93** (1998) 2330
5. A. Zullo, F. Perna, C. Hassan, C. Ricci, I. Saracino, S. Morini, D. Vaira, *Aliment. Pharmacol. Ther.* **25** (2007) 1429
6. N. Ebrahimi-Dariani, S. Mirmomen, F. Mansour-Ghanaei, P. Noormohammadpoor, R. Sotodehmanesh, B. Haghpanah, H. Bahrami, *Med. Sci. Monit.* **9** (2003) 105
7. A. Foroumadi, A. Rineh, S. Emami, F. Siavoshi, S. Massarrat, F. Safari, S. Rajabalian, M. Falahati, E. Lotfali, A. Shafiee, *Bioorg. Med. Chem. Lett.* **18** (2008) 3315
8. M. H. Moshafi, M. Sorkhi, S. Emami, M. Nakhjiri, A. Yahya-Meymandi, A. S. Negahbani, F. Siavoshi, M. Omrani, E. Alipour, M. Vosooghi, A. Shafiee, A. Foroumadi, *Arch. Pharm. Chem. Life Sci.* (2010), doi: 10.1002/ardp.201000013

9. N. Mohammadhosseini, B. Letafat, F. Siavoshi, S. Emami, F. Safari, A. Shafiee, A. Foroumadi, *Med. Chem. Res.* **17** (2008) 578
10. A. Foroumadi, M. Sorkhi, M. H. Moshafi, M. Safavi, A. Rineh, F. Siavoshi, A. Shafiee, S. Emami, *Med. Chem.* **5** (2009) 529
11. B. Letafat, S. Emami, A. Aliabadi, N. Mohammadhosseini, M. H. Moshafi, A. Asadipour, A. Shafiee, A. Foroumadi, *Arch. Pharm. Chem. Life Sci.* **341** (2008) 497
12. A. Foroumadi, M. Daneshtalab, A. Shafiee, *Arzneim.-Forsch./Drug Res.* **49** (1999) 1035
13. E. Alipour, S. Emami, A. Yahya-Meymandi, M. Nakhjiri, F. Johari, S. K. Ardestani, F. Poorrajab, M. Hosseini, A. Shafiee, A. Foroumadi, *J. Enzyme Inhib. Med. Chem.* **26** (2011) 123
14. J. Mirzaie, F. Siavoshi, S. Emami, F. Safari, M. R. Khoshayand, A. Shafiee, A. Foroumadi, *Eur. J. Med. Chem.* **43** (2008) 1575
15. A. Fallah-Tafti, T. Akbarzadeh, P. Saniee, F. Siavoshi, A. Shafiee, A. Foroumadi, *Turk. J. Chem.* (2010), doi: 10.3906/kim-1004-522.

Journal of the Serbian Chemical Society
JSCS-info@shd.org.rs • www.shd.org.rs/JSCS
J. Serb. Chem. Soc. *76* (2) 211–220 (2011)
JSCS–4113
UDC **Haberlea rhodopensis*:577.121:57–188
Original scientific paper

GC–MS profiling of bioactive extracts from *Haberlea rhodopensis*: an endemic resurrection plant

STRAHIL H. BERKOV[1], MILENA T. NIKOLOVA[2], NEVENA I. HRISTOZOVA[3], GEORGI Z. MOMEKOV[4], ILIANA I. IONKOVA[4] and DIMITAR L. DJILIANOV[1]*

[1]*AgroBio Institute, 8 Dragan Tzankov Blvd., 1164-Sofia,* [2]*Institute of Botany, Bulgarian Academy of Sciences, 23 Acad. G. Bonchev Str., 1113-Sofia,* [3]*Faculty of Biology, Sofia University, 8 Dragan Tzankov Blvd., 1164-Sofia and* [4]*Faculty of Pharmacy, Medical University of Sofia, 2 Dunav Str., 1000- Sofia, Bulgaria*

(Received 24 March, revised 6 July 2010)

Abstract: GC–MS metabolic profiling of the apolar and polar fractions from methanolic extracts of *Haberlea rhodopensis* revealed more than one hundred compounds (amino acids, fatty acids, phenolic acids, sterols, glycerides, saccharides, *etc*.). Bioactivity assays showed that the polar fractions possessed strong free radical scavenging activity (IC_{50} = 19.95±14.11 μg ml^{-1} for fresh leaves and 50.04±23.16 μg ml^{-1} for desiccated leaves), while both the polar and apolar fractions failed to provoke any significant cytotoxic effects against the tested cell lines. Five compounds possessing antiradical activity were identified – syringic, vanillic, caffeic, dihydrocaffeic and *p*-coumaric acids.

Keywords: *Haberlea rhodopensis*; metabolites; free radical scavenging activity.

INTRODUCTION

Haberlea rhodopensis Friv. is a very rare Balkan endemite belonging to the group of extremely desiccation-tolerant (ressurection) plants which are capable of withstanding long periods of almost full desiccation and to recover quickly on water availability.[1,2] Carbohydrates and phenols were found to play an important role in the survival of plants under extreme conditions.[3] Phenolic compounds, accumulated in high amounts in ressurection plants, are assumed to protect the membranes against desiccation and free radical-induced oxidation.[4,5]

Ethnobotanical data that *Haberlea* leaves were used for the treatment of wounds and diseases of stock in the Rhodope region of Bulgaria stimulated our interest in this plant species. Similarly, *Myrothamnus flabelifolia*, a desiccation--tolerant plant accumulating gallotannins, is used in traditional folklore and medicine in southern Africa due to its wound-healing properties.[5] Alcoholic extracts

* Corresponding author. E-mail: d_djilianov@abi.bg
doi: 10.2298/JSC100324024B

of *H. rhodopensis* were found to possess strong antioxidant and antimicrobial activities.[6,7] Preliminary phytochemical studies indicated that this plant contains flavonoids, tannins and polysaccharides,[7] in addition to previously reported lipids[8] and saccharides.[3]

The aim of the present study was to perform metabolic profiling of this resurrection plant in parallel with antioxidant and cytotoxicity activity assays in an attempt to make a preliminary evaluation of its potential for application in phytotherapy.

EXPERIMENTAL

Plant material

Micropropagated plants, obtained by an *in vitro* propagation system developed in our laboratory,[9] were used in this study to avoid possible damage of natural habitats and problems resulting from handling material of unknown age, size and stage of plant growth. The plants were maintained routinely in culture rooms under a 16/8 h light/dark photoregime, at 22 °C with a light intensity of 75 μmol m^{-2} s^{-1}. The micropropagated *Haberlea* plants possess the same resurrection behaviour as plants taken from natural habitats.[6] Leaves from well-developed plantlets (about 3 months in culture) were taken out from the culture vessels and left to dry to the full air-dried stage in a culture room under controlled conditions (22–25 °C and 60 % relative humidity in the dark) or lyophilized to obtain the desiccated and fresh leaf samples, respectively.

Sample preparation

For metabolite analysis, 50 mg (DW) of leaf samples were macerated in 500 μl of methanol in Eppendorf tubes. 20 μl of nonadecanoic acid (C19:0, 2 mg ml^{-1}) and ribitol (2 mg ml^{-1}) were added as internal standards and the material was extracted for 30 min at 70 °C. Subsequently, 500 μl of chloroform was added and the material was extracted for a further 5 min at room temperature with vortex. Then, 300 μl of distilled water was added and the extract was centrifuged at 13,000 rpm for 10 min to separate the apolar and polar fraction. 300 μl aliquots of the polar and apolar fractions were dried by lyophilisation. Dried polar and apolar fractions were dissolved in 50 μl of pyridine and derivatized with *N*,*O*-bis(trimethylsilyl)-trifluoroacetamide (BSTFA, 50 μl) for 90 min at 40 °C. The derivatized extracts were dissolved in 100 μl chloroform and injected into the GC–MS system. BSTFA and pyridine were purchased from Sigma-Aldrich (St. Louis, MO, USA).

For the bioactivity assays, about 420 mg of dry plant material was extracted in a similar manner to the above-described method, using 4 ml of both methanol and chloroform and 2.5 ml of water to obtain the polar and apolar fractions. No internal standards were added.

GC–MS analyses

The GC–MS analyses were performed on a Hewlett Packard 7890 instrument coupled with MSD 5975 equipment (Hewlett Packard, Palo Alto, CA, USA) operating in EI mode at 70 eV. An HP-5 MS column (30 m×0.25 mm×0.25 μm) was used. The temperature programme was: 100–180 °C at 15 °C min^{-1} and 180–300 °C at 5 °C min^{-1} with a 10 min hold at 300 °C. Injector temperature was 250 °C. The flow rate of the carrier gas (helium) was 0.8 ml min^{-1}. A split ratio of 1:20 was used for the injection of 1 μl of the solutions.

Metabolites identification

The compounds contained in the polar and apolar fractions were identified as TMS derivatives with the help of the NIST 05 database (NIST Mass Spectral Database, PC-Version 5.0 – 2005, National Institute of Standardization and Technology, Gaithersburg, MD, USA), and other plant-specific databases: the Golm Metabolome Database (http://csbdb.mpimp-golm.mpg.de/ /csbdb/gmd/home/gmd_sm.html) and the lipid library (http://www.lipidlibrary.co.uk/ms/ ms01/ /index.htm), as well as literature data[10] based on the matching of the mass spectra and the Kovats retention indexes (*RI*). A syringic acid standard, purchased from Sigma-Aldrich (St. Louis, MO, USA), was co-chromatographed for confirmation of the major phenolic acid in the polar fraction. The measured mass spectra were deconvoluted using AMDIS 2.64 software before comparison with the databases. The groups of unidentified compounds were determined based on the specific mass spectral fragmentation and in comparison with the mass spectra of the known metabolites. All unknown compounds, comprising more than 0.1 % of the TIC (total ion current), were used to calculate the relative contribution of each metabolite group. The response ratios were calculated for each analyte relative to the internal standard (ribitol for the polar and nonadecanoic acid for the apolar metabolites) using the calculated areas for both components. The *RI* values of the compounds were measured with a standard *n*-hydrocarbon calibration mixture (C9–C36) (Restek, Cat No. 31614, supplied by Teknokroma, Spain) using AMDIS 2.64 software.

Determination of the free radical scavenging activity

The stable radical 1,1-diphenyl-2-picrylhydrazyl (DPPH) was used for the determination of the free radical scavenging activity of the extracts.[11] Different concentrations of the extracts (5, 10, 20, 50, 100 and 200 μg mL^{-1} in methanol) were added to an equal volume (2.5 mL) of a methanolic solution of DPPH$^{\bullet}$ (0.3 mM, 1 mL). After 30 min at room temperature, the *Ab* values were measured at 517 nm using a Jenway 6320D spectrophotometer and converted into the percentage antioxidant activity using the following equation: DPPH$^{\bullet}$ anti-radical scavenging capacity (%) = 100((*Ab*(sample) – *Ab*(blank)×100/*Ab*(control)). Methanol (1.0 mL) plus plant extract solution (2.5 mL) was used as the blank, while DPPH$^{\bullet}$ solution plus methanol was used as the control. The extracts were measured in triplicate on two different days. The results are presented as the mean±standard error of IC_{50}.

Cytotoxic activity

The cell lines used in this study, namely HL-60 (acute myelocyte leukaemia), its multi--drug resistant sub-line HL-60/Dox, SKW-3 (KE-37 derivative) (T-cell leukaemia), and MDA-MB-231 (breast cancer), were purchased from the German Collection of Microorganisms and Cell Cultures (DSMZ GmbH, Braunschweig, Germany). They were cultured under standard conditions – RPMI-1640 liquid medium supplemented with 10 % foetal bovine serum (FBS) and 2 mM L-glutamine, in cell culture flasks, housed at 37 °C in an incubator "BB 16-Function Line" Heraeus (Kendro, Hanau, Germany) with a humidified atmosphere and 5 % CO_2. The cell cultures were maintained in the logarithmic growth phase by supplementation with fresh medium two or three times weekly. The mdr-phenotype of HL-60/Dox was maintained by culturing cells in the presence of 0.2 μM doxorubicin. In order to avoid synergistic interactions, HL-60/Dox were maintained in an anthracycline-free medium (90 % RPMI 1640, 10 % FCS) for at least 72 h prior to the cell viability experiments.

Cellular viability after exposure to the tested compounds was assessed using the standard MTT-dye reduction assay as described by Mosmann[12] with some modifications.[13] The method is based on the reduction of the yellow tetrazolium dye MTT to a violet formazan pro-

duct *via* mitochondrial succinate dehydrogenase in viable cells. The exponentially growing cells were seeded in 96-well flat-bottomed microplates (100 μl well^{-1}) at a density of 1×10^5 cells per ml and after 24 h incubation at 37 °C, they were exposed to various concentrations of the tested compounds for 72 h. At least 8 wells were used for each concentration. After the incubation with the test compounds, 10 μl MTT solution (10 mg ml^{-1} in PBS) aliquots were added to each well. The microplates were further incubated for 4 h at 37 °C, after which the formed MTT-formazan crystals were dissolved by adding 100 μl well^{-1} of 5 % HCOOH-acidified 2-propanol. The MTT-formazan absorption was determined at 580 nm using a microprocessor-controlled microplate reader (Labexim LMR-1). Cell survival fractions were calculated as percentage of the untreated control.

Data processing and statistics

The cell survival data were normalized as percentage of the untreated control (set as 100 % viability). The IC_{50} values (concentrations causing 50 % scavenge of the DPPH$^{\bullet}$) were calculated using non-linear regression analysis (GraphPad Prism Software). The statistical processing of the biological data included the Student's *t*-test, whereby values of $p \leq 0.05$ were considered as statistically significant.

RESULTS AND DISCUSSION

The free radical scavenging activity assays (Table I) showed that the polar fractions of both desiccated and fresh samples possessed strong antioxidant activity; the fraction from the desiccated leaves being more active ($p < 0.05$). Mainly saccharides, as well as organic acids, phenolic acids, phosphate-containing compounds and amino acids, showing high levels of biological variability[14] were found by GC–MS (Table II). The total amounts of disaccharides and trisaccharides were about two-times more in the samples obtained from the desiccated as compared to those from the fresh samples (Table III). The amounts of phosphate-containing compounds tended to decrease in the desiccated leaves, while glycerides, mainly glycerol, increased. There were no detectable changes in the total amount of amino acids.

TABLE I. Free radical scavenging activity of *H. rhodopensis* fractions

Fractions of *H. rhodopensis*	$IC_{50}\pm SE$ / μg ml^{-1}
Polar fraction of desiccated leaves	19.95±3.42[b]
Polar fraction of fresh leaves	50.04±3.44[b]
Apolar fraction of desiccated leaves	>200
Apolar fraction of fresh leaves	>200
Quercetin[a]	3.23±0.39
Syringic acid[a]	4.40±0.37

[a]Reference compound; [b]significantly different at $p < 0.05$

The antiradical activity of plant extracts may be explained by the presence of phenolic compounds.[15,16] Five free phenolic acids were detected in these fractions, with syringic acid dominating (**46**, more than 86 % of all the free phenolic acids) (Tables II and III). This compound was reported to be a potent antioxidant,

effectively inhibiting linoleic acid (fatty acid) peroxidation.[15] The concentration of syringic acid and of the other free phenolic compounds were found to be about 3-times less ($p < 0.05$) in the desiccated (2.8 % of the total ion current, TIC) than in the fresh leaves (7.8 % of the TIC) of *H. rhodopensis.* Similar results concerning the total phenolic acids were reported for *Ramonda serbica*, another resurrection plant. The predominant phenolic compounds found in *R. serbica*, however, were protocatechuic and chlorogenic acids.[4]

TABLE II. Metabolites found in *H. rhodopensis* fractions; identification: Golm database, NIST05, the lipid library, Madeiros and Simoneit[10] and standard; results represent the means±*SE* of the response ratios of measurements on 3 different fractionations from different samples (50 mg). The response ratios represent peak area ratios using ribitol (40 μg) for polar and nonadecanoic acid (40 μg) for apolar metabolites as quantitative internal standards

Compound	M^+/base ion	R_t min	Apolar fraction		Polar fraction	
			Fresh leaves	Desiccated samples	Fresh leaves	Desiccated samples
Glycolic acid (**1**)	205[a]/147	3.69	–	–	0.1±0.1	tr
L-Valine (**2**)	174/72	3.77	–	–	tr	0.1±0.03
Lactic acid (**3**)	234[a]/147	4.35	–	–	tr	tr
Phosphoric acid methyl ester (**4**)	256/241	4.76	–	–	tr	tr
Malonic acid (**5**)	248/147	4.98	–	–	tr	
4-Hydroxybutanoic acid (**6**)	233[a]/147	5.29	–	–	tr	tr
L-Serine (**7**)	–/132	5.54	–	–	tr	tr
Hydrocarbon – branched (**8**)	–/57	4.96	0.2±0.2	0.1±0.02	–	–
Glycerol (**9**)	293[a]/147	5.71	1.5±0.6	1.0±0.3	0.6±0.1	4.1±4.2
Phosphoric acid (**10**)	314/299	5.75	9.4±3.5	4.9±2.5	8.2±3.2	3.4±0.5
Succinic acid (**11**)	262/147	6.07	0.1±0.1	tr	2.0±1.0	0.5±0.1
Hydrocarbon – branched (**12**)	–/71	6.16	0.6±0.4	0.2±0.1		
2,3-Dihydroxypropanoic acid (**13**)	307/147	6.28	–	–	0.5±0.4	tr
UC (**14**)	–/145	6.32	2.9±0.4	–	–	–
Fumaric acid (**15**)	–/245	6.39	–	–	0.1±0.1	tr
3,4-Dihydroxyl-2-furanone (**16**)	262/147	6.71	–	–	0.3±0.1	tr
Hydrocarbon – branched (**17**)	–/57	7.03	0.4±0.01	0.3±0.1	–	–
Hexadecane (**18**)	–/57	7.31	0.3±0.2	0.2±0.1	–	–
Hydrocarbon – branched (**19**)	–/57	7.39	0.5±0.3	0.2±0.2	–	–
Hydrocarbon – branched (**20**)	–/71	7.51	0.2±0.1	tr	–	–
Hydrocarbon – branched (**21**)	–/71	7.72	3.4±2.8	1.2±0.3	–	–
Malic acid (**22**)	335[a]/147	7.73	0.5±0.3	0.3±0.03	10.4±5.5	4.0±0.7
Erythritol (**23**)	–/217	7.97	–	–	0.7±0.5	0.2±0.1
UC[b] (**24**)	–/355	8.62	1.9±0.5	–	–	–
Glutamine (**25**)	363/246	9.13	0.1±0.1	–	–	–
UC (**26**)	–/220	9.2	–	–	18.1±9.2	6.8±1.6
Xylonic acid (**27**)	364/217	9.34	–	–	4.0±3.0	7.8±1.8
UC (**28**)	–/355	9.34	1.9±0.2	–	–	–
Dodecanoic acid (**29**)	272/257	9.4	0.2±0.2	0.2±0.03	–	–
UM (**30**)	–/220	10.09	–	–	2.4±2.0	0.4±0.1

TABLE II. Continued

Compound	M^+/base ion	R_t min	Apolar fraction		Polar fraction	
			Fresh leaves	Desiccated samples	Fresh leaves	Desiccated samples
Hydrocarbon – branched (**31**)	–/71	10.1	2.2±1.7	0.9±0.1	–	–
UM (**32**)	–/218	10.15	–	–	15.5±18.2	0.2±0.2
UM (**33**)	–/205	10.32	–	–	5.1±1.9	0.2±0.03
Vanillic acid (**34**)	312/297	10.97	–	–	1.0±0.5	0.3±0.3
UM (**35**)	–/292	11.01	–	–	26.5±10.1	25.0±13.3
Ribonic acid (**36**)	511/292	11.05	–	–	23.4±5.4	22.7±3.0
Glycerol phosphate (**37**)	445/357	11.12	13.7±1.0	4.4±0.6	tr	0.7±0.4
UM (**38**)	–/217	11.34	–	–	4.6±2.9	2.0±0.9
Glucofuranose (**39**)	–/217	11.64	–	–	5.9±2.6	0.8±0.3
Fructose I (**40**)	–/217	11.81	–	–	10.2±2.2	6.6±3.8
Phytol I (**41**)	–/95	11.88	7.5±4.4	2.8±0.8	–	–
Fructose II (**42**)	–/217	11.94	–	–	11.5±2.8	5. 5±2.5
Tetradecanoic acid (**43**)	300/285	12.12	0.9±0.4	0.3±0.1	–	–
Fructose III (**44**)	–/204	12.28	–	–	6.0±3.0	1.0±0.4
UM (**45**)	–/217	12.36	–	–	14.2±5.6	2.7±1.1
Syringic acid (**46**)	342/327	12.94	4.3+0.9	8.8±4.2	43.8±10.5	24.9±2.6
Hydrocarbon – branched (**47**)	–/71	13.14	1.2±1.2	0.6±0.1	–	–
Glucose (**48**)	–/204	13.28	–	–	6.7±3.3	3.6±1.9
Caffeic acid (**49**)	396/293	13.5	–	–	0.1±0.1	tr
Dihydrocaffeic acid (**50**)	398/179	13.7	–	–	5.4±2.1	2.1±1.5
Ascorbic acid (**51**)	464/332	13.94	–	–	0.4±0.4	0.1±0.2
9-Hexadecenoic acid (**52**)	326/117	14.64	0.1±0.1	0.1±0.03	–	–
Hexadecanoic acid (**53**)	328/313	15.04	16.0±6.2	10.8±1.3	–	–
UC (**54**)	397/218	15.18	0.8±0.4	–	–	–
Heptadecanoic acid (**55**)	342/327	16.18	0.3±0.1	0.3±0.1	–	–
p-Coumaric acid (**56**)	396/396	16.7	–	–	0.4±0.2	0.1±0.1
Phytol II (**57**)	–/143	17.15	1.5±0.2	0.8±0.1	–	–
9.12-Octadecadienoic acid (**58**)	352/337	17.68	2.5±1.5	1.6±0.9	–	–
9-Octadecenoic acid (**59**)	354/339	17.78	1.9±0.7	2.3±0.8	–	–
UC (glyceride) (**60**)	402/314	17.9	12.0±7.3	7.3±0.2	–	–
Octadecanoic acid (**61**)	356/341	18.19	5.7±0.6	6.2±1.3	–	–
UC (Polyolphosphate) (**62**)	602/587	18.31	25.1±2.0	7.0±2.9	–	–
Uridine (**63**)	445[a]/217	21.76	–	–	–	0.2±0.02
2-Hexadecanoylglycerol (**64**)	459[a]/218	23.16	0.3±0.2	0.1±0.1	–	–
UD (**65**)	–/217	23.32	–	–	7.1±1.3	tr
UD (**66**)	–/361	23.44	–	–	72.9±14.4	183.2±52.0
1-Hexadecanoylglycerol (**67**)	459[a]/371	23.66	2.7±1.0	3.2±0.5	–	–
?UD (**68**)	–/361	23.78	–	–	67.7±19.4	59.3±24.1
?UD (**69**)	–/217	24.1	–	–	8.4±5.1	tr
?UD (**70**)	–/217	24.38	–	–	59.9±16.0	168.3±60.3
?UD (**71**)	–/361	24.48	–	–	21.9±9.6	32.9±32.3
?UD (**72**)	–/217	24.55	–	–	9.6±5.9	2.4±0.5
?UD (**73**)	–/217	24.7	–	–	14.3±1.0	7.1±12.9
?UD (**74**)	–/217	24.85	–	–	0.8±0.6	tr

TABLE II. Continued

Compound	M^+/base ion	R_t min	Apolar fraction		Polar fraction	
			Fresh leaves	Desiccated samples	Fresh leaves	Desiccated samples
UD (**75**)	–/361	25.07	–	–	11.0±7.1	55.5±30.0
UD (**76**)	–/361	25.18	–	–		47.3±59.5
Sucrose (**77**)	–/361	25.26	–	–	40.1±15.7	160.3±61.4
UD (**78**)	–/217	25.74	–	–	0.8±0.5	tr
UD (**79**)	–/191	25.85	–	–	1.0±0.7	2.0±1.8
1-Octadecanoylglycerol (**80**)	487[a]/399	26.39	3.6±1.2	4.5±0.7	0.9±0.6	1.0±0.2
Squalene (**81**)	409/69	26.83	0.4±0.1	0.4±0.1	–	–
Tetracosanoic acid (**82**)	440/425	26.99	0.1±0.1	0.1±0.1	–	–
UC(glycerol) (**83**)	530/193	29.14	27.9±0.2	21.9±4.4	–	–
UT (**84**)	–/217	30.27			1.1±0.4	0.7±0.2
Tocopherol (**85**)	502/502	31.05	7.0±2.9	6.2±1.0	–	–
Cholesterol (**86**)	458/329	31.15	1.2±0.4	1.9±0.3	–	–
UC(glycerol) (**87**)	558/133	31.57	27.6±6.1	24.3±0.6	–	–
Campestrol (**88**)	472/382	32.45	9.2±1.1	10.1±1.4	–	–
Stigmasterol (**89**)	484/83	32.82	0.6±0.1	0.6±0.3	–	–
UT (**90**)	–/217	33.46	–	–	6.7±2.4	13.8±5.3
UT (**91**)	–/217	33.57	–	–	10.8±2.5	11.9±2.1
β-Sitosterol (**92**)	486/396	33.6	39.4±5.2	41.4±4.3	–	–
UC (**93**)	396/381	33.79	–	–	4.4±3.0	0.7±0.7
UT (**94**)	–/361	33.83	–	–	–	26.2±22.1
UT (**95**)	–/217	34.33	–	–	14.9±10.9	29.8±6.1
UT (**96**)	–/217	34.75	–	–	3.0±1.4	4.2±3.8
UT (**97**)	–/217	35.18	–	–	3.7±2.4	6.9±1.9
UT (**98**)	–/217	35.42	–	–	7.8±5.7	21.4±12.9
UT (**99**)	–/217	35.81	–	–	9.8±2.4	33.4±33.4
UT (**100**)	–/361	35.97	–	–	10.8±7.3	24.9±7.1
Raffinose (**101**)	–/361	36.21	–	–	22.7±6.1	15.0±3.2
UT (**102**)	–/217	36.61	–	–	5.0±2.9	5.3±3.3
UT (**103**)	–/217	37.04	–	–	3.0±0.8	–
UC-diglyceride (**104**)	–/129	38.36	16.0±1.6	9.6±7.7	–	–
Total	–	–	255.6± ±39.7	187.0± ±12.3	648.1± ±114.4	1034.8± ±305.15

[a][M-15]$^+$; [b]compounds with "U" are unknown

As compared to desiccated leaves, the higher concentration of free phenolic acids in the fresh leaves is not in correlation with their lower antiradical activity, which indicates that other unidentified compounds contribute to the antiradical activity of the polar fractions. The presence of flavonoids and tannins was reported for *H. rhodopensis*[6] but, due to the limitations of GC–MS, such compounds were not detected in the present study.

The apolar fraction of the methanolic extract showed relatively weak antioxidant activity (Table I). This fraction consisted of glycerides (29 and 33 % of TIC of the fresh and desiccated samples, respectively), sterols (20 and 29 %,

respectively), phosphate-containing compounds (19 and 9 %, respectively), free fatty acids (11 and 12 %, respectively), polyenes (6%), phenolic acids and hydrocarbons. The relatively weaker antioxidant activity could be explained by the presence of small amounts of α-tocopherol and free phenolic acids.

TABLE III. Main groups of compounds in the extracts of *H. rhodopensis*; the results represent the means±*SE* of the response ratios and % of TIC (total ion current) of the measurements on 3 different fractionations from different samples (50 mg). The response ratios represents peak area ratios using ribitol (40 μg) for polar and nonadecanoic acid (40 μg) for apolar metabolites as quantitative internal standards

Compound	Apolar fraction				Polar fraction			
	Fresh leaves		Desiccated leaves		Fresh leaves		Desiccated leaves	
	Response ratio	% of TIC	Response ratio	% of TIC	Response ratio	% of TIC	Response ratio	% of TIC
Hydrocarbons	8.8±6.9	3.2	3.7±1.0	2.0	–	–	–	–
Phosphates	48.1±6.4	18.9	16.3±6.0	8.6	8.3±3.2	1.3	4.0±0.8	0.4
Organic acids	0.7±0.3	0.3	0.3±0.1	0.2	40.9±15.9	6.21	35.3±5.8	3.6
Phenolic acids	4.3±0.9	1.7	8.8±4.2[a]	4.6	50.6±13.4	7.8	27.4±4.4[a]	2.8
Fatty acids								
Saturated	23.2±7.6	8.9	17.8±2.8	9.5	–	–	–	–
Unsaturated	4.5±2.2	1.7	4.0±1.7	2.1	–	–	–	–
Polyenes	16.4±7.7	6.48	10.3±2.0	5.5	–	–	–	–
Glycerides	74.1±16.0	29.3	61.2±6.5	32.7	1.5±0.7	0.2	5.0±4.4	0.6
Sterols	50.4±6.8	20.0	54.0±6.3	28.8	–	–	–	–
Amino acids	–	–	–	–	0.1±0.003	0.02	0.1±0.1	0.01
Saccharides								
Mono-	–	–	–	–	109.7±55.2	17.0	48.3±24.6	4.6
Di-	–	–	–	–	315.2±106.7	48.8	720.5±334.8	70.0
Tri-	–	–	–	–	99.2±45.0	15.4	184.8±101.4	17.2
Syringic acid	4.3±0.9	1.7	8.8±4.2	4.6	43.8±10.5	6.7	24.9±2.6[a]	2.5

[a]Significantly different at $p < 0.05$

The polar and apolar fractions of *H. rhodopensis* were screened for their cytotoxic activity against a panel of four human tumour cell lines, representative for some important types of neoplastic diseases, including a multi-drug resistant cell line (Table IV). Both tested fractions failed to evoke any significant cytotoxic effects against any of the cell lines.

TABLE IV. Cytotoxic effects of the polar and apolar fractions of *H. rhodopensis* after 72 h continuous exposure (MTT-dye reduction assay); each value represents the arithmetic mean± ±*SE* from 8 independent experiments

Concentration mg/ml	HL-60 cells		HL-60/Dox cells		SKW-3 cells		MDA-MB-231 cells	
	Hc 30[a]	*Hc* 70[b]	*Hc* 30	*Hc* 70	*Hc* 30	*Hc* 70	*Hc* 30	*Hc* 70
0.00	100±2	100±2	100±7	100±7	100±2	100±2	100±5	100±2
0.10	103±2	101±2	103±3	100±3	101±3	95±6	100±3	100±3

TABLE IV. Continued

Concentration	HL-60 cells		HL-60/Dox cells		SKW-3 cells		MDA-MB-231 cells	
mg/ml	*Hc* 30	*Hc* 70	*Hc* 30	*Hc* 70	*Hc* 30	*Hc* 70	*Hc* 30	*Hc* 70
0.20	101±1	100±3	99±3	95±7	100±2	97±4	97±3	99±4
0.25	102±2	104±2	114±6	104±3	106±6	99±3	111±7	102±3
0.40	95±4	99±3	94±6	94±4	93±7	96±4	96±6	94±7
0.50	102±2	107±4	109±6	102±5	107±4	97±4	103±2	102±5

[a]Polar fractions; [b]apolar fractions

CONCLUSIONS

In conclusion, the polar fractions of *H. rhodopensis* showed potent free radical scavenging activity. GC–MS metabolic profiling of the polar and apolar fractions resulted in the detection of more than one hundred compounds, including several phenolic acids. In depth quantitative analysis of the phenolic complex (free and conjugated phenolic acids, flavonoids and polyphenols), however, is needed to reveal the relationship between antiradical activity and metabolites in the extracts of *H. rhodopensis*. The lack of any cytotoxic activity of the extracts indicates that the plant may be used in phytotherapy for its antiradical properties. In this respect, the desiccated leaves of *H. rhodopensis* are more suitable due to their higher antiradical activity.

Acknowledgment. Financial support from Ministry of Education and Science, Sofia, Bulgaria (Grant D002-128/08 I. Ionkova) is acknowledged.

ИЗВОД

ГАСНОМАСЕНА АНАЛИЗА БИОЛОШКИ АКТИВНИХ ЕКСТРАКАТА ЕНДЕМСКЕ БИЉКЕ *Haberlea rhodopensis*

STRAHIL H. BERKOV[1], MILENA T. NIKOLOVA[2], NEVENA I. HRISTOZOVA[3], GEORGI Z. MOMEKOV[4], ILIANA I. IONKOVA[4] и DIMITAR L. DJILIANOV[1]

[1]AgroBio Institute, 8 Dragan Tzankov Blvd., 1164-Sofia, [2]Institute of Botany, Bulgarian Academy of Sciences, 23 Acad. G. Bonchev Str., 1113-Sofia, [3]Faculty of Biology, Sofia University, 8 Dragan Tzankov Blvd., 1164-Sofia и [4]Faculty of Pharmacy, Medical University of Sofia, 2 Dunav Str., 1000-Sofia, Bulgaria

Гасномасена анализа поларних и неполарних метаболита биљке *Haberlea rhodopensis* изолованих екстракцијом метанолом детектовала је више од сто једињења (амино-киселина, масних киселина, фенолних киселина, стерола, глицерида, сахарида, итд.). Тестови за одређивање биолошке активности су показали да поларне фракције имају изражену активност према слободним радикалима (IC_{50} = 19,95±14,11 μg ml^{-1} за свеже листове и 50,04±23,16 μg ml^{-1} за осушене листове), док ни поларне ни неполарне фракције нису испољиле значајне цитотоксичне ефекте на тестираним ћелијским линијама. Пет једињења са антирадикалском активношћу је идентификовано: сирингинска, ванилинска, кофеинска, дихидрокофеинска и *p*-кумаринска киселина.

(Примљено 24. марта, ревидирано 6. јула 2010)

REFERENCES

1. J. Markovska, T. Tsonev, G. Kimenov, A. Tutekova, *J. Plant Physiol.* **144** (1994) 100
2. K. Georgieva, S. Lenk, C. Buschmann, *Photosynthetica* **46** (2008) 208
3. J. Muller, N. Sprenger, K. Bortlik, T. Boiler, A. Wiemken, *Physiol. Plant.* **100** (1997) 153
4. C. Sgherri, B. Stevanovic, F. Navari-Izzo, *Physiol. Plant.* **122** (2004) 478
5. J. Moore, K. Westall, N. Ravenscroft, J. Farrant, G. Lindsey, W. Brandt, *Biochem. J.* **385** (2005) 301
6. I. Ionkova, S. Ninov, I. Antonova, D. Moyankova, T. Georgieva, D. Djilianov, *Pharmazija* **1–4** (2009) 22
7. R. Radev, G. Lazarova, P. Nedialkov, K. Sokolova, D. Rukanova, Z. Tsokeva, *Trakia J. Sci.* **7** (2009) 34
8. K. Stefanov, Y. Markovska, G. Kimenov, S. Popov, *New Chem.* **31 (**1992) 2309
9. D. Djilianov, G. Genova, D. Parvanova, N. Zapryanova, T. Konstantinova, A. Atanassov, *Plant Cell Tissue Organ Cult.* **80** (2005) 115
10. P. Medeiros, B. Simoneit, *J. Chromatogr. A* **1141** (2007) 271
11. C. Cimpoiu, *J. Liq. Chromatogr. Relat. Technol.* **29** (2006) 1125
12. T. Mosmann, *J. Immunol. Met.* **65** (1983) 55
13. S. Konstantinov, H. Eibl, M. Berger, *Br. J. Haematol.* **107** (1999) 365
14. U. Roessner, C. Wagner, J. Kopka, R. Trethewey, L. Willmitzer, *Plant J.* **23** (2000) 131
15. F. Liu, T. Ng, *Life Sci*. **66** (2000) 725
16. D. Szwajgier, J. Pielecki, Z. Targonski, *Acta Sci. Pol.* **4** (2005) 129.

Journal of the Serbian Chemical Society
JSCS-info@shd.org.rs • www.shd.org.rs/JSCS
J. Serb. Chem. Soc. *76* (2) 221–233 (2011)
JSCS–4114
UDC 546.77–31+547.298.61:543.57:542.9+547.571+547.551
Original scientific paper

Synthesis and characterization of oxomolybdenum(V) and dioxomolybdenum(VI) complexes derived from *N*'-(2-hydroxy-3-methoxybenzylidene)isonicotinohydrazide

MADHAVAN NAIR LEKSHMY HARIKUMARAN NAIR* and DEVAKIAMMA THANKAMANI

Department of Chemistry, University College, Thiruvananthapuram-695 034, India

(Received 8 February, revised 23 August 2010)

Abstract: Several novel complexes of oxomolybdenum(V) and dioxomolybdenum(VI) were synthesized with the Schiff base, *N*'-(2-hydroxy-3-methoxybenzylidene)isonicotinohydrazide (HL) derived from 3-methoxysalicylaldehyde and isonicotinohydrazide. The complexes were characterized by elemental analyses, molar conductance and magnetic susceptibility, as well as IR, ^{1}H-NMR, FAB mass and UV–Vis spectral studies. The complexes have the general formulae [MoO(L)XCl] and [MoO_2(L)X], where X=NO_3 or ClO_4. The IR spectra of these complexes indicate that the ligand HL acts as a monoanionic tridentate chelating agent. The spectra indicate the monodentate mode of coordination for the nitrate and perchlorate groups. The X-ray diffraction studies of [MoO(L)NO_3Cl] correspond to an orthorhombic crystal lattice with unit cell dimensions a = 15.49 Å, b = 12.44 Å and c = 10.11 Å. All the complexes were found to have distorted octahedral geometry. Thermal studies of the complex [MoO_2(L)NO_3] showed that it was stable up to 240 °C, above which it started to decompose. The optimized geometry of ligand and one of its complexes, [MoO(L)NO_3Cl], have been obtained by a molecular mechanics method. Antibacterial studies of the present complexes show that the oxomolybdenum(V) complexes were more potent bactericides than the ligand and the dioxomolybdenum(VI) complexes.

Keywords: oxomolybdenum(V); dioxomolybdenum(VI); 3-methoxysalicylaldehyde isonicotinoylhydrazone; thermal analysis; 3D modelling.

INTRODUCTION

Coordination chemistry of molybdenum still engages the attention of researchers due to the chemistry of its oxidation state, coordination number, ligating atom, their impact on structure, reactivity and because of the potential

* Corresponding author. E-mail: drmlhnair@gmail.com
doi: 10.2298/JSC100208009N

applications of molybdenum compounds.[1–8] Molybdenum is a biologically important trace metal that occurs in the redox-active sites of molybdo-enzymes involved in nitrogen, carbon or sulphur metabolism. Molybdenum is a micronutrient for microorganisms, plants and animals. The biochemical importance of molybdenum is due to its ability a) to provide facile electron-transfer pathways, a consequence of the easy inter-convertibility of the different oxidation states and b) to form bonds with nitrogen-, oxygen-, and sulphur-donors, which are sufficiently strong to permit the existence of stable complexes but also sufficiently labile to permit facile ligand exchange reactions or changes in the molybdenum co-ordination number. Hydrazones derived from isonicotinohydrazide and their complexes have applications in various fields, such as biological, analytical and pharmacological areas and are reported to have lower toxicity than the hydrazide.[9,10]

In view of the versatile importance of hydrazones and molybdenum, the synthesis, characterization, thermal behaviour, and biological and 3D molecular modelling studies of some nitrate and perchlorate complexes of oxomolybdenum(V) and dioxomolybdenum(VI) species with a Schiff base (HL), derived from 3-methoxysalicylaldehyde and isonicotinohydrazide are reported herein.

EXPERIMENTAL

Materials and methods

Molybdenum pentachloride (Alfa Aesar, Lancaster) and molybdenum trioxide (Loba Chemie, Mumbai, India) were used. All other chemicals were of A R grade.

Synthesis of the ligand (HL)

The Schiff base ($C_{14}H_{13}N_3O_3$) (Fig. 1) was prepared[1] by mixing methanolic solutions of 3-methoxysalicylaldehyde (0.05 mol, 50 mL) and isonicotinohydrazide (0.05 mol, 50 mL) and refluxing the mixture for ≈30 min. The pale yellow solid which separated was filtered, washed with methanol and dried. The purity of the ligand was monitored by TLC. It was characterized by elemental analysis, IR, UV and ^{1}H-NMR spectroscopy. Yield: 70 %; m.p. 260 °C; Anal. Calcd. for $C_{14}H_{13}N_3O_3$: C, 61.99; H, 4.83; N, 15.49 %. Found: C, 61.50; H, 4.95; N, 15.24 %. ^{1}H-NMR (300 MHz, DMSO-d_6, δ / ppm): 12.27 (1H, *s*, –OH), 10.74 (1H, *s*, –NH), 8.70 (1H, *s*, CH=N), 3.97 (3H, *s*, –OCH_3), 6.85–8.9 (7H, *m*, aromatic H).

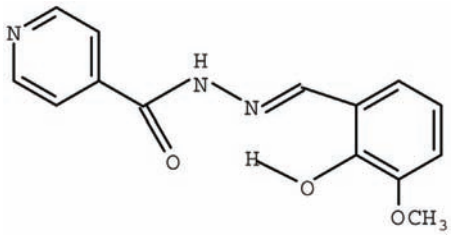

Fig. 1. Structural formula of the ligand (HL).

Synthesis of the oxomolybdenum(V) complexes

The following general method was adopted for the preparation of the complexes.[11] A methanolic solution of $MoCl_5$ (2 mmol, 20 mL) containing ≈0.3 g $LiNO_3$/2–3 drops of perchloric acid as the case may be, was added to a hot methanolic solution of the ligand (2 mmol, 20mL). The pH of the mixture was adjusted to ≈4 with NaOAc/HOAc buffer. The complexes precipitated on refluxing the solution for 20–30 min. The precipitated complexes were suction filtered, washed with aqueous methanol (1:1) followed by dry diethyl ether and dried over P_4O_{10} *in vacuo.*

Synthesis of the dioxomolybdenum(VI) complexes

The dioxomolybdenum(VI) complexes were prepared by adding, dropwise a solution of MoO_3 (2 mmol, 20 mL) in hot conc. HCl (2 mL) containing ≈0.3 g $LiNO_3$/2–3 drops of perchloric acid to a methanolic solution of the ligand (2 mmol, 20 mL) under constant stirring. The complexes precipitated on refluxing the solution for 0–30 min. The separated solid was suction filtered, washed with aqueous methanol, then with diethyl ether and dried over P_4O_{10} *in vacuo.*

Metal, chloride and perchlorate were estimated by standard methods.[12] The elemental analyses (C, H and N) were realised at the Sophisticated Test and Instrumentation Centre (STIC), Kochi, India. The IR spectra (KBr, cm^{-1}) of the ligand and the complexes were recorded in the region 4000–400 cm^{-1} on a Perkin-Elmer 397 spectrophotometer. The room temperature molar conductances of the complexes in DMF were recorded on an Elico direct reading conductivity meter at a concentration of ≈10^{-3} M. The electronic absorption spectral measurements of the complexes in methanol were measured using a Jasco-V-550-UV-Vis spectrophotometer. The ^{1}H-NMR spectra of the ligand and the complexes were recorded on a 300 MHz FT-NMR instrument using TMS as the reference. The FAB mass spectrum of $[MoO_2(L)NO_3]$ was recorded in a JEOL JMS600H mass spectrometer. Thermal analysis of the complex $[MoO_2(L)NO_3]$ was performed by heating in air at a rate of 10 °C/min on a Mettler TG-50 thermobalance. The X-ray powder diffraction patterns were recorded using a Philips X-ray PW1710 diffractometer. The magnetic susceptibilities were recorded at room temperature by the Gouy method. Diamagnetic corrections for various atoms and structural units were computed using Pascal's constants.[13]

Antibacterial activity

The ligand, HL, and the complexes were screened *in vitro* for their possible antibacterial activities against *Salmonella typhi* MTCC734, *Pseudomonas aeruginosa* MTCC 2642, *Escherichia coli 585*, *Proteus vulgaris* 177, *Bacillus subtilis* 2248 and *Streptococcus thermophilus* 1938 using the disc diffusion method (Kirby Bauer Method).[14]

All the plates were allowed to air dry under sterile conditions and swabbed with the pure culture of the bacteria on the Mueller Hinton Agar (MHA) plates (100 mm). The already prepared sterile discs (6 mm) impregnated with the studied compounds were aseptically placed above the seeded plates using sterile forceps. A disc was also used in pure chloroform to provide a control. The plates were incubated for 24 h at 37 °C and the zones of inhibition caused by the antibiotic compounds against the bacteria were measured in millimetres.

RESULTS AND DISCUSSION

All the four complexes were coloured, non-hygroscopic solids, which were stable in air. They were sparingly soluble in common organic solvents, such as acetone and chloroform, and completely soluble in methanol, DMF and DMSO.

The analytical and spectroscopic data (Tables I and II, respectively) showed that all the complexes were mononuclear with the general formulae [MoO(L)ClX] and [MoO_2(L)X], where X = ClO_4 or NO_3. The low conductance values[15] of the chelates support the non-electrolytic nature of the complexes. The magnetic susceptibility values of the oxomolybdenum(V) complexes at room temperature were close to the spin-only value (1.73 μ_B) of oxomolybdenum(V) species. This shows the absence of Mo–Mo interaction[16] in these complexes. Due to Mo=O in oxomolybdenum(V) complexes, strong tetragonal distortion may occur and this causes a slight reduction in the magnetic moment values. All the dioxomolybdenum(VI) complexes were found to be diamagnetic, as expected for d^0 systems.

TABLE I. Analytical data of the complexes

Complex[a]	Yield %	Found (Calc.), %					Λ_M S cm^2 mol^{-1}	μ_{eff} μ_B
		Mo	C	H	N	Cl		
[MoO(L)NO_3Cl]	72	20.35 (20.00)	35.64 (35.06)	2.64 (2.52)	11.82 (11.68)	7.94 (7.39)	42	1.70
[MoO(L)ClO_4Cl]	65	18.36 (18.55)	32.86 (32.52)	2.43 (2.3)	8.42 (8.13)	13.98 (13.7)	54	1.69
[MoO_2(L)NO_3]	78	20.58 (20.85)	36.79 (36.54)	2.72 (2.63)	12.41 (12.17)	–	45	–
[MoO_2(L)ClO_4]	67	19.47 (19.28)	34.11 (33.79)	2.21 (2.43)	8.32 (8.44)	7.34 (7.12)	56	–

[a]L = $C_{14}H_{12}N_3O_3$

TABLE II. IR spectral data in cm^{-1} of the ligand and the complexes (abbreviations as in Table I)

Complexes	$\nu_{N–H}$	$\nu_{C=O}$	$\nu_{C=N}$	$\nu_{C–O}$	$\nu_{N–N}$	$\nu_{M=O}$ (sym)	$\nu_{M=O}$(asym)
HL	3201	1670	1626	1317	998	–	–
[MoO(L)NO_3Cl]	3205	1640	1600	1337	1026	945	–
[MoO(L)ClO_4Cl]	3205	1650	1601	1341	1018	945	
[MoO_2(L)NO_3]	3205	1637	1604	1338	1022	945	902
[MoO_2(L)ClO_4]	3202	1636	1604	1339	1024	955	920

IR spectra

In order to study the binding mode of the Schiff base to the metal in the complexes, the IR spectrum of the free ligand was compared with the spectra of the complexes. Important infrared spectral bands of the ligand and complexes and their tentative assignments are given in Table II. In all complexes, the keto-form of the ligand coordinates through the carbonyl oxygen and the azomethine nitrogen as evidenced by the shift of $\nu_{C=O}$ and $\nu_{C=N}$ to lower frequencies.[17,18] The coordination through the azomethine nitrogen atom was further supported by the shift of the $\nu_{N–N}$ vibration observed at 998 cm^{-1} in the ligand to a higher frequency in the complexes by ≈20 cm^{-1}.[17] This is due to a reduction of lone pair repulsive forces in the adjacent nitrogen atoms.[19] The deprotonated OH group

was also involved in the coordination. This is supported by the disappearance of the free ligand bands at 3438 and 1353 cm^{-1} due to the phenolic OH groups. The intense ligand band at 1317 cm^{-1}, due to phenolic C–O, was also shifted to ≈1340cm^{-1}, which further supports the same conclusion.[1]

The dioxomolybdenum(VI) complexes displayed two Mo=O stretching bands at 945–955 cm^{-1} and 900–920 cm^{-1} due to the symmetric and antisymmetric stretching of the *cis*-MoO_2^{2+} core.[20] The MoO_2^{2+} prefers to form the *cis* configuration due to the maximum utilization of the dπ groups. A very strong band observed at ≈940 cm^{-1} in the spectra of oxidomolybdenum(V) complexes corresponds to the Mo=O stretching frequency.[21] New weak bands at ≈550 cm^{-1} and at ≈460 cm^{-1} in the metal complexes are assigned to the ν_{Mo-O} and ν_{Mo-N} modes, respectively.[22]

The IR spectra of the nitrate complexes suggest monocoordination of the nitrate group (ν_4, 1530 cm^{-1}; $\nu_1 \approx 1380$ cm^{-1} and $\nu_2 \approx 1034$ cm^{-1}). For the perchlorate complexes, two bands (split bands), observed at ≈1114 and ≈1060 cm^{-1}, are assigned to ν_4 and ν_1. The bands at ≈640 and ≈620 cm^{-1} can be assigned, respectively, to ν_3 and ν_5 of monodentately coordinated perchlorate group. The medium intensity absorption band expected at ≈925 cm^{-1} in the spectra of the complexes cannot be located because of ligand vibrations in this region.[23]

^{1}H-NMR spectra

The ^{1}H-NMR spectra of HL and $[MoO_2(L)NO_3]$ were recorded in DMSO-d_6. The signal at δ 12.27 ppm in the spectrum of the ligand disappeared because of complexation, suggesting coordination through the deprotonated phenolic oxygen. Presence of a sharp singlet at δ 10.8 ppm in the complex indicates that the ligand exists in the keto-form. The signal at δ 8.7 ppm of the ligand was shifted to 9.1 ppm, indicating coordination of azomethine nitrogen in the complexes. The methoxy protons and the seven aromatic protons of the ligand and complex appeared at nearly the same positions.[1]

Electronic spectra

The electronic spectra of the tridentate ONO donor hydrazone ligand and the oxomolybdenum(V) complexes were recorded in methanol. The electronic spectrum of the ligand showed intense bands at 246 and 298 nm. Similar bands of lower intensity were observed at 362 and 377 nm. These bands are assigned to π→π*and n→π* transitions, respectively.[24] They suffered considerable shifts in intensity and wavelength on coordination.

The electronic spectra of the $[MoO(L)NO_3Cl]$ and$[MoO(L)ClO_4Cl]$ complexes are characterized by strong absorption bands in the UV region at ≈230 nm and at ≈270 nm and less intense bands at ≈320 nm and at ≈370 nm. The latter bands may be assigned to metal–ligand charge transfer, possibly superposed by ligand n→π*transitions.[25]

The electronic spectra of octahedral oxomolybdenum (V) complexes usually exhibit three distinct bands in the regions 690–740 nm, 520–450 nm and 380––440 nm, assignable to $^2B_2 \rightarrow {}^2E$ ($d_{xy} \rightarrow d_{xz}$, d_{yz}), $^2B_2 \rightarrow {}^2B_1$ ($d_{xy} \rightarrow d_{x^2-y^2}$) and $^2B_2 \rightarrow {}^2A_1$ ($d_{xy} \rightarrow d_{z^2}$) transitions, respectively.[26] In the present study, [MoO(L)NO_3Cl] showed a medium intensity band at ≈459 nm and a weak broad band at ≈660 nm. The corresponding bands for [MoO(L)ClO_4Cl] were at ≈468 nm and at ≈665 nm. However, the third band was not observed in these complexes, probably due to masking by the low energy tail of the much more intense charge-transfer transitions O(π)→d(Mo), involving the excitation of an electron from the highest filled MO associated with oxygen to the d-orbital of Mo. The electronic spectra indicate an octahedral environment for all the complexes and are in conformity with the Ballhausen-Gray scheme for octahedral geometry.[27]

FAB mass spectra

The FAB mass spectrum of the complex [MoO_2(L)NO_3] showed the characteristic molecular ion peak at *m*/*z* = 459.91 (M^+), which corresponds to the molecular weight of the complex. The other important peaks are due to the formation of various fragments,[28] such as $(M–OCH_3)^{+\bullet}$, $(M–NO_3)^{+\bullet}$, $(C_6H_5N_2O)^{\bullet}$, $(C_8H_7NO_2)^+$, $(C_{14}H_{12}N_3O_3)^+$, etc.

X-Ray diffraction studies

The complex [MoO(L)NO_3Cl] was found to be orthorhombic by the X-ray powder diffraction method and was indexed (Fig. 2 and Table III) using the Hesse and Lipson procedure.[29] The lattice constants were found to be: *A* =

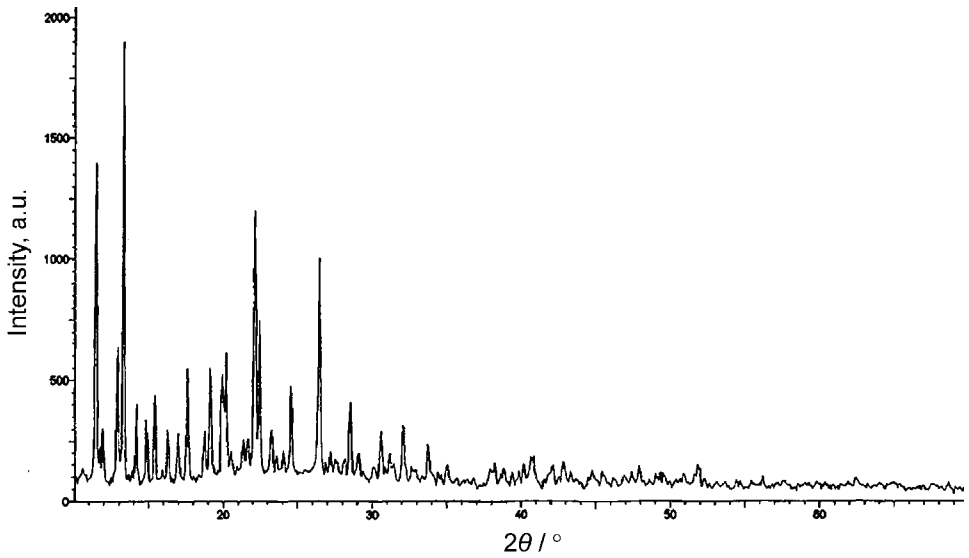

Fig. 2. X-ray diffractions pattern of [MoO(L)NO_3Cl].

= 0.0024742, B = 0.003831 and C = 0.0058091, and the unit cell dimensions were a = 15.49 Å, b = 12.44 Å and c = 10.11 Å.

TABLE III. X-Ray diffraction data of $[MoO(L)NO_3Cl]$ (abbreviations as in Table I)

Line	$\sin^2\theta$ (obs)	$\sin^2\theta$ (Calcd.)	Intensity
1	0.008556	0.008274	3.89
2	0.009895	0.009897	61.85
3	0.012502	0.012114	22.19
4	0.013376	0.013728	100.00
5	0.01517	0.015324	18.27
6	0.01786	0.017798	21.21
7	0.020004	0.019537	13.51
8	0.021666	0.021133	10.48
9	0.023298	0.023236	26.69
10	0.027576	0.027067	26.04
11	0.030131	0.029541	19.05
12	0.036596	0.036953	59.2
13	0.040336	0.040288	13.01
14	0.045135	0.045505	24.45
15	0.052209	0.052282	51.19
16	0.060592	0.607210	19.27
17	0.062755	0.062823	7.64
18	0.067307	0.067606	5.03
19	0.069485	0.069579	13.21
20	0.072426	0.071193	5.53
21	0.076238	0.077002	15.16
22	0.079404	0.079876	4.06
23	0.084189	0.084532	9.77
24	0.090387	0.089387	5.54
25	0.105813	0.105672	4.23
26	0.109906	0.109029	3.02
27	0.120846	0.121486	6.20
28	0.128667	0.129894	4.98
29	0.133522	0.137322	4.08
30	0.144992	0.145228	3.33
31	0.149316	0.149059	3.06
32	0.164578	0.167796	5.30
33	0.174162	0.175434	2.56
34	0.184266	0.182820	3.53
35	0.191142	0.191195	4.54
36	0.221449	0.228308	2.89
37	0.267035	0.263271	1.55
38	0.308593	0.302859	1.08

Thermal studies

Thermal behaviour of the $[MoO_2(L)NO_3]$ complex was studied by non-isothermal thermogravimetric, TG, and differential TG, DTG, analyses by heating

the sample in air at a rate of 10 °C min^{-1} (Fig. 3). The stability range extended from ambient temperature to 240 °C. The decomposition of the complex occurred in three stages as indicated by the DTG peaks at 302, 439 and 760 °C. First decomposition stage started at 250 °C and ended at 350 °C. The mass loss of 25.9 % (Calcd. 26.3 %) corresponded to the loss of ≈0.5 mol of the ligand. The second stage was more complicated and it ranged from 350 to 560 °C. The weight loss in this stage was 57.7 % (Calcd. 57.5 %). The weight of the sample at 560 °C was consistent with the formation of MoO_3. The sample showed another weight loss in the region 700–790 °C. The weight of the sample, 15.8 % (Calcd. 27.8 %), at 790 °C was less than that expected if MoO_2 was formed. This may be due to the volatilization of MoO_3 above 700 °C.[30]

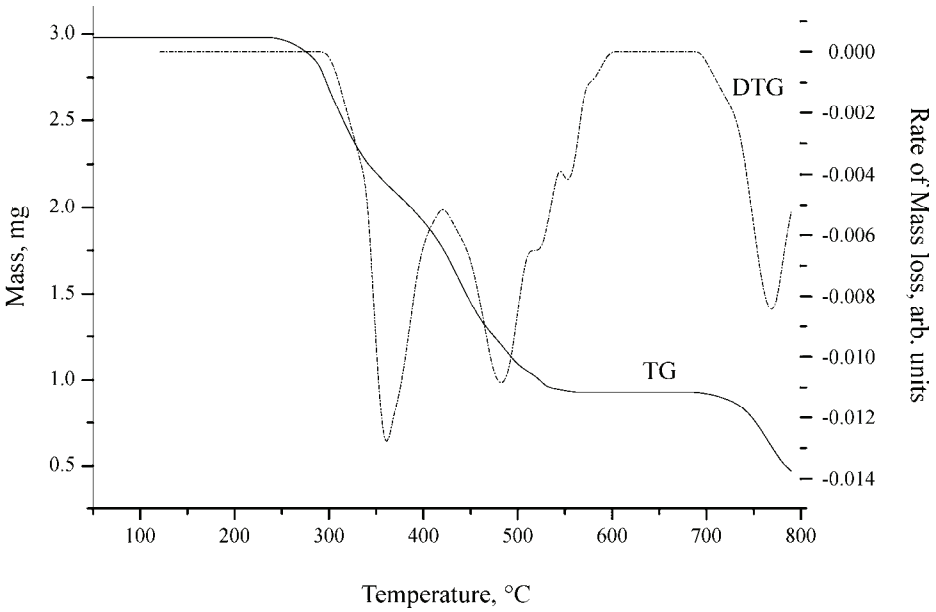

Fig. 3. TG and DTG curves of $[MoO_2(L)NO_3]$.

Antibacterial studies

The ligand and the complexes were screened for their antibacterial activity and the results obtained are presented in Table IV. A comparative study of the ligand and the complexes revealed that the oxo-complexes showed higher activity than the dioxo-complexes. The ligand was inactive against all the applied pathogenic bacteria *P. aeruginosa.* appeared to be resistant to all the tested compounds.

The antibacterial activity of the complexes may result from various modes by which these antibacterials act on bacteria. It may be due to factors such as inhibition of cell wall formation leading to lysis, damage of the cell wall leading to

loss of cell contents and hence to cell death, inhibition of protein production and thereby arresting bacterial growth and inhibition of the production of nucleic acids, thereby preventing bacterial reproduction. Metal chelates have simultaneously polar and non-polar properties; this makes them suitable for permeation into cells and tissues. Changing hydrophilicity and lipophilicity probably leads to a reduction of the solubility and permeability barriers of cells, which in turn enhances the bioavailability of chemotherapeutics on the one hand and their potentiality on the other.[31] The low activity of dioxo-complexes may be due to low lipid solubility, steric and pharmacokinetic factors which play vital roles in deciding the potency of an antibacterial agent.

TABLE IV. Antibacterial activity of the ligand and its complexes against pathogenic bacteria (abbreviations as in Table I)

Compound	Zone of inhibition, mm					
	S. typhi MTCC 734	*P. aeruginosa MTCC 2642*	*E. coli MTCC 585*	*P. vulgaris 1771*	*B. subtilis 2248*	*S. thermophilus 1938*
HL	–	–	–	–	–	–
$[MoO(L)NO_3Cl]$	T	–	T	14	11	14
$[MoO(L)ClO_4Cl]$	T	–	10	15	12	15
$[MoO_2(L)NO_3]$	–	–	–	11	–	–
$[MoO_2(L)ClO_4]$	–	–	–	12	–	–
Control (chloroform at 10 µl/disc)	–	–	–	–	–	–

3D molecular modelling

The molecular modelling was constructed using modelling and analysis software[32] CHEM Bio3D Ultra 11.0. The possible 3D structures of the ligand and one of the complexes, $[MoO(L)NO_3Cl]$, as a representative, were optimized by molecular mechanics calculations, MM_2 giving the lowest energy CHEM 3D models. The CHEM 3D model of the ligand HL is shown in Fig. 4, while that of $[MoO(L)NO_3Cl]$ is shown in Fig. 5. Selected bond angles and the bond angle

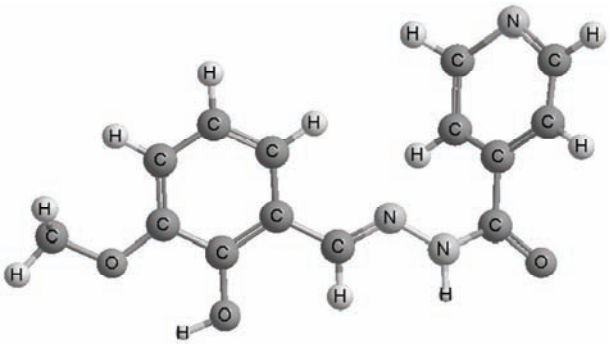

Fig. 4. Proposed 3D structure of the ligand (HL).

around the octahedral surrounding, given in Table V, are calculated values after energy minimization[33,34] in CHEM 3D.

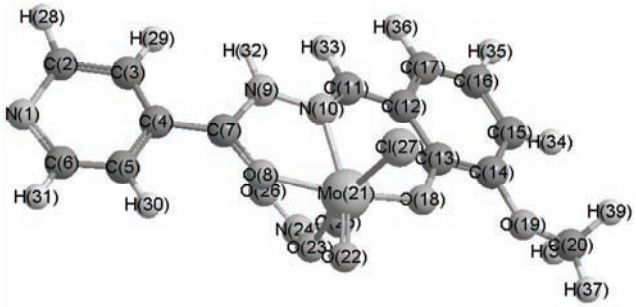

Fig. 5. Proposed 3D structure of the complex [MoO(L)NO_3Cl].

TABLE V. Selected bond lengths/bond angles of the complex [MoO(L)NO_3Cl] (abbreviations as in Table I)

Bond	Bond length, Å	Bond	Bond angle, deg.
Mo(21)–Cl(27)	2.2973	Cl(27)–Mo(21)–O(23)	169.1658
Mo(21)–O(23)	1.9534	Cl(27)–Mo(21)–O(22)	87.3513
O(22)–Mo(21)	1.6773	Cl(27)–Mo(21)–O(18)	88.7829
Mo(21)–O(18)	1.9432	Cl(27)–Mo(21)–N(10)	85.8183
N(10)–Mo(21)	2.0074	Cl(27)–Mo(21)–O(8)	103.5166
O(8)–Mo(21)	1.9352	O(23)–Mo(21)–O(22)	84.4090
		O(23)–Mo(21)–O(18)	86.6129
		O(23)–Mo(21)–N(10)	104.5423
		O(23)–Mo(21)–O(8)	83.8798
		O(22)–Mo(21)–O(18)	105.2278
		O(22)–Mo(21)–N(10)	155.3596
		O(22)–Mo(21)–O(8)	92.3625
		O(18)–Mo(21)–N(10)	98.2704
		O(18)–Mo(21)–O(8)	159.0781
		N(10)–Mo(21)–O(8)	66.4086

Based on all the above spectral data and physicochemical studies, a distorted octahedral geometry (Figs. 6 and 7) are tentatively proposed for all the complexes.

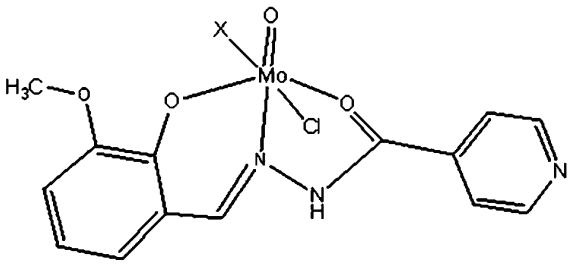

Fig. 6. Proposed 2D structure of [MoO(L)XCl], X = NO_3, ClO_4.

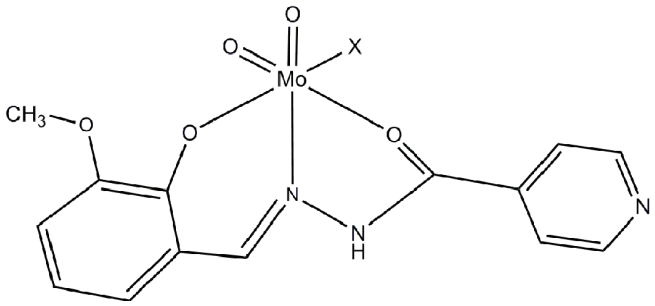

Fig. 7. Proposed 2D structure of $[MoO_2(L)X]$, X = NO_3, ClO_4.

CONCLUSIONS

From the spectroscopic, analytical and thermal analyses data, it can be concluded that the molybdenum existed in a distorted octahedral environment with the ligand as a monoanionic tridentate chelating agent. The FAB mass spectral data suggest the monomeric nature of the complexes. The results of antibacterial studies revealed that the oxomolybdenum complexes exhibited much higher activity than the ligand and the dioxomolybdenum complexes.

Acknowledgement. The authors are thankful to NIIST, Thiruvananthapuram, STIC, Kochi and the Department of Chemistry, University of Kerala, Thiruvananthapuram for the facilities. One of us (DT) expresses her gratitude to the UGC for the award of a Teacher fellowship under FDP.

ИЗВОД

СИНТЕЗА И КАРАКТЕРИЗАЦИЈА ОКСОМОЛИБДЕН(V) И ДИОКСОМОЛИБДЕН(VI) КОМПЛЕКСА СА *N*'-(2-ХИДРОКСИ-3-МЕТОКСИБЕНЗИЛИДЕН)-ИЗОНИКОТИНОХИДРАЗИДОМ

M. L. HARIKUMARAN NAIR и D. THANKAMANI

Department of Chemistry, University College, Thiruvananthapuram-695 034, India

Синтетизовано је неколико нових оксомолибден(V)- и диоксомолибден(VI)-комплекса који као лиганд садрже Шифову базу *N*'-(2-хидрокси-3-метоксибензилиден)изоникотинохидразид (HL), који је изолован у реакцији између 3-метокси-салицилалдехида и изоникотинохидразида. Поред елементалне микроанализе, моларне проводљивости, магнетних мерења, за карактеризацију комплекса употребљене су IR, ^{1}H-NMR, FAB масена и UV–Vis спектроскопске методе. Нађено је да комплекси имају општу формулу $[MoO(L)XCl]$ и $[MoO_2(L)X]$ (X = NO_3 или ClO_4). На основу IR спектроскопије закључено да је лиганд HL у овим комплексима моноанјонског типа и да је тридентатно координован, док су нитратни и перхлоратни анјони у овим комплексима монодентатно координовани. На основу рендгенске дифракционе анализе нађено је да $[MoO(L)NO_3Cl]$ комплекс има орторомбичну кристалну решетку са јединичном ћелијом димензија a = 15,49 Å, b = 12,44 Å и c = 10,11 Å, као и да је дисторговане октаедарске геометрије. Термална анализа $[MoO_2(L)NO_3]$ комплекса је показала да су сви комплекси стабилни до температуре од 240 °C, а да изнад ове температуре долази до њиховог разлагања. Методом молекулске механике оптимизована је геометрија лиганда и комплекса формуле $[MoO(L)NO_3Cl]$. Антибактеријска испитивања су показала да

комплекси оксомолибдена(V) имају већу активност од комплекса диоксомолибдена(VI), као и од самог лиганда.

(Примљено 8. фебруара, ревидирано 23. августа 2010)

REFERENCES

1. a) M. L. Harikumaran Nair, D. Thankamani, *Indian J. Chem*. **48A** (2009) 1212; b) E. L. Steifel, *Prog. Inorg. Chem.* **22** (1977) 1
2. N. R. Pramanik, S. Ghosh, T. K. Raychaudhuri, S. S. Mandal, *J. Coord. Chem*. **62** (2009) 3845
3. M. L. Harikumaran Nair, V. L. Siji, *J. Indian Chem. Soc.* **86** (2009) 449
4. M. L. Harikumaran Nair, A. Sheela, *Indian J. Chem.* **47A (**2008) 87
5. A. S. Ahamed, A. A. Saadia , A. Orabi, *Spectrochim. Acta* **65A** (2006) 841
6. A. M. Martins, C. C. Romão, M. Abrantes, M. C. Azevedo, J. Cui, A. R. Dias, M. T. Duarte, M. A. Lemos, T. Lourenço, R. Poli, *Organometallics* **24** (2005) 2582
7. J. A. Gnecco, G. Borda, P. Reyes, *J. Chil. Chem. Soc.* **49** (2004) 179
8. M. Tamm, B. Dreßel, V. Urban, T. Lügger, *Inorg. Chem. Commun.* **5** (2002) 837
9. S. Rollas, Ş. G. Küçükgüzel, *Molecules* **12** (2007) 1910
10. Z. H. Chohan, M. Arif, Z. Shafiq, M. Yaqub, C. T. Supuran, *J. Enzyme Inhib. Med. Chem.* **21** (2006) 95
11. A. Sheela, M. S. Pramila Gladis, M. L. Harikumaran Nair, *J. Indian Chem. Soc.* **84** (2007) 329
12. A. I. Vogel, *A Text Book of Quantitative Inorganic Analysis*, Wiley, New York, 1963, p. 462
13. R. L. Dutta, A. Syamal, *Elements of Magneto Chemistry*, East West Press, New Delhi, 1992, p. 8
14. R. Ananthanarayan, J. C. Panikar, *Text Book of Microbiology*, Orient Longman, Hyderabad, 1999, p. 578
15. A. Kilic, E. Tas, *Synth. React. Inorg. Met.-Org. Nano-Met. Chem.* **37** (2007) 583
16. M. L. Harikumaran Nair, V. L. Siji, *J. Indian Chem. Soc.* **85** (2008) 589
17. N. Singh, S. Hingorani, J. Srivastava, V. Puri, B. V. Agarwala, *Synth. React. Inorg. Met--Org. Chem.* **22** (1992) 1283
18. V. P. Singh, A. Singh, *Russ. J. Coord. Chem.* **34** (2008) 374
19. K. Singh, B. V. Agarwala, G. A. Naganagowda, *Indian J. Chem.***35A** (1996) 66
20. M. L. Harikumaran Nair, M. S. Pramila Gladis, *Asian J. Chem.* **20** (2008) 2504
21. M. L. Harikumaran Nair, K. R. Kumari Nisha, *Asian J. Chem.* **19** (2007) 468
22. N. Gupta, R. V. Singh, *Indian J. Chem*. **37A** (1998) 75
23. a) S. Thomas, M. L**.** Harikumaran Nair, *Asian J. Chem.* **19** (2007) 3461; b) K. Nakamoto, *Infrared and Raman Spectra of Inorganic and Coordination Compounds*, Wiley, New York, 1978
24. N. A. Mangalam, M. R. Prathapachandra Kurup, *Spectrochim. Acta A* **71** (2009) 2040
25. E. Kahroic, K. Molcanov, L. Tusek-Bozic, B. Kojic-Prodic, *Polyhedron* **25** (2006) 2459
26. M. L. Harikumaran Nair, C. P. Prabhakaran, *Indian J. Chem*. **39A** (2000) 989
27. C. J. Ballhausen, H. B. Gray, *Inorg. Chem.* **1** (1962) 111
28. R. K. Dubey, U. K. Dubey, C. M. Mishra, *Indian J. Chem.* **47A** (2008) 1208
29. a) M. L. Harikumaran Nair, L. Shamla, *J. Indian Chem. Soc.* **86** (2009) 133; b) R. Hesse, *Acta Crystallogr.* **1** (1948) 200; c) H. Lipson, *Acta Crystallogr*. **2** (1949) 43

30. N. Sridevi, K. K. M. Yusuff, *Indian J. Chem.* **47A** (2008) 836
31. K. Mohanan, S. Nirmala Devi, B. Murukan, *Synth. React. Inorg. Met.-Org. Nano-Met. Chem.***36** (2006) 441
32. Chem Bio Office 2008 Ultra Molecular Modeling and Analysis, Cambridge, available from www.cambridgesoft.com
33. R. C. Maurya, S. Sahu, P. Bohre, *Indian J. Chem.* **47A** (2008) 1333
34. B. Ghosh, S. R. Parag, *Indian J. Chem*. **46A** (2007) 1587.

Journal of the Serbian Chemical Society
JSCS-info@shd.org.rs • www.shd.org.rs/JSCS
J. Serb. Chem. Soc. *76* (2) 235–247 (2011)
JSCS–4115
UDC 546.712:548.7:543.42–74:547–327
Original scientific paper

The crystal structure and spectroscopic properties of *catena*-(2-methylimidazolium bis(μ_2-chloro)aquachloromanganese(II))

BARBARA HACHUŁA[1]*, MONIKA PĘDRAS[1], MARIA NOWAK[2], JOACHIM KUSZ[2], DANUTA PENTAK[1] and JERZY BOREK[1]

[1]*Institute of Chemistry, University of Silesia, 9 Szkolna Street, 40-006 Katowice and* [2]*Institute of Physics, University of Silesia, 4 Uniwersytecka Street, 40-007 Katowice, Poland*

(Received 18 February, revised 27 September 2010)

Abstract: A novel manganese(II) coordination polymer, *catena*-(2-methylimidazolium bis(μ_2-chloro)aquachloromanganese(II)), $\{(C_4H_7N_2)[MnCl_3(H_2O)]\}_n$, was synthesized, structurally characterized by FTIR spectroscopy and confirmed by single crystal X-ray diffraction analysis. Thermogravimetric analysis and EPR spectroscopy of the compound were also performed. The colourless crystals of the complex were monoclinic, space group *P*21/*c*, with the cell parameters a = 11.298(2) Å, b = 7.2485(14) Å, c = 14.709(5) Å, β = 128.861(18)°, V = 938.0(5) Å^3, Z = 4 and R_1 = 0.03. The title compound consisted of one-dimensional infinite anionic chains $[MnCl_3(H_2O)]_n$ and isolated 2-methylimidazolium cations. The Mn(II) atom was octahedrally coordinated to four bridging chloride anions (Mn–Cl = 2.5109(6) – 2.5688(7) Å), one terminal chloride anion (Mn–Cl = 2.5068(11) Å) and a H_2O molecule (Mn–O = 2.2351(17) Å). A three-dimensional layer structure was constructed *via* hydrogen bonds and by weak π–π stacking interactions. A four-step thermal decomposition occurred in the temperature range 25–900 °C under nitrogen.

Keywords: manganese(II) complex; 2-methylimidazole; X-ray crystal structure; IR spectra; EPR spectra.

INTRODUCTION

Complexes of imidazole derivatives with transition metal ions have attracted much attention because of their biological and pharmacological activities, such as antiviral and antimicrobial,[1,2] antifungal and antimycotic,[3] antihistaminic and antiallergic,[4] anthelminthic,[5] antitumoural and antimetastatic properties.[6–13] The biological role of complexes containing an imidazole ring system can be connected with the two N atoms, which have different properties; the deprotonated N

* Corresponding author. E-mail: barbara.hachula@us.edu.pl
doi: 10.2298/JSC100218012H

atom can coordinate with a transition-metal ion, whereas the protonated N atom participates in hydrogen bonding.[14–22]

2-Methylimidazole, a compound widely used as a chemical intermediate (the manufacture of pharmaceuticals, photographic and photothermographic chemicals, dyes and pigments, agricultural chemicals and rubber), has been detected in cigarette smoke, as a result of pyrolysis. It is also an undesirable by-product in food and forage coloured with caramel, such as beer, colas, caramel-coloured syrups and soy sauce.[23–27]

In previous papers, the crystal structures of 2-methylimidazole and diaquadichlorobis(1*H*-imidazole)manganese(II) were reported.[28,29] In this paper, the structural characterization of the polymeric complex, *catena*-(2-methylimidazolium bis(μ_2-chloro)aquachloromanganese(II)) (**I**), which was obtained in the reaction of manganese(II) chloride with 2-methylimidazole (Scheme 1), is reported. In this compound, a protonated 2-methylimidazole can cross-link manganese(II) complexes, $[MnCl_3(H_2O)]_n$, through two M–Cl···H–N interactions. Despite the simplicity of the ligands, no structural report of the title compound was found in a search of the Cambridge Structural Database (CSD, Version 5.31 of November 2009).[30] Moreover, only two manganese(II) complexes with 2-methylimidazolium cation have been investigated, *i.e.*, bis(2-methylimidazolium)-bis(2,6-pyridinedicarboxylato)manganese(II)[31] and *catena*-(bis(2-methylimidazolium)(μ_2-benzene-1,2,4,5-tetracarboxylato-*O*,*O*')tetraaquamanganese(II) pentahydrate).[32] The same $[MnCl_3(H_2O)]$ group was reported in the structure of $[H(2\text{-ampy})][MnCl_3(H_2O)]$.[33]

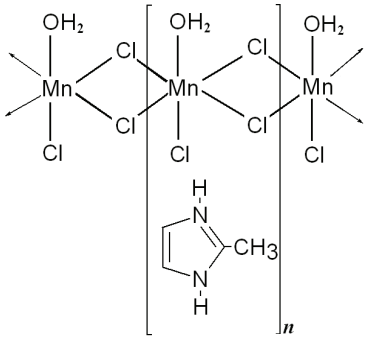

(I)

Scheme. 1. Structure of $\{(2\text{-met}H_2\text{Im})[MnCl_3(H_2O)]\}_n$.

EXPERIMENTAL

Synthesis of $\{(C_4H_7N_2)[MnCl_3(H_2O)]\}_n$

All the employed chemicals were commercial products (Sigma-Aldrich and POCH S.A., Poland), which were used without further purification.

Hydrochloric acid (2 mg, 0.05 mmol), manganese(II) chloride (520 mg, 4 mmol) and 2-methylimidazole (640 mg, 8 mmol) were stirred in 2 ml of water until they had dissolved. The solution was filtered and the filtrate was left to stand undisturbed. After two days, colourless single crystals of **I**, suitable for X-ray crystallographic analysis, were collected and dried in air at room temperature (268.94 mg, yield: 24.92 %). Anal. Calcd. for $C_4H_9Cl_3MnN_2O$: C, 18.29; H, 3.43; N, 10.67 %. Found: C, 18.34; H, 3.39; N, 10.69%.

X-Ray crystal structure determination

The data were collected using an Oxford Diffraction kappa diffractometer with a Sapphire3 CCD detector and MoKα radiation (λ = 0.71073 Å) at 100 K. Accurate cell parameters were determined and refined using the CrysAlis CCD program.[34] For the integration of the collected data, the program CrysAlis RED was used.[34] Absorption corrections were realised using the multi-scan method.[34] The structure was solved by the direct method using SHELXS-97[35] and then the solution was refined by the full matrix least-squares method using SHELXL-97.[35] Non-hydrogen atoms were refined with anisotropic displacement factors. All hydrogen atoms attached to N and C were placed in the geometrically idealized positions (d(N–H) = 0.88 Å and U_{iso}(H) = 1.2U_{eq}(N) for N–H hydrogens; d(C–H) = 0.95 Å and U_{iso}(H) = 1.2U_{eq}(C) for C–H hydrogens; d(C–H) = 0.98 Å and U_{iso}(H) = 1.5U_{eq}(C) for CH_3 hydrogens). Hydrogen atoms attached to O atoms were located from the difference Fourier map and then refined as riding on their parent atoms.

Physical measurements

The IR spectrum of a polycrystalline sample of *catena*-(2-methylimidazolium bis(μ_2-chloro)aquachloromanganese(II)) dispersed in KBr was measured at room temperature using an FT-IR Nicolet Magna 560 spectrometer operating at a resolution of 4 cm^{-1}. The IR spectrum was recorded in the range of 4000–400 cm^{-1} using an Ever-Glo source, a KBr beam splitter and a DTGS detector. The thermal stability of the compound was studied by thermogravimetric analysis (TGA) from 298 to 1173 K at a heating rate of 10 K min^{-1} under a nitrogen atmosphere using a Perkin–Elmer Pyris thermogravimetric analyzer. The X-band electron paramagnetic resonance (EPR) spectrum (9.7 GHz) was recorded using a Bruker EMX spectrometer at room temperature. 2,2-Diphenyl-1-picrylhydrazyl (DPPH) was used as an internal field marker. For the EPR measurement, 0.1 mL of the sample solution was kept in closed quartz capillaries.

RESULTS AND DISCUSSION

The crystal data and final refinement details of the title compound are given in Table I.

The asymmetric unit of the title crystal structure comprises an anionic [$MnCl_3(H_2O)$] fragment and a 2-methylimidazolium (2-metH_2Im) cation (Fig. 1). The crystal structure shows the formation of $[MnCl_3(H_2O)]_n$ polymeric chains developed parallel to axis *b*. The local geometry around Mn(II) ion can be seen as octahedral, involving four bridging chloride anions, one terminal chloride anion and one water molecule. The angles in the octahedron are distorted by less than 7.4° from the ideal values (Table II).

The Mn–Cl distances are in the range from 2.5068(11) to 2.5688(7) Å. The bridging Mn–Cl bond distances, *viz.* Mn–Cl2 and Mn–Cl3, are slightly longer than the terminal one (Mn–Cl1, Table II). The latter bond length Mn–Cl1 bond is

comparable with the corresponding value in other hexacoordinated Mn(II) complexes.[33,36,37] The Mn–O bond length of 2.2351(17) Å is slightly longer than the value found in other manganese(II) structures, *i.e.* [H(2-ampy)][$MnCl_3(H_2O)$] (2.171(2) Å),[33] $Mn_2L_2Cl_4(H_2O)_2$ (where L is 2-(2'-pyridyl)quinoxaline) (2.190(2) Å)[38] and than the average value specified by Orpen *et al.*[36] for a Mn–O distance (terminal OH_2 group = 2.190 Å). The Mn(II) atoms are separated by a distance of 3.6386(7) Å, which is quite large and seems to rule out any strong direct metal–metal interaction.

TABLE I. Crystal data and structure refinement details of $\{(C_4H_7N_2)[MnCl_3(H_2O)]\}_n$ (**I**)

Property	Value
Chemical formula	$[MnCl_3(H_2O)\cdot C_4H_7N_2]$
Compound weight	262.42
Crystal system	Monoclinic
Space group	$P2_1/c$
Crystal dimension, mm^3	0.56 × 0.22 × 0.21
Crystal form, colour	Polyhedron, colourless
Unit cell parameters	
a / Å	11.298(2)
b / Å	7.2485(14)
c / Å	14.709(5)
β / °	128.861(18)
V / $Å^3$	938.0(5)
Z	4
D_c / g cm^{-3}	1.858
$F(000)$	524
θ range for data collection, °	3.33–34.45
Data collection method	ω scan
Absorption coefficient, mm^{-1}	2.208
Final R indices ($I > 2\delta(I)$)	R_1 = 0.0304, wR_2 = 0.1101
R indices (all data)	R_1 = 0.0334, wR_2 = 0.1117
Reflections collected/unique	13649/3653 [R_{int} = 0.0201]
Limiting indices	$-17 \le h \le 17$, $-11 \le k \le 6$, $-23 \le l \le 22$
Refinement method	Full-matrix least-squares on F^2
S	1.0
Parameters refined	104
Extinction method	0.146(5)
$\Delta\rho_{max}$, $\Delta\rho_{min}$ / e $Å^{-3}$	1.42–0.99

The 2-methylimidazolium cations are planar (mean deviation = 0.0013 Å) and canted 88.64(6)° from the chains formed by the anions (*vs.* the plane formed by the two Mn atoms and the bridging Cl atoms). The internal geometry of the 2-metH_2Im cation is different from that in the free 2-methylimidazole (2-metHIm) molecule.[28] The N–C bond distances in **I** show some significant variations. The N1–C2 distance (N1–C2 1.325(3) Å) is shorter than the corresponding bond in

2-metHIm and, conversely, the C2–N3 bond is longer (1.384(3) Å *vs*. 1.3283(11) Å in 2-metHIm). This indicates that the π electrons of C2=N3 and C4=C5 exhibit significant delocalization compared with those of pure 2-metHIm.

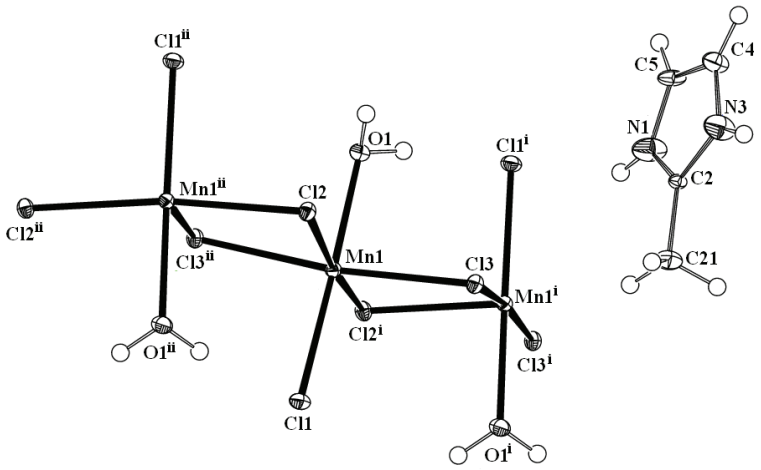

Fig. 1. A view of the molecular structure of **I**, showing the atom-numbering scheme. Displacement ellipsoids are drawn at the 50 % probability level. H atoms are shown as small spheres of arbitrary radius (symmetry codes: *i*) $-x$, $-1/2 + y$, $1/2 - z$; *ii*) $-x$, $1/2 + y$, $1/2 - z$).

Table II. Selected bond lengths (Å), bond angles (°) and torsion angles (°) of $\{(C_4H_7N_2)[MnCl_3(H_2O)]\}_n$. Symmetry codes: *i*) $-x$, $-1/2 + y$, $1/2 - z$; *ii*) $-x$, $1/2 + y$, $1/2 - z$

Bond lengths, Å			
Mn1–O1	2.2351(17)	N1–C2	1.325(3)
Mn1–Cl1	2.5068(11)	N1–C5	1.325(3)
Mn1–Cl2	2.5109(6)	N3–C2	1.384(3)
Mn1–Cl2^i	2.5220(6)	N3–C4	1.358(3)
Mn1–Cl3	2.5567(6)	C4–C5	1.364(3)
Mn1–Cl3^i	2.5688(7)	C2–C21	1.455(3)
Bond angles, °			
O1–Mn1–Cl1	178.01(4)	Cl1–Mn1–Cl3^{ii}	92.93(2)
O1–Mn1–Cl2	86.92(4)	Cl2–Mn1–Cl3^{ii}	87.74(2)
Cl1–Mn1–Cl2	94.05(2)	Cl2^i–Mn1–Cl3^{ii}	91.75(2)
O1–Mn1–Cl2^i	85.66(4)	Cl3–Mn1–Cl3^{ii}	172.754(12)
Cl1–Mn1–Cl2^i	93.37(2)	C2–N1–C5	108.53(18)
Cl2–Mn1–Cl2^i	172.583(12)	C2–N3–C4	106.86(17)
O1–Mn1–Cl3	87.38(4)	N1–C2–N3	108.41(17)
Cl1–Mn1–Cl3	94.32(2)	N1–C2–C21	126.62(17)
Cl2–Mn1–Cl3	91.80(2)	N3–C2–C21	124.96(17)
Cl2^i–Mn1–Cl3	87.77(2)	N3–C4– C5	106.68(18)
O1–Mn1–Cl3^{ii}	85.37(4)	N1–C5–C4	109.53(18)

The packing shows four potentially active H atoms, *viz* the methylimidazolium N–H and the aqua H atoms involved in hydrogen bonds with Cl atoms, forming a three-dimensional hydrogen-bonded network (Fig. 2 and Table III). The $[MnCl_3(H_2O)]$ units are connected in the crystal lattice through O1–H1O···Cl1^{i} and O–H2O···Cl1^{iii} hydrogen bonds (symmetry codes: *i*) $-x$, $-1/2 + y$, $1/2 - z$; *iii*) x, $3/2 - y$, $-1/2 + z$), which are formed between two terminal chloride anions and the hydrogen atoms of the coordinated water molecule. The result of these interactions is the formation of eight-membered rings, with a graph-set motif of $R_4^2(8)$,[39,40] in the *bc* plane. Moreover, each of the $[MnCl_3(H_2O)]$ moieties is also linked to two 2-metH_2Im cations by weaker N1–H1···Cl2^{iv} and N3–H3···Cl1^{v} hydrogen bonds (symmetry codes: *iv*) x, $-1 + y$, z; *v*) $1 - x$, $1 - y$, $1 - z$), joining the molecules into a three-dimensional network. The N–H···Cl interactions are formed to one bridging halogen and one terminal halogen (Fig. 3). In addition, there are weak contacts between the C–H groups of the 2-metH_2Im ring and the Cl, as well as O atoms of the $[MnCl_3(H_2O)]$ unit of neighbouring molecules (Table III). The alternate stacking of the 2-metH_2Im rings results in ring separations of 3.841 Å, indicating weak π–π interactions (Fig. 3).[41]

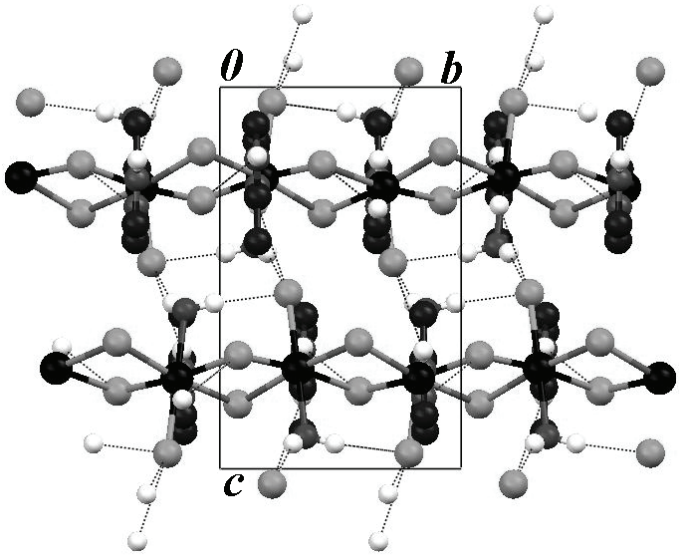

Fig. 2. Packing in the crystal structure of $\{(2\text{-met}H_2Im)[MnCl_3(H_2O)]\}_n$ viewed along the *a* axis. For the sake of clarity, all H atoms bonded to C atoms were omitted.

The structure of the presented complex differs considerably from that of $[MnCl_2(C_3H_4N_2)_2(H_2O)_2]$ (in which the Mn(II) atom was octahedrally coordinated by the monodentate ligands, *i.e.* two *N*-coordinated imidazole groups, two

chloride anions and two O atoms of water molecules) and other Mn(II) systems with imidazole ligands.[29,37,42–47] Thus, the introduction a methyl substituent at the C2 position of imidazole seems to prevent it from being incorporated into the lattice of **I**.

Table III. Hydrogen bonding geometry for $\{(C_4H_7N_2)[MnCl_3(H_2O)]\}_n$. Symmetry codes: *iii*) $x, 1.5 - y, -1/2 + z$; *i*) $-x, -1/2 + y, 1/2 - z$; *iv*) $x, -1 + y, z$; *v*) $1 - x, 1 - y, 1 - z$; *vi*) $x, 1/2 - y, -1/2 + z$;; *vii*) $-x, 1 - y, -z$

Bond	*d* (D–H) / Å	*d* (H···A) / Å	*d* (D···A) / Å	<DHA/ °
O1–H2O···Cl1^{iii}	0.90	2.33	3.1917(16)	161
O1–H2O···Cl1^{i}	0.91	2.26	3.1596(16)	172
N1–H1···Cl2^{iv}	0.88	2.87	3.492(2)	129
N3–H3···Cl1^{v}	0.88	2.87	3.601(2)	141
C5–H5···Cl3^{vi}	0.95	2.47	3.233(2)	138
C5–H5···O1^{vii}	0.95	2.30	2.993(3)	129

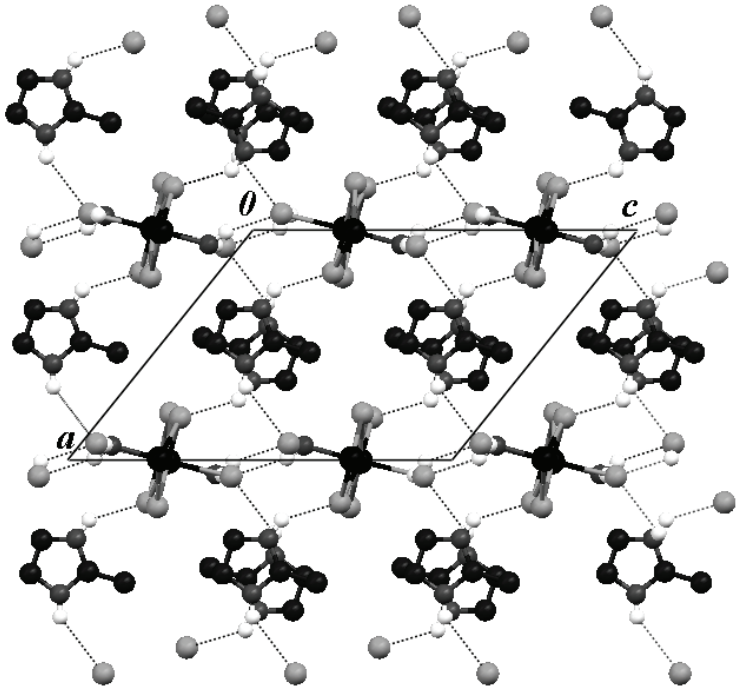

Fig. 3. Structure of a layer of $[MnCl_3(H_2O)]^-$ chains cross-linked by $[2\text{-met}H_2Im]^+$. For the sake of clarity, all H atoms bonded to C atoms were omitted.

IR spectrum of compound ***I***

The IR spectrum of the complex shows a strong and broad band extending over the frequency range 3600–2000 cm^{-1} (Fig. 4). The band in this region is attributed to the stretching vibrations, ν_{O-H}, of the hydroxyl groups in the water

molecules. The essential features of the band in this region indicate the presence of hydrogen bond involving the uncoordinated N–H groups of the 2-metH_2Im cation and aqua H atoms, with Cl atoms. From Raman spectra measurements of free 2-methylimidazole, it is known that the narrow bands at 3127 and 3102 cm^{-1}, disturbing the $\nu_{N–H}$ and $\nu_{O–H}$ band contour shapes of compound **I**, correspond to the $\nu_{C–H}$ stretching modes of the 2-metH_2Im ring.[28] The bands at 1613, 1579 and 1542 cm^{-1} can be due to the stretching of the short Cl···HO bonds.[48] The vibrational bands from 1438 to 1002 cm^{-1} can be assigned to the ring stretching frequency of the 2-metH_2Im cation.[49] The $\nu_{C=N}$ mode can be found at 1438 cm^{-1}. The bands remaining in the 859–686 cm^{-1} region can be associated with deformations of the imidazole ring. The peak at 477 cm^{-1} may be assigned to the bending vibration of the hydrogen bond.[48]

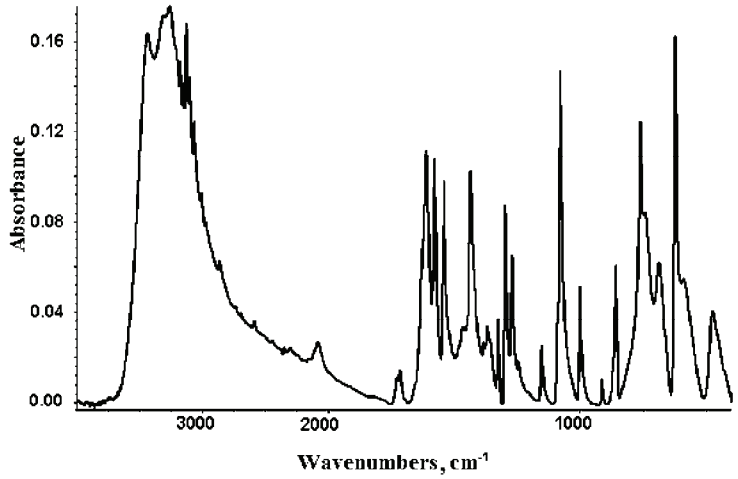

Fig. 4. The IR spectrum of *catena*-(2-methylimidazolium bis(μ_2-chloro)-aquachloromanganese(II)) sample dispersed in a KBr pellet.

*Thermal analysis of compound **I***

The thermogravimetric data in Fig. 5 show a four-step decomposition. The first one, in the temperature range of 298–406 K, seems to correspond to the removal of one coordinated water molecule with a weight loss of 8.92 % (Calcd. 6.86 %). The next mass loss of 34.26 % (Calcd. 31.63 %), occurring in the range 406–558 K, can be attributed to 2-metH_2Im destruction. Further decomposition of the compound of 35.88 % (Calcd. 40.53 %), with the successive release of Cl_2, begins at 558 K and ends at 894 K. The final total mass loss of 78.80 % is much more than the calculated value of 72.97 %. Similarly to other Mn(II) complexes, the final product of the decomposition of $\{(C_4H_7N_2)[MnCl_3(H_2O)]\}_n$ seems to be MnO.[50–53]

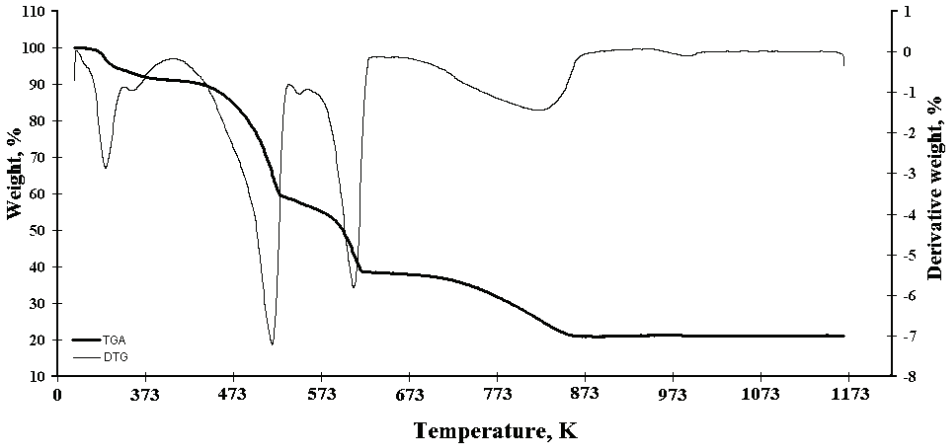

Fig. 5. TGA–DTG curves for compound **I** under a dynamic nitrogen atmosphere at a heating rate of 10 K min^{-1}.

*EPR spectrum of complex **I***

The solid-state EPR spectrum of compound **I** at room temperature shows only one isotropic signal at g = 2.03147, corresponding to manganese(II) in a weakly distorted octahedral environment (predicted by crystal structure analysis). Such an isotropic spectrum consisting of a broad signal without a hyperfine pattern is due to intermolecular dipole–dipole interactions and enhanced spin lattice relaxation.[54] When the manganese ion is magnetically diluted, the hyperfine interaction can be detected.

The EPR spectrum of $\{(C_4H_7N_2)[MnCl_3(H_2O)]\}_n$ in aqueous solution at 298 K brings more detailed information about the coordination sphere of the Mn(II) centre. The ground state of the Mn(II) ion ($3d^5$) is $^6S_{5/2}$. The EPR of Mn(II) ions can be adequately described by the spin-Hamiltonian:

$$H = g\mu_B BS + D(S_z^2 - (1/3)S(S + 1)) + E(S_{x^2} - S_{y^2}) + ASI$$

where: S = 5/2 and I = 5/2; D and E are fine structure (fs) parameters; the last term means that the hyperfine interaction; the g-factor and the hyperfine structure parameter A are isotropic.

The spectrum of **I** exhibits a six line manganese hyperfine pattern centred at g = 1.98093 (Fig. 6). These six hyperfine lines arise from the interaction of the electron spin with the nuclear spin (^{55}Mn, I = 5/2) and correspond to m_I = ±5/2, ±3/2, ±1/2, resulting from allowed transitions (Δm_s = ±1, Δm_I = 0). The observed g values are close to the free electron spin value of 2.0023, which is suggestive of the absence of spin–orbit coupling in the ground state, $^6A_1$.[55–58]

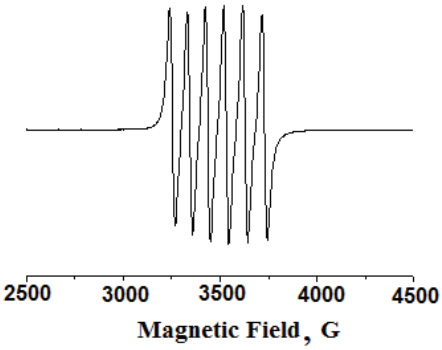

Fig. 6. X-band EPR spectrum of $\{(2\text{-metH}_2\text{Im})[MnCl_3(H_2O)]\}_n$ in aqueous solution.

CONCLUSIONS

In the present paper, the synthesis, crystal structure, thermal and spectroscopic properties of a novel manganese(II) coordination polymer, $\{(C_4H_7N_2)[MnCl_3(H_2O)]\}_n$, which can easily be prepared by the reaction of manganese(II) chloride and 2-methylimidazole, are reported. In the compound, each manganese ion is connected with the neighbouring metal *via* chloride atoms forming a polymeric chain of $[MnCl_3(H_2O)]_n$ anions hydrogen bonded to 2-metH$_2$Im cations, thus forming a three-dimensional hydrogen-bonded network. The substitution of imidazole by 2-methylimidazole during the synthesis is reflected in the structure and properties of the manganese complex in which the cation is not a metal complex but a protonated 2-methylimidazole ligand. Thus, the imidazole methyl group seems to be a steric feature impeding its insertion in the Mn coordination polymer. Moreover, the above-discussed compound shows the structural role of protonated 2-methylimidazole on the self-assembly of metal complexes through N–H···Cl–M hydrogen bonds.

SUPPLEMENTARY DATA

CCDC-755577 contains the supplementary crystallographic data for this paper. These data can be obtained free of charge at www.ccdc.cam.ac.uk/conts/retrieving.html or from the Cambridge Crystallographic Data Centre (CCDC), 12 Union Road, Cambridge CB2 1EZ, UK; fax: +44(0)1223-336033; e-mail: deposit@ccdc.cam.ac.uk

Acknowledgement. The work of M.N. was partially supported by PhD scholarship within the framework of the 'University as a Partner of the Economy Based on Science' (UPGOW) project, subsidized by the European Social Fund (EFS) of the European Union.

ИЗВОД

КРИСТАЛНА СТРУКТУРА И СПЕКТРОСКОПСКА КАРАКТЕРИЗАЦИЈА *catena*-(2-МЕТИЛИМИДАЗОЛИЈУМ-БИС(μ_2-ХЛОРО)АКВАХЛОРОМАНГАНА(II))

BARBARA HACHUŁA[1], MONIKA PĘDRAS[1], MARIA NOWAK[2], JOACHIM KUSZ[2], DANUTA PENTAK[1] и JERZY BOREK[1]

[1]*Institute of Chemistry, University of Silesia, 9 Szkolna Street, 40-006 Katowice и* [2]*Institute of Physics, University of Silesia, 4 Uniwersytecka Street, 40-007 Katowice, Poland*

Синтетизован је нови координациони полимер мангана(II), *catena*-(2-метилимидазолијум-бис(μ_2-хлоро)аквахлороманган(II)), $\{(C_4H_7N_2)[MnCl_3(H_2O)]\}_n$, и окарактерисан помоћу FT-IR спектроскопије и рендгенске структурне анализе. Такође, приказани су резултати термогравиметријске анализе и EPR спектроскопије испитиваног комплекса. Безбојни кристали комплекса су моноклинични, просторна група $P2_1/c$, са параметрима јединичне ћелије: a = 11,298(2) Å, b = 7,2485(14) Å, c = 14,709(5) Å, β = 128,861(18)°, V = 938,0(5) Å^3, Z = 4 и R_1 = 0,03. Наслovљено једињење се састоји од бесконачних једнодимензионалних $[MnCl_3(H_2O)]_n$ анјонских ланаца и изолованих 2-метилимидазолијум катјона. Mn(II) атом је октаедарски координован за четири мосна хлоридна анјона (Mn–Cl = 2,5109(6) – 2,5688(7) Å), један терминални хлоридни анјон (Mn–Cl = 2,5068(11) Å) и H_2O молекул (Mn–O = 2,2351(17) Å). Тродимензионална слојевита структура је изграђена помоћу водоничних веза и слабих π–π стекинг интеракција. Декомпозициона реакција испитиваног комплекса у струји азота се одвија у четири фазе при температурском интервалу 25–900 °C.

(Примљено 18. фебруара, ревидирано 27. септембра 2010)

REFERENCES

1. J. Cheng, J. Xie, X. Lou, *Bioorg. Med. Chem. Lett.* **15** (2005) 267
2. J. Sheng, P. T. M. Nguyen, J. D. Baldeck, J. Olsson, R. E. Marquis, *Arch. Oral Biol*. **51** (2006) 1015
3. K. A. M. Walter, A. C. Braemer, S. Hitt, R. E. Jones, T. R. Matthews, *J. Med. Chem.* **21** (1978) 840
4. H. Nakano, T. Inoue, N. Kawasaki, H. Miyataka, H. Matsumoto, T. Taguchi, N. Inagaki, H. Nagai, T. Satoh, *Bioorg. Med. Chem*. **8** (2000) 373
5. A. Ts. Mavrova, K. Anichina, D. I. Vuchev, J. A. Tsenov, P. S. Denkova, M. S. Kondeva, M. K. Micheva, *Eur. J. Med*. **41** (2006) 1412
6. A. J. Charlston, *Carbohydr. Res*. **29** (1973) 89
7. B. K. Keppler, W. Rupp, U. M. Juhl, H. Endres, R. Niebl, W. Baizer, *Inorg. Chem.* **26** (1987) 4366
8. B. K. Keppler, M. Henn, U. M. Juhl, M. R. Berger, R. Niebl, F. E. Wagner, *Prog. Clin. Biochem. Med*. **10** (1989) 41
9. B. K. Keppler, K. G. Lipponer, B. Stenzel, F. Kratz, *Metal Complexes in Cancer Chemotherapy*, VCH, Weinheim, 1993, p. 187
10. E. Alessio, G. Balducci, A. Lutman, G. Mestroni, M. Calligaris, W. M. Attia, *Inorg. Chim. Acta* **203** (1993) 205
11. G. Mestroni, E. Alessio, A. Sessanta o Santi, S. Geremia, A. Bergamo, G. Sava, A. Boccarelli, A. Schettino, M. Coluccia, *Inorg. Chim. Acta* **273** (1998) 62
12. P. Mura, A. Casini, G. Marcon, L. Messori, *Inorg. Chim. Acta* **312** (2001) 74

13. B. A. Greiner, N. M. Marshall, A. A. Narducci Sarjeant, C. C. McLauchlan, *Inorg. Chim. Acta* **360** (2007) 3132
14. A. Santoro, A. D. Mighell, M. Zocchi, C. W. Reimann, *Acta Crystallogr*. **B25** (1969) 842
15. C. W. Reimann, A. Santoro, A. D. Mighell, *Acta Crystallogr*. **B26** (1970) 521
16. G. J. M. Ivarsson, W. Forsling, *Acta Crystallogr*. **B35** (1979) 1896
17. F. Lambert, J. P. Renault, C. Policar, I. M. Badarou, M. Cesario, *Chem. Commun*. (2000) 35
18. K.-B. Shiu, C.-H. Yen, F.-L. Liao, S.-L. Wang, *Acta Crystallogr*. **E59** (2003) m1189
19. N. Masciocchi, G. A. Ardizzoia, S. Brenna, F. Castelli, S. Galli, A. Maspero, A. Sironi, *Chem. Commun*. (2003) 2018
20. X. C. Huang, J. P. Zhang, Y. Y. Lin, X. L. Yu, X. M. Chen, *Chem. Commun*. (2004) 1100
21. S. Abuskhuna, M. McCann, J. Briody, M. Devereux, V. McKee, *Polyhedron* **23** (2004) 1731
22. Y. Gong, C. Hu, H. Li, W. Pan, X. Niu, Z. Pu, *J. Mol. Struct.* **740** (2005) 153
23. P. C. Chan, *Toxic. Rep. Ser.* **67** (2004) 1-G12
24. J. M. Sanders, R. J. Griffin, L. T. Burka, H. B. Matthews, *J. Toxicol. Environ. Health* **A54** (1998) 121
25. J. D. Johnson, D. Reichelderfer, A. Zutshi, S. Graves, D. Walters, J. Smith, *Toxicol. Environ. Health* **A65** (2002) 869
26. P. C. Chan, R. C. Sills, G. E. Kissling, A. Nyska, W. Richter, *Arch. Toxicol.* **6** (2008) 399
27. P. Moore-Testa, Y. Saint-Jalm, A. Testa, *J. Chromatogr.* **290** (1984) 263
28. B. Hachuła, M. Nowak, J. Kusz, *J. Chem. Crystallogr*. **3** (2010) 201
29. B. Hachuła, M. Pędras, D. Pentak, M. Nowak, J. Kusz, J. Borek, *Acta Crystallogr*. **C65** (2009) m215
30. F. H. Allen, *Acta Crystallogr*. **B58** (2002) 380
31. J. C. MacDonald, T. J. M. Luo, G. T. R. Palmore, *Cryst. Growth. Des*. **4** (2004) 1203
32. D. Cheng, M. A. Khan, R. P. Houser, *Inorg. Chim. Acta* **351** (2003) 242
33. C.-W. Su, C.-P. Wu, J.-D. Chen, L.-S. Liou, J.-C. Wang, *Inorg. Chem. Commun*. **5** (2002) 215
34. Oxford Diffraction, CrysAlis CCD & CrysAlis RED, Version 1.171.29, Oxford Diffraction Ltd., Wrocław, Poland, 2006
35. G. M. Sheldrick, SHELX-97, Program package for crystal structure solution and refinement, *Acta Crystallogr*. **A64** (2008) 112
36. A. Orpen, K. Brammer, F. H. Allen, O. Kennard, D. G. Watson, R. Taylor, *J. Chem. Soc. Dalton Trans.* (1989) S1–S83
37. M. A. Kurawa, C. J. Adams, A. G. Orpen, *Acta Cryst*. **E64** (2008) m1276
38. A. Garoufis, S. Kasselouri, S. Boyatzis, C. P. Raptopoulou, *Polyhedron* **18** (1999) 1615
39. M. C. Etter, J. C. MacDonald, J. Bernstein, *Acta Cryst.* **B46** (1990) 256
40. J. Bernstein, R. E. Davies, L. Shimoni, N.-L. Chang, *Angew. Chem. Int. Ed. Engl*. **34** (1995) 1555
41. C. Janiak, *J. Chem. Soc. Dalton Trans*. (2000) 3885
42. T. P. J. Garrett, J. M. Guss, H. C. Freeman, *Acta Crystallogr.* **C39** (1983) 1031
43. Y. Liu, D. Xu, J. Liu, *J. Coord. Chem*. **54** (2001) 175
44. S.-Y. Niu, S.-S. Zhang, X.-M. Li, Y.-H. Wen, K. Jiao, *Acta Crystallogr*. **E60** (2004) m209
45. H. Kooijman, *Acta Crystallogr*. **E62** (2006) m2681

46. P. Lemoine, V. Viossat, E. Dayan, N.-H. Dung, B. Viossat, *Inorg. Chim. Acta* **359** (2006) 4274
47. C.-M. Zhong, Y.-J. Zuo, H.-S. Jin, T.-C. Wang, S.-Q. Liu, *Acta Crystallogr.* **E62** (2006) m2605
48. M. Arif, S. Nazir, M. S. Iqbal, S. Anjum, *Inorg. Chim. Acta* **362** (2009) 1624
49. P. Naumov, M. Ristova, B. Soptrajanov, M. Zugik, *J. Mol. Struct.* **598** (2001) 235
50. B. Hachuła, M. Pędras, M. Nowak, J. Kusz, D. Skrzypek, J. Borek, D. Pentak, *J. Coord. Chem.* **63** (2010) 67
51. M. Sikorska-Iwan, R. Mrozek, Z. Rzączyńska, *J. Therm. Anal. Cal.* **60** (2000) 139
52. R. Mrozek, Z. Rzączyńska, M. Sikorska-Iwan, *J. Therm. Anal. Cal.* **63** (2001) 839
53. Z.-Q. Zhang, R.-D. Huang, Y.-Q. Xu, L.-Q. Yu, Z.-W. Jiao, Q.-L. Zhu, C.-W. Hu, *Inorg. Chim. Acta* **362** (2009) 5183
54. 54. B. S. Garg, M. R. P. Kurup, S. K. Jain, Y. K. Bhoon, *Transition Met. Chem*. **13** (1998) 92
55. A. Sreekath, M. Joseph, H.-K. Fun, M. R. P. Kurup, *Polyhedron* **25** (2006) 1408
56. G. H. Reed, G. D. Markham, in *Biological Magnetic Resonance*, L. J. Berliner, J. Reuben, Eds., Plenum Press, New York, 1984, p. 73
57. V. K. Jain, G. Lehmann. *Phys. Status Solidi* **B159** (1990) 495
58. B. Ke, *Photosynthesis: Photobiochemistry and Photobiophysics*, Kluwer Academic Publishers, Dordrecht, 2001, p. 337.

Journal of the Serbian Chemical Society
JSCS-info@shd.org.rs • www.shd.org.rs/JSCS
J. Serb. Chem. Soc. *76* (2) 249–261 (2011) UDC 546.654.3+542.913:543.57:66.095.13/.14
JSCS–4116 *Original scientific paper*

Synthesis and spectroscopic characterization of some lanthanide(III) nitrate complexes of ethyl 2-[2-(1-acetyl-2--oxopropyl)azo]-4,5-dimethyl-3-thiophenecarboxyate

CHEMPAKAM JANARDHANAN ATHIRA, YESODHARAN SINDHU, MATHUNNI SUSAMMA SUJAMOL and KOCHUKITTAN MOHANAN*

Department of Chemistry, University of Kerala, Kariavattom Campus, Trivandrum-695 581, Kerala, India

(Received 14 April, revised 10 September 2010)

Abstract: Ethyl 2-[2-(1-acetyl-2-oxopropyl)azo]-4,5-dimethyl-3-thiophenecarboxyate was synthesized by coupling diazotized ethyl 2-amino-4,5-dimethyl-thiophene-3-carboxylate with acetylacetone. Based on various spectral studies and elemental analysis, an intramolecularly hydrogen-bonded azo-enol structural form was assigned for the ligand. This ligand is versatile in forming a series of lanthanide(III) complexes, *viz.*, lanthanum(III), cerium(III), praseodymium(III), neodymium(III), samarium(III) and gadolinium(III), which were characterized through various spectral studies, elemental analysis, magnetic susceptibility measurements, molar conductance and thermal analysis. The spectral data revealed that the ligand acted as a neutral tridentate, coordinating to the metal ion through one of the azo nitrogen atoms, the ester carbonyl and the enolic oxygen of the acetylacetone moiety, without deprotonation. Molar conductance values adequately supported their non-electrolytic nature. The ligand and lanthanum(III) complex were subjected to X-ray diffraction studies. In addition, the lanthanum(III) complex underwent a facile transesterification reaction on refluxing with methanol for a long period. The thermal behaviour of the lanthanum(III) complex was also examined.

Keywords: azo derivative; lanthanum(III) complex; molar conductance; XRD; transesterification; thermal analysis.

INTRODUCTION

The ever increasing interest in the coordination chemistry of azo derivatives is attributable to their use as complexing agents, dyeing materials, antidepressants and antitubercular agents, models for biological systems and chromogenic reagents.[1–5] Recent years have witnessed a tremendous upsurge of in-

* Corresponding author. E-mail: drkmohanan@rediffmail.com
doi: 10.2298/JSC100414025A

terest in the synthesis and characterization of metal chelates containing heterocyclic azo dyes as ligands. Azo dyes derived from 2-aminothiophene derivatives have many advantages, including a colour deepening effect as an intrinsic property of the thiophene ring, a small molecular structure leading to better dyeability and the heterocyclic structure of thiophene ring resulting in good sublimation fastness of dyed fibres.[6] The colour of these azo derivatives depends on the diazo and the coupling components. The diazo components of 2-aminothiophene derivatives tend to show a bathochromic shift and high tinctorial strength, when compared to analogous dyes derived from a cyclic aromatic system.[7] Due to the presence of the –N=N– group and a β-diketone moiety in a single compound, their effectiveness of complex formation surpasses those of the parent compounds. Metal complexes of lanthanide(III) ions containing azo derivatives have been extensively investigated.[1,8–11] However, due to the instability of aminothiophene, lanthanide(III) complexes of azo dyes formed from 2 or 3-aminothiophene have hitherto only received sporadic attention. Nevertheless, the stability of 2-aminothiophene was increased by suitable substitution at the remaining positions by a versatile synthetic method developed by Gewald.[12] Apart from providing stability to 2-aminothiophene, the introduction of a ethoxycarbonyl group at 3-position of the thiophene ring, provided further scope for reactivity and a new coordination site. In view of this, and as part of our continuing interest on structural and thermal aspects of heterocyclic azo derivatives and their lanthanide(III) complexes, herein the synthesis, spectral and thermal studies are reported of a new series of lanthanide(III) complexes of an azo derivative of aminothiophene, *viz.*, ethyl 2-[2-(1-acetyl-2-oxopropyl)azo]-4,5-dimethyl-3-thiophenecarboxyate (HAAT). Moreover, the structural aspect of the ligand, the bioisosteric relationship of thiophene to benzene, gives added significance to this investigation.

EXPERIMENTAL

Materials

All employed chemicals were of AnalaR grade purchased from Aldrich, Fischer and Sisco chemicals and used without further purification. Lanthanide(III) nitrates were prepared by dissolving the corresponding oxide in 50 % nitric acid, followed by crystallization.

Preparation of the ligand

The thiophene intermediate was synthesized by a reported method.[12] This thiophene intermediate was diazotized at 0–5 °C using $NaNO_2$ and concentrated H_2SO_4. Urea was added to this diazonium salt solution to remove excess nitrous acid. The resulting diazonium salt solution was immediately coupled with acetylacetone in methanol. The pH of the reaction mixture was adjusted to 8–9 by adding the required amount of sodium acetate solution (10 %) while keeping the temperature below 5 °C. The obtained product was filtered off, washed with small amount of water and finally with diethyl ether and dried (m.p. 92 °C; yield: 80 %).

Preparation of the metal complexes

A solution of lanthanide(III) nitrate (0.5 mmol) in methanol was added to a warm methanolic solution (50 cm^3) of the ligand (1 mmol). After 3 h stirring, the pH of the solution was adjusted to 6.5–7.0 and the resulting solution was then refluxed on a water-bath for about 12 h. The solution was then concentrated and kept overnight. The powdery material thus separated was filtered, washed successively with small amounts of MeOH and finally with diethyl ether and dried in vacuum over P_4O_{10} (m.p. <180 °C; yield: 55–60 %).

Physical measurements

Carbon, hydrogen and nitrogen analysis were performed using a Heraeus Carlo Erba 1108-CHN analyzer. The complexes were analyzed for their metal content by the oxalate–oxide method.[13] Molar conductance measurements were performed using 10^{-3} M solution of the metal complexes in DMSO, DMF and nitrobenzene at room temperature using a Systronics direct reading conductivity meter, type 304. Infrared spectral studies were realised using KBr discs on a Shimadzu FT-IR 8000 spectrophotometer in the range 4000–400 cm^{-1} and far infrared spectra were recorded on a Polytec FIR 30 spectrometer in the range 400–200 cm^{-1} using CsI discs. The electronic spectra were recorded on a Hitachi 320 UV–Visible spectrophotometer. Magnetic susceptibility values of the complexes were measured at room temperature with a Magway MSB Mk 1 susceptibility balance. The ^{1}H-NMR spectra were recorded in DMSO-d_6 on a JEOL GSX 400NB 400 MHz FTNMR spectrometer. The X-ray diffraction study was conducted using a Siemens D 5005 model spectrometer. Thermal analysis was performed using a Mettler Toledo Thermogravimetric analyzer in dynamic air at a heating rate of 10 °C min^{-1}.

Transesterification

Transesterification of the lanthanum(III) complex was performed by a reported method.[14] About 0.1 g of lanthanum(III) complex was suspended in hot methanol (100 cm^3) and refluxed for 48 h on a water-bath. The resulting solution was then evaporated to dryness and the solid product obtained was washed repeatedly with diethyl ether and dried over P_4O_{10} in vacuum.

RESULTS AND DISCUSSION

The ligand and the metal complexes were air-stable and possessed good keeping qualities. Analytical data of the ligand and its complexes are in good agreement with their formulation, as given in the Table I. The formulation of these complexes was made based on elemental analysis, molar conductance, magnetic susceptibility measurements and various spectral data. The molar conductance values of the complexes (Table II) support their non-electrolytic nature.[15] The complexes exhibited 1:2 metal-ligand stoichiometry, in which the ligand is coordinated to the metal ion without deprotonation in a tridentate mode. The purity of the ligand and its complexes were confirmed by the TLC technique.

The principal advantage of the diazo component is that the yield is very high, the reaction time is short, and the procedure involves only one facile step. However, one disadvantage of the ester functionality is that its conjugation with amino group reduces the basicity of the nitrogen atom and thus efficient diazotization can only be achieved using nitrosylsulphuric acid obtained from $NaNO_2$

and H_2SO_4.[16] The ligand formed well defined complexes with lanthanum(III), cerium(III), praseodymium(III), neodymium(III), samarium(III) and gadolinium(III) nitrates. The formation of the metal complexes can be represented by the following general equation:

$$M(NO_3)_3 + HAAT \rightarrow [M(HAAT)_2(NO_3)_3]$$

where M = La(III), Ce(III), Pr(III), Sm(III), Nd(III) or Gd(III) and HAAT = ethyl 2-[2-(1-acetyl-2-oxopropyl)azo]-4,5-dimethyl-3-thiophenecarboxyate.

TABLE I. Analytical and magnetic moment data of the ligand and its metal complexes

Compound	Yield	Found (Calcd.), %					μ / μ_B
	%	C	H	N	S	M	
HAAT	80	54.18 (54.12)	5.85 (5.83)	9.02 (9.03)	10.33 (10.31)	–	–
$[La(HAAT)_2(NO_3)_3]$	64	35.56 (35.54)	3.84 (3.85)	10.37 (10.35)	6.78 (6.79)	14.69 (14.67)	Diamagnetic
$[Ce(HAAT)_2(NO_3)_3]$	70	35.52 (35.50)	3.83 (3.82)	10.35 (10.33)	6.77 (6.78)	14.79 (14.78)	2.55
$[Pr(HAAT)_2(NO_3)_3]$	67	35.49 (35.46)	3.82 (3.81)	10.34 (10.33)	6.76 (6.75)	14.86 (14.84)	3.57
$[Nd(HAAT)_2(NO_3)_3]$	65	35.34 (35.33)	3.81 (3.80)	10.30 (10.31)	6.74 (6.72)	(15.22) (15.20)	3.65
$[Sm(HAAT)_2(NO_3)_3]$	67	35.14 (35.15)	3.79 (3.78)	10.24 (10.22)	6.70 (6.68)	15.71 (15.70)	1.52
$[Gd(HAAT)_2(NO_3)_3]$	71	34.89 (34.87)	3.76 (3.73)	10.17 (10.18)	6.65 (6.67)	16.31 (16.30)	7.86

TABLE II. Molar conductance data (S cm^2 mol^{-1}) of the metal complexes

Complex	Solvent		
	DMSO	DMF	Nitrobenzene
$[La(HAAT)_2(NO_3)_3]$	8.6	14.4	5.6
$[Ce(HAAT)_2(NO_3)_3]$	8.9	13.3	4.6
$[Pr(HAAT)_2(NO_3)_3]$	7.5	13.5	4.3
$[Nd(HAAT)_2(NO_3)_3]$	8.8	14.6	4.8
$[Sm(HAAT)_2(NO_3)_3]$	8.5	13.9	5.6
$[Gd(HAAT)_2(NO_3)_3]$	7.9	13.6	4.5

Structure of the ligand

Generally, compounds obtained by the coupling reaction of a 1,3-diketone with an aryl diazonium ion are capable of exhibiting azo-hydrazo tautomerism (Fig. 1). There are reports that the ultraviolet absorption spectrum of monophenyl azo compounds differ from those of monophenyl hydrazones. The former azo compounds exhibit a strong absorption band at a wavelength of 270–280 nm, while the latter hydrazones give a strong band above 320 nm. The ultra-violet spectrum of the ligand HAAT exhibited a strong band at 280 nm characteristic of

the azo form.[17] The IR spectrum of HAAT adequately supported the conclusions made based on UV–Vis spectral data.

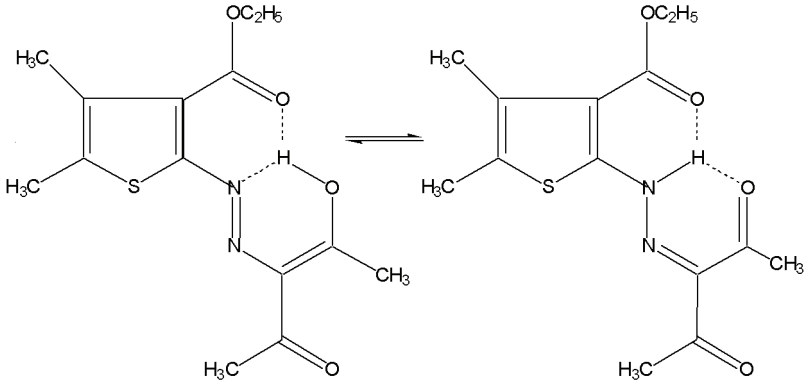

Fig. 1. Tautomeric structure of the ligand.

The IR spectrum of the free ligand (Fig. 2) exhibited a broad medium intensity band in the region 3300–3000 cm^{-1} and centred at 3100 cm^{-1}, which is assignable to the O–H stretching vibration of internally hydrogen bonded enolic group.[18] The medium intensity band observed at 1493 cm^{-1} can be assigned to ν(–N=N–), confirming the formation of the azo derivative.[19] The band observed at 1274 cm^{-1} is attributed to C–O stretching (enolic) vibration.[20] Thus, the IR spectrum strongly supports the existence of the free ligand in an intramolecularly hydrogen bonded azo-enol form. The free acetyl carbonyl band of the acetylacetone moiety was observed at 1690 cm^{-1}.[21] Apart from these vibrations, the infrared spectrum of the ligand also exhibited a strong band at 1678 cm^{-1} due to the ester carbonyl group.[22] The ester carbonyl group was also involved in weak hydrogen bonding with the OH group, forming a sort of bifunctional hydrogen bonding in the free ligand. Nevertheless, in competition with the azo nitrogen for the enolic OH, the ester carbonyl of the thiophene moiety can only manage a partial share. This elucidated the reason for the ester carbonyl frequency appearing relatively higher than that in the free amine (1660 cm^{-1}). In addition to the above frequencies, vibrations characteristic of substituted thiophene ring were observed at 1524, 1396 and 1352 cm^{-1}.[23]

In agreement with the UV and IR spectral data, the ^{1}H-NMR spectrum of the ligand (Fig. 3) clearly evinces its existence in the azo-enol form (Fig. 1). The ^{1}H--NMR spectrum of the ligand recorded in DMSO-d_6 exhibited two methyl proton signals of equal intensity, each around 2.46 and 2.33 ppm of the two acetyl groups on the acetylacetone moiety, which indicates that one of these groups undergoes a shift in the chemical environment because of hydrogen bonding with the azo group. The low intensity signal resonating at 15.42 ppm can be confi-

dently assigned to the intramolecularly hydrogen bonded enolic proton of the ligand.[24] Signals for methyl and methylene protons of the ester function were observed at δ 1.45 and 4.49 ppm, respectively. The signal appearing 2.27 ppm could be attributed to the two methyl groups at 4th and 5th position on the thiophene moiety.

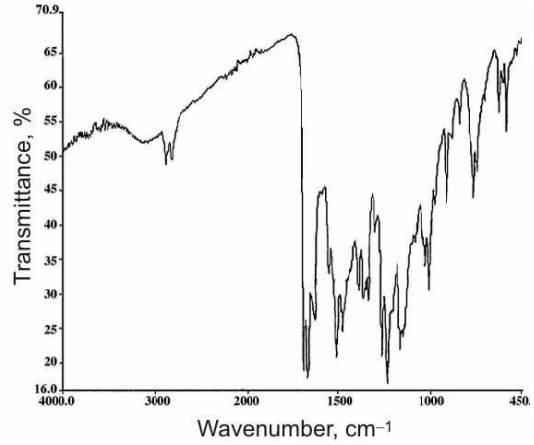

Fig. 2. IR spectrum of the ligand.

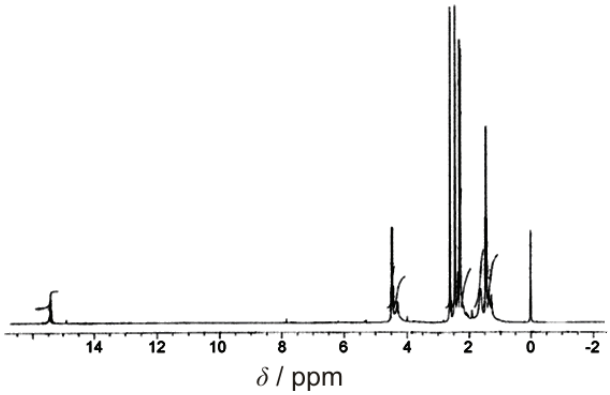

Fig. 3. ^{1}H-NMR spectrum of the ligand.

Structure of metal complexes

The electronic spectra of all the complexes recorded in DMSO are only marginally red shifted from that of the ligand, indicating that the complexes are isostructural and the ligand exhibits the same structural form in the synthesized complexes.

IR spectra. The infrared spectrum of the ligand was compared with those of the metal complexes in order to ascertain the coordination sites that may be involved in chelation (Table III). In the spectra of the metal complexes (Fig. 4),

the band apparently due to the internally hydrogen bonded OH group was shifted to higher frequency and became less broad showing a peak centred at ≈3120 cm^{-1}, indicating that the OH group is coordinated to the metal ion without deprotonation. As the interaction of the lanthanide ion with the enolic oxygen does not increase the acidity sufficiently for the ionization of the proton, the enolic oxygen coordinates to the metal ion without deprotonation.[25] This is further supported by the positive shift of the ν(C–O) plane bending band by about 20 cm^{-1} in the metal complexes. The band due to ν(N=N) shifted appreciably to a lower wave number by 25–30 cm^{-1}, indicating the involvement of the azo nitrogen in the bonding with the metal ion.[26] The free acetyl carbonyl band at 1690 cm^{-1} of the acetylacetone moiety was only marginally shifted during complexation, suggesting its non-participation in the coordination.[27] The ester carbonyl stretching frequency of the ligand was lowered by ≈40 cm^{-1} in the lanthanide(III) complexes, indicating the involvement of the ester carbonyl group in the chelation.[28]

TABLE III. Infrared data of the ligand and its metal complexes (cm^{-1})

Compound	ν(O–H)	ν(C=O) of ester carbonyl	ν(N=N)	ν(C–O)	ν(C=O) of free acetyl carbonyl	ν(Ln–N)	ν(Ln–O)
HAAT	3100	1677	1493	1274	1690	–	–
$[La(HAAT)_2(NO_3)_3]$	3118	1637	1463	1294	1691	365	435
$[Ce(HAAT)_2(NO_3)_3]$	3120	1638	1465	1295	1693	367	437
$[Pr(HAAT)_2(NO_3)_3]$	3121	1636	1468	1294	1691	370	438
$[Nd(HAAT)_2(NO_3)_3]$	3119	1637	1467	1296	1689	366	436
$[Sm(HAAT)_2(NO_3)_3]$	3122	1636	1464	1293	1690	368	439
$[Gd(HAAT)_2(NO_3)_3]$	3120	1639	1466	1294	1692	367	440

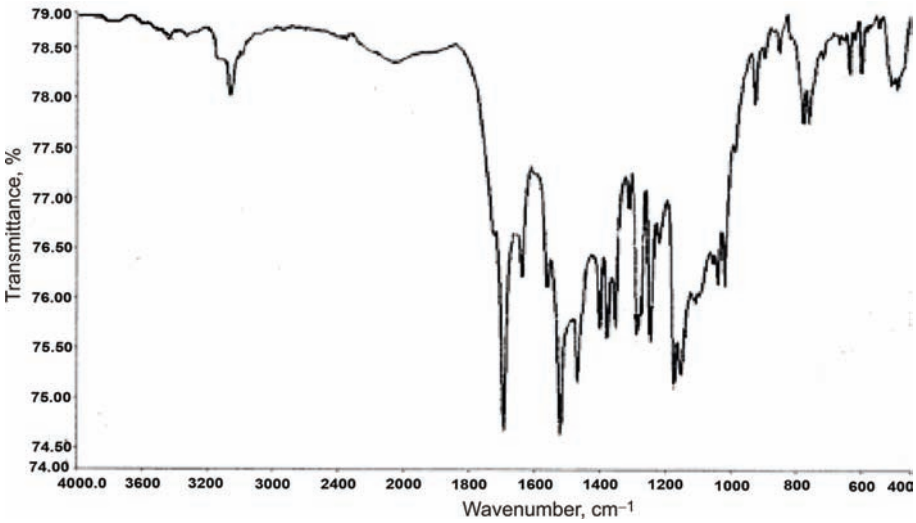

Fig. 4. IR spectrum of the lanthanum(III) complex.

The characteristic vibrations of the substituted thiophene ring remained almost unaffected in the metal chelates. This excludes the possibility of bonding by the ring sulphur atom to the metal ion. The absence of a ν(M–S) band in the far infrared spectra of the metal complexes also gives additional evidence for the non-participation of ring sulphur in coordination with the metal ion. In the spectra of the nitrato complexes, there are two additional bands observed at ≈1457 and ≈1257 cm^{-1}, which were absent in the spectrum of the free ligand. These bands are assigned to the ν_5 and ν_1 modes of the nitrate ions, respectively. Since the magnitude of the separation between ν_5 and ν_1 is >200 cm^{-1}, it is concluded that the nitrate is coordinated in a bidentate fashion.[29] Crystallographically, it has been observed that nitrate is invariably bidentate towards lanthanide ions.[30] "Short bite" ligands, such as nitrate (bidentate), minimize ligand–ligand repulsion and hence are suited to lanthanides, which show a pronounced tendency to attain relatively high coordination numbers. The far infrared spectra of the metal complexes exhibited non-ligand bands in the regions 435–440 and 365–370 cm^{-1}, assignable to ν(M–O) and ν(M–N) vibrations, respectively.[28]

^{1}H-NMR spectrum. The ^{1}H-NMR spectrum of the lanthanum(III) complex recorded in DMSO-d_6 further substantiates the mode of coordination suggested by the electronic and IR spectral studies. The ^{1}H-NMR spectrum of the complex (Fig. 5) also exhibited a signal for OH proton at 15.12 ppm, indicating that the OH group is coordinated to the metal ion without deprotonation. The signals due to other protons are found in the expected regions and shifted by about 0.1–0.2 ppm in the spectra of the metal complexes. Thus, from the above spectral data, it is clear that the ligand is coordinated to the metal ion without deprotonation in a tridentate fashion.

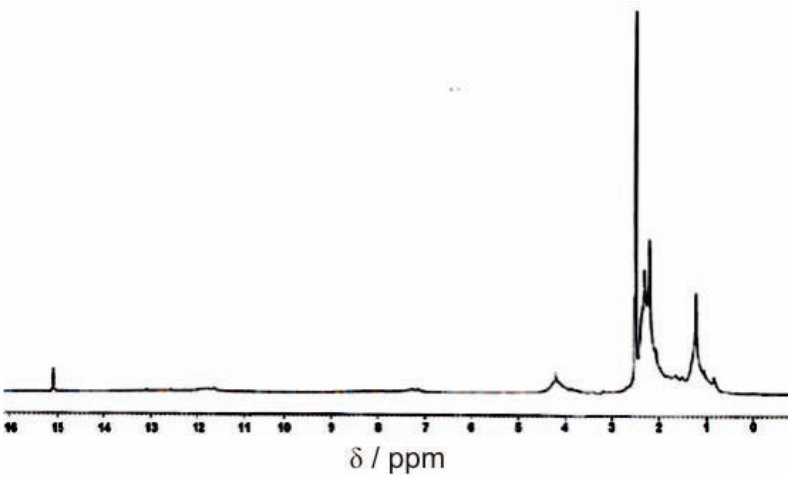

Fig. 5. ^{1}H-NMR spectrum of the lanthanum(III) complex.

Magnetic moment. Unlike the d-electrons of the transition metal ions, the f-electrons of the lanthanide ions are almost unaffected by the chemical environment and the energy levels are the same as in the free ion, due to very effective shielding by the overlying $5s^2$ and $5p^6$ shells. The magnetic moment values of the complexes showed that the lanthanum(III) complex is diamagnetic, while all others are paramagnetic, showing close agreement with the calculated values except for the samarium(III), indicating an insignificant participation of the 4f electrons in the bonding. The relatively high value obtained in the case of the samarium(III) complex may be due to the small J–J separation, which leads to thermal population of the higher energy levels and show susceptibilities due to the first-order Zeeman effect.[31]

Electronic spectra. The lanthanum(III) complex has no significant absorption in the visible region, owing to the absence of 4f orbital electrons. The visible spectral bands of the lanthanide complexes were hypersensitive to stereochemistry. An enhancement of the intensity of certain hypersensitive bands of the praseodymium(III), neodymium(III) and samarium(III) complexes compared to the respective aquated ions was observed. These variations can be attributed to the action of an inhomogeneous electromagnetic field and by changes in the symmetry of the field on the lanthanide ion.[32] The sharp bands due to f–f transitions originating within the $4f^n$ configuration of the lanthanide ions are only slightly affected by the immediate surroundings of the metal ion, and this is commonly attributed to the shielded nature of the 4f orbitals by the overlying $5s^2$ and $5p^6$ orbitals. However, a shift to a lower frequency can be considered as being due to complex formation.

X-Ray diffraction. The diffractogram of the ligand recorded 16 reflections for the 2θ range from 11 to 52° with maxima at 2θ = 25.6069°, which corresponds to interplanar distance d = 3.4758 Å. The X-ray diffraction data are given in Table IV. The X-ray diffraction pattern of the ligand indicates high crystallinity. The obtained $\sin^2\theta$ values were compared with the calculated values. The observed values of the ligand fit well with an orthorhombic crystal system,[33] with lattice parameters, a = 6.50469 Å, b = 7.61705 Å, c = 11.53506 Å and a unit cell volume of 571.52241 $Å^3$. It was observed that the crystallinity of the ligand was lost on complexation.

Transesterification

Transesterification is a process in which an ester fragment is transformed into another through interchange of the alkoxy moiety. It is more advantageous than ester synthesis from carboxylic acids and alcohols. As transesterification is an equilibrium process, the ease with which a target ester is formed is dependent on the combination of alcohol and ester reactants. It was observed that methanol has the strongest replacing power, as the formation of methyl acetate is thermo-

dynamically favoured. Several reports indicate that metal chelates of carboxylic esters undergo facile transesterification on refluxing with an alcohol. However, such studies on heterocyclic azo complexes are rare. In the present investigation, the lanthanum(III) complex was subjected to transesterification reaction in methanol medium according to a reported method.[14]

TABLE IV. XRD Pattern of the ligand

Peak No.	*d* / Å	Relative intensity, %	Observed 2θ	Calculated 2θ	Observed $\sin^2\theta$	Calculated $\sin^2\theta$	*hkl*
1	7.54009	89.62	11.72689	11.55753	0.010426	0.010138	221
2	5.68113	35.02	15.58498	15.62098	0.018365	0.018468	101
3	5.49650	23.09	16.11191	15.34367	0.019619	0.017822	002
4	5.03394	5.37	17.60367	17.91051	0.023391	0.024231	110
5	4.11494	9.20	21.57783	20.55591	0.035005	0.031835	102
6	3.87358	28.57	22.93997	23.10314	0.039504	0.0401	003
7	3.77288	10.54	23.56093	23.66699	0.041641	0.042053	112
8	3.47587	100.00	25.60694	25.92541	0.049061	0.050318	013
9	3.32804	11.59	26.76509	26.90272	0.053517	0.054112	120
10	3.16880	10.07	28.1371	28.198721	0.05903	0.059343	121
11	3.02580	7.39	29.49633	29.38550	0.064742	0.064331	113
12	2.76088	2.91	32.40085	31.54210	0.077763	0.073872	202
13	2.66705	2.31	33.57384	33.71405	0.083331	0.084091	212
14	2.44176	2.69	36.77723	36.27854	0.099418	0.096925	220
15	2.34487	3.61	38.355	38.06944	0.107804	0.106368	213
16	2.06282	4.08	43.85236	43.45189	0.139302	0.137024	223

The crystallinity, appearance and the solubility behaviour of the product obtained after transesterification was distinctly different from those of the ethyl derivative. Apart from these, the ester carbonyl stretching frequency observed for the methyl derivative at 1627 cm^{-1} is a direct indication of the occurrence of transesterification. Substitution of ethyl group by methyl group was further confirmed by the ^{1}H-NMR spectrum of the product.

Although several mechanisms have been proposed to explain transesterification reactions, it appears that increased nucleophilicity of the acyl carbon atom induced by the azo group is of great importance. It was also reported[14] that an alkoxycarbonyl group attached to the carbon atom can be readily transesterified. As difficulties are encountered in the preparation of metal chelates of esters, the general method of synthesis by transesterification has gained acceptance.

Thermogravimetric analysis

Thermogravimetric analysis was performed on the lanthanum(III) complex with the aim of understanding the thermal behaviour of the complex. The TG profile (Fig. 6) showed no weight loss up to 170 °C, which indicates the absence of either crystallization or coordinated water molecules in the complex. The

lanthanum(III) complex underwent a two-stage decomposition, as denoted by the two DTG peaks at 351 and 617 °C. The first stage of decomposition started at 180 °C and was completed at 440 °C, with a mass loss of 26.89 % (Calcd. 28.21 %), corresponding to the loss of the azo group and the acetylacetone moiety. The second stage of decomposition occurred in the temperature range 480–680 °C, with a mass loss of 65.54 % (Calcd. 63.60 %) due to the oxidative decomposition of the complex to La_2O_3. The mass loss agrees fairly well with that found in independent pyrolysis experiments.

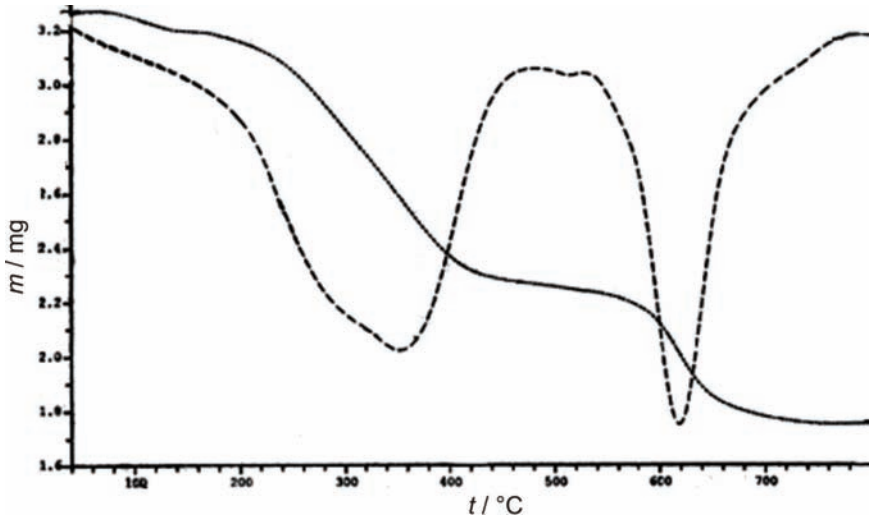

Fig. 6. TG and DTG curve of lanthanum(III) complex.

Based on the analytical, physico–chemical and spectral results, the structure of the metal complex shown in Fig. 7 was assigned.

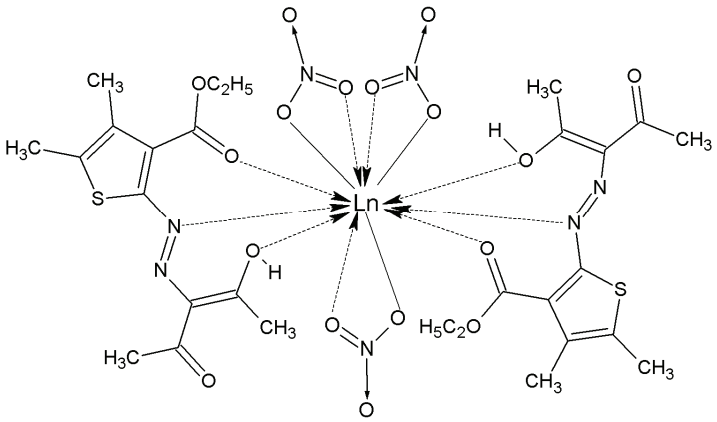

Fig. 7. Proposed structure of the lanthanide(III) complex.

CONCLUSIONS

A heterocyclic ligand obtained by the coupling of diazotized ethyl 2-amino--4,5-dimethylthiophene-3-carboxylate with acetylacetone, *viz*., ethyl 2-[2-(1-acetyl-2-oxopropyl)azo]-4,5-dimethyl-3-thiophenecarboxyate, acted as a neutral tridentate ligand. The ligand formed a series of lanthanide(III) complexes with a 1:2 metal–ligand stoichiometry. Spectral studies revealed that the ligand possessed an azo–enol structure and this structural form of the ligand persisted in the metal complexes. The infrared spectral data adequately supported the bidentate coordination of nitrate ions. Based on the spectral evidence, it could be concluded that the ligand behaved as neutral tridentate, coordinating to the metal ion through one of the azo nitrogen atoms, the ester carbonyl and the enolic oxygen of the acetylacetone moiety without deprotonation. A coordination number of twelve is proposed for the studied lanthanide(III) complexes. Thermal analyses indicated a greater stability of the lanthanum(III) complex compared to the ligand.

Acknowledgements. We express our sincere gratitude to Professor and Head, Department of Chemistry, University of Kerala, Kariavattom Campus, Trivandrum-695 581, Kerala, India, for providing the necessary facilities for carrying out this work. We are also glad to acknowledge the instrumental facilities provided by the Sophisticated Analytical Instrumental Facility, Cochin; IIT Bombay and the National Institute for Interdisciplinary Science and Technology, Trivandrum, India.

ИЗВОД

СИНТЕЗА И СПЕКТРОСКОПСКА КАРАКТЕРИЗАЦИЈА КОМПЛЕКСА ЛАНТАНОИД(III) НИТРАТА СА ЕТИЛ-2-[2-(1-АЦЕТИЛ-2-ОКСОПРОПИЛ)АЗО]-4,5-ДИМЕТИЛ-3-ТИОФЕНКАРБОКСИЛАТОМ КАО ЛИГАНДОМ

CHEMPAKAM JANARDHANAN ATHIRA, YESODHARAN SINDHU, MATHUNNI SUSAMMA SUJAMOL и KOCHUKITTAN MOHANAN

Department of Chemistry, University of Kerala, Kariavattom Campus, Trivandrum-695 581, Kerala, India

У реакцији између диазотованог етил-2-амино-4,5-диметилтиофен-3-карбоксилата и ацетилацетона синтетизован је нови лиганд етил-2-[2-(1-ацетил-2-оксопропил)азо]-4,5-диметил-3-тиофенкарбоксилат. На бази спектроскопских испитивања и резултата елементарне микроанализе нађено је да синтетисани лиганд има интрамолекулским водоничним везама повезану азо-енолну структурну форму. Овај лиганд се показао врло погодним за грађење серије различитих комплекса лантаноида(III), као што су лантан(III), цер(III), празеодим(III), неодим(III), самаријум(III) и гадолинијум(III) комплекси који су у овом раду окарактерисани помоћу различитих спектроскопских метода, елементалне микроанализе, мерења магнетне и моларне проводљивости и термалне анализе. На основу спектроскопских изучавања закључено је да је неутрална форма лиганда тридентатно координована преко азо атома азота, карбонилног кисеониковог атома естарске групе и протонованог енолног атома кисеоника из ацетилацетонског остатка овог лиганда. Вредности за моларну проводљивост ових комплекса указују на њихову неутралну форму. Лиганд и одговарајући комплекси лантана(III) су испитивани методом дифракције X-зрака. Нађено је да комплекси лантана(III) подлежу реак-

ција трансестерификације приликом рефлуктовања у метанолу у току дужег временског периода. Испитивана је термална стабилност изолованих комплекса лантана(III).

(Примљено 14. априла, ревидирано 10. септембра 2010)

REFERENCES

1. A. E. Basheir, L. S. Shanker, S. A. Mohamed, M. M. Mahmoud, *Can. J. Chem.* **66** (1988) 2362
2. S. Zeynel, E. Nermin, Y. Ebru, U. Guven, *Color Technol*. **124** (2007) 27
3. A. A. Salem, Y. M. Issa, E. E. El-Shreafy, *J. Therm. Anal*. **48** (1997) 851
4. A. T. Mubarak, *Spectrochim. Acta A* **61** (2005) 1163
5. A. M. Khedr, M. Gaber, *Spectrosc. Lett.* **38 (**2005) 431
6. S. A. Alaa, H. A. Tarek, *Dyes Pigm.* **70** (2006) 8
7. M. S. Yen, I. J. Wang, *Dyes Pigm.* **62** (2004) 173
8. M. M. Moustafa, *Synth. React. Inorg. Met-Org. Chem.* **27** (1997) 1417
9. B. A. El-Shetary, S. L. Stefan, F. I. Zidan, El-Maraghy, *Monatsh. Chem.* **118** (1987) 1101
10. S. A. Abdel-Latif, *Synth. React. Inorg. Met-Org. Chem*. **31** (2001) 1355
11. K. Mohanan, C. J. Athira, Y. Sindhu, M. S. Sujamol, *J. Rare Earths* **27** (2009) 705
12. K. Gewald, E. Schinke, H. Böllcher, *Chem. Ber*. **99** (1966) 94
13. I. M. Kolthoff, P. J. Elving, *Treatise on Analytical Chemistry, Part II*, Vol. 8, Interscience, New York, 1963, p. 330
14. F. Jursik, B. Hajek, *Inorg. Chim. Acta* **13** (1975) 169
15. W. J. Geary, *Coord. Chem. Rev*. **7** (1971**)** 81
16. H. R. Maradiya, V. S. Patel, *Chem. Heterocycl. Compd*. **38** (2002) 1324
17. H. C. Yao, *J. Org. Chem*. **29** (1964**)** 2959
18. M. B. Ummathur, *J. Iran. Chem. Soc.* **4 (**2007) 244
19. H. B. Hassib, S. A. Abdel-Latif, *Spectrochim. Acta A* **59** (2003) 2425
20. K. Krishnankutty, P. Sayudevi, M. B. Ummathur, *J. Indian Chem. Soc*. **84** (2007) 337
21. E. V. Shchegol'kov, O. G. Khudina, L. V. Anikina, Y. V. Burgart, V. I. Saloutin, *Pharm. Chem. J*. **40** (2006) 373
22. G. Hallas, A. D. Towns, *Dyes Pigm.* **32** (1996**)** 135
23. C. N. R. Rao, *Chemical Applications of Infrared Spectroscopy*, Academic Press, New York, 1963
24. E. Abdel-Latif, F.A. Amer, *Monatsh. Chem.* **139** (2008) 561
25. G. F. De Sa, E. Giesbrecht, L. C. Thompson, *J. Inorg. Nucl. Chem.* **37** (1975*)* 109
26. R. Sherif, K. Mohanan, *Asian J. Chem*. **13** (2001) 177
27. M. Thankamony, K. Mohanan, *Indian J. Chem. A* **46** (2007) 247
28. K. Mohanan, S. N. Devi, *Russ. J. Coord. Chem*. **32** (2006) 600
29. S. Kavita, B. V. Agarwala, *Synth. React. Inorg. Met-Org. Chem.* **26** (1996) 473
30. J. I. Bullock, H. A.T. Riahi, *Inorg. Chim. Acta* **38** *(*1980*)* 141
31. T. J. Marks, *Prog. Inorg. Chem*. **24** (1978) 51
32. D. G. Karraker, *Inorg. Chem*. **6** (1967) 1863
33. R. W. M. D'Eye, E. Wait, *X-ray Powder Photography in Inorganic Chemistry*, Butterworths, London, 1960.

Journal of the Serbian Chemical Society
JSCS-info@shd.org.rs • www.shd.org.rs/JSCS

J. Serb. Chem. Soc. 76 (2) 263–281 (2011)
JSCS–4117

UDC 615.214:547.95/.96:539.219
Original scientific paper

QSAR–CoMSIA applied to antipsychotic drugs with their dopamine D_2 and serotonine $5HT_{2A}$ membrane receptors

SPERANTA AVRAM[1], DANIEL DUDA-SEIMAN[2], FLORIN BORCAN[3]* and PETER WOLSCHANN[4]

[1]*University of Bucharest, Faculty of Biology, Physiology and Biophysics Dept., 91–95 Spl. Independentei, Bucharest-76201,* [2]*University of Medicine and Pharmacy "Victor Babes" Timisoara, Clinic of Preventive Cardiology and Cardiovascular Rehabilitation, 49 C.D. Loga Bvd., Timisoara-300020,* [3]*West University Timisoara, Faculty of Chemistry, Biology and Geography, Chemistry Dept., 16 Pestalozzi Str., Timisoara-300115, Romania and* [4]*University of Vienna, Institute for Theoretical Chemistry, 17 Währingerstrasse, Vienna-1090, Austria*

(Received 6 August, revised 9 September 2010)

Abstract: Antipsychotic drugs are psychiatric medication primarily used to manage psychosis (*e.g.*, delusions or hallucinations), particularly in schizophrenia and bipolar disorder. First and second generations of antipshychotics tend to block receptors in the brain's dopamine pathways, but antipsychotic drugs encompass a wide range of receptor targets. The inhibition constant, K_i, at the level of membrane receptors is a major determinant of their pharmacokinetic behavior and, consequently, it can affect their antipsychotic activity. Here, predicted inhibition constants, K_i for 71 antipsychotics, already approved for clinical treatment, as well as representative new chemical structures which exhibit antipsychotic activity, were evaluated using 3D-QSAR–CoMSIA models. Significant values of the cross-validated correlation q^2 (higher than 0.70) and the fitted correlation r^2 (higher than 0.80) revealed that these models have reasonable power to predict the biological affinity of the 15 new risperidone and 12 new olanzapine derivatives in interactions with dopamine D_2 and serotonin $5HT_{2A}$ receptors; these compounds are suggested for further studies.

Keywords: antipsychotic; CoMSIA; QSAR; membrane receptors; olanzapine; risperidone.

INTRODUCTION

Schizophrenia is a severe mental illness characterized by positive symptoms, such as delusions and hallucinations, and disorganized speech, and negative symptoms, such as affective flattening, social withdrawal in nature and deficits of attention.[1–5] Moreover, inhibition of inappropriate actions and irrelevant sensory

* Corresponding author. E-mail: fborcan@yahoo.com
doi: 10.2298/JSC100806022A

information are also present.[6,7] Schizophrenia etiology indicates that many factors are involved, namely genetic factors,[8–10] alterations in chemical transmission (dopamine, serotonine, *etc*.),[11–13] obstetrical complications[14–17] and viral infections.[18] The neurobiology of schizophrenia has shown that an enlarged ventricular system accompanied by an overall reduction in brain volume[19] and a regional decrease in the hippocampus, thalamus and frontal lobes are present.[20,21] Neurons in these regions appear reduced in size with abnormal dendritic arborization and synaptic organization.[19,22] Currently there are many classes of chemical structures which can be regarded as typical antipsychotics (*e.g*., haloperidol and chlorpromazine) and atypical antipsychotics (risperidone, olanzapine and clozapine)[23–25] but recently many other chemical structures having antipsychotic activities have been reported.[26–32] A common feature of these drugs is not only their relatively high affinity for dopamine receptors,[33] but also for serotonin receptors.[34,35] In schizophrenia treatment, a strong correlation between therapeutic doses of neuroleptics and their binding affinity to D_2 receptor was noticed.[33,36,37] The important limitations of antipsychotic prescription are their critical side effects, such as extra-pyramidal symptoms (EPS),[38] increased plasma prolactin levels and decreasing tardive dyskinesia (TD),[39] which develop in about 70 % of patients.

Risperidone and olanzapine, two extremely potent antipsychotics, are included in empirical protocols for the treatment of psychosis with good tolerance in patients. They decrease the negative symptoms by acting on the serotonergic and noradrenergic receptors, while the positive symptoms are reduced by their effects on the dopaminergic pathway,[37] with lower side effects. There is currently much interest in the development of new derivatives starting from these antipsychotics.

Structure–activity relationship (QSAR) studies using the classical quantitative structure–activity relationship (2D-QSAR)[27–29,40,41] and a few 3D-QSAR––CoMFA and/or 3D-comparative molecular similarity analysis (3D-CoMSIA) approaches[42–48] have enhanced knowledge concerning the interactions of antipsychotics with different classes of membrane receptors.

In a previous study,[40] six new QSAR models were presented in which correlate the inhibition constants of antipsychotics at the dopamine D_1–D_4 and serotonine ($5HT_{2C}$, $5HT_{2A}$) receptors were correlated with their physicochemical parameters using MOE software (http://www.chemcomp.com/software.htm). In this previous study,[40] MLR-, factor-analyses and discriminant-analyses were used to elucidate the most important physico–chemical properties of the antipsychotics which are responsible for their binding properties, *i.e*., hydrophobic and refractivity properties on subdivided surface areas (SlogP_VSA4, SlogP_VSA8, SlogP_VSA9 (hydrophobicity descriptors, with L_i in different ranges; L_i denotes the contribution to log P(o/w) of atom i as calculated in the *S*log *P* descriptor,

http://www.chemcomp.com/software.htm) and SMR_VSA2, SMR_VSA5, SMR_VSA3, SMR_VSA4, SMR_VSA1, SMR_VSA7 (refractivity descriptors with R_i in different ranges; R_i denotes the contribution to molar refractivity of atom i as calculated in the SMR descriptor, http://www.chemcomp.com/ /software.htm), electronic properties (PEOE_VSA+1, PEOE_VSA-4, PEOE_VSA--0), energetic term E_{sol} (solvation energy), as well as properties due to the solvent accessible surface areas (ASA_H) and the pharmacophore feature vsa-hyd. The 71 antipsychotic drugs analyzed before were used to extend the study by developing new 3D-QSAR-CoMSIA models.

The aim of this study is to develop predictive 3D-QSAR models to observe which structural features are responsible for selective $5HT_{2A}$ antagonism *vs.* D_2 receptor binding.

An objective of this study was to use 3D-QSAR models to predict the effect of molecular properties, for example hydrogen bond donor/acceptor, hydrophobic, steric and electrostatic properties, on the inhibitor constant at dopamine and serotonin receptors of a large number of antipsychotics: *i*) typical and atypical antipsychotics already approved for clinical treatment,[32,49–55] and *ii*) novel potential antipsychotic agents, such as 3-aminoethyl-1-tetralones,[30] piperazine,[26] benzothiazepine[28,29] and pyrrolobenzazepine[27] derivatives, with favorable pharmacokinetic properties. Preliminary, studies[26–31] confirmed the superior pharmacological effects (significant reduction of spontaneous locomotor activity, a negligible increase of prolactine serum levels, therapeutic potential against cognitive and negative symptoms of schizophrenia) of these novel drugs which are administered in much lower doses compared to classical antipsychotics.

This encouraged the present study in which the above-mentioned molecular properties led to powerful 3D-QSAR models for K_i prediction, despite the large variety of chemical structures from different literature sources. The ultimate goal was to design selective, high affinity D_2 and $5HT_{2A}$ receptor antagonists with a superior clinical profile for schizophrenia treatment, with the assistance of the 3D-QSAR models developed herein. Therefore, new 15 risperidone and 11 olanzapine derivatives with possible higher affinity to dopamine D_2 and serotonin $5HT_{2A}$ membrane receptors were designed and their antipsychotic activities were predicted in accordance with the estimated 3D-QSAR models.

EXPERIMENTAL

Dataset for analysis

The inhibitor constant data, K_i, of 71 dopamine D_2 and serotonin $5HT_{2A}$ receptors antagonists (typical and atypical antipsychotics already approved for clinical treatment and novel potential antipsychotic agents) used in this study were collected from the literature.[26–32,49–55]

A large range of observed inhibition constant K_i (pK_i from 5 to 10), favorable pharmacokinetic properties covering the interactions with dopamine and serotonine receptors, various

substituents, covering as many as possible chemical classes of compounds (Tables I–V) were the selection criteria of the compounds considered in this study.

As a rule, a range in affinity of at least three logarithmic units is necessary to develop a statistically significant 3D-QSAR model. The $5HT_{2A}$ receptor affinities spread over a range of nearly five logarithmic units, whereas the D_2 ligands covered four logarithmic units.

Even if the values of the inhibition constants originated from different studies, they were mutually well comparable, as in following examples: clozapine (pK_{i5HT2A} = 8.26,[50] 8.00,[27–29] 8.20,[32] 8.04;[30] pK_{iD1} = 6.45,[27–29] 6.26;[32] pK_{iD2} = 6.59,[50] 6.60,[27–29] 6.84,[32] 6.65)[30] or haldol pK_{iD2} = 8.39,[50] 8.60,[32] 8.32,[27–29] 9.00).[30] This enabled the affinity data of the compounds to be combined in one set. The names of typical and atypical antipsychotics, corresponding to the observed and predicted pK_i values and also the 2D structures of potential antipsychotics are given in Tables I–V.

TABLE I. Typical and atypical antipsychotics which are already approved for clinical treatment[49–55]

Compound	$pK_{i5HT2Aobs}$	$pK_{i5HT2Apred}$	pK_{iD2obs}	$pK_{iD2pred}$
Clozapine (**N1**)	8.26	8.68	6.59	7.12
Flupentixol (**N2**)	7.05	7.24	8.82	8.63
Haloperidol (**N3**)	7.27	7.48	8.39	8.21
Loxapine (**N4**)	8.11	7.86	7.92	7.79
Mesoridazine (**N5**)	8.31	8.08	7.72	7.87
Olanzapine (**N6**)	8.69	8.73	7.46	7.27
Quetiapine (**N7**)	6.99	7.20	6.61	6.47
Risperidone (**N8**)	9.76	9.30	8.18	8.34
Sertindole (**N9**)	9.23	9.15	8.04	7.74
Thiothixene (**N10**)	7.30	7.47	9.20	8.07
Thioridazine (**N11**)	8.00	8.23	7.95	8.06
Campazine (**N12**)	7.82	7.61	8.76	8.00
Ziprazidone (**N13**)	9.52	9.26	8.01	8.07

Molecular modeling and minimum energy performed for antipsychotics

Three dimensional structures of studied compounds were obtained using of the build module from Sybyl 7 software.[56,57] In the first step, 2D structures of the antipsychotics that were automatically changed into 3D structures were saved in Sybyl specific files .mol2.

In this study, the conformation of the antipsychotics with the minimum potential energy was established using the Maxim 2 minimization routine in Sybyl 7, with Tripos force field, conjugate-gradient algorithm and convergence 0.01 without constraint. After energy minimization, the Gasteiger–Marsili partial charges of the compounds[57] were loaded on the chemical structures from the Sybyl 7 dictionary.

CoMSIA strategy and chemometric analyses

The CoMSIA method involves a "common scaffold". As all the inhibitors had a six-membered ring in common (*e.g.*, piperazine and piperidine), in this study, a "common scaffold" was obtained by the superposition of the common six-membered ring belonging to compounds and of the most active antagonist benzothiazepine (derivative, N66, pK_{iD2} = 9.36) to the dopamine D_2 receptor and risperidone, pK_{i5HT2A} = 9.76 to the serotonin $5HT_{2A}$ receptor.

The steric and electrostatic, hydrophobic and hydrogen bond donor/ acceptor properties of each inhibitor were calculated at the intersections of a regularly spaced (2 Å) grid in a grid-

-box ‘‘create automatically’’ in Sybyl. Lennard-Jones 6–12 potential and Coulombic potential functions, hydrophobicity, and hydrogen bond properties of compounds, within the Tripos force field, using a sp^3 carbon probe atom, with a +1 charge, were considered.[56,57]

TABLE II. 3-Aminoethyl-1-tetralones derivatives[30]

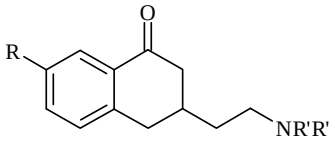

Compound	Radical R	NR’R’	p$K_{i5HT2Aobs}$	p$K_{i5HT2Apred}$	pK_{iD2obs}	p$K_{iD2pred}$
N14	H	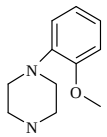	6.59	6.39	6.97	6.11
N15	OCH_3		6.65	6.33	6.55	6.2
N16	H	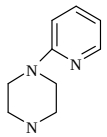	–	–	5	5.07
N17	OCH_3		–	–	5	5.05
N18	H		8.29	8.35	5.98	7.23
N19	OCH_3		8.23	8.24	7.04	7.06
N20	H	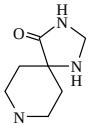	5	5.94	5	5.15
N21	OCH_3		5	4.98	5	5.15
N22	H	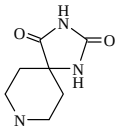	6.15	5.98	5	4.83
N23	OCH_3		5.98	5.94	5	4.87

An energy cutoff of 30 kcal mol^{-1} was used for both the electrostatic and steric contributions. Regression analysis was performed by the partial least squares (PLS) algorithm within Sybyl 7.2. The leave-one-out cross-validation method using the SAMPLS method was employed to evaluate the predictable residual sum squares (*PRESS*), standard deviation (*SD*) and cross-validated correlation coefficient (q^2). The optimal number of orthogonal principal components was chosen based on t the highest q^2 value by the PLS using the leave-one-out cross-validation method.[56,57]

The minimum standard deviation threshold sigma was set to 2.0 kcal mol^{-1} and 2.0 for CoMSIA. Furthermore, the control criteria fitted correlation coefficient r^2, standard error of estimate (*SEE*) and Fisher test (*F*) were calculated using the CoMFA module by the non--cross-validated method.[56,57] In addition, the representation of the hydrophobic and hydrogen

bond acceptor descriptors as a 3D contour plot (the favorable and unfavorable area representation by polygons) formed just around the risperidone were performed in the Sybyl/ QSAR module.[56,57]

TABLE III. Piperazine derivatives[26]

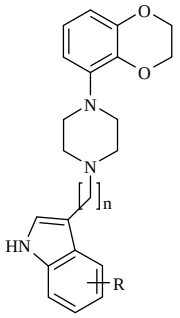

Compound	Radicals		pK_{iD2obs}	$pK_{iD2pred}$
	n	R		
N24	1	H	7.20	7.07
N25	2	H	7.34	7.79
N26	3	H	7.67	7.87
N27	4	H	8.29	8.00
N28	5	H	8.04	7.99
N29	3	4-F	8.09	7.86
N30	3	5-F	7.72	7.86
N31	3	6-F	7.83	7.85
N32	3	7-F	7.97	7.88
N33	3	5-OMe	7.82	7.87
N34	3	4-Cl	7.61	7.87
N35	3	5-Cl	7.50	7.87
N36	3	6-Cl	8.67	7.86
N37	3	7-Cl	7.80	7.9
N38	3	5-Me	7.97	7.88
N39	3	7-Me	7.79	7.93

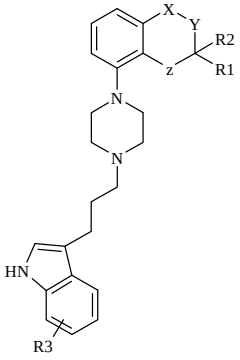

TABLE III. Continued

Compound	Radical						pK_{iD2obs}	$pK_{iD2pred}$
	X	Y	Z	R1	R2	R3		
N40	O	CH_2	CH_2	H	H	H	7.69	7.65
N41	NH	CH_2	CH_2	H	H	H	7.94	7.64
N42	NMe	CH_2	CH_2	H	H	H	7.04	7.62
N43	NH	CH_2	CH_2	Me	H	H	7.82	7.66
N44	NH	C(=O)	CH_2	H	H	H	7.94	8.19
N45	NH	C(=O)	O	H	H	H	8.36	8.56
N46	NH	C(=O)	O	Me	H	H	8.34	8.6
N47	NH	C(=O)	O	Me	Me	H	8.13	8.5
N48	NH	C(=O)	O	(*R*)–Me	H	H	8.06	8.25
N49	NH	C(=O)	O	(*S*)–Me	H	H	9.00	8.51
N50	NH	C(=O)	O	(*R*)–Me	H	5-F	8.16	8.31
N51	NH	C(=O)	O	(*R*)–Me	H	7-F	8.27	8.51
N52	NH	C(=O)	O	(*S*)–Me	H	7-F	9.00	8.63

TABLE IV. Benzothiazepine derivatives[28,29]

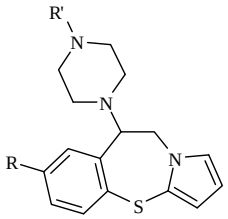

Compound	Radical			$pK_{i5HT2Aobs}$	$pK_{i5HT2Apred}$	pK_{iD2ob}	pK_{iD2pr}
	R	*n*	R’			s	ed
N53	Cl	1	Me	8.94	8.11	8.69	7.99
N54	H	1	Me	7.60	8.17	7.10	7.97
N55	F	1	Me	8.29	8.13	7.63	7.98
N56	Cl	1	Et	8.23	8.01	8.51	7.97
N57	Cl	1	CH_2CH_2OH	8.06	7.79	8.23	8.1
N58	F	1	Et	8.36	8.22	8.02	8.22
N59	F	1	CH_2CH_2OH	7.13	7.70	7.66	7.98
N60	Br	1	Me	7.92	8.40	8.44	8.42
N61	Br	1	Et	7.64	8.29	8.40	8.40
N62	Br	1	CH_2CH_2OH	7.65	7.84	8.30	8.21
N63	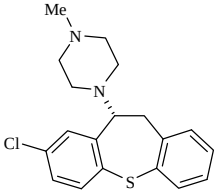			9.64	8.51	9.30	8.5

TABLE IV. Continued

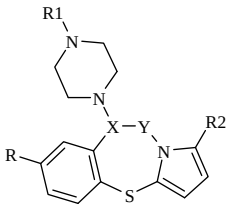

Compound	Radical				$pK_{i5HT2Aobs}$	$pK_{i5HT2Apred}$	pK_{iD2obs}	$pK_{iD2pred}$
	R	R1	R2	X–Y				
N64	H	Me	H	C=CH	9.18	9.08	7.76	8.18
N65	F	Me	H	C=CH	9.45	9.11	8.07	8.29
N66	Cl	Me	H	C=CH	9.46	9.20	9.36	8.4
N67	Br	Me	H	C=CH	9.08	9.26	9.34	8.48
N68	H	Me	Me	C=CH	8.95	9.01	6.89	7.98

TABLE V. Pyrrolobenzazepine derivatives[27]

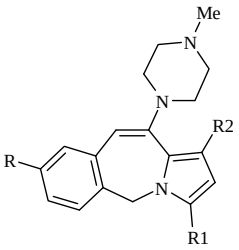

Compound	Radical		$pK_{i5HT2Aobs}$	$pK_{i5HT2Apred}$	pK_{iD2obs}	$pK_{iD2pred}$
	R	R1				
N69	H	H	8.13	8.67	6.23	7.50
N70	Cl	H	8.86	8.85	7.14	7.95
N71	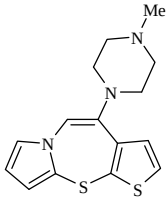		8.66	8.65	8.07	8.21

Training and test sets in the QSAR models

The ability of CoMSIA to predict the biological activities of the antipsychotics to the dopamine D_2 and serotonin $5HT_{2A}$ receptors was evaluated by training and test sets in which a variable number of molecules were used (Tables I–V). Traditionally, external test sets are used to check the predictive power of models derived from training sets. The predicted binding affinities for the test sets are given in Tables I–V in bold numbers/characters.

Initially, to validate 3D-QSAR CoMSIA D_2 and $5HT_{2A}$ models, individual hydrophobic, hydrogen bond acceptor, hydrogen bond donor, steric and electrostatic fields in different com-

binations were considered. Finally, choosing a set of descriptors sufficient to enable an accurate validation of the QSAR models (q^2 (cross-validated r^2) not less than 0.6, r^2 higher than 0.9), two 3D-QSAR models were presented: *i*) the 3-QSAR-CoMSIA D_2 model contains 5 compounds in test set (thiothixene (**N10**), campazine (**N12**), 3-aminoethyl-1-tetralones derivative (**N18**), benzothiazepine derivative (**N68**) and pyrrolobenzazepine derivative (**N69**) and the other 66 compounds in the training set) assessed with hydrogen bond acceptor, hydrophobic, steric and electrostatic as descriptors; *ii*) the 3D-QSAR-CoMSIA $5HT_{2A}$ model contains 4 compounds in the test set (benzothiazepine derivatives: **N53**, **N54**, **N61** and **N63**) and the other 38 compounds in training set, assessed with hydrogen bond donor, hydrophobic and steric and electrostatic as descriptors.

Design of new D_2 and $5HT_{2A}$ antagonist derivatives from risperidone and olanzapine with possibly improvement in the antagonist potency

Taking into account the best correlations between the observed and predicted pK_i for risperidone and olanzapine to dopamine and serotonin receptors, 15 molecules derived from risperidone and another 11 derivatives from olanzapine were designed and proposed as possible antipsychotic drugs, and their pK_{iD2} and pK_{i5HT2A} values were evaluated. Molecular modeling of risperidone and olanzapine derivatives was performed under the above-described procedure. The risperidone and olanzapine derivatives were generated using the added atoms (Cl, F) and groups (ethyl, *iso*-propyl, cyclohexyl, *n*-butyl, methyl, $CH_3NC_2H_5$, OH, COOH, NH_2) from the Sybyl data base. The minimum potential energy for the risperidone and olanzapine derivatives was established using the Maxim 2 minimization routine in Sybyl 7, with Tripos force field, conjugate-gradient algorithm, and convergence 0.01. During energy minimization, only the specific substituents were allowed free movement while the rest of the molecule was kept rigid. After energy minimization, the Gasteiger–Marsili partial charges of the compounds[57] were loaded on the chemical structures from the Sybyl 7 dictionary. Prediction of inhibitor constants to dopamine D_2 and serotonin $5HT_{2A}$ receptors of the obtained derivatives was realized using QSAR models statistically validated during previous phases of the study.

RESULTS AND DISCUSSION

The 3D-QSAR-CoMSIA D_2 model predicted antagonist potency of 66 compound by the leave-one-out cross-validated PLS analysis running with four principal components led to a q^2 cross-validated correlation coefficient of 0.71 and by non-cross-validated PLS analysis, a fitted correlation coefficient r^2 = 0.86, standard error estimate of 0.40 and *F* value of 96.72 were obtained (Table VI).

The other goal of this study was to establish by 3D-QSAR/CoMSIA the contribution of molecular properties, such as hydrogen bond donor/acceptor property, hydrophobic and also steric/electrostatic fields, to the D_2 receptor antagonist potency.

The statistic parameters q^2 – cross-validated correlation coefficient, r^2 – fitted correlation coefficient and the standard error estimate (*SEE*) were statistically significant when the hydrogen bond acceptor, hydrophobic and steric and electrostatic fields were considered (Table VI). It was noticed that the hydrogen bond acceptor (1.397) and hydrophobic (0.60) properties contributed significantly more compared with the steric and electrostatic (0.283/ 0.496) properties.

When the antagonist potency of compounds referred were studied to the serotonin 5HT2A receptor, a second CoMSIA model was obtained and the statistic parameters q^2 cross-validated of 0.78, fitted correlation coefficient r^2 of 0.95 and *SEE* of 0.34 were evaluated (Table VI).

TABLE VI. Summary of the 3D-QSAR-CoMSIA statistical data

Statistical parameter	3D-QSAR D_2 model	3D-QSAR $5HT_{2A}$ model
Molecules	66	38
Q2 cv	0.71	0.78
Component used	4	3
*SEE*stimate	0.40	0.34
R squared	0.86	0.95
F value	96.72	250.53
Steric contribution	0.28	0.35
Electrostatic contribution	0.49	0.75
Acceptor contribution	1.39	–
Hydrophobic contribution	0.60	0.67
Donor contribution	–	0.77

Analysis of the contribution of the molecular descriptors showed that the significant statistical q^2 cross-validated and fitted correlation coefficient r^2 parameters were obtained when the descriptors steric and electrostatic, hydrophobic and hydrogen bond donor were considered (Table VI). Noteworthy is that three (electrostatic (0.75), hydrophobic (0.67) and hydrogen bond donor (0.77)) of the four descriptors had contributions higher than 0.65; the most involved descriptor in the interaction between the described compounds and the serotonine $5HT_{2A}$ receptors seemed to be hydrogen bond donor.

Modeling of new risperidone and olanzapine derivatives with potentially superior antagonist potency at the dopamine D2 and serotonin 5HT2A membrane receptors

Due to their low affinities, the currently used atypical antipsychotics suffer the disadvantage of high dose administration. Currently, the major problem of using antipsychotic drugs is governed by the above-mentioned side-effects. Due to the before-mentioned high importance of risperidone and olanzapine as antipsychotic agents, two sets of 15 new risperidone and 11 olanzapine derivatives were made in order to predict improved pK_i values for D_2 and $5HT_{2A}$ receptors using the above-presented 3D-QSAR models (Tables VII and VIII).

In designing the new risperidone and olanzapine derivatives, two strategies were followed: first, the number of hydrophobic contacts on *i*) risperidone by adding methyl, ethyl, *iso*-propyl, *n*-propyl, *n*-butyl, cyclohexyl and phenyl substituents at 2,6-diazabicyclo[4.4.0]deca-1,3-dien-5-one and ethyl chain and *ii*) olanzapine by adding methyl, ethyl, *iso*-propyl, *iso*-butyl and phenyl at piperazinyl and 10*H*-thieno rings, respectively.

Secondly, Cl, hydroxyl, carboxyl or amino substituents were generated on risperidone. In addition, Cl, F and hydroxyl were generated on olanzapine (Tables VII and VIII). The chemical structures of the risperidone and olanzapine derivatives, residual pK_i values (the difference between template antipsychotics and predicted pK_i derivatives) and the predicted pK_i values for the risperidone and olanzapine derivatives are presented in Tables VII and VIII.

TABLE VII. Antagonist potency pK_{iD2} and pK_{i5HT2A} for the risperidone derivatives and residual values (differences in the antagonist potency of the risperidone derivatives to the parent antagonist potency are given in brackets)

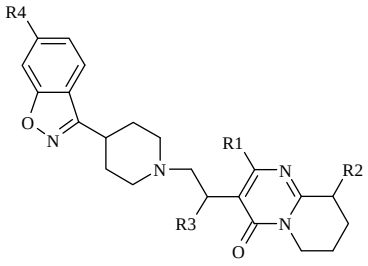

Risperidone derivate	Group				Predicted pK_{iD2}	Predicted pK_{i5HT2A}
	R1	R2	R3	R4		
1	C_2H_5	H	H	F	8.7 (0.54)	9.37(–0.39)
2	$(CH_3)_2CH$	H	H	F	8.74 (0.56)	9.46 (–0.3)
3	CH_3	$(CH_3)_2$	H	F	8.55 (0.37)	9.10 (–0.66)
4	$(CH_3)_2CH$	H	OH	F	8.60 (0.42)	9.41(–0.35)
5	C_6H_{13}	H	H	F	7.46 (–0.72)	8.41 (–1.35)
6	$H_3C–NH_2$	H	H	F	8.12 (–0.06)	9.30 (–0.46)
7	$CH_2N(CH_3)_2$	H	H	F	8.66 (0.48)	9.42 (–0.34)
8	OH	H	H	F	8.23 (0.05)	9.36 (–0.4)
9	C_4H_7	H	H	F	8.18 (0)	9.00 (–0.76)
10	C_4H_7	H	NH_2	F	8.27 (0.09)	8.94 (–0.82)
11	CH_3	H	C_6H_5	F	8.75 (0.57)	9.30 (–0.46)
12	C_4H_7	H	H	OH	8.25 (0.07)	9.52 (–0.24)
13	C_4H_7	H	H	Cl	8.27(0.09)	9.60 (–0.16)
14	C_4H_7	H	H	COOH	8.42 (0.24)	8.06 (–1.7)
15	C_4H_7	CH_3	H	F	7.42 (–0.76)	8.15 (–1.61)

In this study, good correlations between the observed and predicted antagonist potency of the compounds to the dopamine D_2 receptor (Tables I–V) were obtained. As examples, the correlation between the observed and predicted antagonist potency of compounds included in the training set were piperazine derivative **N40** ($pK_{iD2observed} - pK_{iD2predicted} = 0.04$), benzothiazepine **N60** ($pK_{iD2observed} - pK_{iD2predicted} = 0.02$) and **N61** ($pK_{iD2observed} - pK_{iD2predicted} = = 0.001$) derivatives. However, the residual value was not good when the anta-

gonist potency was predicted for the 3-aminoethyl-1-tetralones derivative **N18** ($pK_{iD2observed} - pK_{iD2predicted} = -1.03$).

Data presented in Tables I–V are illustrated by graphical presentations of the correlation between the observed and the predicted antagonist potency of the compounds to the dopamine D_2 membrane receptor in Fig. 1.

TABLE VIII. Antagonist potency pK_{iD2} and pK_{i5HT2A} for olanzapine derivatives and residual values (differences in the antagonist potency of the olanzapine derivatives to the parent antagonist potencyare given in brackets)

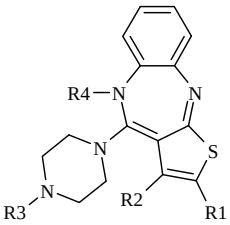

Olanzapine derivate	Group				Predicted pK_{iD2}	Predicted pK_{i5HT2A}
	R1	R2	R3	R4		
1	CH_3-CH_2	H	CH_3	H	7.31 (–0.15)	8.42 (–0.27)
2	CH_3	CH_3	CH_3	H	7.49 (0.03)	8.48 (–0.21)
3	CH_3	C_3H_7	CH_3	H	7.46 (0)	8.99 (0.30)
4	CH_3	isobutyl	CH_3	H	7.51(0.05)	8.94 (0.25)
5	CH_3	H	CH_3	CH_3	6.97 (–0.49)	8.69 (0)
6	C_6H_5	H	CH_3	H	7.30 (–0.16)	8.27 (–0.42)
7	CH_3	H	H_3C–CH_2	H	7.20 (–0.26)	8.15 (–0.54)
8	CH_3	H	C_3H_7	H	7.16 (–0.3)	8.10 (–0.59)
9	CH_3	H	CH_2F	H	7.26 (–0.2)	8.20 (–0.49)
10	CH_3	H	CH_2Cl	H	7.26 (–0.2)	8.65 (–0.04)
11	CH_3	H	CH_2OH	H	7.02 (–0.44)	7.95 (–0.74)

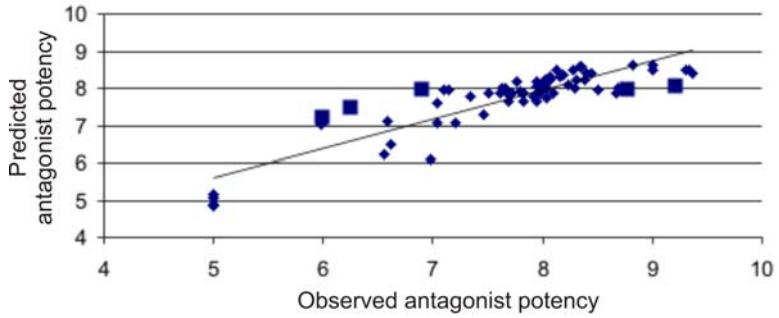

Fig. 1. Correlation between the observed and predicted antagonist potency pK_{iD2} of the antipsychotic drugs when the hydrophobic, hydrogen acceptor bond, electrostatic and steric properties are regarded as descriptors (the molecules from the test set are represented by the square shape).

The observed and predicted antagonist potency of serotonin $5HT_{2A}$ receptor for the training and test (bold letters) sets are shown in Tables I–V.

CoMSIA statistic validation in this case leads to a good correlation of observed and predicted antagonist potency for the pyrrolobenzazepine derivatives **N71** ($pK_{i5HT2Aobserved} - pK_{i5HT2Apredicted} = 0.01$) and **N70** ($pK_{i5HT2Aobserved} - - pK_{i5HT2Apredicted} = 0.01$). A graphical presentation of the correlation between the observed and predicted antagonist potency of the compounds in interaction with the serotonin $5HT_{2A}$ receptor is presented in Fig. 2.

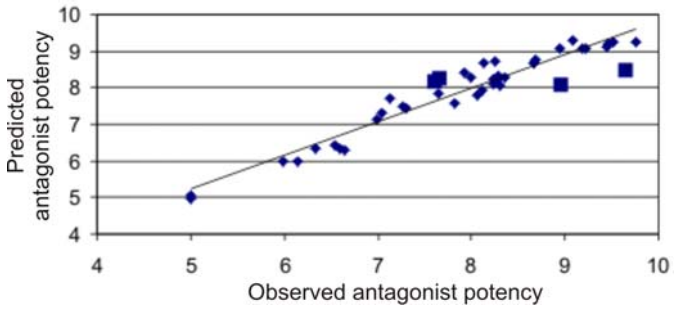

Fig. 2. Correlation between the observed and predicted antagonist potency pK_{i5HT2A} of the antipsychotic drugs belong to the training set when the hydrophobic, hydrogen donor bond, electrostatic and steric properties are regarded as descriptors (the molecules from the test set are represented by the square shape).

Graphical interpretation of the 3D-QSAR–CoMSIA models

The great advantage of the CoMSIA method is its ability to visualize the descriptor fields as 3D contour plots (the favorable and unfavorable descriptor areas are represented by polygons) formed just around the target molecule. Accordingly, in this study, with the contribution of the descriptors to the biological activity, CoMSIA contour maps of the hydrophobic field and hydrogen bond acceptor were used for graphical analysis.

The favorable hydrogen acceptor bond areas (white polygons) and the unfavorable hydrophobic areas (grey polygons) formed around risperidone when its antagonist potencies at the dopamine D_2 and setotonine $5HT_{2A}$ receptors were considered ($pK_{iD2} = 8.18$ and $pK_{i5HT2A} = 9.76$) are shown in Figs. 3–5.

The contour maps for hydrophobic property obtained from risperidone (Fig. 3) show that the presence of large unfavorable hydrophobic areas (2,6-diazabicyclo[4.4.0]deca-1,3-dien-5-one and also isoxazol-rings) could be responsible for the relatively low affinity of risperidone at D_2. On the contrary, the hydrophobic property distribution presented in Fig. 4 looks around risperidone and shows the presence of favorable areas (white areas) around the isoxazol ring and ethyl group, which might be a good explanation for the high antagonist potency of risperidone at $5HT_{2A}$ receptor.

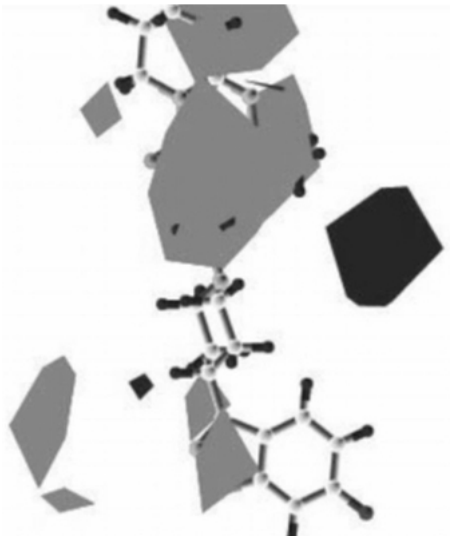

Fig. 3. Representation of the favorable (white polygons) and unfavorable (grey polygons) hydrophobic areas of risperidone (pK_{iD2} = 8.18) when its antagonist potency at dopamine D_2 receptor is considered.

Fig. 4. Representation of the favorable (white polyhedra) and unfavorable (grey polyhedra) hydrophobic areas of risperidone (pK_{i5HT2A} = 9.76) when its antagonist potency at the serotonin $5HT_{2A}$ receptor is considered.

CoMSIA maps showing the hydrogen acceptor bond property are depicted in Fig. 5; they correspond to regions of the putative protein environment which are capable of donating hydrogen bonds. The three favorable regions which formed around the 1,3-dien-5-one and piperidine rings could be important for the D_2 receptor affinity.

Following the employed design strategy, four risperidone derivatives with affinity for the dopamine D_2 receptor (**1** (R1=C_2H_6, R2=H, R3=H, R4=F, pK_{iresD2} = 0.54), **2** (R1=$(CH_3)_2CH$, R2=H, R3=H, R4=F, pK_{iresD2} = 0.56), **7** (R1=$CH_2N(CH_3)_2$, R2=H, R3=H, R4=F, pK_{iresD2} = 0.48) and **11** (R1=CH_3, R2=H,

R3=C_6H_5, R4=F, pK_{iresD2} = 0.57)) had higher predicted pK_{iD2} values than risperidone. It should be mentioned that the presence of additional hydrophobic contacts on R1 in 2,6-diazabicyclo-dione and R3, while simultaneously maintaining F on R4, lead to an increased affinity of the new risperidone derivatives to the dopamine D_2 receptor. The same observation could not be made if a substantial increase of the hydrophobic effect was obtained (derivatives **5** (R1=C_6H_{13}, R2=H, R3=H, R4=F, pK_{iresD2} = –0.72) and **15** (R1=C_4H_7, R2=CH_3, R3=H, R4=F, pK_{iresD2} = –0.76)). In the present study, it is interesting to note that an increased number of hydrophobic contacts on risperidone did not result in a higher affinity for the serotonin 5HT2A receptor and sometimes a decrease in affinity could be found (derivatives **5** (R1=C_6H_{13}, R2=H, R3=H, R4=F, p$K_{ires5HT2A}$ = –1.35), **14** (R1=C_4H_7, R2=H, R3=H, R4=COOH, p$K_{ires5HT2A}$ = –1.70) and **15** (R1=C_4H_7, R2=CH_3, R3=H, R4=F, p$K_{ires5HT2A}$ = –1.61)).

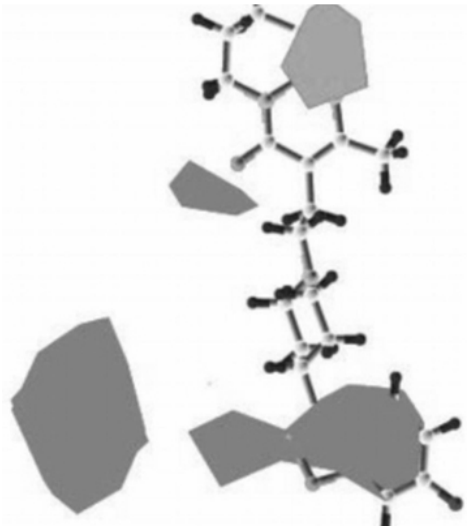

Fig. 5. Representation of the favorable (grey polyhedra) and unfavorable (black polyhedra) hydrogen acceptor bond areas of risperidone when its antagonist potency at the dopamine D2 receptor is considered.

Analysis of the antagonist potency of the olanzapine derivatives at the dopamine D_2 receptor led to the observation that ten had a lower antagonist potency, except derivative **3** (R1=CH_3, R2=C_3H_7, R3=CH_3, R4=H, pK_{iresD2} = 0), for which an identical pK_{iD2} was recorded The same observation could not be made when the affinity of the olanzapine derivate **3** at the serotonin $5HT_{2A}$ receptor was analyzed. The additional hydrophobic contacts on R2 led to clear affinity increases for derivative **3**, p$K_{ires5HT2A}$ = 0.30 and derivative **4** (R1=CH_3, R2= isobutyl, R3=CH_3, R4=H, p$K_{ires5HT2A}$ = 0.25). However, the addition of a hydrophobic contact on R4, *i.e.*, a methyl group, resulted in the same affinity as the template compound (derivative **5** (R1=CH_3, R2=H, R3=CH_3, R4=CH_3, p$K_{ires5HT2A}$ = 0.00).

CONCLUSIONS

3D-QSAR–CoMSIA models can give different information, for example reliable prediction of the affinity of compounds belonging to a data set and chemical interpretation of the results obtained. In this paper, alignment-dependent 3D-QSAR–CoMSIA studies using two QSAR models are reported of a series of 71 antipsychotic drugs already used in clinical practice, as well as representative new chemical structures which exhibit antipsychotic activity and 15 risperidone and 11 olanzapine derivatives proposed as possible antagonists of dopamine D_2 and serotonin $5HT_{2A}$ receptors. The models were used to elucidate the most important physico–chemical properties responsible for the antagonist potency of the chemical structures to dopamine D_2 and serotonin $5HT_{2A}$ receptors. In this study, hydrogen donor/acceptor and hydrophobic properties supplied by steric and electrostatic fields were considered.

Significant PLS results were obtained when a hydrogen acceptor bond and the simultaneous presence of hydrophobic, electrostatic and steric properties were considered in the study of the antagonist potency at the dopamine D_2 receptor. However, the serotonin $5HT_{2A}$ receptor affinity of the antipsychotics was governed by the hydrogen bond donor ability and the simultaneous presence of hydrophobic, electrostatic and steric properties.

Thus, judicious modulation of the physico–chemical properties, particularly hydrogen bond acceptor/donor and hydrophobic properties may be very useful for the design of new chemical structures as possible antagonists of D_2 and $5HT_{2A}$ receptors. Considering the above set of 15 risperidone and 11 olanzapine derivatives, the established equations could be used to enhance or reduce the antagonist potency pK_i, in accordance with the biological requirements.

It was noticed that additional hydrophobic contacts on R1 and R3 on risperidone rings, while simultaneously retaining F in R4, increased the antagonist potency of risperidone derivatives to the dopamine D_2 receptor. In addition, hydrophobic contacts on R2 resulted in a clearly enhanced antagonist potency of two olanzapine derivatives.

Acknowledgement. S. Avram thanks the Federation of European Biochemical Societies (FEBS) for a research grant.

ИЗВОД

QSAR–CoMSIA МОДЕЛИ ПРИМЕЊЕНИ НА АНТИПСИХОТИЧКЕ ЛЕКОВЕ И ЊИХОВЕ ДОПАМИН D_2 И СЕРОТОНИН $5HT_{2A}$ МЕМБРАНСКЕ РЕЦЕПТОРЕ

SPERANTA AVRAM[1], DANIEL DUDA-SEIMAN[2], FLORIN BORCAN[3] и PETER WOLSCHANN[4]

[1]University of Bucharest, Faculty of Biology, Physiology and Biophysics Dept., 91–95 Spl. Independentei, Bucharest-76201, [2]University of Medicine and Pharmacy "Victor Babes" Timisoara, Clinic of Preventive Cardiology and Cardiovascular Rehabilitation, 49 C.D. Loga Bvd., Timisoara-300020, [3]West University Timisoara, Faculty of Chemistry, Biology and Geography, Chemistry Dept., 16 Pestalozzi Str., Timisoara-300115, Romania и [4]University of Vienna, Institute for Theoretical Chemistry, 17 Währingerstrasse, Vienna-1090, Austria

Антипсихотици су лекови који се користе у терапији психоза, првенствено схизофреније и биполарног поремећаја. Антипсихотици делују на широк спектар рецептора који учествују у бројним системима трансмисије у мозгу, али главни терапијски ефекат остварују блокирајући допаминске рецепторе. Константа инхибиције, K_i, на нивоу мембранских рецептора је главна детерминанта фармакокинетике и дејства ових лекова. У раду су коришћењем 3D--QSAR–CoMSIA модела оцењене предсказане инхибиционе константе K_i за низ од 71 антипсихотика већ одобрених за клиничку праксу, као и за репрезентативне нове хемијске структуре које показују антипсихотичну активност. Значајне вредности унакрсне корелације q^2 (изнад 0,70) и фитоване корелације r^2 (изнад 0,80), показале су да ови модели могу да предвиде биолошке афинитете 15 нових респеридонских и 12 нових оланзапинских деривата за допаминске D_2 и серотонинске $5HT_{2A}$ рецепторе, те се ова једињења предлажу за даље испитивање.

(Примљено 6. августа, ревидирано 9. септембра 2010)

REFERENCES

1. W. T. Carpenter Jr., D. W. Heinrichs, T. E. Hanlon, *Am. Psychiatry* **144** (1987) 1466
2. M. Matsui, H. Arai, M. Yonezawa, T. Sumiyoshi, M. Suzuki, M. Kurachi, *Appl. Neuropsychol.* **16** (2009) 158
3. C. Dubertret, I. Bidard, J. Ades, P. Gorwood, *Schizophr. Res.* **86** (2006) 284
4. G. M. James, C. A. Sugar, R. Desai, R. A. Rosenheck, *Schizophr. Res.* **86** (2006) 309
5. P. Sirota, I. Pannet, A. Koren, E. Tchernichovsky, *Hum. Psychopharmacol.* **21** (2006) 227
6. D. Dickinson, V. N. Iannone, C. M. Wilk, J. M. Gold, *Biol. Psychiatry* **55** (2004) 826
7. S. K. Hill, J. L. Reilly, M. S. Harris, C. Rosen, R. W. Marvin, O. Deleon, J. A. Sweeney, *Schizophr. Res.* **113** (2009) 167
8. D. L. Levy, M. J. Coleman, H. Sung, F. Ji, S. Matthysse, N. R. Mendell, D. Titone, *J. Neuroling.* **23** (2010) 176
9. M. Alaerts, J. Del-Favero, *Hum. Mutat.* **30** (2009) 1139
10. J. Hirvonen, T. G. van Erp, J. Huttunen, K. Nagren, M. Huttunen, S. Aalto, J. Lonnqvist, J. Kaprio, T. D. Cannon, J. Hietala, *Psychiatry Res.* **146(1)** (2006) 13
11. B. K. Lipska, G. E. Jaskiw, D. R. Weinberger, *Neuropsychopharm.* **9** (1993) 67
12. B. K. Lipska, *J. Psychiatry Neurosci.* **29** (2004) 282
13. A. H. Wong, H. H. Van Tol, *Neurosci. Biobehav. Rev.* **27** (2003) 269
14. H. J. Sorensen, E. L. Mortensen, J. M. Reinisch, S. A. Mednick, *Brit. J. Psychiatry* **185** (2004) 366
15. B. C. Ho, V. Magnotta, *Neuroimage* **49** (2010) 3385
16. C. Van Mullem, J. Tillett, *J. Perinat. Neonatal. Nurs.* **23** (2009) 124

17. G. Boog, *Eur. J. Obstet. Gynecol. Reprod. Biol.* **114** (2004) 130
18. A. S. Brown, E. J. Derkits, *Am. J. Psychiatry* **167** (2010) 261
19. G. S. Robertson, S. E. Hori, K. J. Powell, *J. Psychiatry Neurosci.* **31** (2006) 157
20. M. Marcelis, J. Suckling, P. Hofman, P. Woodruff, E. Bullmore, J. van Os, *Schizophr. Res.* **86** (2006) 45
21. F. M. Benes, *Neuropsychopharm.* **35** (2010) 239
22. B. Gisabella, M. G. Cunningham, V. Y. Bolshakov, F. M. Benes, *Biol. Psychiatry* **65** (2009) 464
23. D. Tarsy, R. J. Baldessarini, F. I. Tarazi, *CNS Drugs* **16** (2002) 23
24. J. P. Kelleher, F. Centorrino, M. J. Albert, R. J.; Baldessarini, *CNS Drugs* **16** (2002) 249
25. S. Miyamoto, G. E. Duncan, C. E. Marx, J. A. Lieberman, *Mol. Psychiatry* **10** (2005) 79
26. P. Smid, H. K. Coolen, H. G. Keizer, R. van Hes, J. P. de Moes, A. P. den Hartog, B. Stork, R. H. Plekkenpol, L. C. Niemann, C. N. Stroomer, M. T. Tulp, H. H. van Stuivenberg, A. C. McCreary, M. B. Hesselink, A. H. Herremans, C. G. Kruse, *J. Med. Chem.* **48** (2005) 6855
27. G. Campiani, S. Butini, C. Fattorusso, F. Trotta, S. Gemma, B. Catalanotti, V. Nacci, I. Fiorini, A. Cagnotto, I. Mereghetti, T. Mennini, P. Minetti, M. A. Di Cesare, M. A. Stasi, S. Di Serio, O. Ghirardi, O. Tinti, P. Carminati, *J. Med. Chem.* **48** (2005) 1705
28. G. Campiani, S. Butini, C. Fattorusso, B. Catalanotti, S. Gemma, V. Nacci, E. Morelli, A. Cagnotto, I. Mereghetti, T. Mennini, M. Carli, P. Minetti, M. A. Di Cesare, D. Mastroianni, N. Scafetta, B. Galletti, M. A. Stasi, M. Castorina, L. Pacifici, M. Vertechy, S. Di Serio, O. Ghirardi, O. Tinti, P. Carminati, *J. Med. Chem.* **47** (2004) 143
29. G. Campiani, S. Butini, S. Gemma, V. Nacci, C. Fattorusso, B. Catalanotti, G. Giorgi, A. Cagnotto, M. Goegan, T. Mennini, P. Minetti, M. A. Di Cesare, D. Mastroianni, N. Scafetta, B. Galletti, M. A. Stasi, M. Castorina, L. Pacifici, O. Ghirardi, O. Tinti, P. Carminati, *J. Med. Chem.* **45** (2002) 344
30. M. Alvarado, A. Coelho, C. F. Masaguer, E. Ravina, J. Brea, J. F. Padin, M. I. Loza, *Bioorg. Med. Chem. Lett.* **15** (2005) 3063
31. J. Arora, M. Bordeleau, L. Dube, K. Jarvie, L. Mazzocco, J. Peragine, A. Tehim, I. Egle, *Bioorg. Med. Chem. Lett.* **15** (2005) 5253
32. J. Fernandez, J. M. Alonso, J. I. Andres, J. M. Cid, A. Diaz, L. Iturrino, P. Gil, A. Megens, V. K. Sipido, A. A. Trabanco, *J. Med. Chem.* **48** (2005) 1709
33. A. Takano, *Curr. Pharm. Des.* **16** (2010) 371
34. L. S. Kegeles, A. Abi-Dargham, W. G. Frankle, R. Gil, T. B. Cooper, M. Slifstein, D. R. Hwang, Y. Huang, S. N. Haber, M. Laruelle, *Arch. Gen. Psychiatry* **67** (2010) 231
35. S. Snigdha, M. Horiguchi, M. Huang, Z. Li, M. Shahid, J. C. Neill, H. Y. Meltzer, *J. Pharmacol. Exp. Ther.* **332** (2010) 622
36. S. Kapur, G. Remington, *Biol. Psychiatry* **50** (2001) 873
37. H. Uchida, T. K. Rajji, B. H. Mulsant, S. Kapur, B. G. Pollock, A. Graff-Guerrero, M. Menon, D. C. Mamo, *J. Clin. Psychopharmacol.* **29** (2009) 571
38. S. Potvin, T. Pampoulova, A. Mancini-Marie, O. Lipp, R. H. Bouchard, E. Stip, *J. Neurol. Neurosurg. Psychiatry* **77** (2006) 796
39. I. Wonodi, L. E. Hong, G. K. Thaker, *Adv Neurol.* **96** (2005) 336
40. S. Avram, H. Berner, A. L. Milac, P. Wolschann, *Monatsh. Chem.* **139** (2008) 407
41. S. Agatonovic-Kustrin, P. Davies, J. V. Turner, *Med. Chem.* **5** (2009) 271
42. T. Balle, K. Andersen, K. K. Soby, T. Liljefors, *J. Mol. Graph. Model.* **21** (2003) 523

43. H. Lanig, W. Utz, P. Gmeiner, *J. Med. Chem.* **44** (2001) 1151
44. J. Bostrom, M. Bohm, K. Gundertofte, G. Klebe, *J. Chem. Inf. Comput. Sci.* **43** (2003) 1020
45. J. Bostrom, K. Gundertofte, T. Liljeforsa, *J. Comput. Aided Mol. Des.* **14** (2000) 769
46. K. Audouze, E. O. Nielsen, D. Peters, *J. Med. Chem.* **47** (2004) 3089
47. B. G. Tehan, E. J. Lloyd, M. G. Wong, *J. Mol. Graph. Model.* **19** (2001) 417
48. E. Ravina, J. Negreira, J. Cid, C. F. Masaguer, E. Rosa, M. E. Rivas, J. A. Fontenla, M. I. Loza, H. Tristan, M. I. Cadavid, F. Sanz, E. Lozoya, A. Carotti, A. Carrieri, *J. Med. Chem.* **42** (1999) 2774
49. *PDSP KI Database*, http://kidb.cwru.edu/pdsp.php (accessed 23May, 2010)
50. W. K. Kroeze, S. J. Hufeisen, B. A. Popadak, S. M. Renock, S. Steinberg, P. Ernsberger, K. Jayathilake, H. Y. Meltzer, B. L. Roth, *Neuropsychopharm.* **28** (2003) 519
51. E. S. Burstein, J. Ma, S. Wong, Y. Gao, E. Pham, A. E. Knapp, N. R. Nash, R. Olsson, R. E. Davis, U. Hacksell, D. M. Weiner, M. R. Brann, J. Pharmacol. Exp. Ther. 315 (2005) 1278
52. D. A. Shapiro, S. Renock, E. Arrington, L. A. Chiodo, L. X. Liu, D. R. Sibley, B. L. Roth, R. Mailman, *Neuropsychopharm.* **28** (2003) 1400
53. P. Seeman, *Clin. Neurosci. Res.* **1** (2001) 53
54. J. M. Elliott, A. Kent, *Neurochem.* **53** (1989) 191
55. E. Richelson, *Ann. N. Y. Acad. Sci.* **537** (1988) 435
56. C. L. Waller, T. I. Oprea, A. Giolitti, G. R. Marschall, *J. Med. Chem.* **36** (1993) 4152
57. *Sybyl Basic Ligand-Based Design Manual*, Tripos Associates Inc., 1699 South Hanley Road, St. Louis, MO, 1988.

Journal of the Serbian Chemical Society
JSCS-info@shd.org.rs • www.shd.org.rs/JSCS
J. Serb. Chem. Soc. *76* (2) 283–303 (2011)
JSCS–4118
UDC 546.151–128.2+546.48–128.4+ 544.723:546.57
Original scientific paper

Processes of adsorption/desorption of iodides and cadmium cations onto/from Ag(111)

VLADIMIR D. JOVIĆ*# and BORKA M. JOVIĆ#

Institute for Multidisciplinary Research, P.O. Box 33, 11030 Belgrade, Serbia

(Received 1 July, revised 23 August 2010)

Abstract: In this work, the adsorption/desorption processes of iodides and cadmium cations in the presence of iodides onto/from Ag(111) were investigated. It was shown that both processes were complex, characterized by several peaks on the cyclic voltammograms (CVs). By PeakFit analysis of the recorded CVs and subsequent fitting of the obtained peaks by the Frumkin adsorption isotherm, the interaction parameter (f) and the Gibbs energy of adsorption (ΔG_{ads}) for each adsorbed phase were determined. In the case of iodide adsorption, four peaks were characterized by negative values of f, indicating attractive lateral interaction between the adsorbed anions, while two of them possessed value of $f < -4$, indicating phase transition processes. The adsorption/desorption processes of cadmium cations (underpotential deposition – UPD of cadmium) in the presence of iodide anions was characterized by two main peaks, each of them being composed of two or three peaks with negative values of f. By the analysis of charge *vs*. potential dependences obtained either from the CVs or current transients on potentiostatic pulses, it was concluded that adsorbed iodides did not undergo desorption during the process of Cd UPD, but became replaced by Cd ad-atoms and remained adsorbed on top of a Cd layer and/or in between Cd the ad-atoms.

Keywords: Ag(111); iodide adsorption; iodide desorption; Cd underpotential deposition; phase transition.

INTRODUCTION

The first ordered iodide structures on Ag(111) emersed from dilute HI solutions were observed by Salaita *et al.*[1] using the Ultra high vacuum–electrochemical (UHV–EC) technique: one with triangular splitting of subspots in the negative potential range and the other with hexagonal splitting in the positive potential range. Several adlayer structures were also reported for iodine on Ag(111):

* Corresponding author. E-mail: vladajovic@imsi.rs
# Serbian Chemical Society member.
doi: 10.2298/JSC100701026J

scanning tunneling microscopy (STM) images of a flat adlayer of I/Ag(111) obtained in air being ascribed to the so-called ($5\times\sqrt{3}$) structure;[2–4] contracted ($\sqrt{3}\times\sqrt{3}$)R–30° adlattice detected by X-ray photoelectron spectroscopy (XPS) performed on iodine-covered Ag(111).[5] Adsorption/desorption process of iodides from iodide-containing solutions on oriented silver single crystal surfaces has been investigated by capacitance, voltammetric and surface analytical techniques.[6,7] A common characteristic of the voltammetric investigations was the presence of a broad peak at more negative potentials and a sharp peak at less negative potentials. The broad peak was ascribed to the formation of a randomly distributed adlayer at potentials negative of –0.8 V *vs*. SHE and its transformation to a ($\sqrt{3}\times\sqrt{3}$)R30° ordered structure between –0.8 and –0.13 V *vs*. SHE. Further compression of such an ordered structure into an (8×8) iodide structure, expressed by a sharp peak on the CVs, was detected at potentials slightly positive of –0.13 V *vs*. SHE.[6,7] Detailed *in situ* STM and *ex situ* low energy electron diffraction (LEED) studies of Yamada *et al*.[8] in KI buffered with KF–KOH at pH 10 and HI solutions confirmed the continuous compression of the iodide adlattice from square ($\sqrt{3}\times\sqrt{3}$ R–30°), *via* ($\sqrt{3}\,qR\beta°\times\sqrt{3}$ R–30°) ($q \approx 1$, $0 \leq \beta \leq 30$), to ($\sqrt{3}\times\sqrt{3}$)R30° with increasing electrode potential, followed by an abrupt phase transition into a rotated hexagonal ($\sqrt{3}\times\sqrt{3}$)R(30°+α°) phase at potentials more positive than the potential of the sharp peak on the CV. Their CV recorded in 0.1 mM KI + 10 mM KF + 0.1 mM KOH at a sweep rate of 5 mV s^{-1} was characterized by a nucleation loop at –0.06 V *vs*. SHE, by pair of sharp, phase transition peaks, at around –0.16 V *vs*. SHE and a pair of broad peaks between around –0.61 and –0.96 V *vs*. SHE. The pair of broad peaks possessed two pairs of small sharp peaks at potentials around –0.68 and –0.76 V *vs*. SHE. Except the ($\sqrt{3}\times\sqrt{3}$)R(30°+α°) phase detected by *in situ* STM at potentials more positive that the potential of the sharp (phase transition) peaks on the CV at around –0.16 V *vs*. SHE, all the other above-mentioned structures were detected in the so-called double layer region, between the broad and the sharp peak on the CV. The CV recorded at the same sweep rate in a solution of 0.1 mM HI possessed only a nucleation loop at –0.06 V *vs*. SHE and a pair of sharp, phase transition peaks, at around –0.16 V *vs*. SHE. From this solution, only *ex situ* LEED–Auger electron spectroscopy (LEED–AES) experiments were performed. At an emersion potential of –0.48 V *vs*. SHE, a ($\sqrt{3}\times\sqrt{3}$)R30° adlayer structure was detected; at an emersion potential of –0.28 V *vs*. SHE, a $c(p\times\sqrt{3}$ R–30°) adlayer structure with p = 0.264 was detected, while a ($\sqrt{3}\times\sqrt{3}$)R(30°+α°) phase was detected at an emersion potential of –0.1 V *vs*. SHE, positive of a phase transition peak. Hence, the appearance of different ordered structures was found to depend on the solution composition.

Underpotential deposition (UPD) of cadmium onto silver single crystals has not been studied extensively. Bort *et al*.[9] found that on a Ag(111) surface, the

UPD of Cd commenced at a potential of about –0.18V *vs*. SHE, with the formation of a ($\sqrt{3}\times\sqrt{3}$)R30° structure. The voltammetric peaks associated with this process were reversible. A second cathodic peak, observed at about –0.41 V *vs*. SHE, was reported to correspond to a monolayer deposition of Cd, while the charge associated with a third cathodic peak was consistent with that required for a second monolayer of Cd. Almost identical results were obtained in the work of Garcia *et al*.[10] By *in situ* STM, it was shown that the Cd UPD process starts with the formation of an expanded (diluted) adlayer with a superlattice structure Ag(111)–($\sqrt{3}\times\sqrt{19}$)R23.4°, being transformed to a condensed close packed Cd monolayer *via* a first order phase transition. During long time polarization in the potential range of monolayer formation, the monolayer transforms into an Ag–Cd surface alloy by place exchanging between Cd atoms and surface Ag atoms. At more negative potentials, the formation of a second Cd monolayer, with pronounced alloying between Ag and Cd, was found to occur.[10] The formation of the superlattice and both monolayers was clearly detected by *in situ* STM.[10] The kinetics of the alloying process was also investigated showing that de-alloying led to the appearance of large number of 2D islands and monoatomic deep steps, which rapidly disappeared at more positive potentials, suggesting a relatively high mobility of the surface Ag atoms under such conditions.[10] The same processes (UPD and alloying of Ag with Cd) were also investigated in a chloride--containing solution.[11] Identical conclusion were reached concerning UPD and alloying, except that it was concluded in this work that chloride ad-atoms, which are adsorbed on the silver substrate when UPD of Cd starts, did not undergo desorption. They became replaced by Cd ad-atoms and remained adsorbed and discharged on top of a Cd layer.[11]

In the present work, an attempt to investigate the adsorption/desorption process of iodides and the UPD of Cd onto Ag(111) in the presence of iodides was made.

EXPERIMENTAL

All experiments were performed in a two-compartment electrochemical cell at 25±1 °C. The single crystal electrode (Monocrystals Company, d = 0.9 cm) was sealed in epoxy resin in such a way that only the (111) disc surface was exposed to the solution. The surface area of the electrode exposed to the electrolyte was 0.636 cm^2. The counter electrode (CE) was a Pt sheet, which was placed parallel to the working electrode. The reference electrode (RE) was a saturated silver chloride electrode (Ag/AgCl). All results are given *vs*. SHE. The RE was placed in a separate compartment and connected to the working compartment by means of a Luggin capillary. Solutions of 0.1 M NaI and 0.05 M CdI_2 were made from supra pure (99.999 % – Aldrich) chemicals and extra pure UV water (Smart2PureUV, TKA).

The single crystals were prepared by a mechanical polishing procedure followed by chemical polishing in the solution containing NaCN and H_2O_2, as explained in a previous paper.[12] Before each experiment, the electrolyte was purged with high purity nitrogen (99.999 %)

for 45 min, while a nitrogen atmosphere was maintained over the solution during the experiment to prevent contamination with oxygen.

All experiments were performed using a potentiostat Reference 600 and PHE 200 software (Gamry Instruments Inc.).

The deconvolution of the experimentally recorded peaks on the CVs was performed by the computer program PeakFit for Win32, version 4.05 (AISN Software). All fits were performed with the Gauss + Lorenz Amp function. With this function it was possible to vary the width and shape of the resulting peaks. In such a way, it was possible to obtain a fitting curve identical to the experimental one.

RESULTS AND DISCUSSION

Iodide adsorption/desorption in 0.1 M NaI

CV recorded at a sweep rate of 200 mV s^{-1} in 0.1 M NaI is presented in Fig. 1. The process of iodide adsorption/desorption is characterized by one pair of broad peaks, composed of several small, sharp peaks in the negative potential region (from ≈ –0.7 to ≈ –1.0 V) and one pair of sharp peaks at less negative potentials (around –0.16 V). It is important to note that in the investigated solution (pH around 7), the process of hydrogen evolution should commence at about –0.42 V *vs.* SHE. Taking into account a certain overvoltage for hydrogen evolution onto an Ag electrode, this value should be more negative (by about 0.2–0.3 V). According to the CVs presented in the work of Yamada *et al.*[8] in a solution containing 0.1 mM KI + 10 mM KF + 0.1 mM KOH (pH 10) at the sweep rate of 5 mV s^{-1}, the CV started declining to the cathodic direction at about –0.68 V *vs.* SHE (Fig. 1A), while in a solution containing 0.1 mM HI (pH 4.3), the process of iodide adsorption could not be seen since the massive hydrogen evolution (at a

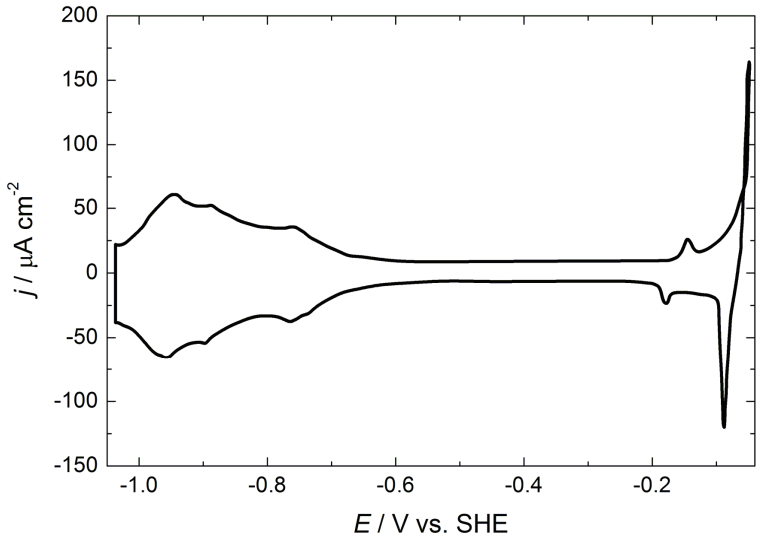

Fig. 1. CV of Ag(111) in 0.1 M NaI recorded at a sweep rate v = 200 mV s^{-1}.

sweep rate of 5 mV s^{-1}) started already at about –0.6 V *vs.* SHE (Fig. 1B). In order to avoid simultaneous hydrogen evolution, taking into account that the processes of anion adsorption are much faster, it was necessary to apply sweep rates higher than 100 mV s^{-1}. Hence, on the CVs recorded at the sweep rates ≥ 100 mV s^{-1}, the declining of the CVs to the cathodic direction could be avoided and well-defined CVs down to –1.0 V were recorded (see Figs. 1 and 4a), with no charge of hydrogen evolution contributing to the charge required for iodide adsorption. The sudden increase of the cathodic current density corresponding to the hydrogen evolution was recorded immediately after the cathodic limit on the presented CVs (not presented in Figs. 1 and 4a). As can be seen in Fig. 1, at potentials close to zero, an anodic nucleation loop was obtained as a result of the beginning of 3D nucleation of AgI, as was the case in other investigations.[1–8] If the anodic potential limit was set to more positive values, a large amount of AgI (probably 3D islands) would form on the Ag(111) surface and its original orientation would be destroyed, causing significant changes on the CV of the iodide adsorption/desorption process (a similar effect was recorded for AgCl formation,[13] but this effect is much more pronounced in the case of AgI).

By integrating the surface under the cathodic and anodic parts of the CV shown in Fig. 1, the corresponding charge *vs.* potential curves were obtained, which are presented in Fig. 2. As can be seen, mirror-like dependences were obtained with a maximum anodic charge (Q_a) of ≈ 90 μC cm^{-2} and a maximum cathodic charge (Q_c) of ≈ 97 μC cm^{-2}. Taking into account that the theoretical charge (assuming complete charge transfer) for an $(\sqrt{3}\times\sqrt{3})$R30° iodide ad-

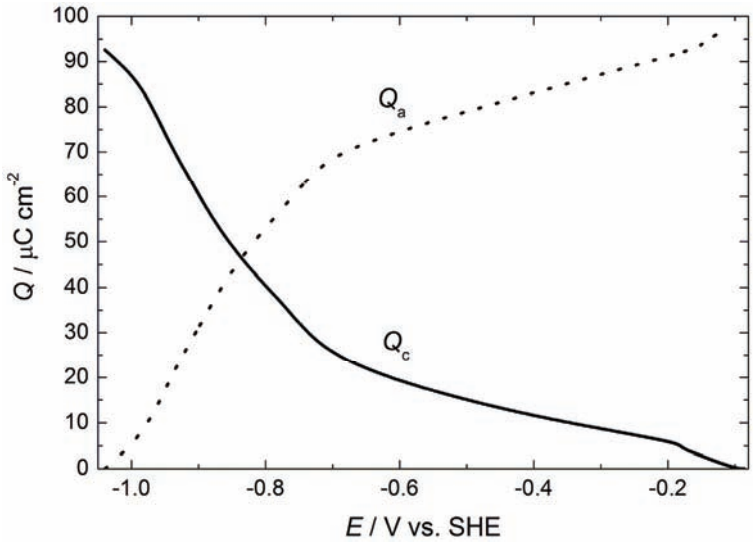

Fig. 2. Cathodic (Q_c) and anodic (Q_a) charges as a function of the potential obtained by integration of the corresponding parts (from –1.02 to –0.1 V) of the CV presented in Fig. 1.

layer[1–8] amounts to 74 μC cm^{-2}, it seems that this adlayer forms under the broad peak (sharp increase of the Q_a *vs.* E up to about 70 μC cm^{-2} at a potential of ≈ –0.65 V), with its further compression expressed by the slow increase of the anodic charge. Such behavior is in accordance with the findings of Yamada *et al.*,[8] although their solution was composed of a mixture of iodide, fluoride and hydroxide of mM concentrations.

In order to investigate more precisely the process of iodide adsorption, the anodic part of the CV shown in Fig. 1 (as well as in Fig. 4a) was analyzed by the PeakFit program. The results of such an analysis are presented in Fig. 3. As can be seen in Fig. 3a, all peaks obtained by deconvolution overlap, indicating that during this dynamic process, different structures could start forming during the formation of some other structure. The sum of all peaks, A, A1–A4 gives the curve presented with solid line showing the best fit of this part of the experimental curve (○). This is most likely the reason why *in situ* STM could not detect any ordered structure in this potential region[8] and ordered structures were detected at more positive potentials in the "double layer region". Simultaneously, the process of "random adsorption" (characterized by peak A) occurs in the potential range between –1.0 and –0.7 V, which is most likely adsorption of iodides at the monoatomic steps, since this type of adsorption is energetically favorable and usually finishes when the whole electrode surface is covered with the adsorbed anions. Hence, all these processes occur more or less simultaneously and deconvolution of the recorded anodic *j*–*E* curve was necessary for their differentiation. After deconvolution, five peaks were obtained. Each of them is considered as a CV of a single adsorption process and each peak was separately analyzed. After integration of the anodic *j*–*E* curve for each peak, the total charge for this particular peak was obtained and this value was used as Q_{max}. θ was calculated as Q/Q_{max}. In such a way, θ varied from 0 to 1 for each peak. The sharp peak at less negative potentials (around –0.16 V) could be fitted with only one peak B. Adsorption isotherms (θ *vs.* E dependences, presented with squares and circles) for peaks A and B are shown in Fig. 3b. Those for the peaks A1–A4 (presented with squares, circles and triangles) are shown in Fig. 3c. All adsorption isotherms presented in Figs. 3b and 3c were fitted with the Frumkin adsorption isotherm (fitting results are presented with solid, dashed, dotted, and dash–dot lines) expressed by the Equation:[14]

$$E = \frac{RT}{F}\left\{\ln\left(\frac{\theta}{1-\theta}\right) + f\theta - \ln\left(K_{\text{ads},\theta\to 0}c_0\right)\right\} \quad (1)$$

where $K_{\text{ads},\theta\to 0}c_0$ is the equilibrium constant for adsorption, $f = r/\text{RT}$ representing interaction parameter (with r being the rate of change of the Gibbs energy of adsorption with coverage), c_0 concentration of anions, while R, T and F have their usual meaning.

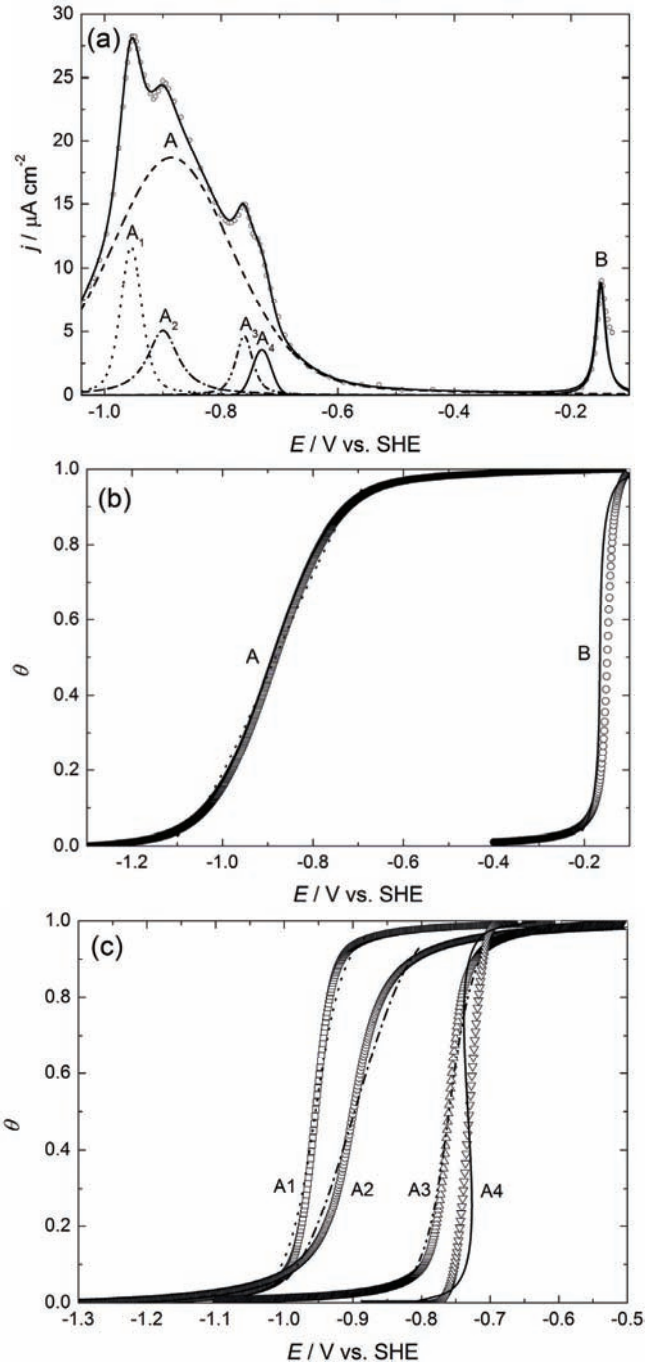

Fig. 3. a) Anodic part of the CV presented in Fig. 4a (v = = 100 mV s^{-1}): ○ – experimental curve; solid line – curve obtained by the PeakFit procedure; all peaks obtained by this procedure are marked with A, A1–A4 and B; b) adsorption isotherms obtained by the analysis of the corresponding peaks in (a): □ – experimental curve for peak A; dotted line – curve obtained after fitting the θ *vs.* E dependence for peak A with the Frumkin adsorption isotherm; ○ – experimental curve for peak B; solid line – fitting curve; c) adsorption isotherms obtained by analysis of the corresponding peaks in (a): □ – experimental curve for peak A1; dotted line – fitting curve; ○ – experimental curve for peak A2; dash-dot line – fitting curve; △ – experimental curve for peak A3; dash-dot-dot line – fitting curve; ▽ – experimental curve for peak A4; solid line – fitting curve.

The values of the Gibbs energies of adsorption were obtained from a following relation:[14]

$$\Delta G_{\text{ads}} = -2.3RT \log K_{\text{ads},\theta\to 0} \quad (2)$$

The best fits for the isotherms presented in Figs. 3b and 3c were obtained with the parameters given in Table I. As could be expected, the adsorption isotherm for peak A (Fig. 3b) is characterized by a high positive value of the interaction parameter (f = 9.1), indicating repulsive lateral interaction between the adsorbed iodides. The adsorption equilibrium constant is also very high, 9.4×10^{20} and an accordingly high negative value of the Gibbs energy of adsorption is obtained (–119.8 kJ mol^{-1}). The interaction parameter f of the adsorption isotherm for the peak B, which, according to Yamada *et al.*[8] represents the phase transition of the $(\sqrt{3}\times\sqrt{3})$R30° adlayer into the rotated hexagonal $(\sqrt{3}\times\sqrt{3})$R(30°+α°) phase, possess a negative value (f = –4.3), confirming the attractive lateral interaction between the adsorbed iodide anions and the phase transition process, since it is more negative than the critical value of f for the phase transition (f = –4).[14] The adsorption equilibrium constant is by several orders of magnitude lower than that for peak A, 1.1×10^{6} and, accordingly, a much smaller negative value of the Gibbs energy of adsorption is obtained (–34.5 kJ mol^{-1}), Table I. Taking into account the shape of the CV (there are no peaks between –0.6 and –0.2 V, this part practically represents the double layer region), it seems reasonable to ascribe peak B to the process of phase transition of the $(\sqrt{3}\times\sqrt{3})$R30° adlayer into the rotated hexagonal $(\sqrt{3}\times\sqrt{3})$R(30°+α°) phase. The values of f for peaks A1, A3 and A4 are also negative, indicating attractive lateral interaction between the adsorbed anions, but only one, for peak A4, is more negative than f = –4, confirming the phase transition process at the end of the broad peak between –1.0 and –0.7 V. Taking into account that continuous compression of the iodide adlattice from square $(\sqrt{3}\times\sqrt{3}$ R–30°), *via* $(\sqrt{3}\ qR\beta$ °$\times\sqrt{3}$ R–30°) ($q \approx 1$, $0 \le \beta \le$ ≤ 30), to $(\sqrt{3}\times\sqrt{3})$R30° occurs with increasing electrode potential, it seems reasonable to ascribe peaks A1, A3 and A4 to the processes of the formation of these three ordered adlayers. While their compression is a dynamic process accompanied with the adsorption of new anions, it appears that the final step, the formation of the $(\sqrt{3}\times\sqrt{3})$R30° adlayer represents a phase transition process, which is in good agreement with an *in situ* STM analysis.[8] Peak A2 should also represent a process of iodide adsorption in which some disordered – random structure, characterized by a positive value of f is formed, most probably at the beginning of the formation of the ordered structure characterized by peak A3. This is often the case in anion adsorption.[15] The main difference between the results and those presented previously[8] is the potential region in which the abovementioned ordered structures (peaks A1, A3, and A4) were formed. From the present analysis, it appears that these three structures were formed under the

broad peak, at more negative potentials than those in the literature.[8] There are two reasons for such a difference: first, STM can detect only stable, ordered structures and during the dynamic change of the adsorbing conditions under the broad peak, the formation of ordered structures most likely cannot be seen; second, the solution for *in situ* STM study[8] contained KOH at the same concentration as KI, with the adsorption of OH^- onto Ag(111) starting at more positive potentials than –0.56 V *vs.* SHE;[7,15] thus in the *in situ* STM investigations, competitive adsorption of iodide and hydroxide anions, influencing the potential of stable iodide adlayer formation, was possible. Considering results for the HI solution,[8] in which the peaks of iodide adsorption/desorption were not seen (they were overridden by hydrogen evolution), while the adlayer $(\sqrt{3}\times\sqrt{3})$R30° was detected by *in situ* STM at the potential of hydrogen evolution (–0.76 V *vs.* SHE), it seems that the difference between the previous and present results could be the consequence of both the above-mentioned reasons. Hence, it could be stated that although by the presented analysis it is not possible to obtain information about the exact structure of the adsorbed adlayers, valuable information concerning their adsorption kinetics could be obtained.

TABLE I. Results of the fitting peaks presented in Fig. 3 by Frumkin adsorption isotherms

Peak	f	$K_{\mathrm{ads},\theta\to0}$	ΔG_{ads} / kJ mol^{-1}
A	9.1	9.4×10^{20}	–119.8
B	–4.3	1.1×10^{6}	–34.5
A1	–1.6	6.6×10^{19}	–113.2
A2	1.5	3.7×10^{19}	–111.8
A3	–1.7	3.7×10^{16}	–94.6
A4	–4.5	2.6×10^{15}	–88.1

Cadmium UPD from 0.05 M CdI_2 + 0.1 M NaI

Since both ions, Cd^{2+} and I^- adsorb with the formation of ordered structures, this system is very convenient to investigate the influence of anion adsorption on cation adsorption. The process of Cd UPD onto Ag(111) in the presence of iodide anions was investigated in this work for the first time by the cyclic voltammetry and potentiostatic pulse techniques.

The CVs of Ag(111) recorded at a sweep rate of 100 mV s^{-1} in the absence (solid line) and presence of CdI_2 in the solution (dotted line) are shown in Fig. 4a. As can be seen, the UPD of Cd starts at about –0.25 V with a sharp increase in the cathodic current density, while the shape of the CV at more positive potentials only slightly changes and still shows the sharp peak of the phase transition of the $(\sqrt{3}\times\sqrt{3})$R30° iodide adlayer into the rotated hexagonal $(\sqrt{3}\times\times\sqrt{3})$R(30°+$\alpha$°) phase. The slightly different shape of this peak is most probably the consequence of the presence of Cd^{2+} in the double layer. The shape and position of this peak does not depend on the cathodic potential limit. Hence, al-

though the process of Cd adsorption/desorption (UPD) occurs at a more negative potential of –0.25 V, after Cd desorption, the $(\sqrt{3}\times\sqrt{3})$R30° adlayer of iodide still remains adsorbed on the Ag(111) surface and its transformation into the $(\sqrt{3}\times\sqrt{3})$R(30°+α°) phase occurs at the same potential as in the absence of Cd^{2+}. If the anodic limit is set to a more positive value, a well-defined nucleation loop of AgI formation and dissolution was detected, Fig. 4b.

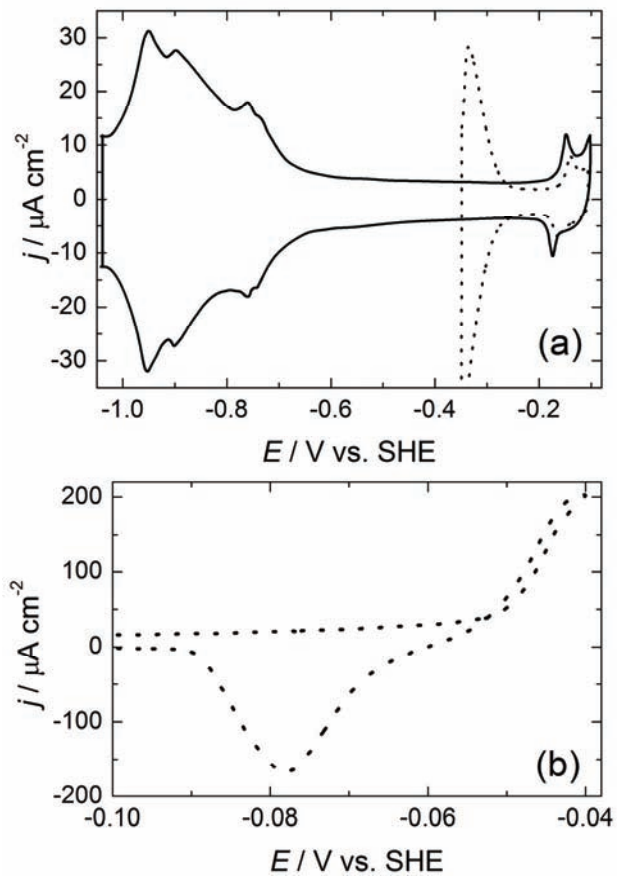

Fig. 4. a) CV of Ag(111) recorded at a sweep rate v = 100 mV s^{-1} in a solution of 0.1 M NaI (solid line) and in a solution containing 0.1 M NaI + 0.05 M CdI_2 (dotted line); b) CV of AgI formation and reduction recorded at a sweep rate v = 100 mV s^{-1} in the solution containing 0.1 M NaI + 0.05 M CdI_2.

In order to obtain much better insight into the UPD process, CVs were recorded at a low sweep rate of 5 mV s^{-1}. The corresponding CVs and Q *vs.* E dependences are presented in Figs. 5a and 5b, respectively. Three cathodic potential limits were set: one after the first peak C (solid line), one after the second peak D

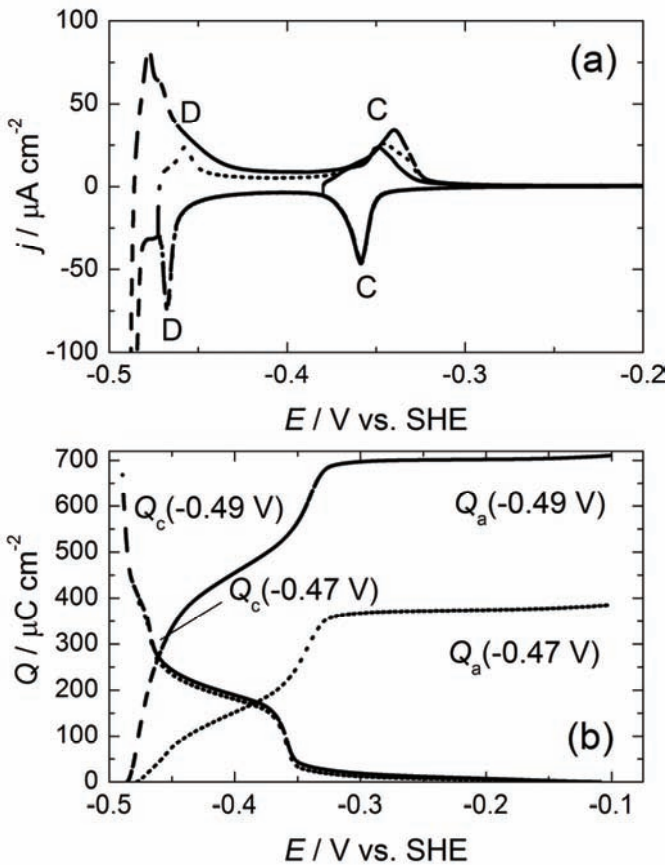

Fig. 5. a) CVs of the process of UPD of Cd onto Ag(111) recorded at a sweep rate v = 5 mV s^{-1} in the solution containing 0.1 M NaI + 0.05 M CdI_2: cathodic potential limit –0.38 (solid line), –0.47 (dotted line) and –0.49 V (dashed line); b) corresponding cathodic (Q_c) and anodic (Q_a) charges as a function of potential obtained by integration of the CVs presented in (a).

(dotted line) and one at –0.49 V (dashed line). The corresponding *Q vs. E* dependences, obtained for cathodic limits of –0. 47 and –0.49 V clearly indicate that the charge obtained for peak C (inflection point at Q_c *vs. E* at around –0. 36 V) amounts to ≈ 150 μC cm^{-2}, confirming the formation of the $(\sqrt{3}\times\sqrt{3})$R30° structure of Cd. In order for Cd to occupy the same $(\sqrt{3}\times\sqrt{3})$R30° sites, all of the iodide ad-atoms must first be desorbed from the (111) face of silver, contributing with an additional charge[1–8] of approximately 74 μC cm^{-2} (since a small charge was exchanged during the rearrangement of this ordered structure into randomly arranged adsorbed anions) to the 149 μC cm^{-2} cathodic charge associated with the adsorbed $(\sqrt{3}\times\sqrt{3})$R30° Cd structure.[11] The results presented in Fig. 5b clearly show that this was not the case since the charge attributed to the early stage of Cd UPD is about 150 μC cm^{-2}, which is quite close to the theo-

retical charge required for the ($\sqrt{3}\times\sqrt{3}$)R30° Cd structure (assuming complete charge transfer between Cd and Ag). Based on these results, it is obvious that desorption of iodide ad-atoms does not occur during Cd UPD, but they become replaced by cadmium ad-atoms, remaining adsorbed onto Cd layer and/or in between the adsorbed Cd ad-atoms. The sharp increase in the cathodic charge between –0.47 and –0.49 V overcomes the charge needed for the formation of a close packed monolayer (≈ 450 μC cm^{-2}) of Cd (Q_c(–0.49 V) and Q_a(–0.49 V) curves of Fig. 5b), indicating alloying of Ag and Cd,[9–11] as well as 3D deposition of Cd. Since the process of alloying has already been investigated in sulfates[9,10] and chlorides[11] containing solution, the intention in the present study was to investigate more closely the processes occurring under peaks C and D. In the first instance, by considering the shape of the CVs shown in Fig. 5a, it is clear that the anodic peaks are composed of more than one peak, while for cathodic peaks, it appears that they could be fitted with one peak only. The results of the PeakFit analysis for both the cathodic and anodic peaks are presented in Figs. 6–6c and 7a–7c, respectively. Since the current density between cathodic and anodic peaks C and D was not small as the one before the peak C (representing the double layer charging current density), it was decided to correct these voltammograms for the base line in order to avoid the influence of all the processes that are not represented by peaks C and D (replacement of ad-atoms, double layer charging, exchange of anions in the inner and outer Helmoholtz layer, *etc*.) and the correction for the base line is presented in Fig. 6a for the cathodic CV and in Fig. 7a for the anodic CV. As can be seen in Fig. 6b, the cathodic peaks C and D are composed of two peaks each, 1 (dashed line), 2 (dash-dot-dot line), 3 (dash-dot line) and 4 (dotted line), respectively. By the same procedure as in the previous analysis, adsorption isotherms (θ *vs. E* dependences) for all four peaks were obtained and fitted with the Frumkin adsorption isotherm (Eq. (1)). The experimental points are presented with squares, circles, and triangles, while the corresponding fitting results are presented by dashed, dotted, dash-dot and dash-dot-dot lines in Fig. 6c. The results of the fitting procedure are given in Table II. As can be seen, all peaks are characterized by the negative values of the interaction parameter *f*, indicating that the UPD in all cases is characterized by attractive lateral interaction between the adsorbed cadmium ad-atoms. This value for peaks 1, 3 and 4 overcomes the critical one of –4, confirming phase transition process. These results are in good agreement with the findings of other authors[9–11] that peak C represents phase transition into the ($\sqrt{3}\times\sqrt{3}$)R30° ordered Cd structure, while under peak D, phase transition of this structure into a close packed monolayer occurs. However, the shape of peak C, as well as the shape of a whole CV, changes in dependence of the presence of sulfates,[9,10] chlorides[11] and iodides. In sulfate and chloride electrolytes, peak C is characterized with a broad (broader in sulfate than in chloride) and a sharp peak. The broad peak corresponds to the random ad-

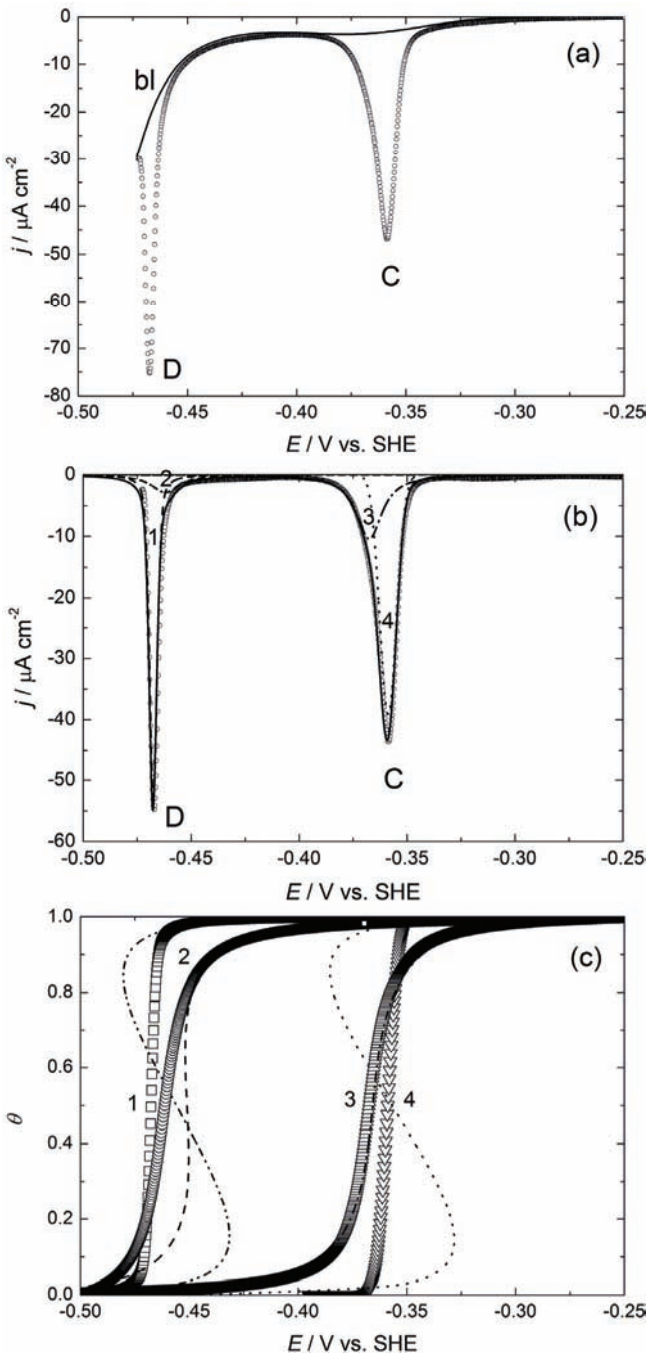

Fig. 6. a) Cathodic part of the CV presented in Fig. 5a: experimental points (○) and corresponding baseline (bl – solid line) – cathodic potential limit –0.47 V; b) cathodic part corrected for the base line; ○ – experimental curve; solid line – curve obtained by the PeakFit procedure; all peaks obtained by this procedure are marked with 1 (dashed line), 2 (dash-dot-dot line), 3 (dash-dot line), and 4 (dotted line); c) adsorption isotherms obtained by analysis of the corresponding peaks in (b): □ – experimental curve for peak 1; dash-dot--dot line – fitting curve; ○ – experimental curve for peak 2; dashed line – fitting curve; △ – experimental curve for peak 3; dash-dot line – fitting curve; ▽ – experimental curve for peak 4; dotted line – fitting curve.

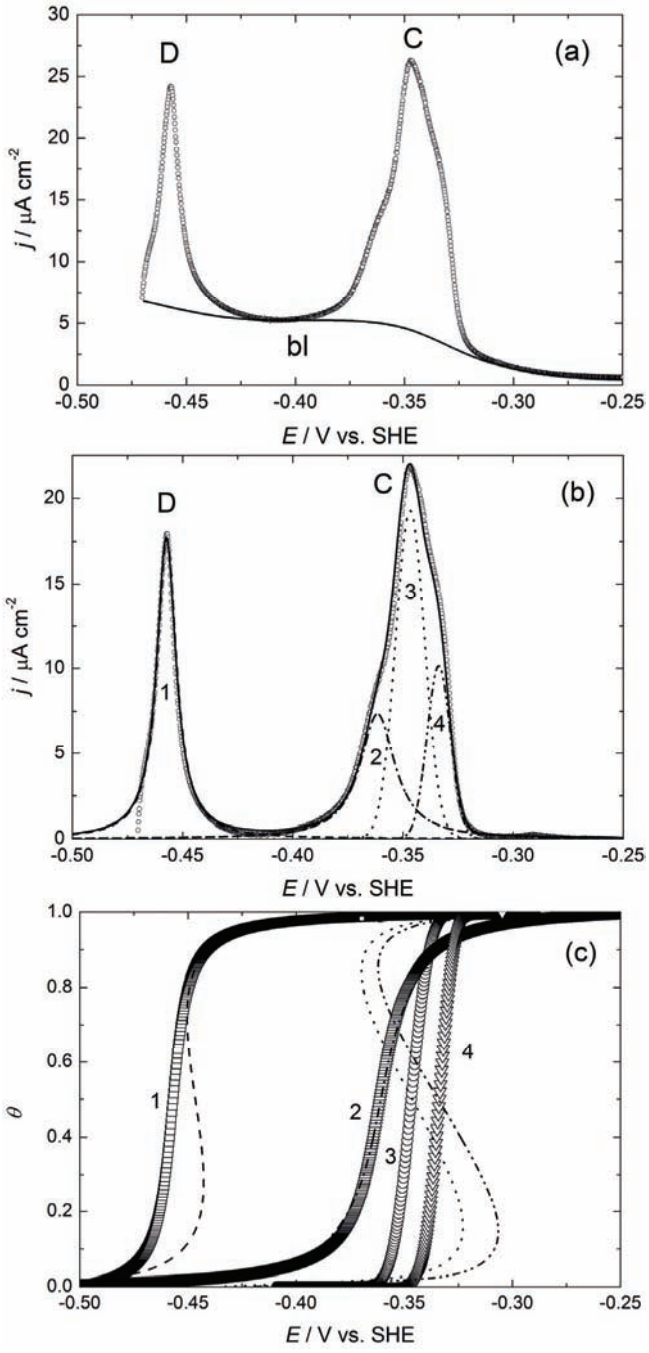

Fig. 7. a) Anodic part of the CV presented in Fig. 5a: experimental points (○) and corresponding baseline (bl – solid line) – cathodic potential limit –0.47 V; b) anodic part corrected for the base line; ○ – experimental curve; solid line – curve obtained by the PeakFit procedure; all peaks obtained by this procedure are marked with 1 (dashed line), 2 (dash-dot line), 3 (dotted line), and 4 (dash-dot-dot line); c) adsorption isotherms obtained by analysis of the corresponding peaks in (b): □ – experimental curve for peak 1; dashed line – fitting curve; △ – experimental curve for peak 2; dash–dot line – fitting curve; ○ – experimental curve for peak 3; dotted line – fitting curve; ▽ – experimental curve for peak 4; dash-dot-dot line – fitting curve.

sorption of Cd (the value of f is positive), while the sharp one represents phase transition into the $(\sqrt{3}\times\sqrt{3})$R30° ordered Cd structure ($f \leq -4$). In both solutions, anions (sulfate or chloride) are already adsorbed on the Ag(111) surface when the UPD of Cd commences (peak C). The adsorbed adlayer of chlorides is known to transform from $(\sqrt{3}\times\sqrt{3})$R30° chloride adlayer into a randomly adsorbed chloride adlayer just before the commencement of Cd UPD.[1,6,11,13,16–20] The structure of adsorbed sulfate ad-atoms is unknown and there are only three papers dealing with the structure and coverage of the adsorbed sulfate onto Ag(111).[21–23] Schweizer and Kolb[21] detected a $c(3\times3\sqrt{3})$ ordered sulfate structure on Ag(111), but this "structure was found to be stable only for a relatively short time (about 1 h) at potentials between –0.25 and 0.05 V *vs*. SCE". These experiments were performed in 0.1 M H_2SO_4, in which HSO_4^- prevail, while most of the Cd UPD experiments were performed in solutions of high concentrations of Na_2SO_4, in which SO_4^{2-} prevail.[9,10] In a previous paper,[23] it was found that in 0.2 M Na_2SO_4, the adsorption of sulfates onto Ag(111) is characterized by two peaks at potentials between –0.45 and –0.15 V *vs*. SHE. The adsorbed sulfate structure is less dense than that expected for a sulfate monolayer and the process of sulfate adsorption follows a Frumkin adsorption isotherm with a high positive value of the interaction parameter f = 16.5, indicating repulsive lateral interaction between the adsorbed anions,[23] *i.e.*, randomly distributed sulfate ad-atoms (it was also found that complete charge transfer occurs). Hence, it could be concluded that in both cases, the Cd UPD starts on the Ag(111) surface which is not covered with adsorbed anions characterized by attractive forces between each other. The beginning of the Cd UPD in sulfate solution is placed at around –0.17 V *vs*. SHE and in chloride solution at around –0.20 V *vs*. SHE. In the case of iodide solution, the $(\sqrt{3}\times\sqrt{3})$R30° iodide adlayer is on the surface[8] when the Cd UPD process commences at around –0.34 V *vs*. SHE. From this behavior, it is obvious that the Cd UPD moves to more negative potentials with increasing attractive forces between the adsorbed anions, *e.g.*, more energy is required to replace the adsorbed iodides with Cd cations. Simultaneously, peak C, representing this process, changes its shape from a combination of a broad and sharp peak to one sharp peak only. As can be seen in Fig. 6b, this process is actually the simultaneous occurrence of two processes, both characterized with attractive forces between the adsorbed ad-atoms (Table II). It is not possible to determine the origin of both peaks. Peak 4 corresponds to the formation of the $(\sqrt{3}\times\sqrt{3})$R30 structure of the adsorbed Cd, while peak 3 might be ascribed to the rearrangement of the $(\sqrt{3}\times\sqrt{3})$R30° iodide adlayer into some undefined, ordered structure on top of the Cd adlayer and/or in between the Cd ad-atoms, or to a continuation of the formation of the $(\sqrt{3}\times\sqrt{3})$R30° structure of the adsorbed Cd. A similar supposition could be made for peak D, corresponding to the formation of a close packed Cd monolayer, with peak 1 representing the phase tran-

sition of the ($\sqrt{3}\times\sqrt{3}$)R30° Cd adlayer into a close packed monolayer and peak 2 representing a rearrangement of the adsorbed structure of iodide on top of a Cd monolayer, or a continuation of the process of close packed Cd monolayer formation. Slightly different results were obtained by the deconvolution of the anodic peaks C and D presented in Figs. 7a–7c. It appears that peak 1 corresponds to the phase transition of the Cd monolayer into a ($\sqrt{3}\times\sqrt{3}$)R30° Cd adlayer, while peaks 2 and 3 correspond to the process of desorption of the ($\sqrt{3}\times\sqrt{3}$)R30° Cd adlayer. This is consistent with the observations of Stuhlmann *et al.*[24] that the Cd adlayer is stabilized by chloride, thereby forming a $CdCl_2$-like layer on the copper surface. It appears that in the case of Ag(111) in iodide solution, the cadmium adlayer replaces the surface iodide, with the iodide remaining adsorbed on the Cd monolayer. Hence, peak 4 could be ascribed to the formation of ($\sqrt{3}\times\sqrt{3}$)R30° iodide adlayer on the Ag(111) surface, since it is characterized with an f value more negative than the critical one for phase transition (f = –8.0, Table II), as well as with the lowest value (1.3×10^8) of adsorption equilibrium constant for all peaks reflecting the UPD process (Table II). Taking into account that the ($\sqrt{3}\times\sqrt{3}$)R30° iodide adlayer in the absence of Cd ad-atoms is formed at a potential around –0.75 V (Fig. 3), it seems reasonable that its formation at more positive potentials should be faster, which is reflected by the high negative value of f and the small value of the equilibrium adsorption constant. It should be stated here that it is quite possible that Cd and iodide ad-atoms form some kind of mixed structures in the potential region between and around peaks C and D, as was the case with the Tl and bromide ad-atoms,[25] but to prove this it would be necessary to perform *in situ* X-ray investigations with accelerated electrons.

TABLE II. Results of fitting the peaks C and D presented in Figs. 6 and 7 by Frumkin adsorption isotherms

Cathodic peak	f	$K_{ads,\theta\to0}$	ΔG_{ads} / kJ mol^{-1}
1	–7.6	1.7×10^{10}	–52.1
2	–4.3	7.4×10^{10}	–55.6
3	–3.3	4.6×10^{9}	–71.6
4	–8.1	3.0×10^{8}	–61.3
Anodic peak			
1	–5.0	4.5×10^{10}	–62.1
2	–2.7	5.2×10^{9}	–57.2
3	–7.5	2.7×10^{8}	–51.7
4	–8.0	1.3×10^{8}	–49.9

Considering the adsorption isotherms presented in Figs. 3b (B), 3c (A4), 6c (1, 2 and 4) and 7c (1, 3 and 4), it can be seen that the fitting curves deviate from the experimental ones, having an "S" shape. This is typical for f values more negative than –4. The experimental curves are characterized with a sudden increase of coverage with potential, while the fitted ones show that the "coverage in-

creases with decreasing potential". Such a behavior obviously does not represent the physical reality of the process.[14] Hence, for all isotherms with $f \leq -4$, the experimental curves would show sudden transition from low to high coverage, while the fitted ones will possess an "S" shape. Complete discontinuity on the isotherms was discussed previously in more details (Fig. 15 in Ref. 12). It is obvious that in the cyclic voltammetry experiments, particularly those recorded at sweep rates higher than 1 mV s^{-1}, such discontinuity cannot be obtained. It is possible to record discontinuous isotherm only with pulse experiments if the potential step is about 1 mV, as shown in Fig. 5 of Ref. 26 for the Pb UPD onto Ag(111).

The UPD of Cd was also investigated by the potentiostatic pulse technique. The initial potential was set at –0.1 V and cathodic pulses were applied in a sequence of 10 mV starting from –0.3 V. The duration of the cathodic pulses was either 40 or 50 ms and then an anodic pulse back to the initial potential was applied. Since the anodic *j–t* transients were much better defined, they were used for further analysis. The anodic *j–t* transients for most of the applied potentials are presented in Fig. 8. As can be seen, monotonously falling transients of short duration (up to 2 ms) were recorded for potentials more positive and in the region of the beginning of peak C (from –0.30 to –0.35 V). For cathodic potentials more negative than the potentials of peak C (from –0.37 to –0.41 V), the shape of the anodic *j–t* transients changed indicating the occurrence of the Cd UPD process and a much larger charge was recorded for these pulses. At more negative pulse potentials (from –0.45 to –0.49 V), two waves could be detected on the anodic *j–t* transients, indicating that two processes occurred (desorption of both the Cd monolayer and the $(\sqrt{3}\times\sqrt{3})$R30° Cd adlayer). By integration of the anodic *j–t* transients, the *Q vs*. *E* dependence was obtained, which is presented in Fig. 9 (the same dependence was obtained by the integration of the cathodic *j–t* transients, not shown here). This dependence is characterized by three inflection points: the first one (I) corresponding to the beginning of the Cd UPD process, the second one (II) corresponding to the formation of a $(\sqrt{3}\times\sqrt{3})$R30° Cd adlayer (at around 150 μC cm^{-2}) and the third one (III) reflecting the beginning of the formation of a close packed Cd monolayer. The charge required for the formation of the close packed Cd monolayer is reached at a potential of –0.49 V. Comparing the shape of *Q vs*. *E* dependence obtained by the analysis of potentiostatic pulse results (Fig. 9) with the one obtained by integration of the CV recorded at a sweep rate of 5 mV s^{-1} (Fig. 5b, Q_c(–0.49 V)), it can be seen that they are practically identical.

Finally, as stated for iodide adsorption, the presented analysis cannot give information about the exact structure of the adsorbed adlayers but valuable information concerning their adsorption kinetics could be obtained. In the case of Cd

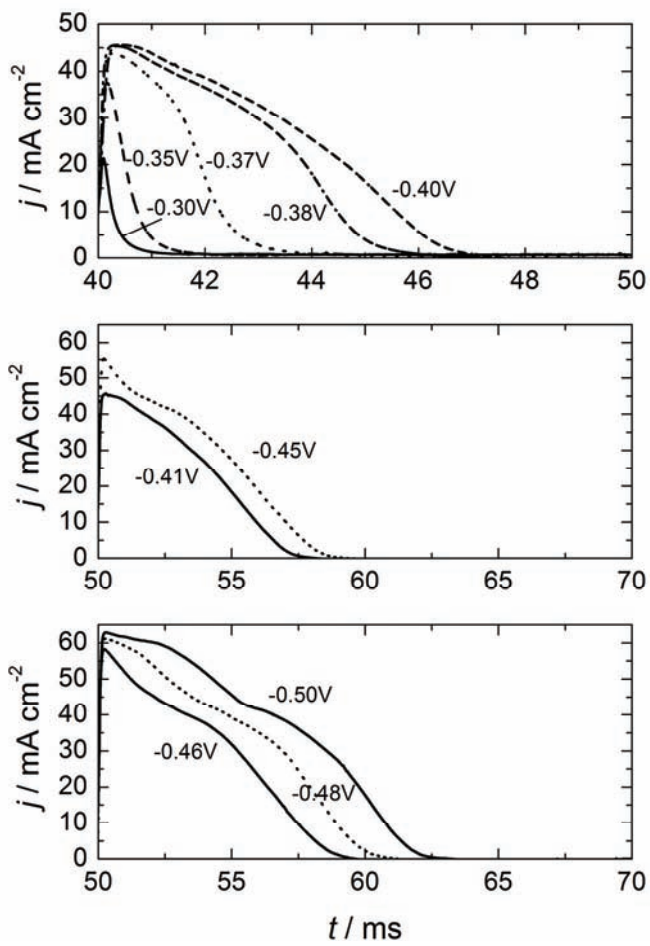

Fig. 8. Anodic *j*–*t* transients (potentials were stepped from the applied cathodic potentials to a potential of –0.1 V) recorded after applying pulse potentials at the values marked in the Figure.

UPD in the presence of iodide anions, the question arises whether it would be possible to detect the ($\sqrt{3}\times\sqrt{3}$)R30° Cd adlayer and close packed Cd monolayer if some ordered structure of iodide ad-atoms is formed on top of the Cd layer. For sulfate solution,[10] as well as for chloride solution,[24] this was possible since the formation of the ($\sqrt{3}\times\sqrt{3}$)R30° Cd adlayer commences on an (111) surface covered with randomly adsorbed anions, and it seems unrealistic to expect an ordered structure of these anions on top of the Cd layer. In the case of iodide anions, the formation of the ($\sqrt{3}\times\sqrt{3}$)R30° Cd adlayer starts on an Ag(111) surface covered with the same structure of adsorbed iodide and it is possible that the same, or a similar ordered structure of iodide, could be formed on top of the Cd adlayer and/or in between the Cd ad-atoms, which would make the determination

of the Cd under-layer difficult by *in situ* STM. According to the STM analysis of Pd monolayer formation onto Pt(111)[27] from a sulfate containing electrolyte, it appears that the ordered sulfate structure ($\sqrt{3}\times\sqrt{7}$)R19.1° adsorbed onto the Pd monolayer masks the structure of the under-layer (Pd monolayer). Hence, if something similar occurs in the case of Cd UPD onto Ag(111) in the presence of iodide anions, it would be (most likely) possible to detect some adlayer of iodide ad-atoms only on the bare Ag(111) surface (between the adsorbed Cd ad-atoms in the ($\sqrt{3}\times\sqrt{3}$)R30° structure). This is obviously a problem which deserves attention and it is believed that someone having the possibility to perform *in situ* STM measurements on this system (which is not the case for us), should investigate this process.

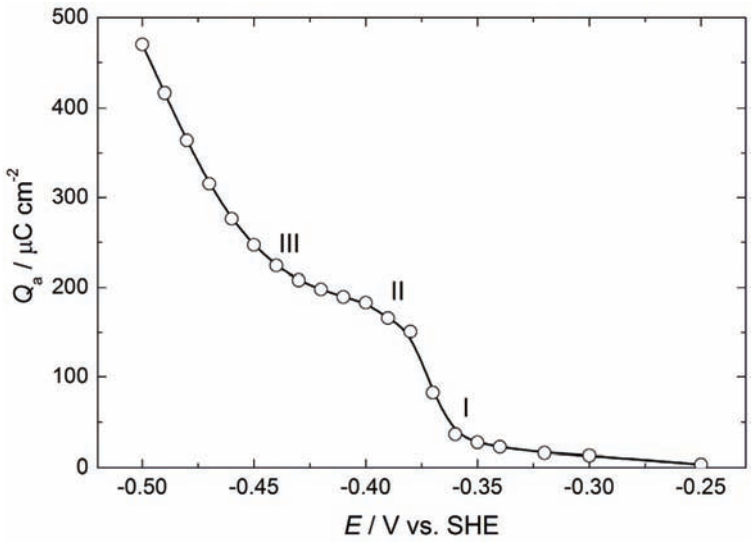

Fig. 9. Charge *vs.* potential curve obtained by integration of the anodic *j–t* transients presented in Fig. 8.

CONCLUSIONS

From the results presented in this paper, it could be concluded that the process of iodide adsorption is characterized by one broad and one sharp peak. The broad peak could be deconvoluted into five peaks: A, A1–A4. Peak A represents the random adsorption of iodide anions, mainly at the monoatomic steps as favorable locations for adsorption, while peaks A1, A3 and A4 are characterized by negative values of *f*, indicating attractive lateral interaction between the adsorbed anions. Only one peak, A4, possesses a value of $f < -4$, indicating a phase transition process. Peak B also corresponds to the phase transition process of the ($\sqrt{3}\times\sqrt{3}$)R30° iodide adlayer into a rotated hexagonal ($\sqrt{3}\times\sqrt{3}$)R(30°+α°) phase.

The adsorption/desorption process of cadmium cations in the presence of iodides is characterized by two main peaks, each of them being composed of two or three peaks with negative values of *f*. By analysis of the charge *vs*. potential dependences obtained either from the CVs or the current transients on potentiostatic pulses, it was concluded that the adsorbed iodide anions did not undergo desorption during the process of Cd UPD, but became replaced by Cd ad-atoms and remained adsorbed on top of a Cd layer and/or in between Cd ad-atoms.

Acknowledgement. The authors are indebted to the Ministry of Science and Technological Development of the Republic of Serbia (Project No. 172054) for the financial support of this work.

И З В О Д

ПРОЦЕСИ АДСОРПЦИЈЕ/ДЕСОРПЦИЈЕ ЈОДИДА И КАТЈОНА КАДМИЈУМА НА Ag(111)

ВЛАДИМИР Д. ЈОВИЋ и БОРКА М. ЈОВИЋ

Институт за мултидисциплинарна истраживања, п. пр. 33, 11030 Београд

У овом раду су испитивани процеси адсорпције/десорпције јодида и катјона кадмијума у присуству јодида на Ag(111). Показано је да су оба процеса комплексна и да су окарактерисани са по неколико пикова на цикличним волтамограмима. Помоћу PeakFit анализе добијених волтамограма и накнадног фитовања сваког регистрованог пика Фрумкиновом адсорпционом изотермом одређени су параметри процеса адсорпције, фактор интеракције (*f*) и Гибсова енергија адсорпције (ΔG_{ads}) за сваку адсорбовану фазу. У случају адсорпције јодида четири пика су поседовала негативне вредности *f*, указујући на привлачне силе између адсорбованих анјона, док су вредности *f* за два пика биле негативније од –4 што је била потврда одигравања процеса фазне трансформације при адсорпцији јодида. Процес адсорпције/десорпције катјона кадмијума (UPD) у присуству јодида окарактерисана је са два главна пика, при чему је сваки пик био састављен од два или три пика са вредностима *f* негативнијим од –4. Анализом зависности наелектрисања од потенцијала закључено је да се адсорбовани јодиди не десорбују при процесу адсорпције катјона кадмијума, већ их на површини монокристала замењују ад-атоми кадмијума док јодиди остају адсорбовани на слоју адсорбованог кадмијума и/или између адсорбованих ад-атома кадмијума.

(Примљено 1. јула, ревидирано 23. августа 2010)

REFERENCES

1. G. N. Salaita, F. Lu, L. Laguren-Davison, A. T. Hubbard, *J. Electroanal. Chem.* **229** (1987) 1
2. J. H. Schott, H. S. White, *J. Phys. Chem.* **98** (1994) 291
3. J. H. Schott, H. S. White, *J. Phys. Chem.* **98** (1994) 297
4. J. H. Schott, H. S. White, *Langmuir* **10** (1994) 486
5. M. Kawasaki, H. Ishii, *Langmuir* **11** (1995) 832
6. M. L. Foresti, G. Aloisi, M. Innocenti, H. Kobayashi, R. Guidelli, *Surf. Sci.* **335** (1995) 241
7. K. J. Stevenson, X. Gao, D. W. Hatchett, H. S. White, *J. Electroanal. Chem.* **447** (1998) 43
8. T. Yamada, K. Ogaki, S. Okubo, K. Itaya, *Surf. Sci.* **369** (1996) 321

9. H. Bort, K. Jüttner, W. J. Lorenz, G. Staikov, *Electrochim. Acta* **28** (1983) 993
10. S. G. Garcia, D. R. Salinas, G. Staikov, *Surf. Sci.* **576** (2005) 9
11. V. D. Jović, B. M. Jović, *Electrochim. Acta* **47** (2002) 1777
12. J. N. Jovićević, V. D. Jović, A. R. Despić, *Electrochim. Acta* **29** (1984) 1625
13. B. M. Jović, V. D. Jović, D. M. Dražić, *J. Electroanal. Chem.* **399** (1995) 197
14. E. Gileadi, *Electrode Kinetics for Chemists, Chemical Engineers, and Materials Scientists*, VCH Publishers Inc., New York, 1993, p. 305
15. B. M. Jović, V. D. Jović, G. R. Stafford, *Electrochem. Commun.* **1** (1999) 247
16. M. L. Foresti, M. Innocenti, F. Forni, R. Guidelli, *Langmuir* **14** (1998) 7008
17. M. Innocenti, M. L. Foresti, A. Fernandez, F. Forni, R. Guidelli, *J. Phys. Chem. B* **102** (1998) 9667
18. M. S. Zei, *J. Electroanal. Chem.* **308** (1991) 295
19. D. D. Sneddon, A. A. Gewirth, *Surf. Sci.* **343** (1995) 185
20. D. D. Sneddon, D. M. Sabel, A. A. Gewirth, *J. Electrochem. Soc.* **142** (1995) 3027
21. M. Schweizer, D. M. Kolb, *Surf. Sci.* **544** (2003) 93
22. S. Smolinski, P. Zelenay, J. Sobkowski, *J. Electroanal. Chem.* **467** (1998) 41
23. B. M. Jović, D. M. Dražić, V. D. Jović, *J. Serb. Chem. Soc.* **64** (1999) 539
24. C. Stuhlmann, Z. Park, C. Bach, K. Wandelt, *Electrochim. Acta* **44** (1998) 993
25. J. X. Wang, I. K. Robinson, R. R. Adžić, *Surf. Sci.* **412/413** (1998) 374
26. V. D. Jović, J. N. Jovićević, A. R. Despić, *Electrochim. Acta* **30** (1985) 1455
27. R. Hoyer, L. A. Kibler, D. M. Kolb, *Electrochim. Acta* **49** (2003) 63.

Journal of the Serbian Chemical Society
JSCS-info@shd.org.rs • www.shd.org.rs/JSCS
J. Serb. Chem. Soc. *76* (2) 305–315 (2011)
JSCS–4119
UDC 547.594+547.412.23:536.423.4+541.121:536.7
Original scientific paper

Isothermal vapour–liquid equilibria in cyclohexanone + dichloroalkane binary mixtures at temperatures from 298.15 to 318.15 K

DANA DRAGOESCU*, ALEXANDRU BARHALA, MARIANA TEODORESCU and DANIELA CHISCAN

"Ilie Murgulescu" Institute of Physical Chemistry, Splaiul Independentei 202, 060021 Bucharest, Romania

(Received 27 January, revised 21 September 2010)

Abstract: The vapour pressures of binary mixtures of cyclohexanone + dichloroalkane (1,3-dichloropropane and 1,4-dichlorobutane) were measured at temperatures between 298.15 and 318.15 K. The vapour pressures *vs.* liquid phase composition data were used to calculate the activity coefficients of the two components and the excess molar Gibbs energies G^E for the mixtures, using the Barker method and the Redlich–Kister, Wilson, NRTL and UNIQUAC equations, taking into account the vapour phase imperfection in terms of the 2nd virial coefficient. No significant difference between the G^E values obtained with these equations was observed.

Keywords: vapour pressure; vapour–liquid equilibria; excess Gibbs energy; mixtures; cyclohexanone; dichloroalkanes.

INTRODUCTION

As part of a series of experimental vapour–liquid equilibria (VLE) studies on mixtures of cycloketones with chloroalkanes, measurements on (cyclohexanone + 1,3-dichloropropane and + 1,4-dichlorobutane) binary mixtures, for which no such experimental data are available,[1,2] are reported herein.

In addition, no experimental excess Gibbs free energy, G^E, or excess enthalpy, H^E, data for these mixtures could be found in the literature.[2]

In previous papers, experimental VLE data for cyclopentanone + 1,2-dichloroethane and + 1,1,1-trichloroethane,[3] 1,1,2,2-tetrachloroethane + cyclopentanone and + cyclohexanone,[4] cyclopentanone + 1,3-dichloropropane, + 1,4-dichlorobutane, + 1-chlorobutane,[5] 1,2-dichloroethane + cyclohexanone, chloro-

* Corresponding author. E-mail: ddragoescu@chimfiz.icf.ro
doi: 10.2298/JSC090127020D

form + cyclopentanone and chloroform + cyclohexanone[6] and cyclohexanone + + 1-chlorobutane, + 1,1,1-trichloroethane[7] were reported.

To correlate the experimental VLE data, different expressions for excess Gibbs energy G^E, *i.e.*, Redlich–Kister,[8] Wilson,[9] NRTL[10] and UNIQUAC[11] equations were used.

These studies will be used to estimate the interaction parameters for the group contribution methods DISQUAC, for a possible comparison with *n*-alkanone + chloroalkane systems in terms of molecular surface interaction, steric and ring strain effects, and electron-donor ability of the cyclo-carbonyl group with chloroalkanes.

EXPERIMENTAL

Materials

The chemicals used, of the highest available purity, were commercial products from Aldrich (cyclohexanone and 1,3-dichloropropane) and Merck (1,4-dichlorobutane). The purity of the substances, checked by gas chromatography, was not less than 99.8 mol %. Evidence of chemical purity was also provided by comparison of the measured refractive indices, n_D(298.15 K), densities, ρ(298.15 K) and vapour pressure with the literature values, given in Table I.

The liquids were dried and stored over 4Å molecular sieves and used without further purification.

TABLE I. Physical properties of the pure compounds at 298.15 K

Temperature, K	n_D		ρ / kg m^{-3}		p / kPa	
	This work	Literature	This work	Literature	This work	Literature
Cyclohexanone						
298.15	1.4482	1.4480[12]	943.0	942.5[12]	0.64	0.58[13]
308.15					1.16	1.05[13]
318.15					1.92	1.79[13]
1,3-Dichloropropane						
298.15	1.4459	1.4460[14]	1181.4	1181.8[14]	2.72	2.24[15]
308.15					4.40	3.82[15]
318.15					6.89	6.26[15]
1,4-Dichlorobutane						
298.15	1.4519	1.4518[14] 1.4522[16]	1132.8	1134.02[16] 1133.1[17]	0.78	0.56[13], 0.77[18]
308.15					1.38	1.00[13], 1.25[18]
318.15					2.10	1.74[13], 1.99[18]

Apparatus and procedure

The vapour pressure, *p*, of the pure compounds and the binary mixtures were measured by a static method, in which the total pressure was measured as a function of the overall composition in an equilibrium cell.

Use was made of an isoteniscope based on the Surovy design.[19] The working procedure and the performance of the apparatus were described in previous papers[20,21] and detailed in other.[6,7]

The equilibrium cell, of total volume of 80 cm^3, was tightly connected with an Hg-filled U-tube as a null manometer surrounded by a thermostated jacket. The cell was equipped with other fittings-on the thermostated mantle. The temperature of this mantle was the actually equilibrium temperature, *T*, while the temperature of the jacket of the null manometer was maintained 1 to 2 K higher in order to prevent the partial condensation of vapours in the upper part of the apparatus. The isoteniscope was joined *via* the null manometer to an external mercury manometer, which enabled the pressure to be accurately measured within the range of 0.1–100 kPa.

After thermostating the equilibrium cell at the required temperature, the difference of the mercury levels in the null manometer was equalized with dry air and the pressure, *p*, was read on the precision Hg manometer connected to the apparatus. The manometric readings were performed with a Griffin and George Ltd. (London, UK), type 4214 cathetometer, to within ±0.01 mm, equivalent to an uncertainty of ±3 Pa. The measured equilibrium pressures were reproducible to better than 20 Pa. In order to avoid modifications of the cell volume, the level of the mercury in the null manometer was maintained always at the same position. In this way, the volume of the vapour space in the cell was kept nearly constant (70 cm^3).

Mixtures of known composition of about 10 cm^3 were prepared by weighing to within 10^{-7} kg and thorough degassing in the equilibrium cell by alternate freezing, high vacuum pumping and thawing, as described by Ronc[22] and Young.[23] During the vapour pressure measurement, the liquid in the equilibrium cell was stirred by means of a magnetic stirrer.

The equilibrium temperature, *T*, was measured with an accuracy of 0.1 K against IST-90 (International Temperature Scale of 1990) by means of mercury thermometers previously checked at the National Institute of Metrology, Bucharest, Romania.

Finally, the experimental uncertainties were: σT = 0.1 K, σp = 0.02 kPa, σx_i = 0.001 for temperature, pressure and molar fraction, respectively.

RESULTS

The vapour pressures of the pure components, cyclohexanone, 1,3-dichloropropane and 1,4-dichlorobutane, were measured in the same apparatus at the working temperatures and were in good agreement with the literature values (Table I).

The direct experimental values, *x*–*p*–*T*, and the calculated vapour phase compositions, *y*, for the binary systems cyclohexanone + 1,3-dichloropropane and + 1,4-dichlorobutane at temperatures from 298.15 to 318.15 K are presented in Tables II and III.

Figures 1 and 2 show the experimental and calculated isotherms fitted to the 3rd order Redlich–Kister Equation for G^E:

$$G^E = RTx_1x_2\sum A_i\left(x_1 - x_2\right)^{i-1} \quad (1)$$

A good agreement between the data was observed.

TABLE II. Experimental VLE data for 1,3-dichloropropane (x) + cyclohexanone (1–x) mixtures

x	y_{calc}	p_{exp} / kPa	(p_{exp}–p_{cal}) / kPa	G^E / J mol^{-1}
		T = 298.15 K		
0.000	0.000	0.64	0	0
0.100	0.210	0.72	0.00	–163
0.176	0.368	0.79	–0.02	–259
0.267	0.533	0.92	–0.02	–343
0.348	0.654	1.12	0.03	–390
0.430	0.751	1.28	0.00	–414
0.565	0.861	1.62	0.03	–403
0.667	0.915	1.88	0.02	–356
0.729	0.940	2.01	–0.02	–312
0.825	0.968	2.22	–0.06	–223
0.909	0.986	2.43	–0.06	–124
0.958	0.994	2.58	–0.03	–60
1.000	1.000	2.72	0	0
		T = 308.15 K		
0.000	0.000	1.16	0	0
0.100	0.207	1.18	–0.12	–135
0.176	0.352	1.40	–0.05	–221
0.267	0.504	1.62	–0.03	–303
0.348	0.620	1.94	0.08	–357
0.430	0.718	2.19	0.07	–391
0.565	0.838	2.61	0.02	–402
0.667	0.901	3.01	0.01	–370
0.729	0.930	3.21	–0.05	–332
0.825	0.964	3.58	–0.10	–246
0.909	0.985	3.90	–0.13	–142
0.958	0.994	4.16	–0.07	–71
1.000	1.000	4.40	0	0
		T = 318.15 K		
0.000	0.000	1.92	0	0
0.100	0.218	2.11	–0.09	–100
0.176	0.361	2.40	–0.05	–168
0.267	0.504	2.76	–0.01	–233
0.348	0.613	3.16	0.05	–279
0.430	0.707	3.62	0.12	–311
0.565	0.825	4.13	–0.06	–327
0.667	0.890	4.84	0.04	–306
0.729	0.921	5.12	–0.07	–278
0.825	0.959	5.75	–0.04	–209
0.909	0.982	6.31	–0.03	–122
0.958	0.993	6.55	–0.09	–61
1.000	1.000	6.89	0	0

TABLE III. Experimental VLE data for 1,4-dichlorobutane (x) + cyclohexanone (1–x) mixtures

x	y_{calc}	p_{xp} / kPa	$(p_{exp}-p_{calc})$ / kPa	G^E / J mol^{-1}
		T = 308.15 K		
0.000	0.000	1.16	0.00	0
0.067	0.086	1.19	0.02	14
0.121	0.149	1.20	0.01	24
0.200	0.241	1.23	0.00	38
0.296	0.344	1.25	–0.00	51
0.418	0.467	1.27	–0.01	61
0.522	0.566	1.30	–0.01	64
0.634	0.669	1.33	–0.00	62
0.712	0.739	1.35	0.00	56
0.812	0.828	1.37	0.01	42
0.898	0.905	1.38	0.01	26
1.000	1.000	1.38	0.00	0
		T = 318.15 K		
0.0000	0.000	1.92	0.00	0
0.067	0.075	1.93	0.00	4
0.121	0.133	1.94	0.00	7
0.200	0.218	1.95	–0.00	10
0.296	0.318	1.99	0.00	13
0.418	0.442	2.00	0.00	16
0.522	0.544	2.03	0.00	16
0.634	0.653	2.04	–0.01	15
0.712	0.728	2.06	0.00	13
0.812	0.823	2.08	0.00	10
0.898	0.904	2.09	0.00	6
1.000	1.000	2.10	0.00	0

CORRELATION AND DISCUSSION

The vapour pressures of the pure component agree fairly well with literature data in the range of the VLE measurements (Table I). The literature values for vapour pressure shown in Table I were calculated using specific equations, as given in the mentioned references.

The isothermal (vapour–liquid) equilibrium data of the mixtures were correlated by Barker's method[24] using well-known expressions for G^E, *i.e.*, the Redlich–Kister,[8] Wilson,[9] NRTL[10] and UNIQUAC Equations.[11]

The model coefficients were determinate by regression through minimization of the objective function Q, Eq. (2):

$$Q = \sum_{j}^{N} \left[\frac{p_{\mathrm{calc},j} - p_{\mathrm{exp},j}}{p_{\mathrm{exp},j}} \right]^2 \qquad (2)$$

where the subscripts calc and exp denote the calculated and experimental values of the pressure of an experimental point *j*, *N* being the total number of experimental points for one isotherm.

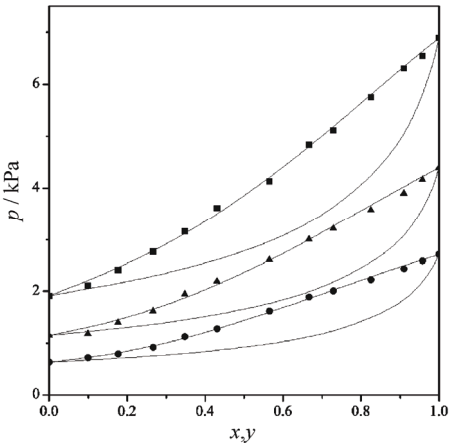

Fig. 1. Isothermal VLE for 1,3-dichloropropane (*x*) + cyclohexanone (1–*x*) mixtures. The symbols represent the experimental data at T = 298.15 (●), 308.15 (▲) and 318.15 (■) K and the curves were obtained from a 3rd-order Redlich–Kister Equation.

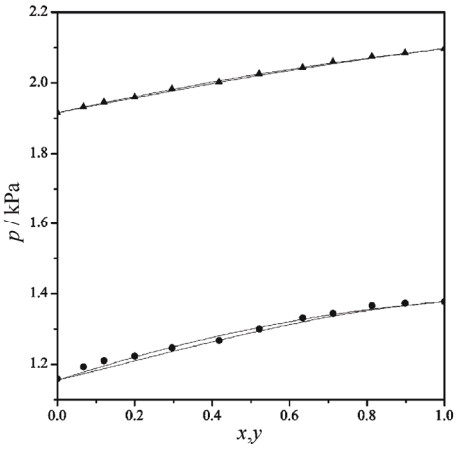

Fig. 2. Isothermal VLE for 1,4-dichlorobutane (*x*) + (1–*x*) cyclohexanone mixture. The symbols represent the experimental data at T = 308.15 (●), 318.15 (▲) K and the curves were obtained from a 3rd-order Redlich–Kister Equation.

Vapour phase imperfection was accounted for in terms of the 2nd molar virial coefficient, estimated by the method of Tsonopoulos[25], while the molar volumes were calculated by the Rackett[26] Equation with coefficients taken from Lide and Kehiaian.[27] Critical properties of substances were used as founded in the report of Ambrose.[28]

For the mixtures under study, the standard deviation σp values were between 3.0 and 76 Pa (Table IV).

In this Table, A_1, A_2 and A_3 denote the binary parameters of the models: (k_{ij} – – k_{ii}) for the Wilson Equation, ($g_{ij} - g_{ii}$) for the NRTL equation and ($u_{ij} - u_{ii}$) for the UNIQUAC Equation and they represent the energies of interactions between unlike molecules 1–2 and 2–1 (being expressed in J mol^{-1}). For the Redlich––Kister Equation, they are without physical significance. The third NRTL parameter, α, is related to the non-randomness in the mixtures that for the studied class of systems had a fixed value of 0.3.

For the mixture 1,3-dichloropropane + cyclohexanone, the correlation with NRTL and UNIQUAC models failed, probably due to some numerical problems in the fitting procedure.

The results presented in Figs. 1 and 2 show that the studied systems behave differently. For the mixture 1,3-dichloropropane + cyclohexanone, the deviations from the Raoult Law were negative, while the mixture 1,4-dichlorobutane + cyclohexanone showed small positive deviations from the Raoult Law.

TABLE IV. Parameters of the equations used to correlate the VLE data for 1,3-dichloropropane (x) + cyclohexanone (1–x) and 1,4-dichlorobutane (x) + cyclohexanone (1–x) binary mixtures and the standard deviation σp at 298.15, 308.15 and 318.15 K

T / K	A_1 or A_{12}	A_2 or A_{21}	A_3	σp[a] / kPa
1,3-Dichloropropane (x) + cyclohexanone (1–x)				
Redlich–Kister Equation (3rd-order)				
298.15	–0.67100	0.007450	–	0.033
308.15	–0.63092	–0.05575	–	0.076
318.15	–0.49198	–0.08619	–	0.068
Redlich–Kister Equation (4th-order)				
298.15	–0.69235	0.21735	–0.27949	0.027
308.15	–0.65264	0.21043	–0.56714	0.040
318.15	–0.49341	0.02619	–0.26056	0.049
Wilson Equation				
298.15	–176.1683	–0.9786	–	0.032
308.15	7.0019	–172.6808	–	0.075
318.15	82.1212	–199.5170	–	0.065
1,4-Dichlorobutane (x) + cyclohexanone (1–x)				
Redlich–Kister Equation (3rd order)				
308.15	0.10047	0.01354	–	0.010
318.15	0.02447	0.0004	–	0.004
Redlich–Kister Equation (4th order)				
308.15	0.06521	0.01080	0.21734	0.003
318.15	0.02113	0.00023	0.02081	0.004
Wilson Equation				
308.15	188.0812	–118.4118	–	0.009
318.15	5.3689	2.4429	–	0.004
NRTL Equation (α = 0.3)				
308.15	195.9862	–137.5274	–	0.010
318.15	6.0756	1.7278	–	0.004
UNIQUAC Equation				
308.15	–86.2824	47.8833	–	0.010
318.15	–79.6637	31.8715	–	0.004

[a]the average standard deviation of the total vapour pressure: $\sigma p = (\sum (p_{exp} - p_{calc})^2 / (N - m))^{1/2}$, where N is the number of experimental points and m is the number of equation parameters

The calculated excess Gibbs energy G^E increases with increasing temperature, for the first mixture and decreases with increasing temperature, for the second mixture, as is observed in Figs. 3 and 4.

The equimolar excess enthalpies, H^E, estimated from the temperature dependence of G^E, for the 1,3-dichloropropane + cyclohexanone mixture are: 1761 J mol^{-1}, at an average temperature of 308.15 K, and 1543 J mol^{-1} for the 1,4-dichlorobutane + cyclohexanone mixture, at an average temperature of 313.15 K. However, it is well known that the calculation of excess enthalpy from vapour pressure data implies a great uncertainty,[29] which was also mentioned by other authors, also very recently[30]; hence, in the absence of the calorimetrical data, the calculated H^E values are qualitative only.

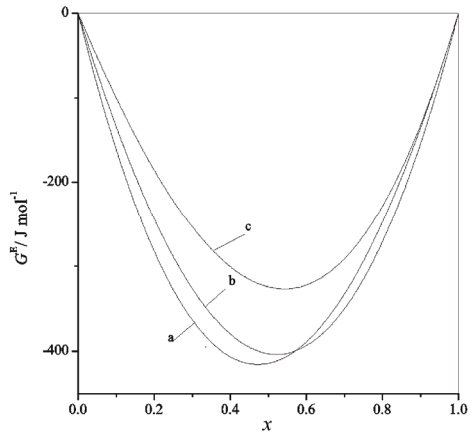

Fig. 3. Molar excess Gibbs energies for 1,3-dichloropropane (x) + cyclohexanone (1–x) mixtures at T = 298.15 (a), 308.15 (b), 318.15 (c) K.

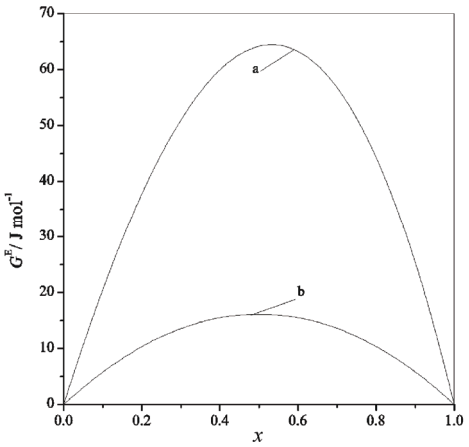

Fig. 4. Molar excess Gibbs energies for 1,4-dichlorobutane (x) + (1–x) cyclohexanone mixtures at T = 308.15 (a), 318.15 (b) K.

The behaviour of the system 1,4-dichlorobutane + cyclohexanone, with small positive values of G^E, unlike the negative values for cyclohexanone + 1,2--dichloroethane[6] and + 1,3-dichloropropane shows a decrease in specific inter-

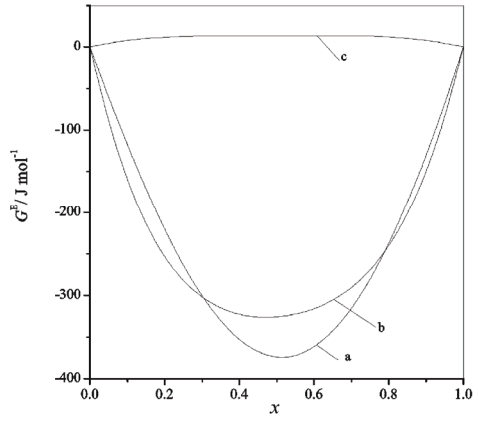

Fig. 5. Molar excess Gibbs energies for dichloroalkane (1–x) + cyclohexanone(1–x) mixtures at T = 318.15 K (a – 1,2-dichloroethane; b – 1,3-dichloropropane; c – 1,4-dichlorobutane).

actions between the Cl groups of the chloroalkanes and the CO group of the cycloketone (Fig. 5), similarly to linear ketone + α,ω-dichloroalkane mixtures.[31] This behaviour agrees with that expected from the proximity effect: the more the two Cl groups are separated, the less they influence each other and the behaviour of these systems is the same of systems with 1-chloroalkane, for which both G^E and H^E are positive.[32,33]

CONCLUSIONS

The experimental vapour–liquid equilibrium data for cyclohexanone + dichloroalkane binary mixtures at temperatures from 298.15 to 318.15 K are reported. For the mixture 1,3-dichloropropane + cyclohexanone, the deviations from the Raoult Law are negative, while the mixture 1,4-dichlorobutane + cyclohexanone shows small positive deviations from this Law.

The vapour pressures *vs*. liquid phase composition data were used to calculate the activity coefficients of the two components, and the excess molar Gibbs energies G^E for the mixtures, using the Barker method. The G^E values were represented by the well-known Redlich–Kister, Wilson, NRTL and UNIQUAC Equations. No significant difference between the G^E values obtained with these equations was observed.

The calculated excess Gibbs energy G^E increases with increasing temperature for the first mixture and decreases with increasing temperature, for the second mixture.

NOMENCLATURE

A_i	– Redlich–Kister parameters
A_{12}, A_{21}	– Binary parameters of the Wilson, NRTL and UNIQUAC Equations
G^E	– Excess Gibbs free energy
H^E	– Excess enthalpy
m	– Number of equation parameters
n_D(298.15 K)	– Refractive index at 298.15 K
N	– Total number of experimental points for one isotherm
p	– Vapour pressure
Q	– Objective function in Eq. (2)
T	– Thermodynamic temperature
x_i	– Liquid-phase mole fraction
y	– Vapour-phase mole fraction
Subscripts	
calc	– calculated
exp	– experimental
j	– j^{th} experimental point
Greek letters	
α	– NRTL parameter
ρ(298.15 K)	– Liquid density at 298.15 K

σ – Standard deviation

И З В О Д

ИЗОТЕРМСКА РАВНОТЕЖА ПАРА–ТЕЧНОСТ БИНАРНИХ СМЕША ЦИКЛОХЕКСАНОН + ДИХЛОРАЛКАН У ТЕМПЕРАТУРНОМ ИНТЕРВАЛУ ОД 298,15 ДО 318,15 K

DANA DRAGOESCU, ALEXANDRU BARHALA, MARIANA TEODORESCU и DANIELA CHISCAN

„Ilie Murgulescu“ Institute of Physical Chemistry, Splaiul Independentei 202, 060021 Bucharest, Romania

Извршена су мерења напона пара бинарних смеша циклохексанон + дихлоралкан (1,3-дихлорпропан, 1,4-дихлорбутан) у температурном интервалу од 298,15 до 318,15 K. Коефицијенти активности компонената и допунске моларне Gibbs-ове енергије (G^E) смеша, израчунати су Баркеровом методом коришћењем експерименталних података зависности напона паре од састава течне фазе. G^E вредности су израчунаване и помоћу Redlich–Kister-ове, Wilson-ове, NRTL и UNIQUAC једначина, при чему је неидеалност гасовите фазе одређена преко другог виријалног коефицијената. Нису добијене значајне разлике при прорачуну G^E помоћу различитих једначина.

(Примљено 27. јануара, ревидирано 21. септембра 2010)

REFERENCES

1. I. Wichterle, J. Linek, Z. Wagner, H. V. Kehiaian, *Vapor–Liquid Equilibrium Bibliographic Database, EVLM‘2003* (CD–ROM, ISBN 2-9521918-0-8), ELDATA, Paris, 2004
2. *The Dortmund Data Bank (DDB), DDBST*, Software and Separation Technology GmbH, Oldenburg, Germany (http://www.ddbst.com/en/online/Online_DDB_Form.php)
3. A. Barhala, D. Dragoescu, M. Teodorescu, I. Wichterle, *J. Chem. Thermodyn.* **38** (2006) 617
4. M. Teodorescu, A. Barhala, D. Dragoescu, *J. Chem. Thermodyn.* **38** (2006) 1432
5. D. Dragoescu, M. Teodorescu, A. Barhala, *J. Chem. Thermodyn.* **39** (2007) 1452
6. D. Dragoescu, A. Barhala, M. Teodorescu, *Fluid Phase Equilib*. **267** (2008) 70
7. D. Dragoescu, A. Barhala, M. Teodorescu, *J. Chem. Thermodyn*. **41** (2009) 1025
8. O. Redlich, A. T. Kister, *Ind. Eng. Chem.* **40** (1948) 345
9. G. M. Wilson, *J. Am. Chem. Soc.* **86** (1964) 127
10. H. Renon, J. M. Prausnitz, *AIChE Journal* **14** (1968) 135
11. D. S. Abrams, J. M. Prausnitz, *AIChE Journal* **21** (1975) 116
12. *Beilstein: Handbook of Organic Chemistry*, 4th ed., R. Luckenback, Ed., Springer, New York, 1984
13. *KDB – Korea thermophysical properties Data Bank*, http://www.cheric.org/kdb/
14. 14. R. R. Dreisbach, *Physical Properties of Chemical Compounds III, Advances in Chemistry Series*, Vol. 29, American Chemical Society, Washington D.C., 1961
15. P. M. Varushchenko, L. O. Loseva, I. A. Druzhinina, *Zh. Fiz. Khim.* **61** (1987) 31
16. M. Teodorescu, J. Linek, *Fluid Phase Equilib.* **146** (1998) 155
17. , *CRC Handbook of Chemistry and Physics*, Internet Version 2007, 87th ed., D. R. Lide, Ed., Taylor and Francis, Boca Raton, FL, 2007 (http://www.hbcpnetbase.com)
18. A. Barhala, D. Dragoescu, *Rev. Roum. Chim.* **47** (2002) 831
19. J. Surovy, E. Graczova, S. Bafrncova, *Collect. Czech. Chem. Commun.* **59** (1994) 1729
20. D. Dragoescu, A. Barhala, R. Vilcu, *ELDATA Int. Electron. J. Phys. Chem. Data* **3** (1997) 85

21. A. Barhala, D. Dragoescu, *Rev. Roum. Chim*. **46** (2001) 773
22. M. Ronc, G. R. Ratcliff, *Can. J. Chem. Eng.* **54** (1976) 326
23. K. L. Young R. A, Mentzer, R. A Greenkorn, K. C Chao, *J. Chem. Thermodyn.* **9** (1977) 979
24. J. A. Barker, *Aust. J. Chem.* **6** (1953) 207
25. C. Tsonopoulos, *AIChE Journal* **20** (1974) 263
26. H. G. Racket, *J. Chem. Eng. Data* **15** (1970) 514
27. D. R. Lide, H. V. Kehiaian, *CRC Handbook of Thermophysical and Thermochemical Data*. CRC Press, Boca Raton, FL, 1994, pp. 1–518
28. D. Ambrose, *Vapour–Liquid Critical Properties*, NPL Report, Teddington, 1980
29. J. S. Rowlinson, F. L. Swinton, *Liquids and Liquid Mixtures*, 3rd ed., Butterworth, London, 1982
30. G. Boukais-Belaribi, B. F. Belaribi, J. Lohmann, J. Jose, *Fluid Phase Equilib*. **262** (2007) 180
31. D. Dragoescu, M. Teodorescu, A. Barhala, I. Wichterle, *Collect. Czech. Chem. Commun*. **68** (2003) 1175
32. J. Wisniak, *Thermochim. Acta*, **257** (1995) 51
33. M. J. Pico, P. C. Menaut, J. Fernandez, L. J. Legido, I. M. Paz Andrade, *J. Solution Chem*. **72** (1994) 304.